

1 **Global Ozone Chemistry And Related Datasets for the**  
2 **Stratosphere (GOZCARDS): methodology and sample results**  
3 **with a focus on HCl, H<sub>2</sub>O, and O<sub>3</sub>**

4 **L. Froidevaux<sup>1</sup>, J. Anderson<sup>2</sup>, H.-J. Wang<sup>3</sup>, R. A. Fuller<sup>1</sup>, M. J. Schwartz<sup>1</sup>,**  
5 **M. L. Santee<sup>1</sup>, N. J. Livesey<sup>1</sup>, H. C. Pumphrey<sup>4</sup>, P. F. Bernath<sup>5</sup>,**  
6 **J. M. Russell III<sup>2</sup>, and M. P. McCormick<sup>2</sup>**

7 <sup>1</sup>Jet Propulsion Laboratory, California Institute of Technology, Pasadena, CA, USA

8 <sup>2</sup>Hampton University, Hampton, VA, USA

9 <sup>3</sup>Georgia Institute of Technology, Atlanta, GA, USA

10 <sup>4</sup>The University of Edinburgh, Edinburgh, UK

11 <sup>5</sup>Old Dominion University, Norfolk, VA, USA

12 *Correspondence to:* L. Froidevaux (lucief@jpl.nasa.gov)

13

14

15

16

17

18

19

20

21

22

23

## 24 **Abstract**

25 We describe the publicly available data from the Global OZone Chemistry And Related Datasets  
26 for the Stratosphere (GOZCARDS) project, and provide some results, with a focus on hydrogen  
27 chloride (HCl), water vapor (H<sub>2</sub>O), and ozone (O<sub>3</sub>). This dataset is a global long-term  
28 stratospheric Earth System Data Record, consisting of monthly zonal mean time series starting as  
29 early as 1979. The data records are based on high quality measurements from several NASA  
30 satellite instruments and ACE-FTS on SCISAT. We examine consistency aspects between the  
31 various datasets. To merge ozone records, the time series are debiased relative to SAGE II values  
32 by calculating average offsets versus SAGE II during measurement overlap periods, whereas for  
33 other species, the merging derives from an averaging procedure during overlap periods. The  
34 GOZCARDS files contain mixing ratios on a common pressure/latitude grid, as well as standard  
35 errors and other diagnostics; we also present estimates of systematic uncertainties in the merged  
36 products. Monthly mean temperatures for GOZCARDS were also produced, based directly on  
37 data from the Modern-Era Retrospective analysis for Research and Applications.

38 The GOZCARDS HCl merged product comes from HALOE, ACE-FTS and lower  
39 stratospheric Aura MLS data. After a rapid rise in upper stratospheric HCl in the early 1990s, the  
40 rate of decrease in this region for 1997-2010 was between 0.4 and 0.7%/yr. On 6-8 yr timescales,  
41 the rate of decrease peaked in 2004-2005 at about 1%/yr, and has since levelled off, at ~0.5%/yr.  
42 With a delay of 6-7 years, these changes roughly follow total surface chlorine, whose behavior  
43 versus time arises from inhomogeneous changes in the source gases. Since the late 1990s, HCl  
44 decreases in the lower stratosphere have occurred with pronounced latitudinal variability at rates  
45 sometimes exceeding 1-2%/yr. Recent short-term tendencies of lower stratospheric and column  
46 HCl vary substantially, with increases from 2005-2010 for northern mid-latitudes and deep  
47 tropics, but decreases (increases) after 2011 at northern (southern) mid-latitudes.

48 For H<sub>2</sub>O, the GOZCARDS product covers both stratosphere and mesosphere, and the same  
49 instruments as for HCl are used, along with UARS MLS stratospheric H<sub>2</sub>O data (1991-1993).  
50 We display seasonal to decadal-type variability in H<sub>2</sub>O from 22 years of data. In the upper  
51 mesosphere, the anti-correlation between H<sub>2</sub>O and solar flux is now clearly visible over two full  
52 solar cycles. Lower stratospheric tropical H<sub>2</sub>O has exhibited two periods of increasing values,

53 followed by fairly sharp drops (the well-documented 2000-2001 decrease and a recent drop in  
54 2011-2013). Tropical decadal variability peaks just above the tropopause. Between 1991 and  
55 2013, both in the tropics and on a near-global basis, H<sub>2</sub>O has decreased by ~5-10% in the lower  
56 stratosphere, but about a 10% increase is observed in the upper stratosphere and lower  
57 mesosphere. However, such tendencies may not represent longer-term trends.

58 For ozone, we used SAGE I, SAGE II, HALOE, UARS and Aura MLS, and ACE-FTS data to  
59 produce a merged record from late 1979 onward, using SAGE II as the primary reference. Unlike  
60 the 2 to 3% increase in near-global column ozone after the late 1990s reported by some,  
61 GOZCARDS stratospheric column O<sub>3</sub> values do not show a recent upturn of more than 0.5 to  
62 1%; continuing studies of changes in global ozone profiles, as well as columns, are warranted.

63 A brief mention is also made of other currently available, commonly-formatted GOZCARDS  
64 satellite data records for stratospheric composition, namely those for N<sub>2</sub>O and HNO<sub>3</sub>.

## 65 **1 Introduction**

66 The negative impact of anthropogenic chlorofluorocarbon emissions on the ozone layer,  
67 following the early predictions of Molina and Rowland (1974), stimulated interest in the trends  
68 and variability of stratospheric ozone, a key absorber of harmful ultraviolet radiation. The  
69 discovery of the ozone hole in ground-based data records (Farman et al., 1985) and the  
70 associated dramatic ozone changes during southern hemisphere winter and spring raised the level  
71 of research and understanding regarding the existence of new photochemical processes (see  
72 Solomon, 1999). This research was corroborated by analyses of aircraft and satellite data (e.g.,  
73 Anderson et al., 1989; Waters et al., 1993), and of independent ground-based data. Global total  
74 column ozone averages in 2006-2009 were measured to be smaller than during 1964-1980 by  
75 ~3%, and larger more localized decreases over the same periods reached ~6% in the southern  
76 hemisphere midlatitudes (WMO, 2011). Halogen source gas emissions have continued to  
77 decrease as a result of the Montreal Protocol and its amendments. Surface loading of total  
78 chlorine peaked in the early 1990s and subsequent decreases in global stratospheric HCl and ClO  
79 have been measured from satellite-based sensors (Anderson et al., 2000; Froidevaux et al., 2006;  
80 Jones et al., 2011) as well as from the ground (e.g., Solomon et al., 2006, Kohlhepp et al., 2012).  
81 A slow recovery of the ozone layer towards pre-1985 levels is expected (WMO, 2011; 2014).

82 High quality long-term datasets for ozone and related stratospheric species are needed to  
83 document past variability and to constrain global atmospheric models. The history of global  
84 stratospheric observations includes a large suite of satellite-based instruments, generally well-  
85 suited for the elucidation of long-term global change. A review of differences between past and  
86 ongoing satellite measurements of atmospheric composition has been the focus of the  
87 Stratosphere-troposphere Processes And their Role in Climate (SPARC) Data Initiative; results  
88 for stratospheric H<sub>2</sub>O and O<sub>3</sub> intercomparisons have been described by Hegglin et al. (2013) and  
89 Tegtmeier et al. (2013), respectively, to be followed by a report on many other species.  
90 Systematic biases reported in these papers mirror past validation work.

91 Under the Global OZone Chemistry And Related Datasets for the Stratosphere (GOZCARDS)  
92 project, we have created monthly zonally averaged datasets of stratospheric composition on a  
93 common latitude/pressure grid, using high quality data from the following satellite instruments:  
94 the Stratospheric Aerosol and Gas Experiments (SAGE I and SAGE II), the Halogen Occultation  
95 Experiment (HALOE) which flew aboard the Upper Atmosphere Research Satellite (UARS), the  
96 UARS Microwave Limb Sounder (MLS), the Atmospheric Chemistry Experiment Fourier  
97 Transform Spectrometer (ACE-FTS) on SCISAT, and Aura MLS. Table 1 provides  
98 characteristics of the original datasets; validation papers from the instrument teams and other  
99 related studies give a certain degree of confidence in these data. However, the existence of  
100 validation references does not imply that there are no caveats or issues with a particular  
101 measurement suite. In this project, we have strived to optimize data screening and mitigate some  
102 undesirable features, such as the impact of outlier values or the effects of clouds or aerosols. All  
103 source data sets still have imperfections, but in creating the GOZCARDS Earth System Data  
104 Record (ESDR) we maintain the integrity of the original data and do not arbitrarily disregard  
105 data, nor do we typically attempt to fill in spatial or temporal gaps in the record.

106 Based on original profiles from the various instruments, GOZCARDS “source” monthly  
107 zonal mean values were derived. After data screening, monthly average profiles were created by  
108 vertical interpolation onto the GOZCARDS pressure levels, followed by binning and averaging  
109 into monthly sets. In order to accommodate the lower vertical resolution of some limb viewers,  
110 such as UARS MLS, the GOZCARDS pressure grid was chosen as

111  $p(i) = 1000 \times 10^{-\frac{i}{6}}$  (hPa) (1)

112 with  $i$  varying from 0 to a product-dependent top; this grid width corresponds to  $\sim 2.7$  km. The  
113 high resolution SAGE O<sub>3</sub> profiles were converted to mixing ratio versus pressure using their  
114 associated NCEP temperature profiles, and smoothed vertically onto this grid. Given the  
115 sampling of solar occultation instruments, which usually provide 15 sunrise and 15 sunset  
116 profiles in two narrow latitude bands every day (versus the denser sampling from MLS, with  
117 almost 3500 profiles/day), we used 10°-wide latitude bins (18 bins from 80°S-90°S to 80°N-  
118 90°N) to construct monthly zonal means. Next, we merged the GOZCARDS source data by  
119 computing average relative biases between source datasets during periods of overlap, and then  
120 adjusting each source dataset to a common reference to remove relative biases. Non-zero biases  
121 always exist between data from different instruments for various reasons, such as systematic  
122 errors arising from the signals or the retrieved values, different vertical resolutions, or sampling  
123 effects. Toohey et al. (2013) studied sampling biases from a large suite of satellite-based  
124 stratospheric profiling instruments, based on simulations using fully-sampled model abundance  
125 averages versus averages of output sampled at sub-orbital locations. Larger sampling errors arise  
126 from occultation than from emission measurements, which often sample thousands of profiles  
127 per day. Toohey et al. (2013) found that sampling biases reach 10-15%, notably at high latitudes  
128 with larger atmospheric variability. Sofieva et al. (2014) have also discussed sampling  
129 uncertainty issues for satellite ozone datasets.

130 We have observed very good correlations between GOZCARDS and other long-term ozone  
131 data, such as the Stratospheric Water vapor and OzOne Satellite Homogenized (SWOOSH) data  
132 (S. Davis, personal communication, 2012) and homogenized Solar Backscatter Ultraviolet  
133 (SBUV) data. Dissemination of trend results arising from analyses of GOZCARDS and other  
134 merged ozone datasets was planned as part of WMO (2014) and the SI<sup>2</sup>N (Stratospheric  
135 Processes And their Role in Climate (SPARC), International Ozone Commission (IOC),  
136 Integrated Global Atmospheric Chemistry Observations (IGACO-O<sub>3</sub>), and the Network for the  
137 Detection of Atmospheric Composition Change (NDACC)) initiative. Profile trend results have  
138 been provided by Tummon et al. (2015), Harris et al. (2015), as well as Nair et al. (2013, 2015).

139 This paper starts with a discussion of data screening issues (Sect. 2 and Appendix A), and  
140 then describes the GOZCARDS data production methodology, followed by some atmospheric

141 results for HCl (Sect. 3), H<sub>2</sub>O (Sect. 4), and O<sub>3</sub> (Sect. 5). We provide specific diagnostics that  
142 indicate generally good correlations and small relative drifts between the source datasets used to  
143 create the longer-term GOZCARDS merged time series. Section 6 briefly mentions GOZCARDS  
144 N<sub>2</sub>O and HNO<sub>3</sub>, as well as temperatures derived from Modern-Era Retrospective analysis for  
145 Research and Applications (MERRA) fields. The version of GOZCARDS described here is  
146 referred to as ESDR version 1.01 or ev1.01.

147

## 148 **2 GOZCARDS source data and data screening**

149 Data provenance information regarding the various measurements used as inputs for  
150 GOZCARDS is provided in Appendix A (Sect. A.1).

### 151 **2.1 GOZCARDS data screening and binning**

152 The screening of profiles for GOZCARDS has largely followed guidelines recommended by  
153 the various instrument teams and/or relevant publications, **and we have documented these issues**  
154 **and procedures in Appendix A (Table A1)**. Unless otherwise noted, we only provide monthly  
155 means constructed from 15 or more (good) values in a given latitude/pressure bin. For ACE-FTS  
156 data, we also found it necessary to remove occasional large outlier values that could significantly  
157 impact the monthly zonal means. Our outlier screening removed values outside 2.5 times the  
158 standard deviation, as measured from the medians in each latitude/pressure bin, for each year of  
159 data. This was deemed close to optimum by comparing results to Aura MLS time series, which  
160 typically are not impacted by large outliers, and to ACE-FTS zonal means screened (in a slightly  
161 different way) by the ACE-FTS instrument team. Up to 5% of the profile values in each bin in  
162 any given month were typically discarded as a result, but the maximum percentage of discarded  
163 values can be close to 10% for a few months of ACE-FTS data, depending on year and species.  
164 Moreover, because of poor ACE-FTS sampling, the threshold for minimum number of good  
165 ACE-FTS values determining a monthly zonal mean was allowed to be as low as 10 for mid- to  
166 high latitudes, and as low as 6 for low latitudes (bins centered from 25°S to 25°N). Zonal mean  
167 data from ACE-FTS become too sparse in some years if such lower threshold values are not  
168 used. **Finally, no v2.2 ACE-FTS data are used after September 2010 (or after December 2009 for**

169 ozone) because of a data processing problem that affected this data version; a newly reprocessed  
170 ACE-FTS dataset was not available before we made the GOZCARDS data public.

171 Placing profiles on a common pressure grid is straightforward when pressures are present  
172 in the original files, as is the case for most data used here. Also, the vertical resolutions are  
173 similar for most of the instruments used for GOZCARDS. The UARS MLS, HALOE, and Aura  
174 MLS native pressure grids are either the same as or a superset of the GOZCARDS pressure grid,  
175 so these datasets were readily sampled for the construction of monthly means. For ACE-FTS,  
176 pressures are provided along with the fixed altitude grid, and we used linear interpolation versus  
177  $\log(\text{pressure})$  to convert profiles to the GOZCARDS grid. More details are provided later for  
178 SAGE I and SAGE II  $\text{O}_3$ , for which density versus altitude is the native representation.

179 The binning of profiles occurs after the screened values are averaged (in each  
180 latitude/pressure bin). Note that for the species discussed here, sunset and sunrise occultation  
181 values in the same latitude bin during a given month are averaged together. Negative monthly  
182 means are set to -999.0 in the GOZCARDS files; while negative mixing ratios smaller (in  
183 absolute value) than the associated standard errors can in theory be meaningful, negative  
184 monthly means are unlikely to be very useful scientifically. Quantities other than mixing ratios  
185 are provided in the netCDF GOZCARDS files, which are composed of one set of individual  
186 yearly files for all source datasets, and one set of yearly files for the merged products. The main  
187 quantities are monthly averages, plus standard deviations and standard errors. The GOZCARDS  
188 source files also provide the number of days sampled each month as well as minimum and  
189 maximum values for the source datasets. Other information includes average solar zenith angles  
190 and local solar times for individual sources. Finally, formulae for monthly standard deviations of  
191 the merged data are given in Appendix A, where sample time series of the standard deviations  
192 and standard errors (not systematic errors) for both source and merged data are also shown.

193

### 194 **3 GOZCARDS HCl**

#### 195 **3.1 GOZCARDS HCl source data records**

196 We used HCl datasets from HALOE, ACE-FTS and Aura MLS to generate the monthly zonal  
197 mean source products for GOZCARDS HCl. In addition to the procedures mentioned before, a

198 first-order aerosol screening was applied to the HALOE HCl profiles: all HCl values at and  
199 below a level where the 5.26  $\mu\text{m}$  aerosol extinction exceeds  $10^{-3} \text{ km}^{-1}$  were excluded. Regarding  
200 Aura MLS HCl, Froidevaux et al. (2008a) found anomalously high values versus aircraft data at  
201 147 hPa at low latitudes; these values are not used in the production of the merged HCl product.  
202 Also, the ongoing standard MLS HCl product is retrieved using band 14 rather than band 13,  
203 which targeted HCl for the first 1.5 years after launch, but started deteriorating rapidly after Feb.  
204 2006. As the remaining lifetime for band 13 is expected to be short, this band has been turned on  
205 only for a few days since Feb. 2006. MLS HCl data are not recommended for trend analyses at  
206 pressures  $< 10$  hPa. However, for pressures  $\geq 10$  hPa, band 14 HCl is deemed robust, because of  
207 the broader emission line in this region, in comparison to the measurement bandwidth.

208 Past validation studies have compared MLS HCl (v2.2), ACE-FTS (v2.2) and HALOE (v19)  
209 datasets using coincident pairs of profiles; such work was described by Froidevaux et al. (2008a)  
210 for MLS HCl validation and by Mahieu et al. (2008) for ACE-FTS HCl validation. The MLS  
211 version 3.3/3.4 HCl data used here (see Livesey et al., 2013) compare quite well with v2.2 HCl  
212 (average relative biases are within 5%). HALOE HCl values were found to be biased low by  
213  $\sim 10\text{-}15\%$  relative to both MLS and ACE-FTS, especially in the upper stratosphere; this low bias  
214 versus other (balloon- and space-based) measurements had been noted in past HALOE validation  
215 studies (Russell et al., 1996). Also, HALOE (v19) and ACE-FTS (v2.2) HCl data tend to lose  
216 sensitivity and reliability for pressures less than  $\sim 0.4$  hPa.

### 217 **3.2 GOZCARDS HCl merged data records**

218 *Although Aura MLS HCl data for pressures less than 10 hPa do not contribute to the time*  
219 *dependence of the merged HCl product, the 2004-2005 absolute Aura HCl measurements in this*  
220 *region are used to compute the offsets for the ACE-FTS and HALOE zonal mean source data in*  
221 *a consistent manner versus pressure.* Figure 1 illustrates the merging process for HCl at 32 hPa  
222 for the 45°S latitude bin (covering 40°S-50°S). Given that there exists very little overlap between  
223 the three sets of measurements in the same months in 2004 and 2005, especially in the tropics, a  
224 simple 3-way averaging of the datasets would lead to significant data gaps. Our methodology is  
225 basically equivalent to averaging all three datasets during this period, and we use Aura MLS as a  
226 transfer dataset. This was done by first averaging ACE-FTS and Aura MLS data, where the



227 datasets overlap, and then including the third dataset (HALOE) into the merging process with the  
228 temporary merged data. As the HALOE HCl values are generally lower than both the MLS and  
229 ACE-FTS values, the merged HCl dataset is generally further away from HALOE than it is from  
230 either ACE-FTS or Aura MLS. The top left panel in Fig. 1 shows GOZCARDS source data for  
231 HALOE, ACE-FTS, and Aura MLS during the overlap period, from August 2004 (MLS data  
232 start) through November 2005 (HALOE data end). The top right panel illustrates the result of  
233 step 1 in the merging procedure, with the temporary merged data values (orange) resulting from  
234 the adjustment of ACE-FTS and Aura MLS values to the mean reference (black dashed line);  
235 this reference is simply the average of the two series for all months when both values exist. The  
236 middle left panel shows step 2, namely the values (brown) obtained from merging HALOE  
237 values with the temporary merged values from step 1; the temporary merged values are weighted  
238 by  $2/3$  and HALOE values by  $1/3$  (giving the black dashed line as mean reference), so this is  
239 equivalent to averaging the three datasets with a weight of  $1/3$  each. A simple mathematical  
240 description of the above procedure is provided in Appendix A. The middle right panel shows the  
241 source data along with the final merged values during the overlap period, whereas the bottom  
242 panel shows the full time period, after the additive offsets are applied to the whole source series,  
243 thus removing relative biases; the three adjusted series are then averaged together wherever  
244 overlap exists, to obtain the final merged dataset. We tested this procedure by using one or the  
245 other of the two occultation data as the initial one (for step 1) and the results were not found to  
246 differ appreciably. We also found that the use of multiplicative adjustments generally produces  
247 very similar results as additive offsets. Some issues were found on occasion with multiplicative  
248 offsets, when combining very low mixing ratios, but additive offsets can also have drawbacks if  
249 the merged values end up being slightly negative, notably as a result of changes that modify the  
250 already low HCl values during Antarctic polar winter. This occurs on occasion as additive offsets  
251 tend to be weighted more heavily by larger mixing ratios found during non-winter seasons; as a  
252 result, we decided not to offset lower stratospheric HCl source datasets in the polar winter at  
253 high latitudes for any of the years. Further specifics and procedural details regarding the merging  
254 of HCl data are summarized in Appendix A.

255 In Fig. 2, we display the offsets that were applied to the three HCl source datasets as a result  
256 of the merging process in each latitude/pressure bin; a positive value means that a dataset is

257 biased low relative to the reference mean and needs to be increased by the offset value. These  
258 offsets show that in general, ACE-FTS and Aura MLS HCl values were adjusted down by 0.1-  
259 0.2 ppbv (a decrease of about 2-10%), while HALOE HCl was adjusted upward by 0.2-0.4 ppbv.  
260 Offset values tend to be fairly constant with latitude and the sum of the offsets equals zero. The  
261 generally homogeneous behaviour versus latitude is a good sign, as large discontinuities would  
262 signal potential issues in the merging (e.g., arising from large variability or lack of sufficient  
263 statistics). Figure S1 provides more detailed examples of upper and lower stratospheric offsets  
264 versus latitude, including standard errors based on the variability in the offsets during the overlap  
265 period (error bars provide an indication of robustness). Another indication of compatibility  
266 between datasets is provided by a comparison of annual cycles. Figure S2 provides average  
267 annual cycle amplitudes obtained from simple regression model fits to HALOE, ACE-FTS, and  
268 Aura MLS series over their respective periods. While there are a few regions where noise or  
269 spikes exist (mainly for ACE-FTS), large annual amplitudes in the polar regions occur in all time  
270 series; this arises from HCl decreases in polar winter, followed by springtime increases.

271 A more detailed analysis of interannual variability and trend consistency is provided from  
272 results in Fig. 3, which shows an example of ACE-FTS and Aura MLS time series. We have  
273 used coincident points from these time series to compare the deseasonalized anomalies (middle  
274 panel in Fig. 3) from both instrument series; correlation coefficient values (R values) are also  
275 computed. Very good correlations are obtained and no significant trend difference between the  
276 anomalies (bottom panel in Fig. 3) exists for ACE-FTS versus Aura MLS HCl. A view of these  
277 correlations and drifts at all latitudes/pressures is provided in Fig. 4, where the top panel gives R  
278 values for deseasonalized anomalies, and the bottom panel gives the ratio of the difference trends  
279 over the error in these trends. The results in Fig. 4 confirm that there are significant trend  
280 differences between the upper stratospheric HCl time series from ACE-FTS and Aura MLS (as a  
281 reminder, we did not use Aura MLS HCl for pressures less than 10 hPa). Fig. 4 also shows very  
282 low correlation coefficients from the deseasonalized HCl series in the uppermost stratosphere,  
283 because Aura MLS HCl exhibits unrealistically flat temporal behavior, whereas ACE-FTS HCl  
284 varies more. In the lower stratosphere, there is generally good agreement between the ACE-FTS  
285 and Aura MLS HCl time series, with R values typically larger than 0.7 and difference trend to

286 error ratios smaller than 1.5. The few low R values for 100 hPa at low latitudes likely reflect  
287 more infrequent ACE-FTS sampling and some (possibly related) outlier data screening issues.

288 Figure S3 illustrates GOZCARDS merged 46 hPa HCl variations versus time; there is clearly  
289 a much more complete global view (with no monthly gaps) after the launch of Aura MLS. Gaps  
290 at low latitudes in 1991 and 1992 are caused by post-Pinatubo aerosol-related issues in the  
291 HALOE record, and gaps in later years arise from the decrease in coverage from UARS. In the  
292 upper stratosphere, there are more gaps compared to 10 hPa and below, as a result of the much  
293 poorer tropical coverage from ACE-FTS and the elimination of MLS data in this region.

294 An indication of systematic errors in the merged values is given by the range of available  
295 monthly mean source data. For each bin, we compute the ranges of monthly means above and  
296 below the merged values that include 95% of the available source data monthly means. These  
297 error bars are not usually symmetric about the merged values, especially if one dataset is biased  
298 significantly more than others, in a relative sense. We did not have enough datasets here to  
299 consider a more statistical approach (such as the standard deviations among source datasets).  
300 Figure 5 shows the result of such a systematic error calculation at 46 hPa for the 35°S latitude  
301 bin. The lower shaded region range gives the lower bound, determined by HALOE data, and the  
302 upper limit of the grey shading originates from ACE-FTS data. Figure 6 shows contour plots of  
303 these estimated systematic errors in HCl. These are fairly conservative error bars; however, even  
304 the source data averages at the 95% boundaries have their own systematic errors (rarely smaller  
305 than 5%), so our estimates do not really encompass all error sources. Error bars representing a  
306 range within which 95% of the source data values reside (see Figs. 5 and 6) can be a useful guide  
307 for data users or model comparisons; although this is not an official product, users can readily  
308 calculate such ranges (or we can provide these values).

### 309 **3.3 GOZCARDS HCl sample results and discussion**

310 Stratospheric HCl is important because it is the main reservoir of gaseous chlorine and it can be  
311 used to follow the chlorine budget evolution over the past decades. This includes a significant  
312 increase before the mid-1990s as a result of anthropogenic chlorofluorocarbon (CFC) production,  
313 followed by a slower decrease as a result of the Montreal Protocol and subsequent international

314 agreements to limit surface emissions that were correctly predicted to be harmful to the ozone  
315 layer (Molina and Rowland, 1974; Farman et al., 1985).

316 In Fig. 7, we provide an overview of the HCl evolution since 1991, based on GOZCARDS  
317 average merged HCl for 3 different latitude regions at 4 pressure levels, from the upper  
318 stratosphere to the lower stratosphere. In the upper stratosphere (at 0.7 hPa shown here), the  
319 rapid early rise in HCl was followed by a period of stabilization (1997-2000) and subsequent  
320 decreases. Rates of decrease for stratospheric HCl and total chlorine have been documented  
321 using satellite-based upper stratospheric abundances, which tend to follow tropospheric source  
322 gas trends with a time delay of order 6 years, with some uncertainties in the modeling of this  
323 time delay and related age of air issues (Waugh et al., 2001; Engel et al., 2002; Froidevaux et al.,  
324 2006). As summarized in WMO (2011), the average rate of decrease in stratospheric HCl has  
325 typically been measured at -0.6 %/yr to -0.9 %/yr, in reasonable agreement with estimated rates  
326 of change in surface total chlorine; see also the HCl upper stratospheric results provided by  
327 Anderson et al. (2000) for HALOE, Froidevaux et al. (2006) for the one and a half year band 13  
328 Aura MLS data record, and Jones et al. (2011) and Brown et al. (2011) for a combination of  
329 HALOE and ACE-FTS datasets. The WMO (2011) summary of trends also includes results from  
330 column HCl data at various NDACC Fourier transform infrared (FTIR) measurement sites; see  
331 Kohlhepp et al. (2012) for a comprehensive discussion of ground-based results, showing some  
332 scatter as a function of latitude. Figure 7 demonstrates that a global-scale decline in mid- to  
333 lower stratospheric HCl is visible since about 1997. We also notice that at 68 hPa in the tropics,  
334 the long-term rate of change appears to be near-zero or slightly positive. In addition, there are  
335 shorter-term periods in recent years when an average increasing “trend” would be inferred rather  
336 than a decrease; in particular, see the northern hemisphere from 2005 through 2012 at 32 hPa.

337 We created deseasonalized GOZCARDS merged monthly zonal mean HCl data at different  
338 latitudes and we show in Fig. 8 the linear rate of change that results from simple fits through  
339 such series. The long-term trends (1997 - 2013 for lower and 1997 - 2010 for upper stratosphere)  
340 are generally negative and between about -0.5%/yr (upper stratosphere) and -1%/yr (lower  
341 stratosphere). Some separation between northern and southern hemisphere results is observed in  
342 the lower stratosphere, with less negative trends in the northern hemisphere. Also, the scatter  
343 increases from 68 hPa to 100 hPa, where some positive trends occur at low latitudes; however,

344 we have less confidence in the 100 hPa results, given the larger scatter and errors (and smaller  
345 abundances) in that region. Without trying to assign exact linear trends from these simple  
346 analyses, we observe considerable latitudinal variability in lower stratospheric HCl short-term  
347 behavior, especially after 2005. Such lower stratospheric changes in HCl have been captured in  
348 column HCl FTIR data (Mahieu et al., 2013, 2014). The latter reference shows that total column  
349 (FTIR) results and GOZCARDS lower stratospheric HCl trends agree quite well, and the authors  
350 imply that a relative slowdown in the northern hemispheric circulation is responsible for  
351 observed recent changes in the lower stratosphere. However, we note (Fig. 7) that changes in  
352 lower stratospheric HCl appear to be fairly short-term in nature, with an apparent reversal in  
353 behavior occurring at both northern and southern midlatitudes since 2011 (e.g., at 32 hPa).  
354 Lower stratospheric changes are distinct from the upper stratospheric long-term decrease, which  
355 we expect to continue, as long as the Montreal Protocol and its amendments are followed and  
356 total surface chlorine keeps decreasing.

357 In Figure 9, we provide simple rates of upper and lower stratospheric change in HCl for 6-yr  
358 sliding time periods (e.g., a 2004 value means a 2001-2006 average) for various latitudes. These  
359 results indicate that there has been an acceleration in the rate of decrease of upper stratospheric  
360 HCl between 2000 and 2004, followed by a period with somewhat smaller rates of change. This  
361 is roughly in agreement with curves showing the rates of change for surface total chlorine based  
362 on National Oceanic and Atmospheric Administration (NOAA) surface data (Montzka et al.,  
363 1999), as shown in Fig. 9 (top panel) with the Earth System Research Laboratory Global  
364 Monitoring Division data, time shifted by 6 or 7 years to account for transport delays into the  
365 upper stratosphere. Chlorine source gases have indeed shown a reduction in their rate of decrease  
366 during the second half of the past decade, as discussed by Montzka et al. (1999) and summarized  
367 in WMO (2011, 2014). Reasons include the initial rapid decrease in methyl chloroform, slower  
368 rates of decrease from the sum of CFCs in recent years, and increases in  
369 hydrochlorofluorocarbons (HCFCs). The lower stratospheric HCl behavior in Fig. 9 (bottom  
370 panel) shows rates of change in partial column density between 68 hPa and 10 hPa. These  
371 changes show more variability with latitude than in the upper stratosphere for short (6-yr) time  
372 periods, and a hemispheric asymmetry exists, peaking in 2009, when positive tendencies are seen  
373 in the northern hemisphere, as opposed to decreases in the south (Mahieu et al., 2014). These

374 results do not depend much on whether 6-yr or 8-yr periods (not shown) are used, but longer  
375 periods smooth out the rates of change; interannual variations, such as those arising from the  
376 quasi-biennial oscillation (QBO), will affect short-term results. Temporal patterns in the upper  
377 and lower stratosphere are qualitatively similar, and rates of change in surface emissions will  
378 impact both regions, but carefully disentangling this from changes in dynamics or in other  
379 species (e.g., CH<sub>4</sub>) that can affect chlorine partitioning will require more analyses and modeling.

## 380 **4 GOZCARDS H<sub>2</sub>O**

### 381 **4.1 GOZCARDS H<sub>2</sub>O source data records**

382 We used water vapor datasets from HALOE, UARS MLS, ACE-FTS, and Aura MLS to generate  
383 the monthly zonal mean source products for GOZCARDS H<sub>2</sub>O. In addition to the data screening  
384 procedures mentioned in Appendix A, we screened HALOE H<sub>2</sub>O data for high aerosol extinction  
385 values, closely following the screening used for merged H<sub>2</sub>O in the Stratospheric Water vapor  
386 and OzOne Satellite Homogenized (SWOOSH) dataset (S. Davis, personal communication,  
387 2012). This method (see Fig. S4) screens out anomalous HALOE H<sub>2</sub>O values that occurred  
388 mainly in 1991-1992, when the aerosol extinction near 22 hPa exceeded  $5 \times 10^{-4} \text{ km}^{-1}$ ; for  
389 pressure levels at and below 22 hPa, we have excluded the corresponding H<sub>2</sub>O values. **While this  
390 method may exclude some good data points, the lowest values (< 3 ppmv) do get screened out;  
391 such outliers are not corroborated by 22 hPa UARS MLS data (with most values > 3 ppmv).**  
392 Also, for upper mesospheric HALOE data, care should be taken during high latitude summer  
393 months, as no screening was applied for the effect of polar mesospheric clouds (PMCs). High  
394 biases (by tens of percent) in H<sub>2</sub>O above ~70 km have been shown to occur as a result of PMCs  
395 in the HALOE field of view (McHugh et al., 2003). Indeed, monthly means larger than 8-10  
396 ppmv are observed in GOZCARDS H<sub>2</sub>O merged data and in HALOE source data for pressures  
397 less than ~0.03 hPa. A more recent HALOE data version (V20 or VPMC) could be used to  
398 largely correct such PMC-related effects, although this was not implemented for GOZCARDS  
399 H<sub>2</sub>O. Aura MLS and ACE-FTS measurements, obtained at longer wavelengths than those from  
400 HALOE, do not yield such large H<sub>2</sub>O values; a rough threshold of 8.5 ppmv could also be used  
401 (by GOZCARDS data users) to flag the pre-2005 merged dataset.

402 UARS MLS stratospheric H<sub>2</sub>O for GOZCARDS was obtained from V6 (or V600) H<sub>2</sub>O data.  
403 This data version is identical to the original prototype (named V0104) from Pumphrey (1999),  
404 who noted that UARS MLS H<sub>2</sub>O often exhibits drier values (by 5-10%) than HALOE H<sub>2</sub>O (see  
405 also Pumphrey et al., 2000). The resulting UARS MLS H<sub>2</sub>O source data span the period from  
406 Sep. 1991 through April, 1993; a significant fraction of this dataset in the tropics at 100 hPa is  
407 flagged bad, as a result of diminishing sensitivity.

408 Summarizing past validation results, SPARC WAVAS (2000) analyses pointed out the  
409 existence of a small low bias in HALOE stratospheric H<sub>2</sub>O versus most other measurements,  
410 except for UARS MLS. Lambert et al. (2007) showed agreement within 5-10% between Aura  
411 MLS version 2.2 H<sub>2</sub>O and other data, including ACE-FTS H<sub>2</sub>O. From the mid-stratosphere to the  
412 upper mesosphere, excellent agreement between ground-based data from the Water Vapor  
413 Millimeter-wave Spectrometer and H<sub>2</sub>O profiles from Aura MLS and ACE-FTS has been  
414 demonstrated by Nedoluha et al. (2007, 2009, 2011). Changes from MLS v2.2 to v3.3 led to an  
415 increase of 0.2-0.3 ppmv in stratospheric H<sub>2</sub>O (Livesey et al., 2013). Recent comparisons by  
416 Hurst et al. (2014) of MLS v3.3 H<sub>2</sub>O data versus Cryogenic Frost point Hygrometer time series  
417 above Boulder show excellent overall agreement, indicating that systematic uncertainties for  
418 lower stratospheric MLS data may be as low as ~5%; this reinforces MLS H<sub>2</sub>O validation work  
419 by Read et al. (2007) and Voemel et al. (2007). Aura MLS stratospheric H<sub>2</sub>O v3.3 values are  
420 slightly larger (by up to ~5%) than the multi-instrument average from a number of satellite  
421 datasets, as discussed in satellite intercomparisons by Hegglin et al. (2013), who observed only  
422 small disagreements in interannual variations from various series for pressures less than 150 hPa.

## 423 **4.2 GOZCARDS H<sub>2</sub>O merged data records**

424 The merging process for H<sub>2</sub>O is nearly identical to the method used for HCl. The main difference  
425 is an additional step that merges UARS MLS data with the already combined datasets from  
426 HALOE, ACE-FTS, and Aura MLS, by simply adjusting UARS MLS values to the average of  
427 the previously merged series during the early (1991-1993) overlap period; see Fig. S5 for an  
428 illustration. Typically, this requires an upward adjustment of UARS MLS H<sub>2</sub>O data, as these  
429 values are biased low versus most other datasets; nevertheless, the short but global record from  
430 UARS MLS helps to fill the time series. After considering the channel drift issues for SAGE II

431 H<sub>2</sub>O (and following past advice from the SAGE II team itself), we decided to use caution and did  
432 not include that dataset for GOZCARDS, as trend results could be affected. Other minor  
433 procedural merging details or issues for H<sub>2</sub>O are included in the Supplement. Also, data users  
434 should be aware of anomalous effects arising in merged average series from non-uniform  
435 latitudinal sampling when no MLS data exist, in regions with large latitudinal gradients, as for  
436 H<sub>2</sub>O at 147 hPa, the largest pressure for merged GOZCARDS H<sub>2</sub>O. Latitudinal averages can be  
437 biased in certain months and month-to-month variability is increased because of relatively poor  
438 global sampling (in this region) prior to Aug. 2004, after which Aura MLS data are used.

439 In Fig. 10, we display the average offsets that were applied to the four H<sub>2</sub>O source datasets;  
440 these offsets follow previously known relative data biases. For example, low biases in UARS  
441 MLS H<sub>2</sub>O, especially in the mesosphere, were discussed by Pumphrey (1999) and the UARS  
442 MLS offsets (see Fig. 10) correct that dataset upward. The application of offsets derived for  
443 HALOE and UARS MLS raises the H<sub>2</sub>O time series from these instruments, whereas negative  
444 offsets lower the H<sub>2</sub>O source data from ACE-FTS and Aura MLS. As we found for HCl, the  
445 offset values generally display small variations versus latitude and are therefore fairly stable  
446 systematic adjustments to the time series. Figure S6 displays the amplitudes of the fitted annual  
447 cycles for HALOE, ACE-FTS, and Aura MLS. As for HCl, similar patterns emerge for these  
448 datasets. Wintertime descent into the polar vortex regions is responsible for large annual cycles  
449 at high latitudes, especially in the mesosphere; also, the seasonal impact of dehydration in the  
450 lower stratospheric Antarctic region causes a large annual cycle in Aura MLS high southern  
451 latitude data. Figure 11 provides some statistical information, as done for HCl in Sect. 3.2,  
452 regarding the correlations and trend differences between ACE-FTS and Aura MLS. There are a  
453 few regions with noisier relationships. While slow increases in H<sub>2</sub>O are generally observed by  
454 both instruments in the stratosphere and mesosphere, the tropical region near 0.1 hPa shows a  
455 slight decreasing trend for the ACE-FTS points, thus leading to larger discrepancies; it is not  
456 clear what the source of these discrepancies is. While the tropical ACE-FTS data are generally  
457 sampled with a significantly lower temporal frequency, the same applies for all pressure levels;  
458 however, a few outlier points can have a much larger impact when sampling is poorer. There are  
459 also a few other spots, such as near 65°S and 65°N and near 5 hPa, with a large drift in the  
460 difference time series; this may be caused by a combination of poorer sampling by ACE-FTS



461 and higher atmospheric variability, which can lead to more scatter. At the highest latitudes in the  
462 lower stratosphere, the observed slope differences are more within error bars, but the larger  
463 variability means that a longer record is needed to determine if the time series trend differently.  
464 The merged dataset tends to be much closer to Aura MLS in terms of trends because there are  
465 many more months of Aura MLS than ACE-FTS data; the overall impact of  
466 ACE-FTS data on the merged H<sub>2</sub>O series is fairly small.

467 Figure S7 provides a visual representation of the merged GOZCARDS H<sub>2</sub>O fields at  
468 3 hPa and 68 hPa, respectively. Well-known features are displayed in these plots, given the good  
469 global coverage in the post-2004 period in particular. In the upper stratosphere, descent at high  
470 latitudes during the winter months leads to larger H<sub>2</sub>O values, and low latitude QBO features are  
471 also observed. In the lower stratosphere, one observes dehydration evidence at high southern  
472 latitudes in the winter months, as well as a low latitude seasonal “tape recorder” signal; this  
473 phenomenon is driven by tropopause temperatures and has been measured in satellite data since  
474 the early 1990s (Mote et al., 1996; Pumphrey, 1999). A vertical cross-section of this lower  
475 stratospheric tropical (20°S to 20°N) tape recorder in GOZCARDS merged H<sub>2</sub>O for 1991-2013  
476 is shown in Fig. 12; periods of positive anomalies alternate with negative anomalies, including  
477 the post-2000 lows, as well as the most recent decreases in 2012-2013 (see also next section).

478 As we discussed for HCl, we have estimated systematic errors for the merged H<sub>2</sub>O product.  
479 This is illustrated by the contour plots in Fig. 13; these ranges encompass at least 95% of the  
480 monthly mean source data values from HALOE, UARS MLS, ACE-FTS, and Aura MLS above  
481 or below the merged series. These errors typically span 5 to 15% of the mean between 100 and  
482 0.1 hPa; errors larger than 30% exist in the tropical upper troposphere (147 hPa), and large  
483 values in the upper mesosphere arise from the low bias in UARS MLS H<sub>2</sub>O.

### 484 **4.3 GOZCARDS H<sub>2</sub>O sample results and discussion**

485 Stratospheric H<sub>2</sub>O variations have garnered attention because of the radiative impacts of water  
486 vapor in the UTLS and the connection to climate change (Solomon et al., 2010), as well as the  
487 stratospheric chemical significance of H<sub>2</sub>O oxidation products. Individual water vapor datasets  
488 have been used here to produce a merged stratospheric H<sub>2</sub>O record spanning more than two  
489 decades. We do not attempt here to characterize trends or to imply that recent tendencies will

490 carry into the next decade or two. Rather, as variability is also of interest to climate modelers, we  
491 focus here on observed decadal-type (longer-term) variability in stratospheric water vapor.

492 Figure 14 illustrates monthly, annual, and longer-term changes in stratospheric water vapor,  
493 based on GOZCARDS merged H<sub>2</sub>O; this shows the well-known H<sub>2</sub>O minimum in the lower  
494 tropical stratosphere as well as an increases in the upper stratosphere (as a result of methane  
495 oxidation). As we know from past studies (e.g., Randel et al., 2004), medium- to long-term  
496 changes in H<sub>2</sub>O are large-scale in nature. However, lower stratospheric H<sub>2</sub>O variations are more  
497 accentuated at low latitudes, in comparison to near-global (60°S-60°N) results. It has long been  
498 known (e.g., from the *in situ* balloon-borne measurements of Kley et al., 1979) that the  
499 hygropause is typically located a few km higher than the thermal tropopause. We observe that  
500 the tropical stratosphere is drier at 68 hPa than at 100 hPa (near the tropopause). According to  
501 the 22-year GOZCARDS data record, annually-averaged H<sub>2</sub>O values in the tropics (20°S-20°N)  
502 have varied between about 3.2 and 4.2 ppmv at 68 hPa. The rapid drop between 2000 and 2001  
503 is observed at 100 and 68 hPa, with some dilution of this effect at higher altitudes. There is a  
504 clear difference in long-term behavior between the upper stratosphere, where changes in methane  
505 should have the clearest influence, and the lower stratosphere, where cold point temperatures and  
506 dynamical changes have a significant impact. To first-order, the last few years show ~10% larger  
507 values in the upper stratosphere than in the early 1990s, while the opposite holds in the lowest  
508 stratospheric region, where a decrease of order 10% is observed over the same period. Figure 14  
509 also shows that month-to-month and seasonal variations are usually somewhat larger than the  
510 long-term changes in the lower stratosphere, most notably at 100 hPa.

511 In order to provide longer-term variability diagnostics for water vapor, we show in Fig. 15 the  
512 minimum to maximum spread in annual averages (tropics and mid-latitudes) from Fig. 14 for the  
513 22-yr period. We observe that the tropical variability is largest just above the tropopause (here  
514 this means at the 68 hPa GOZCARDS level), where it reaches ~27% (1 ppmv). Such diagnostics  
515 of variability should be useful for comparisons to various chemistry climate models.

516 The longer-term variability in water vapor increases above the stratopause and reaches close  
517 to 30% in the uppermost mesosphere, as seen in Fig. 16(a); this plot shows the monthly and  
518 annual near-global (60°S-60°N) H<sub>2</sub>O variations at 0.01 hPa. Large seasonal changes in this  
519 region are driven by vertical advection associated with the mesospheric circulation, with each

520 hemisphere's summertime peaks contributing to the maxima (two per year) in these near-global  
521 averages; such seasonal variations were compared to model results by Chandra et al. (1997),  
522 based on the first few years of HALOE H<sub>2</sub>O data. The strong upper mesospheric variability in  
523 annual-mean H<sub>2</sub>O is known from previous studies of ground-based and satellite H<sub>2</sub>O data  
524 (Chandra et al., 1997; Nedoluha et al., 2009; Remsberg, 2010), and this region is where the solar  
525 (Lyman  $\alpha$ ) influence on H<sub>2</sub>O is strongest. Figure 16(b) displays the near-global variations in  
526 annual upper mesospheric H<sub>2</sub>O from 0.1 to 0.01 hPa. We clearly see increased variability in the  
527 uppermost mesosphere, and decreases in the mixing ratios as a result of H<sub>2</sub>O photodissociation.

## 528 **5 GOZCARDS ozone**

529 A number of discussions relating to signs of ozone recovery have been presented before  
530 (Newchurch et al., 2003; Wohltmann et al., 2007; Yang et al., 2008; Jones et al., 2009; Hassler  
531 et al., 2011; Salby et al., 2011, 2012; Ziemke and Chandra, 2012; Gebhardt et al., 2014;  
532 Kuttipurath et al., 2013; Kirgis et al., 2013; Nair et al., 2013, 2015; Shepherd et al., 2014, Frith et  
533 al., 2014). While there are some indications of small increases in O<sub>3</sub> in the past 10-15 years,  
534 further confirmation of an increase in global O<sub>3</sub> and its correlation with column increases is  
535 needed in order to more clearly distinguish between long-term forcings, notably from the 11-yr  
536 solar cycle, slow changes in halogen source gases, temperature changes, and shorter-term  
537 variability. Continuing, good long-term ozone datasets are clearly needed for such studies.

### 538 **5.1 GOZCARDS ozone source data records**

539 We used ozone datasets from SAGE I, SAGE II, HALOE, UARS MLS, ACE-FTS, and Aura  
540 MLS to generate the monthly zonal mean source products for GOZCARDS. Due to time  
541 constraints, we did not use the newer SAGE II version 7 ozone (see Damadeo et al., 2013) as  
542 part of the GOZCARDS merged dataset. Our studies indicate that there are systematic  
543 differences of only a few percent between SAGE II V6.2 and V7 O<sub>3</sub> on their native coordinates  
544 (number density versus altitude). However, these 2 versions exhibit some differences if the data  
545 are converted to mixing ratios on pressure surfaces. These differences result mainly from  
546 different temperatures (and their trends) between MERRA and analyses from the National  
547 Centers for Environmental Prediction (NCEP), used by SAGE II V7 and V6.2 retrievals,

548 respectively. The main differences between MERRA and NCEP temperatures occur in the upper  
549 stratosphere for time periods before 1989 and after mid-2000 (see further details in Sect. 5.2).

### 550 **5.1.1 Treatment of SAGE ozone profiles**

551 Both SAGE I and SAGE II used solar occultations during satellite sunrise and sunset to measure  
552 vertical profiles of ozone, along with other composition data and aerosol extinction (McCormick  
553 et al., 1989; Cunnold et al., 1989). It takes about 1 month for SAGE I and II to provide near  
554 global coverage (about 80°N to 80°S), with some dependence on season. The SAGE I  
555 measurements started in February 1979 and stopped in November 1981, while SAGE II provided  
556 data between October 1984 and August 2005. In the middle of July 2000, SAGE II had a  
557 problem in its azimuth gimbal system. Although this was corrected by November 2000, the  
558 instrument operation was switched to a 50% duty cycle, with either sunrise or sunset occultations  
559 occurring in monthly alternating periods, until the end of the mission.

560 It is known that there were altitude registration errors in SAGE I (V5.9) data (Veiga et al.,  
561 1995; Wang et al., 1996). To correct this problem, an empirical altitude correction method based  
562 on Wang et al. (1996) had been applied to SAGE I (V5.9) data; these corrected SAGE I V5.9  
563 profiles, which had been evaluated in previous trend studies (e.g. SPARC, 1998; WMO, 2003),  
564 were used to create the GOZCARDS SAGE I product (denoted as version V5.9\_rev). We did not  
565 use reprocessed version 6.1 SAGE I data (L. W. Thomason, personal communication, 2012)  
566 because the altitude registration problems had not been completely fixed and new altitude  
567 correction criteria should be derived and validated.

568 Ozone data screening details for the original SAGE I and SAGE II datasets are provided in  
569 Appendix A. The number density profiles were converted to mixing ratios on pressure levels by  
570 using NCEP temperature and pressure data provided with each profile. Derived ozone profiles  
571 were then interpolated to fixed pressure levels on the following grid:

$$572 \quad p(i) = 1000 \times 10^{-\frac{i}{30}} \text{ (hPa)} \quad i = 0, 1, 2, \dots \quad (2)$$

573 Ozone values at each of the 5 levels centered on every GOZCARDS pressure level were then  
574 averaged (weighted by pressure) to derive mixing ratios at each GOZCARDS pressure level. By  
575 doing this, the SAGE profiles were smoothed to a vertical resolution comparable to that of the

576 other satellite instruments used in this GOZCARDS work. Monthly zonal means were then  
577 computed for the SAGE ozone datasets on the GOZCARDS-compatible grid.

### 578 **5.1.2 Comparisons of ozone zonal means**

579 Ozone differences between SAGE II and other satellite data are shown in Fig. S8. Zonal mean  
580 differences between SAGE II and HALOE are generally within 5% for 1.5 to 68 hPa at mid-  
581 latitudes, and for 1.5 to 46 hPa in the tropics; relative biases are larger outside those ranges and  
582 increase to ~10% near the tropopause and also near 1 hPa. This good level of agreement was  
583 demonstrated in the past (e.g., SPARC, 1998). SAGE II data show better agreement with UARS  
584 and Aura MLS in the upper stratosphere and lower mesosphere, within 5% up to 0.68 hPa and  
585 for latitudes outside the polar regions. Aura MLS O<sub>3</sub> compares better with SAGE II data than  
586 does UARS MLS in the tropics for pressures larger than 68 hPa; the high bias in UARS MLS O<sub>3</sub>  
587 at 100 hPa has been discussed previously (Livesey et al., 2003). There are no months that include  
588 both SAGE II and ACE-FTS data in the northern hemisphere tropics (see the gap in Fig. S8,  
589 bottom right panel), largely due to the poorer coverage from ACE-FTS in the tropics. ACE-FTS  
590 O<sub>3</sub> shows the largest positive bias (greater than 10%) with respect to SAGE II, for pressures less  
591 than 1.5 hPa. The high bias in upper stratospheric ACE-FTS ozone has been mentioned in past  
592 validation work using ACE-FTS data (e.g., Froidevaux et al., 2008b; Dupuy et al., 2009). The  
593 biases shown here are also consistent with recent O<sub>3</sub> intercomparison studies from a  
594 comprehensive array of satellite instruments by Tegtmeier et al. (2013). It has been known for  
595 some time that the HALOE and SAGE II ozone datasets, which govern the main variations of the  
596 GOZCARDS merged ozone values before 2005, agree quite well (within 5%) in absolute value,  
597 and also in terms of temporal trends (Nazaryan et al., 2005), and versus ozonesondes (mostly  
598 above ~20 km or ~50 hPa). Larger percentage differences occur in the lowest region of the  
599 stratosphere at low latitudes, and especially in the upper troposphere, where HALOE values  
600 become significantly smaller than SAGE II data, which are already biased low (by ~50%) versus  
601 sondes (Wang et al., 2002); see also Morris et al. (2002), as well as results of SAGE II and  
602 HALOE comparisons versus solar occultation UV-Visible spectrometer measurements from long  
603 duration balloons (Borchi et al., 2005). We should note here that in this GOZCARDS merging  
604 work, we have largely avoided the upper tropospheric region.

605 Zonal mean differences between SAGE II and Aura MLS show some latitudinal structure  
606 between 1 and 3 hPa, with larger (5-10%) biases in the southern hemisphere, especially for 0 to  
607 30°S (see Fig. S8). There are no such features between SAGE II and HALOE or UARS MLS.  
608 We found that this results from anomalous NCEP temperatures after 2000, which affect SAGE II  
609 data converted from number density/altitude to GOZCARDS VMR/pressure coordinates.  
610 Figure 17 shows an example of the ozone series from SAGE II and other satellite data for 10°S to  
611 20°S from 1 to 6.8 hPa. At 1 hPa, the SAGE II ozone values (converted to mixing ratios) drift  
612 relative to HALOE and are elevated after mid-2000; this can be attributed to abnormal NCEP  
613 temperature trends compared to MERRA and HALOE during the same time period (for detailed  
614 views, see Figs. S9 and S10). Similar features are found down to pressures near 3 hPa. These  
615 issues relating to anomalous upper stratospheric NCEP temperature trends were noted by  
616 McLinden et al. (2009). Because such artifacts are confirmed by using either MERRA or  
617 HALOE temperatures, we decided not to include in the merging process any SAGE II O<sub>3</sub> values  
618 after June 30, 2000 for pressures equal to or less than 3.2 hPa. SAGE II ozone is not significantly  
619 affected by the conversion to mixing ratio/pressure coordinates at 4.6 and 6.8 hPa (Fig. 17).

## 620 **5.2 GOZCARDS ozone merged data records**

### 621 **5.2.1 Methodology for GOZCARDS merged ozone**

622 Ozone measurements from SAGE I, SAGE II, HALOE, UARS MLS, Aura MLS and ACE-FTS,  
623 were used to establish a near-continuous monthly zonal mean record from late 1979 through  
624 2012 for the GOZCARDS merged O<sub>3</sub> product (ESDR version 1.01). The SAGE II dataset was  
625 used as a reference standard, since it has the longest period of measurements and has been  
626 extensively validated. A GOZCARDS ozone merged data record is constructed by combining  
627 these measurements after removing systematic biases with respect to SAGE II. This is done by  
628 applying additive offsets to all other instrument series, as determined from average differences  
629 between monthly zonal means and SAGE II during overlap time periods. The merged data are  
630 then derived by averaging all available adjusted datasets. Because there are gaps in overlap  
631 between SAGE II and ACE-FTS monthly mean data in some latitudes (Fig. S7), and as SAGE II  
632 ozone VMRs obtained from the vertical grid transformation were affected by anomalous NCEP  
633 temperatures after mid-2000 for pressures smaller than or equal to 3.2 hPa, a two-step approach

634 is used to generate the merged product. First, SAGE II data are used as reference for pressures  
635 larger than 3.2 hPa to adjust HALOE, UARS MLS and Aura MLS based on overlapping months  
636 between 1991 and Nov. 2005; see the method overview schematic in Fig. 18. For  $p \leq 3.2$  hPa,  
637 SAGE II O<sub>3</sub> is still used as a reference through June 2000, and HALOE and UARS MLS data are  
638 adjusted accordingly. This eliminates the effect of anomalous NCEP temperatures on SAGE II  
639 ozone and leads to more accurate offsets based on HALOE values, after they have been adjusted  
640 to SAGE II. Adjusted HALOE data (HALOE\* in Fig. 18) are then used as a reference to derive  
641 estimated offsets for Aura MLS O<sub>3</sub>, using the overlap period with HALOE from Aug. 2004 to  
642 Nov. 2005. In step 2, a new reference value is derived by averaging all available data from  
643 SAGE II, HALOE\*, UARS MLS\* and Aura MLS\*. This value is used to adjust ACE-FTS ozone  
644 based on all overlapping months between March 2004 and Nov. 2005. By including Aura MLS  
645 in the dataset created in step 1, we obtain more complete spatial and temporal coverage than  
646 possible with SAGE II and HALOE, and ensure that there are overlapping months between this  
647 combined dataset and ACE-FTS source data. At the end of step 2, the final merged ozone is  
648 derived by averaging the temporary merged dataset from step 1 with the adjusted ACE-FTS data.

### 649 **5.2.2 Further considerations regarding GOZCARDS merged ozone data**

650 Even in the absence of diurnal variations, measurements from occultation sensors can yield  
651 larger sampling errors than those from densely-sampled emission measurements (Toohey et al.,  
652 2013). Diurnal changes in ozone can affect data comparisons and could impact data merging.  
653 Recently, Sakazaki et al. (2013) presented diurnal changes measured by the Superconducting  
654 Submillimeter-Wave Limb-Emission Sounder (SMILES) and Parrish et al. (2014) analyzed  
655 ground-based microwave O<sub>3</sub> profile variations versus local time in conjunction with satellite  
656 data. Ozone diurnal variations range from a few percent in the lower stratosphere to more than  
657 10% in the upper stratosphere and lower mesosphere (see also Ricaud et al., 1996; Haeefele et al.,  
658 2008; Huang et al., 2010). SAGE II and other occultation instruments observe ozone at local  
659 sunrise or sunset, and the retrieved values are generally closer to nighttime values in the upper  
660 stratosphere and mesosphere. To characterize systematic differences between satellite data,  
661 coincident profiles with small differences in space and time are most often used; an example of  
662 mean differences and standard deviations between SAGE II and Aura MLS using both  
663 coincident profile and zonal mean methods is provided in Fig. S11. SAGE II and coincident

664 Aura MLS nighttime O<sub>3</sub> values agree within ~5% between 0.46 and 100 hPa, except in the  
665 tropical lower stratosphere where comparisons are noisier. Differences between zonal mean  
666 SAGE II and Aura MLS data are very close to differences from averaged coincident values,  
667 except for pressures less than 2 hPa, where differences increase from a few to ~10% at 0.3 hPa,  
668 consistent with what one expects from the diurnal cycle. Although zonal mean differences are  
669 likely to be less representative of “true” differences, by combining SAGE II with Aura MLS data  
670 adjusted by zonal mean biases, we provide a series adjusted to the average of sunrise and sunset,  
671 as measured by SAGE II. If Aura MLS data were adjusted by biases obtained using the  
672 coincident method, an upper stratospheric offset of more than several percent and artificial trends  
673 due to such a diurnal cycle effect could be introduced. The use of long-term datasets with  
674 consistent sampling should be an advantage for trend detection, even in a region with diurnal  
675 changes. Also, our avoidance of SAGE II upper stratospheric O<sub>3</sub> after mid-2000 mitigates  
676 potential artifacts arising from changing SAGE II sunrise/sunset sampling patterns over time.

677 Figure 19 displays the average ozone offsets obtained from the biases relative to SAGE II. A  
678 high bias in upper stratospheric ACE-FTS O<sub>3</sub> relative to other datasets is evident from the  
679 negative ACE-FTS offsets (as large as 25%). Most of the other instrument offsets are in the 5-  
680 10% range; lowering O<sub>3</sub> from UARS MLS, HALOE, and Aura MLS in the lower mesosphere is  
681 required to match SAGE II. Sampling differences and data sparseness may be mostly responsible  
682 for larger offsets at high latitudes; in these regions, the merged data are less amenable to long-  
683 term analyses because of data gaps and larger variability (especially prior to 2004).

684 As shown in the Supplement (Fig. S12), we observe strong similarities (e.g., peaks at  
685 midlatitudes near 10 and 1.5 hPa) in the O<sub>3</sub> annual cycle amplitude patterns from SAGE II,  
686 HALOE, ACE-FTS, and Aura MLS over their respective measurement periods. Middle  
687 stratospheric peaks are a result of the annual cycle in oxygen photolysis, whereas temperature  
688 variations drive the annual cycle in the upper stratosphere (Perliski et al., 1989). This sort of  
689 comparison provides some reassurance regarding the consistency of various datasets. Figure 20  
690 provides diagnostics similar to those given for HCl and H<sub>2</sub>O, namely correlation coefficients and  
691 significance ratios for the slopes of the deseasonalized anomaly time series from SAGE II versus  
692 HALOE as well as from ACE-FTS versus Aura MLS (for 1992 through 1999, and 2005 through  
693 2009, respectively). These diagnostic results for ACE-FTS and Aura MLS are of a quality that is



694 comparable to the HALOE/SAGE II results; poorer fits occur mostly at high latitudes and in the  
695 upper stratosphere. Poorer correlations at upper altitude appear largely tied to a decrease in the  
696 amount of valid data in this region (especially at high latitudes), coupled with a relatively small  
697 variability. For regions with poorer agreement between ACE-FTS and Aura MLS, we often see  
698 small variability in the series from Aura MLS but larger changes (scatter) in the ACE-FTS series.  
699 Larger differences in trends between SAGE II and HALOE were noted by Nazaryan et al. (2005)  
700 at low latitudes near 50 km; this is also indicated by our simple linear fits (not shown here) to the  
701 GOZCARDS source datasets from these two instruments and the existence of poorer agreements  
702 in Fig. 20 for the slope of the difference series in that region. The existence of good correlations  
703 in interannual ozone variations between a large number of satellite measurements was discussed  
704 by Tegtmeier et al. (2013). Regarding temporal drifts, Nair et al. (2012) have shown that small  
705 drifts (mostly within about  $\pm 0.5\%/yr$  for the 20-35 km region) exist between most of the datasets  
706 from six ozone lidar sites and coincident HALOE, SAGE II, and Aura MLS measurements;  
707 similar results were obtained by Kirgis et al. (2013). Other recent studies (in particular, by  
708 Hubert et al., 2015) corroborate the very good stability of the datasets used for GOZCARDS,  
709 which relies most heavily on O<sub>3</sub> data from SAGE II and Aura MLS. While we feel justified in  
710 the use of the longer-term time series chosen for GOZCARDS O<sub>3</sub>, data users should still note the  
711 existence of a few regions with poorer correlations or trend agreement (and, therefore, larger  
712 uncertainties) between different satellite ozone datasets, as indicated in Fig. 20. Long-term  
713 merged datasets from GOZCARDS and other sources should undergo continued scrutiny from  
714 the community, as done recently for trends by Tummon et al. (2015) and Harris et al. (2015).  
715 Sample cross-sectional views of two slices through the GOZCARDS merged O<sub>3</sub> field are  
716 provided in the Supplement (Fig. S13). Figure 21 shows estimated systematic errors from our  
717 calculation of the 95% ranges for the monthly mean source data used here, both above and below  
718 the merged values. In this case, as SAGE II is used as a reference dataset, the applied offsets  
719 (Fig. 20) correlate quite well with this plot depicting the ranges about SAGE II values. Minimum  
720 error bars can be slightly lower than 5% for the middle stratosphere at low latitudes, where ozone  
721 values are largest. This view of systematic error bars is consistent with results by Tegtmeier et al.  
722 (2013), based on the larger set of data analyzed for the SPARC Data Initiative. They also found

723 that the regions with lowest errors (scatter) are in the middle stratosphere at low to mid-latitudes,  
724 where most monthly mean satellite data fit within  $\pm 5\%$  of the multi-instrument mean.

### 725 **5.3 GOZCARDS ozone sample results and discussion**

726 Nair et al. (2013) used regression analyses to compare profile trend results from GOZCARDS  
727 merged O<sub>3</sub> at northern midlatitudes versus a combined O<sub>3</sub> dataset from lidar and coincident  
728 satellite data at the Observatoire de Haute Provence (OHP), France. They showed that good  
729 consistency exists for the decreasing ozone time period, from the early 1980s to 1997, and for the  
730 upper stratospheric increase since 1997, but some differences exist in the lower stratosphere  
731 during this second time period, when the GOZCARDS results show a near-zero trend in  
732 comparison to small positive trends from the combined (and more localized) dataset. The above  
733 results for the declining time period agree broadly with earlier work (for the 1979-1997 period)  
734 by Jones et al. (2009). Gebhardt et al. (2014) analyzed ozone profile trends from SCIAMACHY  
735 on ENVISAT, and compared this to trends from Aura MLS, Optical Spectrograph and InfraRed  
736 Imager System (OSIRIS) on the Odin satellite, and sondes; their results include the detection of  
737 localized ozone increases in the mid-stratosphere at low latitudes; see also Bourassa et al. (2014),  
738 who analyzed merged SAGE II and (OSIRIS) observations for 1984-2013, as well as results  
739 from Kyrölä et al. (2013) on combined SAGE II and Global Ozone Monitoring by Occultation of  
740 Stars (GOMOS) records for 1984-2012, and Eckert et al. (2014), who investigated ENVISAT  
741 MIPAS trends for 2002-2012. The shortness of data records since 1997, coupled with relative  
742 variability and potential drifts between various measurements may explain some differences in  
743 recent trend results, notably for the post-1997 period. More comprehensive analyses from the  
744 SI<sup>2</sup>N initiative have focused on an intercomparison of profile changes from a variety of datasets,  
745 including GOZCARDS and other merged records (Tummon et al., 2015; Harris et al., 2015).

746 Here, we investigate ozone column results based on the global GOZCARDS data, given the  
747 work by Ziemke and Chandra (2012), hereafter referenced as ZC12. These authors analyzed total  
748 column and stratospheric column data from satellites, and their analyses yielded a rather strong  
749 near-global (60°S-60°N) average ozone increase since 1998. Their stratospheric columns  
750 depend on the convective-cloud differential (CCD) method and use Total Ozone Mapping  
751 Spectrometer (TOMS) and Ozone Monitoring Instrument (OMI) column data over convective

752 clouds near the tropopause (see also Ziemke et al., 2005). In Fig. 22, we compare changes in  
753 60°S-60°N ZC12 column ozone data (J. Ziemke, personal communication, 2013) to changes in  
754 GOZCARDS O<sub>3</sub> columns above 68 hPa for that region; note that GOZCARDS values do not  
755 provide for a continuous long-term time series down to pressures of 100 hPa or more in the  
756 SAGE I years (1979-1981). To eliminate biases between stratospheric columns as calculated  
757 using the CCD methodology and the GOZCARDS fixed bottom pressure approach, we reference  
758 all stratospheric columns to the 1980 total column value. These column series include SAGE I  
759 data and are linearly interpolated between 1981 and 1984, when no GOZCARDS source datasets  
760 exist. We observe that relative changes in GOZCARDS columns follow the ZC12 curves within  
761 a few DU in the downward phase until about 1992, but the 1992-1997 decrease in total columns  
762 does not compare very well. Some of this discrepancy may occur because total columns capture  
763 a stronger decrease from levels below 68 hPa, not fully represented in GOZCARDS. Focusing on  
764 the late period (from Aura MLS and ACE-FTS), we also show the GOZCARDS columns above  
765 68 hPa, referenced to 2007 instead of 1980. There is a good match in the variations between  
766 GOZCARDS and ZC12 columns during 2005-2010, in agreement with the fact that very good  
767 correlations were obtained by ZC12 between Aura MLS columns and stratospheric column data  
768 from the CCD technique. ZC12 values for stratospheric and total columns are in good agreement,  
769 although the stratospheric values have gaps when not enough data were present for near-global  
770 estimates. The increase in ZC12 data from 1997 to 1998 is not matched very well by  
771 GOZCARDS; this is also true if we remove the 11-yr solar cycle from both datasets (not shown  
772 here), as done by ZC12. We also note that recent analyses by Shepherd et al. (2014), who used a  
773 chemistry-climate model constrained by meteorology to investigate causes of long-term total  
774 column O<sub>3</sub> variations, show a partial return, in 2010, towards 1980 ozone column values, but not  
775 nearly as much as implied by ZC12. We note that long-term halogen source gas reductions that  
776 have occurred since the mid-1990s should only lead to column ozone increases of a few DU  
777 since 1997 (Steinbrecht et al., 2011). It is likely that the discrepancies seen here lie in the various  
778 datasets and their merging; for example, it would be worthwhile to check if homogenized SBUV  
779 column O<sub>3</sub> data show results that are substantially different from those of ZC12. Discrepancies  
780 could also arise from differences in ozone column calculations or coverage, because of different  
781 methodologies, grids or sampling to properly determine near-global results.

## 782 **6 Other GOZCARDS data records**

783 We now briefly mention the N<sub>2</sub>O, HNO<sub>3</sub>, and temperature GOZCARDS records that were part of  
784 the delivery for public dissemination in 2013. For N<sub>2</sub>O and HNO<sub>3</sub>, the somewhat simpler  
785 merging procedure consisted of averaging the source datasets from ACE-FTS and Aura MLS  
786 over the overlap time period (Aug. 2004 through Sep. 2010) to obtain the additive offsets for  
787 each of the two individual records. We then simply used the correspondingly-adjusted and  
788 averaged series to create the merged results; this procedure is the same as we described for the  
789 first step in the HCl (or H<sub>2</sub>O) merging process.

### 790 **6.1 N<sub>2</sub>O**

791 This data set starts in August 2004, when the Aura MLS data record began; the only dataset after  
792 Sep. 2010 is the Aura MLS N<sub>2</sub>O (version 3.3) data record. Because of degradation in the main  
793 target MLS N<sub>2</sub>O band (near 640 GHz) after the first few months of 2013, the N<sub>2</sub>O standard MLS  
794 product is being reprocessed for the whole Aura MLS period using an alternate measurement  
795 band; currently, there are no official GOZCARDS N<sub>2</sub>O data after 2012.

796 Excellent agreement (mostly within 5%) exists between stratospheric ACE-FTS and Aura  
797 MLS N<sub>2</sub>O profiles (see Lambert et al., 2007; Strong et al., 2008; Livesey et al., 2013). Plots  
798 showing the average offsets applied to both MLS and ACE-FTS N<sub>2</sub>O series as a function of  
799 latitude and pressure are provided in Fig. S14. These plots are in agreement (in magnitude and in  
800 sign) with the above-referenced studies; the two datasets yield typical offsets (one half of the  
801 average differences) of less than 5%. Also, very good temporal agreement between these two  
802 time series (for 2004-2010) is illustrated by the quality of the N<sub>2</sub>O diagnostic information  
803 displayed in Fig. S15, showing generally highly correlated fields and insignificant drifts.

804 Figure 23 shows sample contour plots for the N<sub>2</sub>O merged field (2004-2012); as seen from the  
805 bottom panel (100 hPa), wintertime descent brings low N<sub>2</sub>O values down at high latitudes inside  
806 the polar vortices. N<sub>2</sub>O is a conserved tracer in the lower stratosphere and its variations near the  
807 tropopause have implications regarding age of air. Variations in upper stratospheric N<sub>2</sub>O are  
808 clearly affected by seasonal and dynamical effects; this is evident from the striking semi-annual,  
809 annual and QBO-related patterns displayed in Fig. 23 for the 6.8 hPa level (top panel).

## 810 **6.2 HNO<sub>3</sub>**

811 As for N<sub>2</sub>O, we merged the HNO<sub>3</sub> data from ACE-FTS (version 2.2) and Aura MLS (version  
812 3.3) from Aug. 2004 onward, and included only the adjusted MLS dataset after Sep. 2010. The  
813 average offsets applied to MLS and ACE-FTS time series as a function of latitude and pressure  
814 for HNO<sub>3</sub> are provided in Fig. S16. The typical offsets (one half of the average differences) for  
815 HNO<sub>3</sub> are less than ~10% (and less than 0.5 ppbv). Despite somewhat larger percent absolute  
816 differences than for N<sub>2</sub>O between Aura MLS and ACE-FTS HNO<sub>3</sub>, there is very good agreement  
817 as a function of time between these two datasets in the stratosphere. This is illustrated by the  
818 HNO<sub>3</sub> diagnostic information provided in Fig. S17; the poorest correlations are obtained at or  
819 below the tropical tropopause.

820 Comparisons of v3.3 Aura MLS and v2.2 ACE-FTS nitric acid profiles have shown good  
821 agreement (see also Livesey et al., 2013), as the MLS HNO<sub>3</sub> v3.3 values are now generally larger  
822 than in v2.2, for which validation results were provided by Santee et al. (2007). Wolff et al.  
823 (2008) also compared MLS (v2.2) and ACE-FTS (v2.2) coincident profiles, and obtained similar  
824 results; in addition, they demonstrated that very good agreement exists between the HNO<sub>3</sub>  
825 profiles from ACE-FTS and coincident profiles from MIPAS on Envisat. Also, comparisons  
826 between Aura MLS HNO<sub>3</sub> (v3.3) profiles and wintertime HNO<sub>3</sub> profiles retrieved by a Ground-  
827 based Millimeter-wave Spectrometer (GBMS) in Thule, Greenland, during the first 3 months of  
828 2010, 2011, and 2012 show agreement mostly within 10-15% (Fiorucci et al., 2013).

829 Figure 24 (top two panels) displays the HNO<sub>3</sub> fields at 46 hPa from the UARS MLS period  
830 (1991-1997) as well as from the 2004-2013 period, for which a merged GOZCARDS product  
831 was produced, based on Aura MLS and ACE-FTS source datasets. Also shown (bottom two  
832 panels) are time series for 45°N and 32 hPa from both these periods; the bottom right panel  
833 includes the source and merged time series. We have performed additional investigations (not  
834 shown here) which lead us to believe that small upward adjustments to the UARS MLS HNO<sub>3</sub>  
835 values (by about 10%) are needed to better cross-correlate these datasets across the two distinct  
836 time periods; such relative biases are within the expected systematic errors. This is based on a  
837 consideration of ground-based Fourier Transform infrared column HNO<sub>3</sub> data covering the full  
838 time period, as well as past GBMS HNO<sub>3</sub> profile retrievals. Also, Aura MLS and ACE-FTS

839 HNO<sub>3</sub> data match ground-based and other correlative data quite well, and typically better than  
840 the intrinsically poorer quality UARS MLS HNO<sub>3</sub> data. However, obtaining an optimum global  
841 set of adjustments for the UARS MLS nitric acid field will be limited by the number of sites with  
842 such ground-based data as well as by the different vertical resolutions for these datasets versus  
843 MLS. More collaborative work regarding such analyses is needed in order to find the optimum  
844 adjustments to help tie together these two time periods for this species. Although we did not  
845 deliver the UARS MLS HNO<sub>3</sub> source data files for GOZCARDS, we could provide these  
846 monthly zonal mean series upon request, keeping the above caveats in mind.

### 847 **6.3 Temperature**

848 Finally, in terms of the initial set of delivered GOZCARDS products, and for the convenience of  
849 stratospheric composition data users, we have used temperatures (T) from the Modern-Era  
850 Retrospective Analysis for Research and Applications (MERRA) to produce a monthly mean  
851 GOZCARDS temperature data set from 1979 onward. MERRA is a NASA Goddard reanalysis  
852 (Rienecker et al., 2011) for the satellite era using Goddard Earth Observing System Data  
853 Assimilation System version 5 (GEOS-5); T is from the DAS 3d analyzed state MAI6NVANA,  
854 version 5.2 files (such as MERRA300.prod.assim.inst6\_3d\_ana\_Nv.20110227.hdf). Data from  
855 four daily MERRA files (for 00, 06, 12, and 18 hr UT) were averaged to provide daily mean  
856 temperature fields (appropriate for a mean time of 09 hr). Vertical interpolation was performed  
857 onto the GOZCARDS pressure grid, which, for temperature, covers 30 pressures levels from  
858 1000 hPa to 0.0147 hPa. Averaged values were stored for the 10° GOZCARDS latitude bins, and  
859 daily results were binned to create the GOZCARDS monthly temperature data set (version 1.0).

## 860 **7 Summary and conclusions**

861 We have reviewed the GOZCARDS project's production of merged data records of stratospheric  
862 composition, mainly for HCl, H<sub>2</sub>O, and O<sub>3</sub>, using carefully screened satellite data, starting in  
863 1979 with SAGE I and continuing through Aura MLS and ACE-FTS data periods. The source  
864 data have a high degree of maturity and we have reinforced our confidence in their usefulness  
865 through investigations of various diagnostics (offsets, annual cycles, correlations and trend  
866 differences of deseasonalized series). These records are publicly available as GOZCARDS  
867 ESDR version 1.01 and can be referenced using DOI numbers (Froidevaux et al., 2013b,

868 Anderson et al., 2013, and Wang et al., 2013, for the above species, respectively). The other  
869 GOZCARDS data records also have references, namely Schwartz et al. (2013) for the MERRA-  
870 based temperature records, and Froidevaux et al. (2013c, 2013d) for N<sub>2</sub>O and HNO<sub>3</sub>,  
871 respectively. Table 2 provides a summary of the GOZCARDS monthly mean datasets. Yearly  
872 netCDF files are available for public access (<http://mirador.gsfc.nasa.gov>). The merging  
873 methodology follows from a determination of mean biases (for each pressure level and 10°  
874 latitude bin) between monthly mean series, based on the overlap periods. For ozone, SAGE II  
875 data are the chosen reference, whereas for other species, the merging basis is equivalent to an  
876 average of the datasets during the periods of overlap. The merged data files contain the average  
877 offset values applied to each source data time series, along with standard deviations and standard  
878 errors. The GOZCARDS README document (Froidevaux et al., 2013a) provides more details  
879 about data file quantities, including local time and solar zenith angle information, and a list of  
880 days with available data. We also display here estimated systematic errors about the merged  
881 values; we find that mixing ratio errors are typically within 5% to 15% and are consistent with  
882 the magnitude of observed relative biases.

883 The GOZCARDS HCl merged record in the upper stratosphere enables long-term tracking of  
884 changes in total stratospheric chlorine. The long-term increase in HCl prior to the late 1990s, and  
885 the subsequent gentler decrease in the 21st century, are delayed manifestations of changes in the  
886 sum of the surface source gas abundances as a result of regulations from the Montreal Protocol  
887 and its amendments. From 1997 to 2010, the average rate of change in upper stratospheric HCl  
888 (50°S to 50°N) was about -0.4 to -0.7%/yr (with the smaller rates of decrease after 2003). In the  
889 lower stratosphere, where Aura MLS data are weighted heavily, recent short-term variations  
890 have shown a flattening out and, in particular for northern midlatitudes and at 50-70 hPa for the  
891 deep tropics, a significant reversal and increasing trend (see also Mahieu et al., 2014), compared  
892 to the decrease from the late 1990s to about 2004. However, lower stratospheric HCl tendencies  
893 appear to be reversing again in recent years (2011-2014), with decreases at northern  
894 midlatitudes and some increasing tendencies at southern midlatitudes. In the future, we expect to  
895 see long-term global HCl decreases in both the upper and lower stratosphere.

896 For water vapor, we have used data from the same instruments as for HCl, with the same  
897 methodology, except for the addition of 1991-1993 UARS MLS data. The H<sub>2</sub>O data record

898 shows large mesospheric variations that are anti-correlated with the solar flux over the past two  
899 11-yr solar cycles. Net long-term trends in lower stratospheric H<sub>2</sub>O are quite small if one  
900 considers the past 22 years, but there has been considerable interannual variability, including the  
901 steep drop from 2000 to 2001, as mentioned in past work. While H<sub>2</sub>O tendencies have been  
902 generally positive after 2001, the 68 and 100 hPa levels show some steep decreases (by 0.5-0.8  
903 ppmv) from 2011 to 2013 (see also Urban et al., 2014). Over the past 22 years, long-term global  
904 H<sub>2</sub>O increases of order 10% are observed in the upper stratosphere and lower mesosphere,  
905 whereas a decrease of nearly 10% has occurred in the lower stratosphere (near 70-100 hPa).  
906 However, there is no regular monotonic change on decadal timescales, especially in the tropical  
907 lower stratosphere, where fairly sharp decreases followed by steadier increases may be a  
908 recurrent pattern (see also Fueglistaler, 2012); this complicates the detection of any small  
909 underlying trend. As one might expect from the well-documented temperature influence on the  
910 tropical lower stratosphere, H<sub>2</sub>O variability (based on maximum minus minimum yearly  
911 averages) is largest in the tropics and just above the tropopause. More accurate studies of  
912 seasonal to decadal water vapor variability will be enabled by continuing such merged H<sub>2</sub>O  
913 datasets in the future. A reduction in model spread for stratospheric H<sub>2</sub>O is likely easier to  
914 achieve than tighter upper tropospheric model results; for the upper troposphere, see the  
915 data/model comparisons (H<sub>2</sub>O and ice water content) by Jiang et al. (2012).

916 For ozone, we have used measurements from SAGE I, SAGE II, HALOE, UARS MLS, Aura  
917 MLS and ACE-FTS to produce a merged record starting in 1979, after adjusting the series to  
918 SAGE II. We observed temporal drifts in the SAGE II series, after conversion to the  
919 GOZCARDS mixing ratio/pressure grid, as a result of the NCEP temperature data used in this  
920 conversion, mostly in the upper stratosphere after June 2000 (see also McLinden et al., 2009). To  
921 mitigate this issue, we used HALOE upper stratospheric O<sub>3</sub> as a reference for July 2000 to  
922 November 2005, after adjusting the HALOE series to SAGE II. The resulting GOZCARDS  
923 merged O<sub>3</sub> data for northern midlatitudes have been used in regression analyses (Nair et al.,  
924 2013) to reveal decreases in the whole stratosphere for 1984-1996. Nair et al. (2015) extended  
925 this work and found increasing trends in upper stratospheric GOZCARDS O<sub>3</sub> since 1997, but no  
926 significant positive trends in the lower stratosphere. Other studies of GOZCARDS O<sub>3</sub> profile  
927 trends have been discussed as part of the WMO (2014) and SI<sup>2</sup>N assessments (Tummon et al.,



928 2015; Harris et al., 2015). Here, we looked at the consistency of column data between  
929 stratospheric GOZCARDS O<sub>3</sub> and work by Ziemke and Chandra (2012), who noted that a fairly  
930 rapid change (“recovery”) in near-global ozone columns from TOMS and OMI could be inferred  
931 since the mid-1990s. We show that the similarly analyzed GOZCARDS column data does not  
932 show an upturn of more than 0.5-1% since that period. Reasons for these differences could  
933 include data coverage or merging-related issues in either dataset, or inaccuracies in globally-  
934 averaged stratospheric columns. A recent global total ozone study (Shepherd et al., 2014) also  
935 points to less of a return towards 1980 levels than implied by ZC12.

936 We also briefly described the creation of N<sub>2</sub>O and HNO<sub>3</sub> GOZCARDS data records, based on  
937 Aura MLS and ACE-FTS. The agreement between these two instruments’ datasets for these  
938 species was shown to be generally very good. For HNO<sub>3</sub>, UARS MLS HNO<sub>3</sub> source datasets in  
939 the GOZCARDS format are available from the authors. However, a small upward adjustment (of  
940 order 10%) to the UARS MLS values is likely needed based on our preliminary work comparing  
941 these series to HNO<sub>3</sub> column results from FTIR measurements. More detailed work should help  
942 determine if global adjustments can indeed be made to UARS MLS HNO<sub>3</sub> data; lacking this, one  
943 should ensure that error bars reflect likely biases that can affect the continuity between HNO<sub>3</sub>  
944 datasets before and after 2000, given the multi-year gap in satellite coverage for this species.

945 **There is a Supplement related to this article.**

946 *Acknowledgements.* Work at JPL was performed under contract with the National Aeronautics  
947 and Space Administration (NASA). We dedicate this work to the memory of Professor Derek  
948 Cunnold (Georgia Institute of Technology) who was a member of the original NASA  
949 MEaSURES (Making Earth System Data Records for Use in Research Environments)  
950 GOZCARDS proposal. The GOZCARDS data generation could not have been possible without  
951 the past work from instrument teams for SAGE I, SAGE II, HALOE, UARS MLS, Aura MLS,  
952 and ACE-FTS, and related data usage documentation. At JPL, we thank Joe Waters for his  
953 leadership role in making MLS instruments and datasets possible and Bill Read for his key role;  
954 thanks to Vince Perun for MERRA-related work, and to Brian Knosp and Robert Thurstans for  
955 database and computer management assistance. We also thank Kaley Walker and Ashley Jones  
956 for comments regarding ACE-FTS data, Gloria Manney and William Daffer for help in making

957 the original ACE-FTS data profiles available, and Joe Zawodny and Larry Thomason for their  
958 contributions and comments regarding SAGE data. We acknowledge the work of the GMAO  
959 team responsible for MERRA data used to generate the GOZCARDS temperatures, specifically,  
960 Steven Pawson and Jianjun Jin for discussions and cross-checks regarding temperature data. We  
961 acknowledge Jerry Ziemke for the ozone column data (from Ziemke and Chandra, 2012), and  
962 Sean Davis for discussions on data usage and screening, and the creation of long-term series. For  
963 early HNO<sub>3</sub>-related work connecting ground-based data to MLS datasets, we thank Giovanni  
964 Muscari and Irene Fiorucci. We are thankful for the NOAA Earth System Research Laboratory  
965 (ESRL) Global Monitoring Division (GMD) website information and data on total surface  
966 chlorine. We obtained solar flux data for the Ottawa/Penticton sites from the NOAA National  
967 Geophysical Data Center (NGDC) website ([www.ngdc.noaa.gov](http://www.ngdc.noaa.gov)), for which we also  
968 acknowledge the National Research Council of Canada.

969 **References**

970

971 Anderson, J. G., Brune, W. H., and Proffitt, M. H.: Ozone destruction by chlorine radicals within the  
972 Antarctic vortex: The spatial and temporal evolution of ClO–O<sub>3</sub> anticorrelation based on in situ ER-2  
973 data, *J. Geophys. Res.*, 94, 11,465-11,479, 1989.

974 Anderson, J., Russell, J. M., Solomon, S., and Deaver, L. E.: HALOE confirmation of stratospheric  
975 chlorine decreases in accordance with the Montreal Protocol, *J. Geophys. Res.*, 105, 4483-4490, 2000.

976 Anderson, J., Froidevaux, L., Fuller, R. A., Bernath, P. F., Livesey, N. J., Pumphrey, H. C., Read, W. G.,  
977 and Walker, K. A.: GOZCARDS Merged Data for Water Vapor Monthly Zonal Means on a Geodetic  
978 Latitude and Pressure Grid, version 1.01, Greenbelt, MD, USA: NASA Goddard Earth Science Data and  
979 Information Services Center, accessible from doi:10.5067/MEASURES/GOZCARDS/DATA3003, 2013.

980 Barath, F., Chavez, M. C., Cofield, R. E., Flower, D. A., Frerking, M. A., Gram, M. B.,  
981 Harris, W. M., Holden, J. R., Jarnot, R. F., Kloezeman, W. G., Klose, G. J., Lau, G. K.,  
982 Loo, M. S., Maddison, B. J., Mattauch, R. J., McKinney, R. P., Peckham, G. E., Pickett, H. M., Siebes,  
983 G., Soltis, F. S., Suttie, R. A., Tarsala, J. A., Waters, J. W., and Wilson, W. J.: The Upper Atmosphere  
984 Research Satellite Microwave Limb Sounder Experiment, *J. Geophys. Res.*, 98, 10751-10762, 1993.

985 Bernath, P. F., McElroy, C. T., Abrams, M. C., Boone, D., Butler, M., Camy-Peyret, C.,  
986 Carleer, M., Clerbaux, C., Coheur, P.-F., Colin, R., DeCola, P., DeMaziere, M., Drummond, J. R.,  
987 Dufour, D., Evans, W. F. J., Fast, H., Fussen, D., Gilbert, K., Jennings, D. E., Llewellyn, E. J., Lowe, R.  
988 P., Mahieu, E., McConnell, J. C., McHugh, M., McLeod, S. D., Michaud, R., Midwinter, C., Nassar, R.,  
989 Nichitiu, F., Nowlan, C., Rinsland, C. P., Rochon, Y. J., Rowlands, N., Semeniuk, K., Simon, P., Skelton,  
990 R., Sloan, J. J., Soucy, M.-A., Strong, K., Tremblay, P., Turnbull, D., Walker, K. A., Walkty, I., Wardle,  
991 D. A., Wehrle, V., Zander, R., and Zou, J.: Atmospheric Chemistry Experiment (ACE): Mission  
992 overview, *Geophys. Res. Lett.*, 32, L15S01, doi:10.1029/2005GL022386, 2005.

993 Bhatt, P. P., Remsberg, E. E., Gordley, L. L., McInerney, J. M., Brackett, V. G., and  
994 Russell, III, J. M.: An evaluation of the quality of Halogen Occultation Experiment ozone profiles in the  
995 lower stratosphere, *J. Geophys. Res.*, 104 (D8), 9261-9275, 1999.

996 Borchi, F., Pommereau, J.-P., Garnier, A., and Pinharanda, M.: Evaluation of SHADOZ sondes, HALOE  
997 and SAGE II ozone profiles at the tropics from SAOZ UV-Vis remote measurements onboard long  
998 duration balloons, *Atmos. Chem. Phys.*, 5, 1381-1397, 2005.

999 Bourassa, A. E., Degenstein, D. A., Randel, W. J., Zawodny, J. M., Kyrölä, E., McLinden, C. A., Sioris,  
1000 C. E., and Roth, C. Z., Trends in stratospheric ozone derived from merged SAGE II and Odin-OSIRIS  
1001 satellite observations, *Atmos. Chem. Phys.*, 14, 6983-6994, doi:10.5194/acp-14-6983-2014, 2014.

1002 Brown, A. T., Chipperfield, M. P., Boone, C., Wilson, C., Walker, K. A., and Bernath, P.: Trends in  
1003 atmospheric halogen containing gases since 2004, *J. Quant. Spec. Rad. Trans.*, 112, 2552-2566, 2011.

1004 Chandra, S., Jackman, C. H., Fleming, E. L., and Russell, J. M.: The seasonal and long term changes in  
1005 mesospheric water vapor, *Geophys. Res. Lett.*, 24, No. 6, 639-642, 1997.

1006 Chu, W. P., and McCormick, M. P.: Inversion of Stratospheric Aerosol and Gaseous Constituents From  
1007 Spacecraft Solar Extinction Data in the 0.38-1.0  $\mu\text{m}$  Wavelength Region, *Appl. Opt.*, 18, No. 9, 1404-  
1008 1413, 1979.

1009 Cunnold, D. M., Chu, W. P., Barnes, R. A., McCormick, M. P., and Veiga, R. E.: Validation of SAGE II  
1010 ozone measurements, *J. Geophys. Res.*, 94, 8447-8460, 1989.

1011 Damadeo, R. P., Zawodny, J. M., Thomason, L. W., and Iyer, N.: SAGE version 7.0 algorithm:  
1012 application to SAGE II, *Atmos. Meas. Tech.*, 6, 3539-3561, doi:10.5194/amt-6-3539-2013, 2013.

1013 Dupuy, E., Walker, K. A., Kar, J., Boone, C. D., McElroy, C. T., Bernath, P. F.,  
1014 Drummond, J. R., Skelton, R., McLeod, S. D., Hughes, R. C., Nowlan, C. R., Dufour, D. G., Zou, J.,  
1015 Nichitiu, F., Strong, K., Baron, P., Bevilacqua, R. M., Blumenstock, T., Bodeker, G. E., Borsdorff, T.,  
1016 Bourassa, A. E., Bovensmann, H., Boyd, I. S., Bracher, A., Brogniez, C., Burrows, J. P., Catoire, V.,  
1017 Ceccherini, S., Chabrillat, S., Christensen, T., Coffey, M. T., Cortesi, U., Davies, J., De Clercq, C.,  
1018 Degenstein, D. A., De Maziere, M., Demoulin, P., Dodion, J., Firanski, B., Fischer, H., Forbes, G.,  
1019 Froidevaux, L., Fussen, D., Gerard, P., Godin-Beekmann, S., Goutail, F., Granville, J., Griffith, D.,  
1020 Haley, C. S., Hannigan, J. W., Hopfner, M., Jin, J. J., Jones, A., Jones, N. B., Jucks, K., Kagawa, A.,  
1021 Kasai, Y., Kerzenmacher, T. E., Kleinbohl, A., Klekociuk, A. R., Kramer, I., Kullmann, H.,  
1022 Kuttippurath, J., Kyrölä, E., Lambert, J.-C., Livesey, N. J., Llewellyn, E. J., Lloyd, N. D., Mahieu, E.,  
1023 Manney, G. L., Marshall, B. T., McConnell, J. C., McCormick, M. P., McDermid, I. S., McHugh, M.,  
1024 McLinden, C. A., Mellqvist, J., Mizutani, K., Murayama, Y., Murtagh, D. P., Oelhaf, H., Parrish, A.,  
1025 Petelina, S. V., Piccolo, C., Pommereau, J.-P., Randall, C. E., Robert, C., Roth, C., Schneider, M., Senten,  
1026 C., Steck, T., Strandberg, A., Strawbridge, K. B., Sussmann, R., Swart, D. P. J., Tarasick, D. W., Taylor,  
1027 J. R., Tetard, C., Thomason, L. W., Thompson, A. M., Tully, M. B., Urban, J., Vanhellefont, F.,

1028 Vigouroux, C., von Clarmann, T., von der Gathen, P., von Savigny, C., Waters, J. W., Witte, J. C., Wolff,  
1029 M., and Zawodny, J. M.: Validation of ozone measurements from the Atmospheric Chemistry Experiment  
1030 (ACE), *Atmos. Chem. Phys.*, 9, 287–343, doi:10.5194/acp-9-287-2009, 2009.

1031 Eckert, E., von Clarmann, T., Kiefer, M., Stiller, G. P., Lossow, S., Glatthor, N., Degenstein, D. A.,  
1032 Froidevaux, L., Godin-Beekmann, S., Leblanc, T., McDermid, S., Pastel, M., Steinbrecht, W., Swart, D.  
1033 P. J., Walker, K. A., and Bernath, P. F.: Drif-corrected trends and periodic variations in MIPAS IMK/IAA  
1034 ozone measurements, *Atmos. Chem. Phys.*, 14, 2571-2589, doi:10.5194/acp-14-2571-2014, 2014.

1035 Engel, A., Strunk, M., Muller, M., Haase, H.-P., Poss, C., Levin, I., and Schmidt, U.: The temporal  
1036 development of total chlorine in the high latitude stratosphere based on reference distributions of mean  
1037 age derived from CO<sub>2</sub> and SF<sub>6</sub>, *J. Geophys. Res.*, 107, 4136, doi:10.1029/2001JD000584, 2002.

1038 Farman, J. C., Gardiner, B. G., and Shanklin, J. D.: Large losses of total ozone in Antarctica reveal  
1039 seasonal ClO<sub>x</sub>/NO<sub>x</sub> interaction, *Nature*, 315, 207-210, 1985.

1040 Fiorucci, I., Muscari, G., Froidevaux, L., and Santee, M. L.: Ground-based stratospheric O<sub>3</sub> and HNO<sub>3</sub>  
1041 measurements at Thule, Greenland: an intercomparison with Aura MLS observations, *Atmos. Meas.*  
1042 *Tech.*, 6, 2441–2453, doi:10.5194/amt-6-2441-2013, 2013.

1043 Frith, S. M., Kramarova, N. A., Stolarski, R. S., McPeters, R. D., Bhartia, P. K., and Labow, G. J.: Recent  
1044 changes in total column ozone based on the SBUV Version 8.6 Merged Ozone Data Set, *J. Geophys.*  
1045 *Res.*, 119, 9735-9751, doi:10.1029/2014JD021889, 2014.

1046 Froidevaux, L., Livesey, N. J., Read, W. G., Salawitch, R. J., Waters, J. W., Drouin, B., MacKenzie, I. A.,  
1047 Pumphrey, H. C., Bernath, P., Boone, C., Nassar, R., Montzka, S., Elkins, J., Cunnold, D., and  
1048 Waugh, D.: Temporal decrease in upper atmospheric chlorine, *Geophys. Res. Lett.*, 33, L23813,  
1049 doi:10.1029/2006GL027600, 2006.

1050 Froidevaux, L., Jiang, Y. B., Lambert, A., Livesey, N. J., Read, W. G., Waters, J. W., Fuller, R. A.,  
1051 Marcy, T. P., Popp, P. J., Gao, R. S., Fahey, D. W., Jucks, K. W., Stachnik, R. A., Toon, G. C.,  
1052 Christensen, L. E., Webster, C. R., Bernath, P. F., Boone, C. D., Walker, K. A., Pumphrey, H. C.,  
1053 Harwood, R. S., Manney, G. L., Schwartz, M. J., Daffer, W. H., Drouin, B. J., Cofield, R. E., Cuddy, D. T.,  
1054 Jarnot, R. F., Knosp, B. W., Perun, V. S., Snyder, W. V., Stek, P. C., Thurstans, R. P., and Wagner, P. A.:  
1055 Validation of Aura Microwave Limb Sounder HCl measurements, *J. Geophys. Res.*, 113,  
1056 doi:10.1029/2007JD009025, D15S25, 2008a.

1057 Froidevaux, L., Jiang, Y. B., Lambert, A., Livesey, N. J., Read, W. G., Waters, J. W.,  
1058 Browell, E. V., Hair, J. W., Avery, M. A., McGee, T. J., Twigg, L. W., Sumnicht, G. K., Jucks, K. W.,  
1059 Margitan, J. J., Sen, B., Stachnik, R. A., Toon, G. C., Bernath, P. F., Boone, C. D., Walker, K. A.,  
1060 Filipiak, M. J., Harwood, R. S., Fuller, R. A., Manney, G. L., Schwartz, M. J., Daffer, W. H., Drouin, B. J.,  
1061 Cofield, R. E., Cuddy, D. T., Jarnot, R. F., Knosp, B. W., Perun, V. S., Snyder, W. V., Stek, P. C.,  
1062 Thurstans, R. P., and Wagner, P. A.: Validation of Aura Microwave Limb Sounder stratospheric and  
1063 mesospheric ozone measurements, *J. Geophys. Res.*, 113, doi:10.1029/2007JD008771, D15S20, 2008b.  
1064

1065 Froidevaux, L., Fuller, R., Schwartz, M., Anderson, J., and Wang, R.: README Document for the  
1066 Global OZoneChemistry And Related trace gas Data records for the Stratosphere (GOZCARDS) project,  
1067 Goddard Earth Sciences Data and Information Services Center (GES DISC), <http://disc.gsfc.nasa.gov>,  
1068 NASA Goddard Space Flight Center, Code 610.2, Greenbelt, MD 20771 USA, 2013a.

1069 Froidevaux, L., Anderson, J., Fuller, R. A., Bernath, P. F., Livesey, N. J., Russell III, J. M., and  
1070 Walker, K.A.: GOZCARDS Merged Data for Hydrogen Chloride Monthly Zonal Means on a Geodetic  
1071 Latitude and Pressure Grid, version 1.01, Greenbelt, MD, USA: NASA Goddard Earth Science Data and  
1072 Information Services Center, accessible from doi:10.5067/MEASURES/GOZCARDS/DATA3002,  
1073 2013b.

1074 Froidevaux, L., Fuller, R. A., Lambert, A., Livesey, N. J., Bernath, P. F., Livesey, N. J., and Walker,  
1075 K.A.: GOZCARDS Merged Data for Nitrous Oxide Monthly Zonal Means on a Geodetic Latitude and  
1076 Pressure Grid, version 1.01, Greenbelt, MD, USA: NASA Goddard Earth Science Data and Information  
1077 Services Center, accessible from doi:10.5067/MEASURES/GOZCARDS/DATA3013, 2013c.

1078 Froidevaux, L., Fuller, R. A., Santee, M. L., Manney, G. L., Livesey, N. J., Bernath, P. F., and Walker,  
1079 K.A.: GOZCARDS Merged Data for Nitric Acid Monthly Zonal Means on a Geodetic Latitude and  
1080 Pressure Grid, version 1.01, Greenbelt, MD, USA: NASA Goddard  
1081 Earth Science Data and Information Services Center, accessible from  
1082 doi:10.5067/MEASURES/GOZCARDS/DATA3008, 2013d.

1083 Fueglistaler, S.: Step-wise changes in stratospheric water vapor? *J. Geophys. Res.*, 117, D13302,  
1084 doi:10.1029/2012JD017582, 2012.

1085 Gebhardt, C., Rozanov, A., Hommel, R., Weber, M., Bovensmann, H., Burrows, J. P., Degenstein, D.,  
1086 Froidevaux, L., and Thompson, A. M.: Stratospheric ozone trends and variability as seen by

1087 SCIAMACHY from 2002 to 2012, *Atmos. Chem. Phys.*, 14, 831–846, doi:10.5194/acp-14-831-2014,  
1088 2014.

1089

1090 Haefele, A., Hocke, K., Kampfer, N., Keckhut, P., Marchand, M., Bekki, S., Morel, B.,  
1091 Egorova, T., and Rozanov, E.: Diurnal changes in middle atmospheric H<sub>2</sub>O and O<sub>3</sub>: Observations in the  
1092 Alpine region and climate models, *J. Geophys. Res.*, 113, D17303, doi:10.1029/2008JD009892, 2008.

1093 Harris, N. R. P., et al., Past changes in the Vertical Distribution of Ozone, Part III: Analysis and  
1094 interpretation of trends, *Atmos. Chem. Phys.*, in press, 2015.

1095 Hassler, B., Bodeker, G. E., Solomon, S., and Young, P. J.: Changes in the polar vortex: Effects on  
1096 Antarctic total ozone observations at various stations, *Geophys. Res. Lett.*, 38, L01805,  
1097 doi:10.1029/2010GL045542, 2011.

1098 Hegglin, M. I., Tegtmeier, S., Anderson, J., Froidevaux, L., Fuller, R., Funke, B., Jones, A., Lingenfelter,  
1099 G., Lumpe, J., Pendlebury, D., Remsberg, E., Rozanov, A., Toohey, M., Urban, J., von Clarmann, T.,  
1100 Walker, K. A., Wang, R., and Weigel, K.: SPARC Data Initiative: Comparison of water vapor  
1101 climatologies from international satellite limb sounders, *J. Geophys. Res. Atmos.*, 118, 11,824–11,846,  
1102 doi: 10.1002/jgrd.50752, 2013.

1103 Hervig, M., and McHugh, M.: Cirrus detection using HALOE measurements, *Geophys. Res. Lett.*, 26,  
1104 No. 6, 719-722, 1999.

1105 Huang, F. T., Mayr, H. G., Russell III, J. M., and Mlynczak, M. G.: Ozone diurnal variations in the  
1106 stratosphere and lower mesosphere, based on measurements from SABER on TIMED,  
1107 *J. Geophys. Res.*, 115, D24308, doi:10.1029/2010JD014484, 2010.

1108 Hubert, D., et al., Ground-based assesment of the bias and long-term stability of fourteen limb and  
1109 occultation ozone profile data records, *Atmos. Meas. Tech.*, in review, 2015.

1110 Hurst, D. F., Lambert, A., Read, W. G., Davis, S. M., Rosenlof, K. H., Hall, E. G., Jordan, A. F., and  
1111 Oltmans, S. J.: Validation of Aura Microwave Limb Sounder stratospheric water vapor measurements by  
1112 the NOAA frost point hygrometer, *J. Geophys. Res. Atmos.*, 119, 1612-1625,  
1113 doi:10.1002/2013JD020757, 2014.

1114 Jiang, J. H., Su, H., Zhai, C., Perun, V. S., Del Genio, A., Nazarenko, L. S., Donner, L. J., Horowitz, L.,  
1115 Seman, C., Cole, J., Gettelman, A., Ringer, M. A., Rotstayn, L., Jeffrey, S., Wu, T., Brient, F., Dufresne,

1116 J.-L., Kawai, H., Koshiro, T., Watanabe, M., L'Écuyer, T. S., Volodin, E. M., Iversen, T., Drange, H.,  
1117 Mesquita, M. D. S., Read, W. G., Waters, J. W., Tian, B., Teixeira, J., and Stephens, G. L.: Evaluation of  
1118 cloud and water vapor simulations in CMIP5 climate models using NASA "A-Train" satellite  
1119 observations, *J. Geophys. Res.*, 117, D14105, doi:10.1029/2011JD017237, 2012.

1120 Jones, A., Urban, J., Murtagh, D. P., Eriksson, P., Brohede, S., Haley, C., Degenstein, D., Bourassa, A.,  
1121 von. Savigny, C., Sonkaew, T., Rozanov, A., Bovensmann, H., and Burrows, J.: Evolution of  
1122 stratospheric ozone and water vapour time series studied with satellite measurements, *Atmos. Chem.*  
1123 *Phys.*, 9, 6055-6075, doi:10.5194/acp-9-6055-2009, 2009.

1124 Jones, A., Urban, J., Murtagh, D. P., Sanchez, C., Walker, K. A., Livesey, N. J., Froidevaux, L., and  
1125 Santee, M. L.: Analysis of HCl and ClO time series in the upper stratosphere using satellite data sets,  
1126 *Atmos. Chem. Phys.*, 11, 5321-5333, doi:10.5194/acp-11-5321-2011, 2011.

1127 Kirgis, G., Leblanc, T., McDermid, I. S., and Walsh, T. D.: Stratospheric ozone interannual variability  
1128 (1995–2011) as observed by Lidar and Satellite at Mauna Loa Observatory, HI and Table Mountain  
1129 Facility, CA, *Atmos. Chem. Phys.*, 13, 5033–5047, doi:10.5194/acp-13-5033-2013, 2013.

1130

1131 Kley, D., Stone, E. J., Henderson, W. R., Drummond, J. W., Harrop, W. J., Schmeltekopf, A. L.,  
1132 Thompson, T. L., and Winkler, R. H.: In Situ Measurements of the Mixing Ratio of Water Vapor in the  
1133 Stratosphere, *J. Atmos. Sci.*, 36, 2513-2524, 1979.

1134

1135 Kohlhepp, R., Ruhnke, R., Chipperfield, M. P., De Maziere M., Notholt, J., Barthlott, S., Batchelor, R. L.,  
1136 Blatherwick, R. D., Blumenstock, T., Coffey, M. T., Demoulin, P., Fast, H., Feng, W., Goldman, A.,  
1137 Griffith, D. W. T., Hamann, K., Hannigan, J. W., Hase, F., Jones, N. B., Kagawa, A., Kaiser, I., Kasai, Y.,  
1138 Kirner, O., Kouker, W., Lindenmaier, R., Mahieu, E., Mittermeier, R. L., Monge-Sanz, B., Morino, I.,  
1139 Murata, I., Nakajima, H., Palm, M., Paton-Walsh, C., Raffalski, U., Reddmann, T., Rettinger, M.,  
1140 Rinsland, C. P., Rozanov, E., Schneider, M., Senten, C., Servais, C., Sinnhuber, B.-M., Smale, D., Strong,  
1141 K., Sussmann, R., Taylor, J. R., Vanhaelewyn, G., Warneke, T., Whaley, C., Wiehle, M., and Wood, S.  
1142 W.: Observed and simulated time evolution of HCl, ClONO<sub>2</sub>, and HF total column abundances, *Atmos.*  
1143 *Chem. Phys.*, 12, 3527–3557, doi:10.5194/acp-12-3527-2012, 2012.

1144



1145 Kuttippurath, J., Lefevre, F., Pommereau, J.-P., Roscoe, H. K., Goutail, F., Pazmino, A., and Shanklin, J.  
1146 D.: Antarctic ozone loss in 1979–2010: first sign of ozone recovery, *Atmos. Chem. Phys.*, 13, 1625–1635,  
1147 doi:10.5194/acp-13-1625-2013, 2013.

1148 Kyrölä, E., Laine, M., Sofieva, V., Tamminen, J., Päivärinta, S.-M., Tukiainen, S., Zawodny, J., and  
1149 Thomason, L.: Combined SAGE II-GOMOS ozone profile data set for 1984-2011 and trend analysis of  
1150 the vertical distribution of ozone, *Atmos. Chem. Phys.*, 13, 10,645-10,658, doi:10.5194/acp-13-10645-  
1151 2013, 2013.

1152 Lambert, A., Read, W. G., Livesey, N. J., Santee, M. L., Manney, G. L., Froidevaux, L.,  
1153 Wu, D. L., Schwartz, M. J., Pumphrey, H. C., Jimenez, C., Nedoluha, G. E., Cofield, R. E., Cuddy, D. T.,  
1154 Daffer, W. H., Drouin, B. J., Fuller, R. A., Jarnot, R. F., Knosp, B. W., Pickett, H. M., Perun, V. S.,  
1155 Snyder, W. V., Stek, P. C., Thurstans, R. P., Wagner, P. A., Waters, J. W., Jucks, K. W., Toon, G. C.,  
1156 Stachnik, R. A., Bernath, P. F., Boone, C. D., Walker, K. A., Urban, J., Murtagh, D., Elkins, J. W., and  
1157 Atlas, E.: Validation of the Aura Microwave Limb Sounder stratospheric water vapour and nitrous oxide  
1158 measurements, *J. Geophys. Res.*, 112, D24S36, doi:10.1029/2007JD008724, 2007.

1159 Livesey, N. J., Read, W. J., Froidevaux, L., Waters, J. W., Santee, M. L., Pumphrey, H. C., Wu, D. L.,  
1160 Shippony, Z., and Jarnot, R. F.: The UARS Microwave Limb Sounder version 5 dataset: Theory,  
1161 characterization and validation, *J. Geophys. Res.*, 108 (D13), 4378, doi:10.1029/2002JD002273, 2003.

1162 Livesey, N. J., Read, W. G., Froidevaux, L., Lambert, A., Manney, G. L., Pumphrey, H. C., Santee, M.  
1163 L., Schwartz, M. J., Wang, S., Cofield, R. E., Cuddy, D. T., Fuller, R. A., Jarnot, R. F., Jiang, J. H.,  
1164 Knosp, B. W., Stek, P. C., Wagner, P. A., and Wu, D. L.: EOS MLS Version 3.3/3.4 Level 2 data quality  
1165 and description document, Tech. rep., Jet Propulsion Laboratory, available from <http://mls.jpl.nasa.gov/>,  
1166 2013.

1167 Mahieu, E., Duchatelet, P., Demoulin, P., Walker, K. A., Dupuy, E., Froidevaux, L., Randall, C., Catoire,  
1168 V., Strong, K., Boone, C. D., Bernath, P. F., Blavier, J.-F., Blumenstock, T., Coffey, M., DeMaziere, M.,  
1169 Griffith, D., Hannigan, J., Hase, F., Jones, N., Jucks, K. W., Kagawa, A., Kasai, Y., Mebarki, Y.,  
1170 Mikuteit, S., Nassar, R., Notholt, J., Rinsland, C. P., Robert, C., Schrems, O., Senten, C., Smale, D.,  
1171 Taylor, J., Tetard, C., Toon, G. C., Warneke, T., Wood, S. W., Zander, R., and Servais, C.: Validation of  
1172 ACE-FTS v2.2 measurements of HCl, HF, CCl<sub>3</sub>F and CCl<sub>2</sub>F<sub>2</sub> using space-, balloon- and ground-based  
1173 instrument observations, *Atmos. Chem. Phys.*, 8, 6199-6221, doi:10.5194/acp-8-6199-2008, 2008.

1174 Mahieu, E., Zander, R., Bernath, P. F., Boone, C. D., and Walker, K. A.: Recent trend anomaly of  
1175 hydrogen chloride (HCl) at northern mid-latitudes derived from Jungfraujoch, HALOE, and ACE-FTS  
1176 infrared solar observations, in: *The Atmospheric Chemistry Experiment ACE at 10: a solar occultation*  
1177 *anthology*, Bernath, P. (Ed.), Deepak Publishing, Hampton, VA, 239-249, 2013.

1178 Mahieu, E., Chipperfield, M. P., Notholt, J., Anderson, J., Bernath, P. F., Blumenstock, T., Coffey, M. T.,  
1179 Dhomse, S., Feng, W., Franco, B., Froidevaux, L., Griffith, D. W. T., Hannigan, J., Hase, F., Hossaini, R.,  
1180 Jones, N. B., Morino, I., Murata, I., Nakajima, H., Palm, M., Paton-Walsh, C., Reddman, T.,  
1181 Russell III, J. M., Schneider, M., Servais, C., Smale, D., and Walker, K. A.: Increase in northern  
1182 stratospheric hydrogen chloride over recent years, submitted, 2014.

1183 McCormick, M. P., Zawodny, J. M., Veiga, R. E., Larsen, J. C., and Wang, P. H.: An overview of SAGE-  
1184 I and II ozone measurements, *Planetary and Space Science*, 37, No. 12, 1567-1586, 1989.

1185 McHugh, M., Hervig, M., Magill, B., Thompson, R. E., Remsberg, E., Wrotny, J., and  
1186 Russell, J. M.: Improved mesospheric temperature, water vapor, and polar mesospheric cloud extinctions  
1187 from HALOE, *Geophys. Res. Lett.*, 30, 8, doi: 10.1029/2002GL016859, 2003.

1188 McLinden, C. A., Tegtmeier, S., and Fioletov, V.: Technical Note: A SAGE-corrected SBUV zonal-mean  
1189 ozone data set, *Atmos. Chem. Phys.*, 9, 7963–7972, doi:10.5194/acp-9-7963-2009, 2009.

1190 McPeters, R. D., Bhartia, P. K., Haffner, D., Labow, G. J. and Flynn, L.: The v8.6 SBUV Ozone Data  
1191 Record: An Overview, *J. Geophys. Res.*, 118, 8032-8039, doi:10.1002/jgrd.50597, 2013.

1192 Molina, M. J., and Rowland, F. S.: Stratospheric sink for chlorofluoromethane: chlorine atom-catalyzed  
1193 destruction of ozone, *Nature*, 249, 810-812, 1974.

1194 Montzka, S. A., Butler, J. H., Elkins, J. W., Thompson, T. M., Clarke, A. D., and Lock, L. T.: Present  
1195 and future trends in the atmospheric burden of ozone-depleting halogens, *Nature*, 398, 690-694, 1999.

1196 Morris, G. A., Gleason, J. F., Russell III, J. M., Schoeberl, M. R., and McCormick, M. P.: A comparison  
1197 of HALOE V19 with SAGE II V6.00 ozone observations using trajectory mapping, *J. Geophys. Res.*,  
1198 107, D13, 4177, doi:10.1029/2001JD000847, 2002.

1199 Mote, P. W., Rosenlof, K. H., McIntyre, M. E., Carr, E. S., Gille, J. C., Holton, J. R., Kinnersley, J. S.,  
1200 Pumphrey, H. C., Russell III, J. M., and Waters, J. W.: An atmospheric tape recorder: The imprint of  
1201 tropical tropopause temperatures on stratospheric water vapor,  
1202 *J. Geophys. Res.*, 101, 3989–4006, 1996.

1203 Nair, P. J., Godin-Beekmann, S., Froidevaux, L., Flynn, L. E., Zawodny, J. M., Russell III, J. M.,  
1204 Pazmino, A., Ancellet, G., Steinbrecht, W., Claude, H., Leblanc, T., McDermid, S., van Gijssel, J. A. E.,  
1205 Johnson, B., Thomas, A., Hubert, D., Lambert, J.-C., Nakane, H., and Swart, D. P. J.: Relative drifts and  
1206 stability of satellite and ground-based stratospheric ozone profiles at NDACC lidar stations, *Atmos.*  
1207 *Meas. Tech.*, 5, 1301–1318, doi: 10.5194/amt-5-1301-2012, 2012.

1208 Nair, P. J., Godin-Beekmann, S., Kuttippurath, J., Ancellet, G., Goutail, F., Pazmiño, A., Froidevaux, L.,  
1209 Zawodny, J. M., Evans, R. D., Wang, H.-J., Anderson, A., and Pastel, M.: Ozone trends derived from the  
1210 total column and vertical profiles at a northern mid-latitude station, *Atmos. Chem. Phys.*, 13, 10373–  
1211 10384, doi:10.5194/acp-13-10373-2013, 2013.

1212

1213 Nair, P. J., Froidevaux, L., Kuttippurath, J., Zawodny, J. M., Russell III, J. M., Steinbrecht, W., Claude,  
1214 H., Leblanc, T., van Gijssel, J. A. E., Johnson, B., Swart, D. P. J., Thomas, A., Querel, R., Wang, R., and  
1215 Anderson, J.: Subtropical and mid-latitude ozone trends in the stratosphere: implications for recovery, *J.*  
1216 *Geophys. Res.*, in press, 2015.

1217 Nazaryan, H., McCormick, M. P., and Russell III, J. M.: New studies of SAGE II and HALOE ozone  
1218 profile and long-term change comparisons, *J. Geophys. Res.*, 110, D09305, doi:10.1029/2004JD005425,  
1219 2005.

1220 Nedoluha, G. E., Gomez, R. M., Hicks, B. C., Bevilacqua, R. M., Russell III, J. M.,  
1221 Connor, B. J., and Lambert, A.: A comparison of middle atmospheric water vapor as measured by  
1222 WVMS, EOS-MLS, and HALOE, *J. Geophys. Res.*, 112, D24S39, doi:10.1029/2007JD008757, 2007.

1223

1224 Nedoluha, G. E., Gomez, R. M., Hicks, B. C., Wrotny, J. E., Boone, C., and Lambert, A.: Water vapor  
1225 measurements in the mesosphere from Mauna Loa over solar cycle 23, *J. Geophys. Res.*, 114, D23303,  
1226 doi:10.1029/2009JD012504, 2009.

1227

1228 Nedoluha, G., Gomez, R. M., Hicks, B. C., Helmboldt, J., Bevilacqua, R. M., and Lambert, A.: Ground-  
1229 based microwave measurements of water vapor from the midstratosphere to the mesosphere, *J. Geophys.*  
1230 *Res.*, 116, D02309, doi:10.1029/2010JD014728., 2011.

1231

1232 Newchurch, M. J., Yang, E. S., Cunnold, D. M., Reinsel, G. C., Zawodny, J. M., and  
1233 Russell III, J. M.: Evidence for slowdown in stratospheric ozone loss: First stage of ozone recovery, *J.*

1234 Geophys. Res., 108, D16, doi:10.1029/2003JD003471, 2003.

1235 Parrish, A., Boyd, I. S., Nedoluha, G. E., Bhartia, P. K., Frith, S. M., Kramarova, N. A.,  
1236 Connor, B. J., Bodeker, G. E., Froidevaux, L., Shiotani, M., and Sakazaki, T.: Diurnal variations of  
1237 stratospheric ozone measured by ground-based microwave remote sensing at the Mauna Loa NDACC  
1238 site: measurement validation and GEOSCCM model comparison, *Atmos. Chem. Phys.*, 7255-7272,  
1239 doi:10.5194/acp-14-7255-2014, 2014.

1240 Perliski, L. M., Solomon, S., and London, J.: On the interpretation of seasonal variations of stratospheric  
1241 ozone, *Planet. Space Sci.*, 37, 12, 1527-1538, 1989.

1242 Pumphrey, H. C.: Validation of a new prototype water vapor retrieval for UARS MLS,  
1243 *J. Geophys. Res.*, 104 (D8), 9399–9412, 1999.

1244 Pumphrey, H. C., Clark, H. L., and Harwood, R. S.: Lower stratospheric water vapor as measured by  
1245 UARS MLS, *Geophys. Res. Lett.*, 27, 1691–1694, 2000.

1246 Randel, W. J., Wu, F., Oltmans, S. J., Rosenlof, K., and Nedoluha, G. E.: Interannual changes of  
1247 stratospheric water vapor and correlations with tropical tropopause temperatures, *J. Atmos. Sci.*, 61,  
1248 2133–2148, 2004.

1249  
1250 Read, W. G., Lambert, A., Bacmeister, J., Cofield, R. E., Chris-  
1251 tensen, L. E., Cuddy, D. T., Daffer, W.  
1252 H., Drouin, B. J., Fetzer, E., Froidevaux, L., Fuller, R., Herman, R., Jarnot, R. F., Jiang, J. H., Jiang, Y.  
1253 B., Kelly, K., Knosp, B. W., Kovalenko, L. J., Livesey, N. J., Liu, H.-C., Manney, G. L., Pickett, H. M.,  
1254 Pumphrey, H. C., Rosenlof, K. H., Sabouchi, X., Santee, M. L., Schwartz, M. J., Snyder, W. V., Stek, P.  
1255 C., Su, H., Takacs, L. L., Thurstans, R. P., Voemel, H., Wagner, P. A., Waters, J. W., Web-  
1256 ster, C. R.,  
1257 Weinstock, E. M., and Wu, D. L.: Aura Microwave Limb Sounder upper tropospheric and lower  
1258 stratospheric H<sub>2</sub>O and relative humidity with respect to ice validation, *J. Geophys. Res.*, 112, D24S35,  
1259 doi:10.1029/2007JD008752, 2007.

1259 Read, W. G., Schwartz, M. J., Lambert, A., Su, H., Livesey, N. J., Daffer, W. H., and  
1260 Booe, C. D.: The roles of convection, extratropical mixing, and in-situ freeze-drying in the Tropical  
1261 Tropopause Layer, *Atmos. Chem. Phys.*, 8, 6051–6067, doi:10.5194/acp-8-6051-2008, 2008.

1262  
1263 Remsberg, E.: Observed seasonal to decadal scale responses in mesospheric water vapor,  
1264 *J. Geophys. Res.*, 115, D06306, doi:10.1029/2009JD012904, 2010.

1265  
1266 Ricaud, P., de La Noë, J., Connor, B. J., Froidevaux, L., Waters, J. W., Harwood, R. S., MacKenzie, I. A.,  
1267 and Peckham, G. E.: Diurnal variability of mesospheric ozone as measured by the UARS microwave limb  
1268 sounder instrument: Theoretical and ground-based validations, *J. Geophys. Res.*, 101 (D6), 10,077–  
1269 10,089, doi:10.1029/95JD02841, 1996.  
1270  
1271 Rienecker, M., Suarez, M. J., Gelaro, R., Todling, R., Bacmeister, J., Liu, E., Bosilovich, M. G.,  
1272 Schubert, S. D., Takacs, L., Kim, G.-K., Bloom, S., Chen, J., Collins, D., Conaty, A.,  
1273 da Silva, A., Gu, W., Joiner, J., Koster, R. D., Lucchesi, R., Molod, A., Owens, T., Pawson, S., Pegion,  
1274 P., Redder, C. R., Reichle, R., Robertson, J., F. R., Ruddick, A. G., Sienkiewicz, M., and Woollen, J.:  
1275 MERRA: NASA's Modern-Era Retrospective Analysis for Research and Applications, *J. Climate*, 24,  
1276 3624–3648, doi:10.1175/JCLI-D-11-00015.1, 2011.  
1277  
1278 Russell III, J. M., Gordley, L. L., Park, J. H., Drayson, S. R., Hesketh, D. H., Cicerone, R. J., Tuck, A. F.,  
1279 Frederick, J. E., Harries, J. E., and Crutzen, P.: The Halogen Occultation Experiment, *J. Geophys. Res.*,  
1280 98, 10777-10797, 1993.  
1281 Russell III, J. M., Deaver, L. E., Luo, M., Park, J. H., Gordley, L. L., Tuck, A. F., Toon, G. C., Gunson ,  
1282 M. R., Traub, W. A., Johnson, D. G., Jucks, K. W., Murcray, D. G., Zander, R.,  
1283 Nolt, I. G., and Webster, C. R.: Validation of hydrogen chloride measurements made by the Halogen  
1284 Occultation Experiment from the UARS platform, *J. Geophys. Res.*, 101 (D6), 10,151– 10,162, 1996.  
1285 Sakazaki, T., Fujiwara, M., Mitsuda, C., Imai, K., Manago, N., Naito, Y., Nakamura, T., Akiyoshi, H.,  
1286 Kinnison, D., Sano, T., Suzuki, M., and Shiotani, M.: Diurnal ozone variations in the stratosphere  
1287 revealed in observations from the Superconducting Submillimeter-Wave Lime-Emission Sounder  
1288 (SMILES) on board the International Space Station (ISS), *J. Geophys. Res. Atmos.*, 118, 2991-3006,  
1289 doi:10.1002/jgrd.50220, 2013.  
1290 Santee, M. L., Lambert, A., Read, W. G., Livesey, N. J., Cofield, R. E., Cuddy, D. T.,  
1291 Daffer, W. H., Drouin, B. J., Froidevaux, L., Fuller, R. A., Jarnot, R. F., Knosp, B. W.,  
1292 Manney, G. L., Perun, V. S., Snyder, W. V., Stek, P. C., Thurstans, R. P., Wagner, P. A.,  
1293 Waters, J. W., Muscari, G., de Zafra, R. L., Dibb, J. E., Fahey, D. W., Popp, P. J., Marcy, T. P., Jucks, K.  
1294 W., Toon, G. C., Stachnik, R. A., Bernath, P. F., Boone, C. D., Walker, K. A.,  
1295

- 1296 Urban, J., and Murtagh, D.: Validation of the Aura Microwave Limb Sounder HNO<sub>3</sub> measurements, *J.*  
1297 *Geophys. Res.*, 112, D24S40, doi:10.1029/2007JD008, 2007.
- 1298 Salby, M., Titova, E., and Deschamps, L.: Rebound of Antarctic ozone, *Geophys. Res. Lett.*, 38, L09702,  
1299 doi:10.1029/2011GL047266, 2011.
- 1300 Salby, M. L., Titova, E. A., and Deschamps, L.: Changes of the Antarctic ozone hole: Controlling  
1301 mechanisms, seasonal predictability, and evolution, *J. Geophys. Res.*, 117, D10111,  
1302 doi:10.1029/2011JD016285, 2012.
- 1303 Schwartz, M. J., Froidevaux, L., Fuller, R. A., and Pawson, S.: GOZCARDS Merged Data for  
1304 Temperature Monthly Zonal Means on a Geodetic Latitude and Pressure Grid, version 1.01, Greenbelt,  
1305 MD, USA: NASA Goddard Earth Science Data and Information Services Center, accessible from  
1306 doi:10.5067/MEASURES/GOZCARDS/DATA3023, 2013.
- 1307 Shepherd, T. G., Plummer, D. A., Scinocca, J. F., Hegglin, M. I., Fioletov, V. E., Reader, M. C., Remsberg,  
1308 E., von Clarmann, T., and Wang, H. J.: Reconciliation of halogen-induced ozone loss with the total-  
1309 column ozone record, *Nature Geoscience*, 7, 443-449, doi:10.1038/NGEO2155, 2014.  
1310
- 1311 Solomon P. M., Barrett, J., Mooney, T., Connor, B., Parrish, A., and Siskind, D. E.: Rise and decline of  
1312 active chlorine in the stratosphere, *Geophys. Res. Lett.*, 33, L18807, doi:10.1029/2006GL027029, 2006.
- 1313 Sofieva, V. F., Kalakoski, N., Päivärinta, S.-M., Tamminen, J., Laine, M., and Froidevaux, L.: On  
1314 sampling uncertainty of satellite profile ozone measurements, *Atmos. Meas. Tech.*, 7, 1891–1900,  
1315 doi:10.5194/amt-7-1891-2014, 2014.
- 1316 Solomon, S.: Stratospheric ozone depletion: A review of concepts and history, *Rev. Geophys.*, 37, 275–  
1317 316, doi:10.1029/1999RG900008, 1999.
- 1318 Solomon, S., Rosenlof, K., Portmann, R., Daniel, J., Davis, S., Sanford, T., and Plattner, G.-K.:  
1319 Contributions of Stratospheric Water Vapor to Decadal Changes in the Rate of Global Warming, *Science*,  
1320 327, 1219-1223, 2010.
- 1321 SPARC: Assessment of Trends in the Vertical Distribution of Ozone, edited by N. Harris, R. Hudson and  
1322 C. Phillips, SPARC/IOC/GAW, SPARC Rep. 1, WMO Ozone Res. Monit. Project Rep. 43, 1998.

1323 SPARC WAVAS: Assessment of upper tropospheric and stratospheric water vapour, World Climate  
1324 Research Programme, WCRP-113, WMO/TD-No.1043, 261-264, 2000.

1325 Steinbrecht, W., Koehler, U., Claude, H., Weber, M., Burrows, J. P., and van der A, R. J.: Very high  
1326 ozone columns at northern mid latitudes in 2010, *Geophys. Res. Lett.*, 38, L06803,  
1327 doi:10.1029/2010GL046634, 2011.

1328 Strong, K., Wolff, M. A., Kerzenmacher, T. E., Walker, K. A., Bernath, P. F., Blumenstock, T., Boone,  
1329 C., Catoire, V., Coffey, M., De Maziere, M., Demoulin, P., Duchatelet, P., Dupuy, E., Hannigan, J.,  
1330 Hopfner, M., Glatthor, N., Griffith, D. W. T., Jin, J. J., Jones, N., Jucks, K., Kuellmann, H., Kuttippurath,  
1331 J., Lambert, A., Mahieu, E., McConnell, J. C., Mellqvist, J., Mikuteit, S., Murtagh, D. P., Notholt, J.,  
1332 Piccolo, C., Raspollini, P., Ridolfi, M., Robert, C., Schneider, M., Schrems, O., Semeniuk, K., Senten, C.,  
1333 Stiller, G. P., Strandberg, A., Taylor, J., Tetard, C., Toohey, M., Urban, J., Warneke, T., and Wood, S.:  
1334 Validation of ACE-FTS N<sub>2</sub>O measurements, *Atmos. Chem. Phys.*, 8, 4759-4786, doi:10.5194/acp-8-  
1335 4759-2008, 2008.

1336 Tegtmeier, S., Hegglin, M. I., Anderson, J., Bourassa, A., Brohede, S., Degenstein, D., Froidevaux, L.,  
1337 Fuller, R., Funke, B., Gille, J., Jones, A., Kasai, Y., Krüger, K., Kyrölä, E., Lingenfelser, G., Lumpe, J.,  
1338 Nardi, B., Neu, J., Pendlebury, D., Remsberg, E., Rozanov, A., Smith, L., Toohey, M., Urban, J., von  
1339 Clarmann, T., Walker, K. A., and Wang, H. J.: The SPARC Data Initiative: A comparison of ozone  
1340 climatologies from international satellite limb sounders, *J. Geophys. Res. Atmos.*, 118, 12,229–12,247,  
1341 doi: 10.1002/2013JD019877, 2013.

1342 Toohey, M., Hegglin, M. I., Tegtmeier, S., Anderson, J., Añel, J. A., Bourassa, A., Brohede, S.,  
1343 Degenstein, D., Froidevaux, L., Fuller, R., Funke, B., Gille, J., Jones, A., Kasai, Y., Krüger, K., Kyrölä,  
1344 E., Neu, J. L., Rozanov, A., Smith, L., Urban, J., von Clarmann, T., Walker, K. A., and Wang, R.:  
1345 Characterizing sampling bias in the trace gas climatologies of the SPARC Data Initiative, *J. Geophys.*  
1346 *Res. Atmos.*, 118, 11,847–11,862, doi: 10.1002/jgrd.5087, 2013.

1347 Tummon, F., Hassler, B., Harris, N. R. P., Staehelin, J., Steinbrecht, W., Anderson, J.,  
1348 Bodeker, G. E., Bourassa, A., Davis, S. M., Degenstein, D., Frith, S. M., Froidevaux, L.,  
1349 Kyrölä, E., Laine, M., Long, C., Penckwitt, A. A., Sioris, C. E., Rosenlof, K. H., Roth, C.,  
1350 Wang, H.-J., and Wild, J.: Intercomparison of vertically resolved merged satellite ozone data sets:  
1351 interannual variability and long-term trends, *Atmos. Chem. Phys.*, 15, 3021-3043, doi: 10.5194/acp-15-  
1352 3021-2015, 2015.

1353 Urban, J., Lautié, N., Murtagh, D. P., Eriksson, P., Kasai, Y., Lossow, S., Dupuy, E.,  
1354 de LaNoë, J., Frisk, U., Olberg, M., Flochmoën, E. Le., and Ricaud, P.: Global observations of middle  
1355 atmospheric water vapour by the Odin satellite: An overview, *Planet. Space Sci.*, 55, 9, 1093-1102, 2007.

1356 Urban, J., Lossow, S., Stiller, G., and Read, W.: Another drop in water vapor, *EOS Transactions,*  
1357 *American Geophysical Union*, 95, 27, 245-252, doi:10.1002/2014EO270001, 2014.

1358 Veiga, R.E., Cunnold, D. M., Chu, W. P., and McCormick, M. P.: Stratospheric Aerosol and Gas  
1359 Experiments I and II comparisons with ozonesondes. *J. Geophys. Res.*, 100 (D5), 9073-9090, 1995.

1360 Voemel, H., Barnes, J. E., Forno, R. N., Fujiwara, M., Hasebe, F., Iwasaki, S., Kivi, R., Komala, N.,  
1361 Kyrölä, E., Leblanc, T., Morel, B., Ogino, S.-Y., Read, W. G., Ryan, S. C., Saraspriya, S., Selkirk, H.,  
1362 Shiotani, M., Valverde Canossa, J., and Whiteman, D. N.: Validation of Aura Microwave Limb Sounder  
1363 water vapor by balloon-borne Cryogenic Frost point Hygrometer measurements, *J. Geophys. Res.*, 112,  
1364 D24S37, doi:10.1029/2007JD008698, 2007.

1365 Wang, H. J., Cunnold, D. M., and Bao, X.: A critical analysis of Stratospheric Aerosol and Gas  
1366 Experiment ozone trends *J. Geophys. Res.*, 101 (D7), 12495-12514, 1996.

1367 Wang, H. J., Cunnold, D. M., Thomason, L. W., Zawodny, J. M., and Bodeker, G. E.: Assessment of  
1368 SAGE version 6.1 ozone data quality, *J. Geophys. Res.*, 107 (D23),  
1369 doi: 10.1029/2002JD002418, 2002.

1370 Wang, H. J., Cunnold, D. M., Trepte, C., Thomason, L. W., and Zawodny, J. M.: SAGE III solar ozone  
1371 measurements: Initial results, *Geophys. Res. Lett.*, 33, L03805, doi:10.1029/2005GL025099, 2006.

1372 Wang, R., Froidevaux, L., Anderson, J., Fuller, R. A., Bernath, P. F., McCormick, M. P., Livesey, N. J.,  
1373 Russell III, J. M., Walker, K. A., and Zawodny, J. M.: GOZCARDS Merged Data for Ozone Monthly  
1374 Zonal Means on a Geodetic Latitude and Pressure Grid, version 1.01, Greenbelt, MD, USA: NASA  
1375 Goddard Earth Science Data and Information Services Center, accessible from  
1376 doi:10.5067/MEASURES/GOZCARDS/DATA3006, 2013.

1377 Waters, J. W., Microwave limb sounding, in *Atmospheric Remote Sensing by Microwave Radiometry*,  
1378 ed. by M. Janssen, chap. 8, John Wiley, New York, 1993.

1379 Waters, J. W., Froidevaux, L., Read, W. G., Manney, G. L., Eslon, L. S., Flower, D. A., Jarnot, R. F., and  
1380 Harwood, R. S.: Stratospheric ClO and ozone from the Microwave Limb Sounder on the Upper  
1381 Atmosphere Research Satellite, *Nature*, 362, 597-602, 1993.



1382 Waters, J. W., Froidevaux, L., Harwood, R. S., Jarnot, R. F., Pickett, H. M., Read, W. G., Siegel, P. H.,  
1383 Cofield, R. E., Filipiak, M. J., Flower, D. A., Holden, J. R., Lau, G. K., Livesey, N. J., Manney, G. L.,  
1384 Pumphrey, H. C., Santee, M. L., Wu, D. L., Cuddy, D. T., Lay, R. R., Loo, M. S., Perun, V. S., Schwartz,  
1385 M. J., Stek, P. C., Thurstans, R. P., Boyles, M. A., Chandra, S., Chavez, M. C., Chen, G.-S., Chudasama,  
1386 B. V., Dodge, R., Fuller, R. A., Girard, M. A., Jiang, J. H., Jiang, Y., Knosp, B. W., LaBelle, R. C., Lam,  
1387 J. C., Lee, K. A., Miller, M., Oswald, J. E., Patel, N. C., Pukala, D. M., Quintero, O., Scaff, D. M.,  
1388 Snyder, W. V., Tope, M. C., Wagner, P. A., and Walch, M. J.: The Earth Observing System Microwave  
1389 Limb Sounder (EOS MLS) on the Aura satellite, *IEEE Trans. Geosci. Remote Sens.*, 44 (5), 1075–1092,  
1390 doi:10.1109/TGRS.2006.873771, 2006.

1391 Waugh, D. W., Considine, D. B., and Fleming, E. L.: Is Upper Stratospheric Chlorine Decreasing as  
1392 Expected?, *Geophys. Res. Lett.*, 28(7), 1187–1190, 2001.

1393 WMO (World Meteorological Organization): Scientific Assessment of Ozone Depletion: 2002, Global  
1394 Ozone Research and Monitoring Project – Report No. 47, Geneva, Switzerland, 2003.

1395 WMO (World Meteorological Organization), Scientific Assessment of Ozone Depletion: 2010, Global  
1396 Ozone Research and Monitoring Project – Report No. 52, Geneva, Switzerland, 2011.

1397 WMO (World Meteorological Organization), Scientific Assessment of Ozone Depletion: 2014, Global  
1398 Ozone Research and Monitoring Project – Report No. 55, Geneva, Switzerland, 2014.

1399 Wohltmann, I., Lehmann, R., Rex, M., Brunner, D., and Mader, J.A.: A process-oriented regression  
1400 model for column ozone, *J. Geophys. Res.*, 112, D12304, doi:10.1029/2006JD007573, 2007.

1401 Wolff, M. A., Kerzenmacher, T., Strong, K., Walker, K. A., Toohey, M., Dupuy, E., Bernath, P. F.,  
1402 Boone, C. D., Brohede, S., Catoire, V., von Clarmann, T., Coffey, M., Daffer, W. H., De Maziere, M.,  
1403 Duchatelet, P., Glatthor, N., Griffith, D. W. T., Hannigan, J., Hase, F., Hopfner, M., Huret, N., Jones, N.,  
1404 Jucks, K., Kagawa, A., Kasai, Y., Kramer, I., Kullmann, H., Kuttippurath, J., Mahieu, E., Manney, G.,  
1405 McElroy, C. T., McLinden, C., Mebarki, Y., Mikuteit, S., Murtagh, D., Piccolo, C., Raspollini, P.,  
1406 Ridolfi, M., Ruhnke, R., Santee, M., Senten, C., Smale, D., Tetard, C., Urban, J., and Wood, S.:  
1407 Validation of HNO<sub>3</sub>, ClONO<sub>2</sub>, and N<sub>2</sub>O<sub>5</sub> from the Atmospheric Chemistry Experiment Fourier Transform  
1408 Spectrometer (ACE-FTS), *Atmos. Chem. Phys.*, 8, 3529–3562, doi:10.5194/acp-8-3529-2008, 2008.

1409 Yang, E.-S., Cunnold, D. M., Newchurch, M. J., Salawitch, R., McCormick, J. M. P., Russell III, J. M.,  
1410 Zawodny, J. M., and Oltmans, S. J.: First stage of Antarctic ozone recovery, *J. Geophys. Res.*, 113,  
1411 D20308, doi:10.1029/2007JD009675, 2008.

1412 Ziemke, J. R., and Chandra, S.: Development of a climate record of tropospheric and stratospheric  
1413 column ozone from satellite remote sensing: evidence of an early recovery of global stratospheric ozone,  
1414 *Atmos. Chem. Phys.*, 12, 5737-5753, doi:10.5194/acp-12-5737-2012, 2012.

1415 Ziemke, J. R., Chandra, S., and Bhartia, P. K.: A 25-year data record of atmospheric ozone from TOMS  
1416 Cloud Slicing: Implications for trends in stratospheric and tropospheric ozone, *J. Geophys. Res.*, 110,  
1417 D15105, doi:10.1029/2004JD005687, 2005.

1418

## 1419 **Appendix A**

### 1420 **A.1. GOZCARDS data provenance**

1421 The general origin of the datasets is summarized here. Data coverage from limb sounders  
1422 (including the instruments used here) is displayed nicely in the work by Toohey et al. (2013).

#### 1423 ***SAGE I***

1424 SAGE I was launched February 18, 1979, aboard the Applications Explorer Mission-B  
1425 (AEM-B) satellite. SAGE I was a sun photometer using solar occultation (Chu and McCormick,  
1426 1979), and it collected a global database for nearly three years on stratospheric aerosol, O<sub>3</sub>, and  
1427 NO<sub>2</sub>. For more information, the reader is referred to <http://sage.nasa.gov/SAGE1>.

#### 1428 ***SAGE II***

1429 SAGE II was launched aboard the Earth Radiation Budget Satellite (ERBS) in October 1984  
1430 and its data gathering period ended in August 2005. During each sunrise and sunset, SAGE II  
1431 measured stratospheric aerosols, O<sub>3</sub>, NO<sub>2</sub>, and H<sub>2</sub>O via solar occultation. This long dataset has  
1432 proven very valuable in determining past ozone trends. For more information on and data access  
1433 to the (V6.2) dataset used for GOZCARDS, the reader is referred to <http://sage.nasa.gov/SAGE2>.

#### 1434 ***HALOE***

1435 Since its launch on September 12, 1991 from the Space Shuttle Discovery until November  
1436 2005, UARS HALOE collected profiles of atmospheric composition and temperature. HALOE  
1437 (Russell et al., 1993) used solar occultation to measure vertical profiles of O<sub>3</sub>, HCl, HF, CH<sub>4</sub>,  
1438 H<sub>2</sub>O, NO, NO<sub>2</sub>, temperature, aerosol extinction, and aerosol composition and size distribution.  
1439 More information and access to the HALOE data can be obtained from <http://haloe.gats-inc.com>  
1440 and <http://disc.sci.gsfc.nasa.gov/UARS/data-holdings/HALOE>. For GOZCARDS purposes, we  
1441 have used Version 19 HALOE netCDF data files available at <http://haloe.gats-inc.com>.

#### 1442 ***UARS MLS***

1443 This instrument observed the Earth's limb in microwave emission using three radiometers, at  
1444 frequencies near 63, 183 and 205 GHz (Waters, 1993; Barath et al., 1993), providing unique

1445 daily global information on stratospheric ClO, along with other profiles, including O<sub>3</sub>, H<sub>2</sub>O,  
1446 HNO<sub>3</sub>, temperature, and cloud ice water content. The stratospheric H<sub>2</sub>O data ceased on April 15,  
1447 1993, after the failure of the 183 GHz radiometer. After March 15, 1994, measurements became  
1448 increasingly sparse in order to conserve the life of the MLS antenna scan mechanism and UARS  
1449 power. Data exist until July 28, 1999, although for GOZCARDS, only data through mid-June  
1450 1997 are used, as data sparseness and degradation of the 63 GHz radiometer led to less ‘trend-  
1451 quality’ data after this. Sampling patterns follow the alternating yaw cycles imposed on MLS by  
1452 the precessing UARS orbit; MLS measurements were obtained continuously for all latitudes  
1453 between 34°S and 34°N, with higher latitudes covered in either the northern or southern  
1454 hemisphere with a roughly 36-day cycle. Livesey et al. (2003) provide more information on the  
1455 UARS MLS instrument, retrievals, and results. For data access, the reader is directed to the  
1456 relevant Goddard Earth Sciences and Information Services Center (GES DISC) data holdings at  
1457 <http://disc.sci.gsfc.nasa.gov/UARS/data-holdings/MLS>. L3AT data files were used as the basis  
1458 for the production of the GOZCARDS UARS MLS monthly source datasets.

#### 1459 *ACE-FTS*

1460 ACE-FTS is the primary instrument onboard the SCISAT satellite, launched on August 12, 2003.  
1461 It is a high spectral resolution (0.02 cm<sup>-1</sup>) Michelson interferometer operating from 2.2 to  
1462 13.3 μm (750-4400 cm<sup>-1</sup>); see Bernath et al. (2005) for an overview of the ACE mission. The  
1463 instrument can simultaneously measure temperature and many trace gases (including all the  
1464 species mentioned here for GOZCARDS), thin clouds, and aerosols, using the solar occultation  
1465 technique. ACE-FTS data version 2.2, along with the version 2.2 update for ozone, were used  
1466 here for GOZCARDS. For access to the public ACE-FTS datasets, with a routine measurement  
1467 start date of March 2004, the reader is directed to <http://www.ace.uwaterloo.ca>.

#### 1468 *Aura MLS*

1469 MLS is one of four instruments on NASA's Aura satellite, launched on July 15th 2004. Aura  
1470 MLS is a greatly enhanced version of the UARS MLS experiment, providing better spatial  
1471 coverage, vertical resolution, and vertical range, along with more continuous data over its  
1472 lifetime (and with ongoing measurements at the time of writing). The instrument includes

1473 radiometers at 118, 190, 240, and 640 GHz, and a 2.5 THz module (Waters et al., 2006). Aura  
 1474 MLS provides measurements of many chemical species, cloud ice, temperature and geopotential  
 1475 height. Continuous measurements have been obtained since August 2004, with the exception of  
 1476 OH, for which sparser measurements exist since August 2010, in order to preserve the life of the  
 1477 THz module. For more information and access to the Aura MLS datasets, the reader is referred to  
 1478 <http://disc.sci.gsfc.nasa.gov/Aura/data-holdings/MLS>. For GOZCARDS, we use the currently  
 1479 recommended Aura MLS data versions (version 2.2/2.3 for ozone and 3.3/3.4 for other species).

## 1480 **A.2. Calculation details for the iterative merging procedure**

1481 Given three time series, the merging procedure that we use first combines two out of the three  
 1482 time series,  $y_1(i)$  and  $y_2(i)$  (where index  $i$  represents time for each monthly mean value in a given  
 1483 latitude/pressure bin). We first obtain the temporary merged series  $m_1(i)$  via:  
 1484 
$$m_1(i) = (1/2) (y_1(i) + y_2(i)) \quad (1)$$

1485 with the average offsets for  $y_1(i)$  and  $y_2(i)$  being  $(1/(2 n_{12})) \sum (y_1(i) - y_2(i))$  and -1 times this value,  
 1486 respectively;  $n_{12}$  is the number of overlapping data points between the two time series. Then, we  
 1487 merge together the time series  $m_1(i)$  and  $y_3(i)$ , keeping the weightings equal for all 3 time series  
 1488 (1/3 for each), so that we calculate the new merged time series  $m(i)$  via:

$$1489 \quad m(i) = w_m m_1(i) + w_3 y_3(i) = (1/3) (y_1(i) + y_2(i) + y_3(i)) \quad (2)$$

1490 which will hold if the weights are  $w_m = 2/3$  and  $w_3 = 1/3$  (given equation (1) for  $m_1(i)$ ). The  
 1491 average reference value (to which the adjustments of  $m_1(i)$  and  $y_3(i)$  in the 2<sup>nd</sup> step are made) is  
 1492 given by  $(1/n_m) \sum ( (2/3) m_1(i) + (1/3) y_3(i) )$ , where  $n_m$  represents the number of (overlapping  
 1493 pairs of) data values used in step 2. For the HCl and H<sub>2</sub>O data merging procedure, we always use  
 1494 the Aura MLS time series as one of the first two series involved in the initial merging step, for  
 1495 example as  $y_1(i)$ , in order to maximize the overlap between the first two series and obtain more  
 1496 robust offset values. Then, we use the 3<sup>rd</sup> time series; the order used for HALOE and ACE-FTS  
 1497 (i.e., whether we use HALOE or ACE-FTS for  $y_2$  or  $y_3$ ) makes very little difference.

## 1498 **Calculation of the standard deviation for the merged data values**

1499 The average and standard deviation (square root of variance) for each  $y_k$  value (i.e. for each  
 1500 monthly zonal mean in a particular lat/p bin) are calculated from equations (3) and (4) below:

1501 
$$\bar{y}_k = \frac{1}{n_{yk}} \sum_j y_{kj} \quad (3)$$

1502 and, for the variance,

1503 
$$\sigma_{yk}^2 = \frac{1}{n_{yk} - 1} \sum_j (y_{kj} - \bar{y}_k)^2 \quad (4)$$

1504 where index “ $j$ ” corresponds to individual data values within a month, index  $k$  represents a given  
 1505 instrument (data source), and  $n$  is the total number of data values for a given bin and source  
 1506 (instrument) time series point in time (or month). Each value  $\bar{y}_k$  above is a monthly average  
 1507 (although we also use instead the simpler notation  $y_k$ ), with standard deviation about the mean  
 1508  $\sigma_{yk}$ . Now, given the merged series  $u(i)$  (where index  $i$  runs over a large number of months), the  
 1509 standard deviation of each merged data point (for a given month) can be obtained by considering  
 1510 the original datasets  $y_{kj}$  that were used to construct  $u$ . Specifically, we have the variance for the  
 1511 merged dataset

1512 
$$\sigma_u^2 = \frac{1}{n_u - 1} \sum_j (u_j - u_{ref})^2 \quad (5)$$

1513 where  $u_{ref}$  is the merged value (which is not necessarily chosen to be the average value  $\bar{u}$ ) and  
 1514 the  $u_j$  values represent the union of adjusted data values that make up the merged product, with  
 1515 the index  $j$  for this combined dataset covering all values (up to the total  $n_u$ ) obtained from the  
 1516 original source values  $y_{kj}$ . In practice, we do not keep track of the individual data values that  
 1517 went into making the averages for the series  $y_k$  that are being merged, and we need to obtain  $\sigma_u$   
 1518 based solely on the values  $\bar{y}_k$ ,  $\sigma_{yk}$ , and the original number of points for each dataset  $y_k$ ,  
 1519 namely  $n_{yk}$ . If we consider all the original values, we have a combined dataset with  $n_u$  points,  
 1520 such that  $n_u = \sum_k n_{yk}$ . Now, expanding equation (5), we get

1521 
$$(n_u - 1) \sigma_u^2 = \sum_j (u_j^2 + u_{ref}^2 - 2u_{ref} u_j) \quad (6)$$

1522 or

1523  $(n_u - 1) \sigma_u^2 = \sum_j u_j^2 + n_u u_{ref}^2 - 2u_{ref} \sum_j u_j$  (7)

1524 Expanding (4) for each individual dataset  $y_k$ , we get

1525  $(n_{yk} - 1) \sigma_{yk}^2 = \sum_j y_{kj}^2 + \bar{y}_k^2 - 2\bar{y}_k \sum_j y_{kj}$  (8)

1526 which leads to

1527  $\sum_j u_j^2 = \sum_{k,j} y_{kj}^2 = \sum_k (n_{yk} - 1) \sigma_{yk}^2 + \sum_k n_{yk} \bar{y}_k^2$ , (9)

1528 so that extracting the variance from equation (7) now leads to

1529  $\sigma_u^2 = \frac{1}{(n_u - 1)} \left( \sum_k (n_{yk} - 1) \sigma_{yk}^2 + \sum_k n_{yk} \bar{y}_k^2 + n_u u_{ref}^2 - 2u_{ref} \sum_k n_{yk} \bar{y}_k \right)$  (10)

1530 The adjusted time series are obtained from the original series  $y_k$  as  $Y_k$ , and we can write

1531 Equation (4) in the same manner for the  $Y_k$  data values, namely

1532  $\sigma_{Yk}^2 = \frac{1}{n_{yk} - 1} \sum_j (Y_{kj} - \bar{Y}_k)^2$  (11)

1533 with  $\sigma_{Yk} = \sigma_{yk}$  as the adjustments (offsets) are performed in an additive manner; if these

1534 adjustments were performed using multiplicative factors, those factors would also have to be

1535 considered in a multiplicative way to get the new  $\sigma_{Yk}$  values. We can thus write (10) for the

1536 adjusted datasets as:

1537  $\sigma_u^2 = \frac{1}{(n_u - 1)} \left( \sum_k (n_{yk} - 1) \sigma_{yk}^2 + \sum_k n_{yk} \bar{Y}_k^2 + n_u U_{ref}^2 - 2U_{ref} \sum_k n_{yk} \bar{Y}_k \right)$  (12)

1538 Equation (12) for the standard deviation of the merged dataset simplifies if the original datasets

1539 are adjusted to exactly the same reference value  $ref$  ( $\bar{Y}_k = ref$ ) and the merged value  $U_{ref}$  is

1540 also equal to that value, as the sum of the last 3 terms in Eq. (10) (with  $Y_k$  replacing  $y_k$ ) then

1541 reduces to  $n_u ref^2 + n_u ref^2 - 2n_u ref^2$ , which is zero. In this case, one obtains

1542 
$$\sigma_u^2 = \frac{1}{(n_u - 1)} \left( \sum_k (n_{yk} - 1) \sigma_{yk}^2 \right) \quad (13)$$

1543 However, in general, one should use equation (12) for the standard deviation of the merged  
 1544 dataset, given the adjusted datasets  $\overline{Y}_k$  and the merged (or reference) value  $U_{ref}$ . Also, we often  
 1545 use a merged value equal to the average of the original data (over a given overlap period), so that

1546 
$$U_{ref} = \frac{1}{n_y} \sum_k \overline{y}_k \quad (14)$$

1547 where  $n_y$  is the total number of datasets ( $y_k$ ), as opposed to having the merged value place more  
 1548 weight on the larger datasets (e.g., for emission-type measurements versus occultation-type), in  
 1549 which case one would consider using  $U_{ref} = \frac{1}{n_u} \sum_k n_{yk} \overline{y}_k$ . For ozone, we use a particular dataset  
 1550 (SAGE II ozone) as the primary reference, but equation (12) can be used to obtain the standard  
 1551 deviation for the merged dataset (about the SAGE II reference) in that case also. While it is  
 1552 useful to have the formalism above for obtaining the merged dataset standard deviation  $\sigma_u$ , we  
 1553 often find significant differences between the standard deviations of various datasets, so that this  
 1554 effect will have the greatest influence on the results, as opposed to the impact of the last 3 terms  
 1555 in the summation (in (12)). Finally, it is easy to test equation (12) (and we have done so) by  
 1556 using synthetic series and calculating the standard deviation of the combined set. In reality, the  
 1557 standard deviations of the time series monthly mean values are typically larger for MLS than for  
 1558 ACE-FTS, mainly because of the more complete sampling of variability from the daily global  
 1559 measurements acquired by MLS. Sample plots for standard deviations and standard errors in the  
 1560 case of HCl are shown in Fig. A1. As expected, merged standard deviations follow the standard  
 1561 deviations from HALOE HCl before Aug. 2004 and those from MLS HCl after this time.  
 1562 However, the merged standard errors for the MLS time period follow the smaller MLS standard  
 1563 errors, because these values vary inversely with the square root of the number of values sampled,  
 1564 and are therefore made smaller by the significantly larger daily and monthly MLS sampling rate  
 1565 and coverage.

1566



1567 **A.3. Procedural details for GOZCARDS HCl, H<sub>2</sub>O, and O<sub>3</sub>**

1568 Data screening procedures for the GOZCARDS source datasets, following previously described  
1569 methods, are provided (with references) in Table A1, along with certain species-related specifics.  
1570 Other GOZCARDS data characteristics and details are provided below for each species.

1571 **A.3.1. HCl**

- 1572 - The vertical data range for valid HCl merged values is between 0.46 hPa and 147 hPa  
1573 (inclusive), as a result of data sparseness or data quality issues outside these ranges.
- 1574 - At 147 hPa, no merged HCl values exist for latitude bins from 35°S to 35°N inclusive,  
1575 because of unrealistically large Aura MLS HCl values in this region; also, there is not enough  
1576 data at this level to provide a meaningful product from HALOE and ACE-FTS data alone.
- 1577 - Because of occasional small negative merged values during southern hemisphere polar  
1578 winter, we did not apply HCl data offsets in the lower stratosphere for the 65°S through 85°S  
1579 bins from June through September and for pressures larger than or equal to 15 hPa. For  
1580 vertical continuity purposes, we applied this method to all lower stratospheric pressure levels,  
1581 although the small negative merged values only occurred in a small fraction of cases.
- 1582 - As Aura MLS and ACE-FTS data exist in the 85°N and 85°S bins, but there are no HALOE  
1583 measurements, we simply extended the offsets from the adjacent bins (at 75°N and 75°S) to  
1584 these two bins to obtain a merged record after 2004 that exhibits continuity versus latitude.
- 1585 - At 100 hPa, we used HCl offsets from the 5°S bin for the 5°N bin, as there was insufficient  
1586 data from the combined data in the latter bin to calculate meaningful offsets. This procedure  
1587 seems reasonable, given that the time series in these two adjacent tropical latitude bins  
1588 (during years outside the 2004/2005 overlap period) look continuous and stable enough to  
1589 justify identical adjustments in both bins and to avoid a data gap in the merged series at 5°N.

1590

1591 **A.3.2. H<sub>2</sub>O**

- 1592 - The vertical data range for valid H<sub>2</sub>O merged values is between 0.01 hPa and 147 hPa  
1593 (inclusive). While H<sub>2</sub>O data exist at 147 hPa for low latitudes, more careful work would be  
1594 needed to extend the merged data globally in such a region.

- 1595 - Users should keep in mind the PMC-related caveats mentioned in Sect. 4 for summer at high  
1596 latitudes in the upper mesosphere, prior to the end of the HALOE dataset (Nov. 2005).
- 1597 - As for HCl, we could not use our standard merging procedure at the two most poleward  
1598 latitude bins; we simply extended the offsets from the adjacent bins (at 75°N and 75°S) to  
1599 these polar bins to obtain a merged record after 2004 that exhibits continuity versus latitude.
- 1600 - Also as for HCl, at 100 hPa, we used H<sub>2</sub>O offsets from the 5°S bin for the 5°N bin, as there  
1601 was insufficient data from the combined datasets in the latter bin to calculate meaningful  
1602 offsets and merge the datasets. This procedure avoids a data gap in the merged series at 5°N.

### 1603 **A.3.3. O<sub>3</sub>**

- 1604 - The vertical range for valid O<sub>3</sub> merged data is from 0.2 hPa to 215 hPa (inclusive), with the  
1605 lower altitude bound varying with latitude; the merged product at 147 and 215 hPa has valid  
1606 data only for the 35° to 85° latitude bins, with values mostly larger than ~ 0.1 ppmv. The  
1607 upper troposphere is more of a merging challenge, given smaller abundances, more difficult  
1608 measurements, and a larger impact from different instrument resolutions. Also, while we  
1609 suggest (see main text) that GOZCARDS merged ozone data should not be subject to a large  
1610 impact from diurnal variations, the highest altitude region should be treated with caution.
- 1611 - SAGE I monthly mean source data are used for the merged dataset in the tropical bins (25°S  
1612 to 25°N) from 1 through 68 hPa only and, at higher latitudes, from 1 through 100 hPa only.
- 1613 - We omitted the use of UARS MLS at 100 hPa for low latitudes (from 25°S to 25°N), as these  
1614 monthly values are biased quite high and also exhibit too large a seasonal cycle amplitude, in  
1615 comparison to HALOE and SAGE II data; this appears to relate to a UARS MLS artifact.
- 1616 - Since there is no (monthly) overlap between SAGE II and HALOE versus UARS MLS or  
1617 Aura MLS in the 85°N and 85°S latitude bins, the same offsets as for 75°N and 75°S  
1618 (respectively) are applied for these bins, in order to minimize discontinuities.
- 1619 - Because of discontinuities that appeared in merged O<sub>3</sub> at high latitudes above the stratopause,  
1620 particularly in the 75°S bin, we flagged merged values for 75° and 85° (N and S) as bad, for  
1621 pressures less than 1 hPa. This issue could be the result of a few bad data points or not  
1622 enough data overlap. To minimize artifacts, we left the resolution of this issue for future  
1623 investigations; also, the reduced amount of occultation data at these high latitudes makes the

1624 usefulness of a merged product with poorly sampled seasonal changes somewhat marginal  
1625 (for certain years at least, the number of monthly values drops significantly at high latitudes).  
1626  
1627

1628 **Table 1.** Characteristics of instrument datasets used to create GOZCARDS ESDRs (version ev1.01).

<b>Instrument and Data Versions</b>	<b>Platform</b>	<b>Type of measurement</b>	<b>Time period (GOZCARDS source files)</b>	<b>Vertical Resolution (km)</b>	<b>Retrieved quantity and stratospheric vertical grid spacing</b>
SAGE I V5.9_rev O <sub>3</sub>	AEM-2	Solar occultation VIS/UV and near-IR	Feb. 1979 - Nov. 1981	1	Density on altitude grid 1 km spacing
SAGE II V6.2 O <sub>3</sub>	ERBS	Solar occultation VIS/UV and near-IR	Oct. 1984 - Aug. 2005	0.5 - 1	Density on altitude grid 0.5 km spacing
HALOE V19	UARS	Solar occultation mid-IR	Oct. 1991 - Nov. 2005	2.5	Volume Mixing Ratio on pressure grid with 30 levels per decade (LPD) change in p
MLS V5 O <sub>3</sub> V6 H <sub>2</sub> O	UARS	Limb emission microwave / sub-mm	Oct. 1991 - June 1997 (May 1993 end for strat. H <sub>2</sub> O)	<b>H<sub>2</sub>O</b> 3 - 4 (strat.) 5 - 12 (mes.)  <b>O<sub>3</sub></b> 3.5 - 5 (strat.) 5 - 8 (mes.)	Volume Mixing Ratio on pressure grid with 6 LPD in stratosphere  6 LPD in stratosphere
ACE-FTS V2.2 (V2.2 update for O <sub>3</sub> )	SCISAT	Solar occultation mid-IR	Mar. 2004 through Sep. 2010 (2009 for O <sub>3</sub> )	3 - 4	Volume Mixing Ratio on 1 km grid spacing (height and p provided)
MLS V3.3 V2.2 O <sub>3</sub>	Aura	Limb emission microwave / sub-mm	Aug. 2004 through 2012	<b>HCl</b> 3 - 5  <b>H<sub>2</sub>O</b> 3 - 4 (p > 0.1 hPa) 5 - 9 (0.1-0.01 hPa)  <b>O<sub>3</sub></b> 3	Volume Mixing Ratio on pressure grid with 6 LPD  12 LPD  6 LPD

1630 **Table 2.** Products and instrument source data making up the available GOZCARDS data records.

<b>Merged Products</b> and pressure range	<b>Source Datasets</b> (and years used)
<b>HCl</b> 147 – 0.5 hPa	HALOE (1991-2005), ACE-FTS (2004-2010), Aura MLS (2004 onward) Note: MLS data for p < 10 hPa not used for merged time series
<b>H<sub>2</sub>O</b> 147 – 0.01 hPa	HALOE (1991-2005), UARS MLS (1991-1993), ACE-FTS (2004-2010), Aura MLS (2004 onward)
<b>O<sub>3</sub></b> 215 – 0.2 hPa	SAGE I (1979-1981), SAGE II (1984-2005), HALOE (1991-2005), UARS MLS (1991-1997), ACE-FTS (2004-2009), Aura MLS (2004 onward)
<b>HNO<sub>3</sub></b> 215 – 1 hPa	ACE-FTS (2004-2010), Aura MLS (2004 onward)
<b>N<sub>2</sub>O</b> 100 – 0.5 hPa	ACE-FTS (2004-2010), Aura MLS (2004 onward)
<b>Temperature</b> 1000 – 0.015 hPa	GMAO MERRA (1979 onward)

1631

1632

1633

1634

1635

1636

1637

1638

1639 **Table A1.** Data screening procedures and related references used for the source dataset generation.

<b>Instrument</b>	<b>Data Screening Issue / Method</b>	<b>Reference</b>
SAGE I (O <sub>3</sub> )	Aerosol interference issue: Remove values at altitudes below which the 1 μm extinction > 10 <sup>-3</sup> km <sup>-1</sup> .	L. Thomason (personal communication, 2012)
SAGE II (O <sub>3</sub> )	Remove entire profile if any error value exceeds 10% of VMR (for 30 to 50 km altitude); this occurred mainly in 1993 & 1994 ("short events").  Use aerosol extinctions and extinction ratios to remove data affected by clouds or by aerosols (from Mt. Pinatubo).  Remove anomalously low values resulting from very small SAGE II transmittances (errors are capped at 300% as a flag).  Remove profiles under high beta angle conditions.	Wang et al. (2002)      See also Wang et al. (1996)
HALOE	Remove cloud-contaminated values. Also remove profiles that may contain artifacts from faulty trip angle or constant lockdown angle registration.  Remove aerosol contamination (O <sub>3</sub> and HCl).	Hervig and McHugh (1999) <a href="http://haloe.gats-inc.com/user_docs/index.php">haloe.gats-inc.com/user_docs/index.php</a>  Bhatt et al. (1999)
UARS MLS	Use screening guidelines based on instrument status, retrieval quality flags, and sign of precision values.	Livesey et al. (2003)
Aura MLS	Use screening guidelines based on instrument status, retrieval quality and convergence flags, and sign of precision values.	Livesey et al. (2013)
ACE-FTS	Remove occultations listed as bad.  Remove data when error value > VMR or error value < 10 <sup>-4</sup> xVMR.  Use a data screening procedure (see Sect. 2.1) to identify and remove the largest outliers.  V2.2 data after Sep. 2010 (2009 for ozone) are not used because of a data processing issue.	<a href="http://databace.scisat.ca/validation/data_issues.php">databace.scisat.ca/validation/data_issues.php</a>  K. Walker (personal communication, 2012)

1641 **Fig. 1.** Merging procedure illustration for HCl. Top left panel shows the HCl monthly mean source data  
1642 during the overlap period (Aug. 2004 - Nov. 2005) for HALOE, ACE-FTS, and Aura MLS. Top right  
1643 panel illustrates step 1 in the merging procedure, with the temporary merged data values (orange)  
1644 resulting from the adjustment of ACE-FTS and Aura MLS values to the mean reference indicated by the  
1645 black dashed line (time mean of co-located ACE-FTS/Aura MLS points). Also, the cyan dashed line is  
1646 the mean of the ACE-FTS points and the red dashed line is the mean of MLS points co-located with  
1647 ACE-FTS. Middle left panel shows step 2 results, namely the merged values arising from merging  
1648 HALOE data with the temporary merged data; the black dashed line is the new average reference value,  
1649 obtained from a 2/3 and 1/3 weighting of the dashed orange (mean of orange points co-located with  
1650 HALOE) and dashed blue line (mean of HALOE) values, respectively. Middle right panel shows all the  
1651 source data and the final merged values during the overlap period. Bottom panel shows the source and  
1652 merged time series from 1991 through 2012 after the calculated additive offsets are applied to the whole  
1653 source datasets, which are then merged (averaged) together wherever overlap between instruments exists.

1654 **Fig. 2.** Offsets applied to the HCl source datasets (top panels for HALOE, middle panels for ACE-FTS,  
1655 bottom panels for Aura MLS) as a function of latitude and pressure. The left column gives offsets in ppbv  
1656 and the right column provides offsets as a percent of the zonal average merged mixing ratios during the  
1657 overlap period (Aug. 2004 – Nov. 2005) used here to compute the average offsets.

1658 **Fig. 3.** Example of HCl time series analyses for 50°N-60°N and 32 hPa. (a) HCl monthly mean source  
1659 data from ACE-FTS and Aura MLS; the MLS dots are filled when there is time overlap with ACE-FTS,  
1660 and open if no such overlap exists. Simple linear fits are shown as colored lines for  
1661 ACE-FTS and for Aura MLS (orange line for all red dots and red line for filled red dots only).  
1662 Correlation coefficient values (R values) for the two time series are provided in the title.  
1663 (b) Deseasonalized anomalies for both ACE-FTS and Aura MLS, with corresponding linear fits (and R  
1664 values). (c) Difference of deseasonalized anomalies (ACE-FTS minus Aura MLS), with linear fit.

1665 **Fig. 4.** Latitude/pressure contours of time series diagnostics obtained from analyses illustrated in  
1666 Fig. 3 for HCl from Aura MLS and ACE-FTS. Top panel: Correlation coefficient for the deseasonalized  
1667 time series. Bottom panel: Ratio of the slope of the difference between deseasonalized series over the  
1668 error in this slope.

1669 **Fig. 5.** Illustration of GOZCARDS HCl monthly averages with systematic error estimates (grey shading)  
1670 at 46 hPa for 30°S-40°S; see text for the meaning of this shaded region. The source data from HALOE,  
1671 Aura MLS, and ACE-FTS are shown in different colors (see legend), along with the merged values.

1672 **Fig. 6.** Systematic error estimates for GOZCARDS HCl. One error (left panels) is relevant for values  
1673 lower than (below) the merged values, and one (right panels) for values larger than the merged values; the

1674 top panels give the error estimates in ppbv, and the bottom panel errors are expressed as percent of the  
1675 average merged values over the relevant time periods (see text). These error bars provide a range within  
1676 which 95% of the source data values lie.

1677 **Fig. 7.** Time series of the GOZCARDS monthly-averaged merged HCl abundance for 3 different latitude  
1678 bin averages (see color legend in panel (a)) for (a) 0.7 hPa, (b) 10 hPa, (c) 32 hPa, and (d) 68 hPa.

1679 **Fig. 8.** The average rate of change (percent per year) for HCl as a function of pressure for different  
1680 latitude bin averages (see legend) for time periods corresponding to the appropriate GOZCARDS HCl  
1681 values (see text) in the upper stratosphere (Jan. 1997 - Sep. 2010) and lower stratosphere (Jan. 1997 -  
1682 Dec. 2012). Deseasonalized monthly data were used to obtain a long-term trend for these time periods;  
1683 two-sigma error bars are shown.

1684 **Fig. 9.** Rates of change for GOZCARDS HCl (connected open circles) are given as a function of latitude  
1685 in 10° latitude bins for sliding 6-year periods centered on Jan. 1 of each year (e.g., the 1998 point is an  
1686 average for data from 1995 through 2000, and the 2011 point is for data from 2008 through 2013). (a) is  
1687 for changes in upper stratospheric HCl at 0.7 hPa and (b) is for the change in the integrated HCl column  
1688 between 68 hPa and 10 hPa. The two additional curves in (a) represent the rates of change in the  
1689 estimated surface total chlorine from NOAA data (green is for a 6-year time shift, and purple for a 7-year  
1690 time shift, to account for transport time to the upper stratosphere); see text for more details. Error bars  
1691 indicate twice the standard errors in the means.

1692 **Fig. 10.** Offsets applied to the H<sub>2</sub>O source datasets as a function of latitude and pressure, similar to  
1693 Fig. 2 for HCl.

1694 **Fig. 11.** Latitude/pressure contours of time series diagnostics for H<sub>2</sub>O from Aura MLS and ACE-FTS;  
1695 this is similar to Fig. 4 for HCl.

1696 **Fig. 12.** A depiction of the “tape recorder” evolution for tropical water vapor abundances from 147 to  
1697 10 hPa for October 1991 through December 2013. This plot was produced from GOZCARDS merged  
1698 H<sub>2</sub>O time series anomalies (differences from the long-term means) for the average of the 4 tropical bins  
1699 covering 20°S to 20°N.

1700 **Fig. 13.** Systematic error estimates for GOZCARDS H<sub>2</sub>O (similar to Fig. 6 for HCl).

1701 **Fig. 14.** Variations in stratospheric water vapor from the GOZCARDS H<sub>2</sub>O merged data records (1992  
1702 through 2013) averaged from (a) 60°S to 60°N and (b) 20°S to 20°N. Monthly average values and annual  
1703 averages are shown by thin and thick lines (connecting similarly-colored dots), respectively, for the  
1704 pressure levels indicated in the plot legend.



1705 **Fig. 15.** Stratospheric water vapor variability on decadal timescales for 1992 through 2013 for tropical  
1706 (20°S-20°N in black) and mid-latitude (20°N-60°N in red and 20°S-60°S in blue) zonal means, based on  
1707 the GOZCARDS merged H<sub>2</sub>O data record. The variability is expressed here as the difference between  
1708 maximum and minimum annual average abundances, from 100 to 1 hPa, in ppmv (left panel) and percent  
1709 (right panel).

1710 **Fig. 16.** (a) Variations in upper mesospheric (0.01 hPa) water vapor mixing ratios averaged from 60°S to  
1711 60°N for Oct. 1991 through Dec. 2013, based on the GOZCARDS merged H<sub>2</sub>O data records. Monthly  
1712 average values and annual averages are shown by connected brown dots and connected black dots,  
1713 respectively. (b) GOZCARDS merged H<sub>2</sub>O annual averages (connected filled symbols) from 60°S to  
1714 60°N for 1992 through 2013 at pressure levels between 0.1 and 0.01 hPa. A time series of annually-  
1715 averaged Lyman  $\alpha$  solar flux values (open circles), scaled to arbitrary units, is also displayed (see text).

1716 **Fig. 17.** Time series of monthly zonal mean O<sub>3</sub> for 10°S - 20°S between 1 hPa and 6.8 hPa (with pressure  
1717 values given by "pre") from SAGE I, SAGE II, HALOE, UARS MLS, Aura MLS, and ACE-FTS, all  
1718 color-coded following the legend in top left panel.

1719 **Fig. 18.** Schematic diagram describing the creation of the merged GOZCARDS monthly zonal mean  
1720 ozone data record from various satellite datasets. Instruments represented in red inside the boxes are used  
1721 as a reference. Instruments whose measurements have already been adjusted to a reference are indicated  
1722 with a "\*" superscript. AMLS refers to Aura MLS and UMLS to UARS MLS. See text for more details.  
1723

1724 **Fig. 19.** Offsets applied to the O<sub>3</sub> source datasets, similar to Fig. 2 for HCl.

1725 **Fig. 20.** Latitude/pressure contours of time series diagnostics for O<sub>3</sub> from Aura MLS and ACE-FTS; this  
1726 is similar to Fig. 4 for HCl. The correlation coefficients (R values) and slope trend diagnostics are  
1727 provided for HALOE versus SAGE II in the top two panels (for 1993-1999 as the trend issue for  
1728 converted SAGE II data occurs after mid-2000 and to avoid Pinatubo-related data gaps before 1993) and  
1729 for ACE-FTS versus Aura MLS in the bottom two panels (for 2005-2009).

1730 **Fig. 21.** Systematic error estimates for GOZCARDS O<sub>3</sub> (similar to Fig. 6 for HCl).

1731 **Fig. 22.** Near-global (60°S to 60°N) results for average column ozone (total and stratospheric, from  
1732 *Ziemke and Chandra, 2012*) compared to GOZCARDS O<sub>3</sub> columns above 68 hPa. Stratospheric columns  
1733 are offset to better match the total column values, in order to more easily compare relative variations

1734 versus time; the black dots and red crosses are referenced to the 1980 total column values, while the cyan  
1735 curves are referenced to 2007 to better illustrate the fits in the later years.

1736 **Fig. 23.** Time evolution (Aug. 2004 through 2012) versus latitude of GOZCARDS merged N<sub>2</sub>O (ppbv) at  
1737 (a) 6.8 hPa and (b) 100 hPa.

1738 **Fig. 24.** Sample results display the time evolution of satellite-retrieved HNO<sub>3</sub> (ppbv) for two different  
1739 periods, 1992-1997 in (a) and (c) versus 2004-2013 in (b) and (d). Panels (a) and (b) are contour plots at  
1740 46 hPa from UARS MLS global data and the merged GOZCARDS global data after 2004, respectively;  
1741 (c) and (d) show time series at 32 hPa and for the 40°N-50°N latitude bin, with (a) from UARS MLS data,  
1742 and (d) from ACE-FTS, Aura MLS, and the merged combination (between the two source data sets).

1743 **Fig. A1.** Illustration of the standard deviations (in (a)) and standard errors (in (b)) for monthly mean  
1744 GOZCARDS HCl (source and merged records) at 46 hPa for 30°S-40°S. Source data from HALOE, Aura  
1745 MLS, and ACE-FTS are given by the filled colored dots (see legend); each standard deviation is simply  
1746 obtained from the range of values measured during the month. The large open brown circles give standard  
1747 deviations for the merged HCl product; this Appendix provides the formulae to calculate these quantities.

1748

1749 **Fig. S1:** Illustration of the latitudinal dependence of the HCl offsets for HALOE, ACE-FTS, and Aura  
1750 MLS at two pressure levels (top panel for 0.46 hPa, bottom panel for 46 hPa). Error bars represent twice  
1751 the standard error in the derived offsets (based on variability during the overlapping period). Larger  
1752 standard error values indicate that there were either fewer points of overlap or larger offset variability  
1753 (standard deviations); we found that both of these factors contribute.

1754 **Fig. S2:** Latitude/pressure contours of the fitted mean annual amplitudes (ppbv) from HCl time series for  
1755 HALOE, ACE-FTS, and Aura MLS, based on their respective measurement periods (see text).

1756 **Fig. S3:** Time evolution (Oct. 1991 through 2013) versus latitude of GOZCARDS merged HCl (ppbv) at  
1757 46 hPa.

1758 **Fig. S4:** HALOE sunrise measurements of H<sub>2</sub>O versus the 3.46 μm extinction coefficient for 1992, 1993,  
1759 and 1999 at 22 hPa. The green vertical line represents the aerosol extinction value ( $5 \times 10^{-4} \text{ km}^{-1}$ ) used to  
1760 screen anomalous HALOE H<sub>2</sub>O values. It is apparent that anomalously low H<sub>2</sub>O values occurred in 1992  
1761 when the 3.46 μm aerosol extinction exceeded about  $5 \times 10^{-4} \text{ km}^{-1}$ . These artifacts were confined to 1991  
1762 and 1992; for these years, and for pressure levels at and below 22 hPa, the corresponding H<sub>2</sub>O data values

1763 were excluded. This screening method eliminates about 10% of the global (lower stratospheric)  
1764 measurements in 1992.

1765 **Fig. S5:** Merging procedure illustration for H<sub>2</sub>O at 5°N and 22hPa. This is similar to Fig. 2 (for HCl), but  
1766 an additional step is illustrated for the end of this procedure, whereby stratospheric H<sub>2</sub>O data from UARS  
1767 MLS are adjusted to the early portion of the merged time series that was obtained after the 2<sup>nd</sup> step; this  
1768 adds more coverage (more brown dots in the bottom panel for 1991-1993).

1769 **Fig. S6:** Latitude/pressure contours of the fitted mean annual amplitudes (ppmv) from H<sub>2</sub>O time series for  
1770 HALOE, ACE-FTS, and Aura MLS, based on their respective measurement periods.

1771 **Fig. S7:** Time evolution (Oct. 1991 through 2013) versus latitude of GOZCARDS merged H<sub>2</sub>O (ppmv) at  
1772 3.2 hPa (top panel) and 68 hPa (bottom panel).

1773 **Fig. S8:** Monthly zonal mean ozone differences (%) between SAGE II and (a) HALOE,  
1774 (b) UARS MLS (UMLS for short), (c) Aura MLS (AMLS for short), and (d) ACE-FTS during their  
1775 respective overlap periods. Differences are expressed (in percent) as  $100 \times [(SAGE II - Other) / (Other)]$ .  
1776 Shaded areas indicate negative values.

1777 **Fig. S9:** Monthly zonal mean temperature differences between NCEP (used by SAGE II) and HALOE  
1778 temperatures relative to MERRA for 10°S - 20°S between 1 and 6.8 hPa, per color-coding indicated in  
1779 bottom left panel; “pre” represents the pressure value. From 1 to 2.1 hPa, differences between NCEP and  
1780 MERRA are generally within  $\pm 4K$  before mid-2000. After that time, NCEP temperatures show a sharp  
1781 increase and are systematically higher than MERRA values by 5 to 10K. However, this divergence and  
1782 trend are not seen in HALOE temperatures. NCEP temperatures between 3.2 and 6.8 hPa are smaller than  
1783 MERRA after mid-2000; negative trends (versus MERRA) also occur in the HALOE data at these levels.

1784 **Fig. S10:** Relative trends (K/decade) in zonal mean temperature differences for NCEP – MERRA and  
1785 HALOE – MERRA (color-coded as in Fig. S9) in the upper stratosphere. NCEP temperatures show  
1786 positive trends versus MERRA of  $\sim 2$ -5 K/decade between 2.1 and 1 hPa for all latitudes. However,  
1787 HALOE temperatures show no significant trends versus MERRA, except at 1.5 hPa in the southern  
1788 hemisphere. For pressures between 3.2 and 6.8 hPa, the temperature analyses are not conclusive; although  
1789 NCEP values show negative trends of  $\sim 2$ -3 K/decade versus MERRA, they agree with HALOE.

1790 **Fig. S11:** Mean differences and standard deviations (horizontal bars) between SAGE II and Aura MLS  
1791 ozone in three different latitude bins: 20°S to 60°S (left panel), 20°S to 20°N (middle panel), and 20°N to  
1792 60°N (right panel). Results based on monthly zonal mean and coincident profiles (see text for coincidence  
1793 criteria) during overlap periods are shown in red and blue, respectively. To choose collocated profiles,

1794 coincidence criteria of  $\pm 1^\circ$  in latitude and  $\pm 8^\circ$  in longitude were used; the time difference criterion was  
1795 chosen as 12 hours, but only nighttime measurements from Aura MLS were used.

1796 **Fig. S12:** Latitude/pressure contours of the fitted mean annual amplitudes (ppmv) from O<sub>3</sub> time series for  
1797 SAGE II, HALOE, ACE-FTS, and Aura MLS, based on their respective measurement periods.

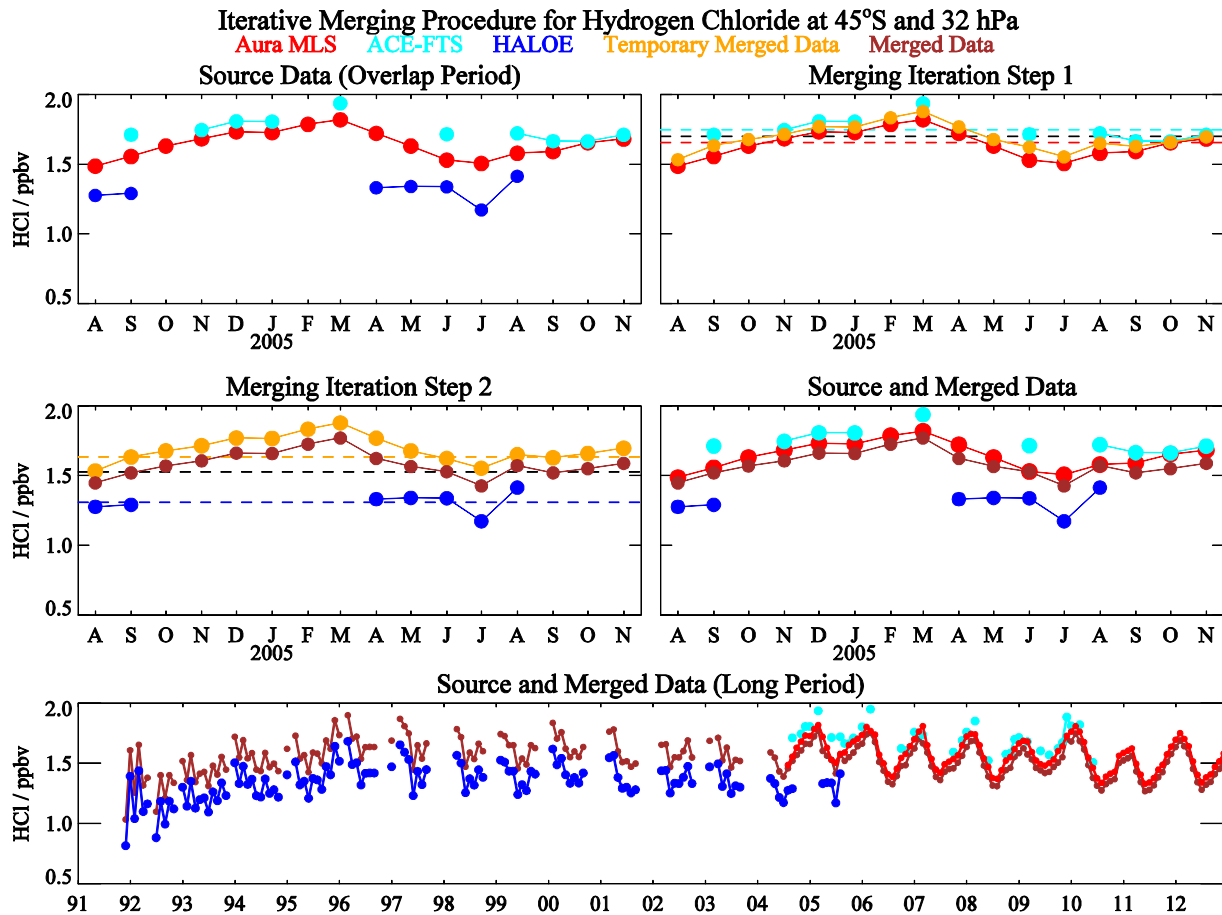
1798 **Fig. S13:** Illustration of the time evolution of the GOZCARDS merged O<sub>3</sub> data field versus latitude at  
1799 68 hPa (top panel) and versus pressure for the 40°N-50°N latitude bin (bottom panel).

1800 **Fig. S14:** Offsets applied to the N<sub>2</sub>O source datasets (top panels for ACE-FTS, bottom panels for Aura  
1801 MLS) as a function of latitude and pressure. The left column gives offsets in ppbv and the right column  
1802 provides offsets as a percent of the zonal average merged mixing ratios during the overlap period (Aug.  
1803 2004 – Sep. 2010) used here to compute the average offsets.

1804 **Fig. S15:** Latitude/pressure contours of time series diagnostics derived from Aura MLS and ACE-FTS  
1805 N<sub>2</sub>O data comparisons (and obtained from analyses similar to those illustrated in Fig. 6 for HCl). Top  
1806 panel: Correlation coefficient for the deseasonalized time series. Bottom panel: Ratio of the slope of the  
1807 difference between deseasonalized series over the error in this slope.

1808 **Fig. S16:** Offsets applied to the HNO<sub>3</sub> source datasets (top panels for ACE-FTS, bottom panels for Aura  
1809 MLS) as a function of latitude and pressure. The left column gives offsets in ppbv and the right column  
1810 provides offsets as a percent of the zonal average merged mixing ratios during the overlap period (Aug.  
1811 2004 – Sep. 2010) used here to compute the average offsets.

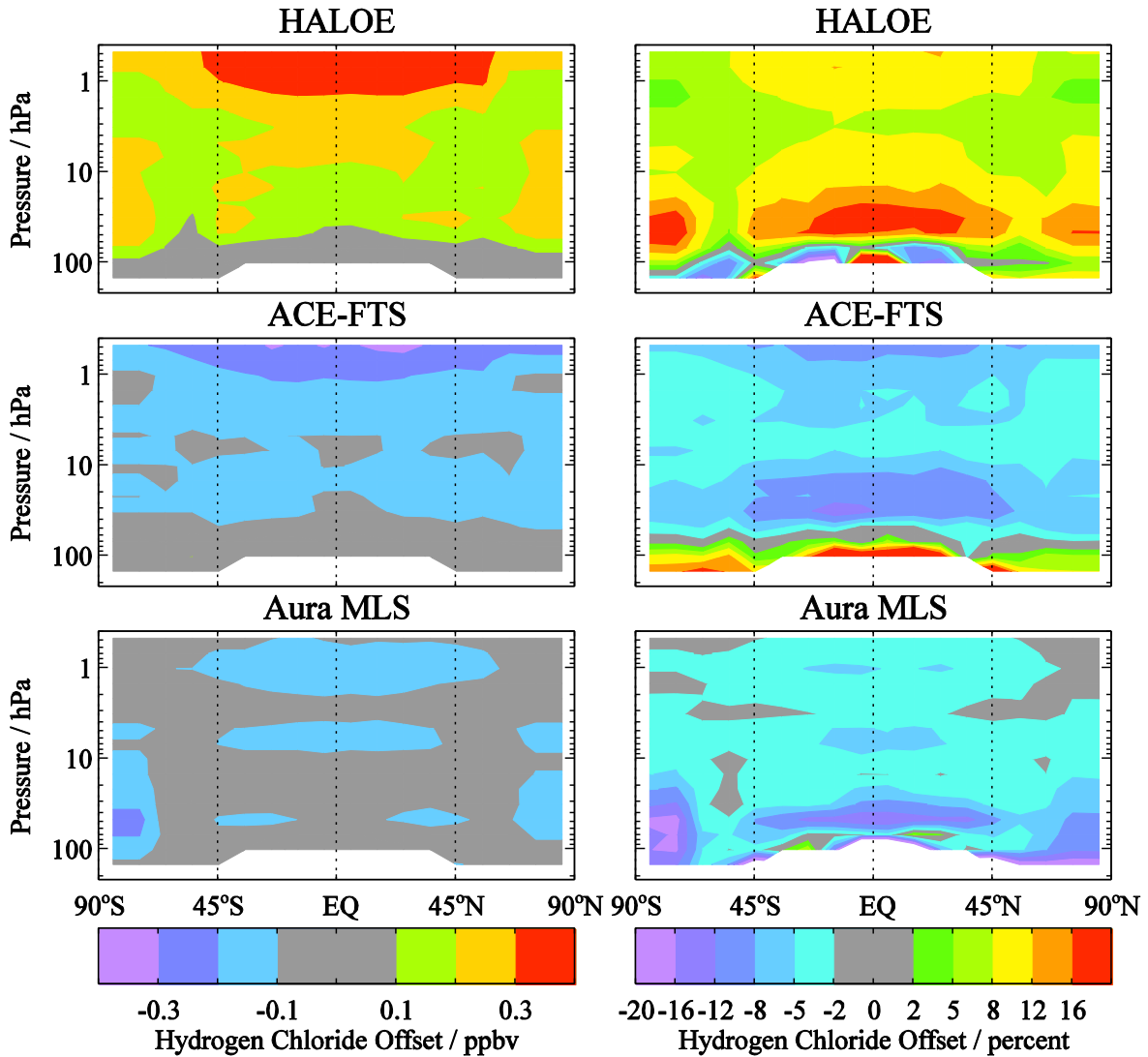
1812 **Fig. S17:** Latitude/pressure contours of time series diagnostics derived from Aura MLS and ACE-FTS  
1813 HNO<sub>3</sub> data comparisons (and obtained from analyses similar to those illustrated in Fig. 6 for HCl). Top  
1814 panel: Correlation coefficient for the deseasonalized time series. Bottom panel: Ratio of the slope of the  
1815 difference between deseasonalized series over the error in this slope.



2

3

4 **Fig. 1.** Merging procedure illustration for HCl. Top left panel shows the HCl monthly mean source data  
 5 during the overlap period (Aug. 2004 - Nov. 2005) for HALOE, ACE-FTS, and Aura MLS. Top right  
 6 panel illustrates step 1 in the merging procedure, with the temporary merged data values (orange)  
 7 resulting from the adjustment of ACE-FTS and Aura MLS values to the mean reference indicated by the  
 8 black dashed line (time mean of co-located ACE-FTS/Aura MLS points). Also, the cyan dashed line is  
 9 the mean of the ACE-FTS points and the red dashed line is the mean of MLS points co-located with  
 10 ACE-FTS. Middle left panel shows step 2 results, namely the merged values arising from merging  
 11 HALOE data with the temporary merged data; the black dashed line is the new average reference value,  
 12 obtained from a 2/3 and 1/3 weighting of the dashed orange (mean of orange points co-located with  
 13 HALOE) and dashed blue line (mean of HALOE) values, respectively. Middle right panel shows all the  
 14 source data and the final merged values during the overlap period. Bottom panel shows the source and  
 15 merged time series from 1991 through 2012 after the calculated additive offsets are applied to the whole  
 16 source datasets, which are then merged (averaged) together wherever overlap between instruments exists.

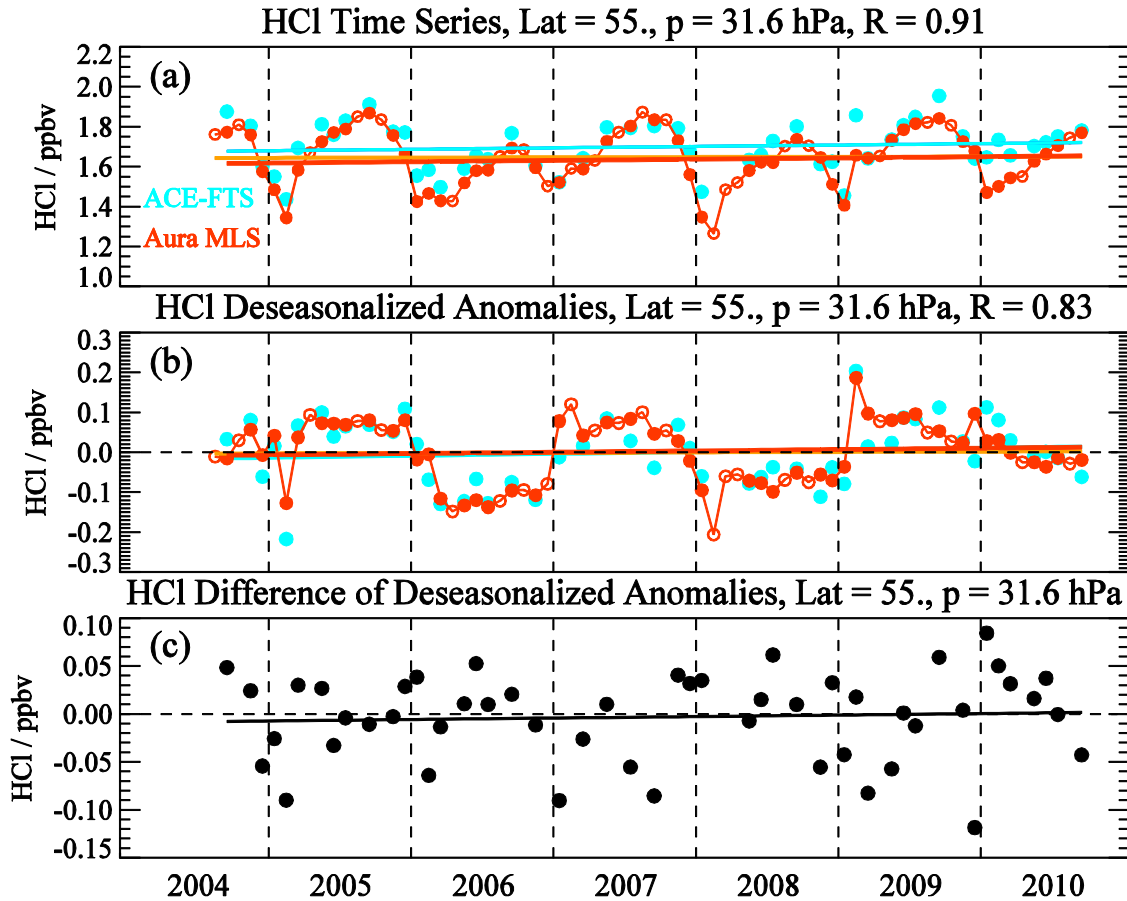


17

18

19 **Fig. 2.** Offsets applied to the HCl source datasets (top panels for HALOE, middle panels for ACE-FTS,  
 20 bottom panels for Aura MLS) as a function of latitude and pressure. The left column gives offsets in ppbv  
 21 and the right column provides offsets as a percent of the zonal average merged mixing ratios during the  
 22 overlap period (Aug. 2004 – Nov. 2005) used here to compute the average offsets.

23



24

25

26

27

28

29

30

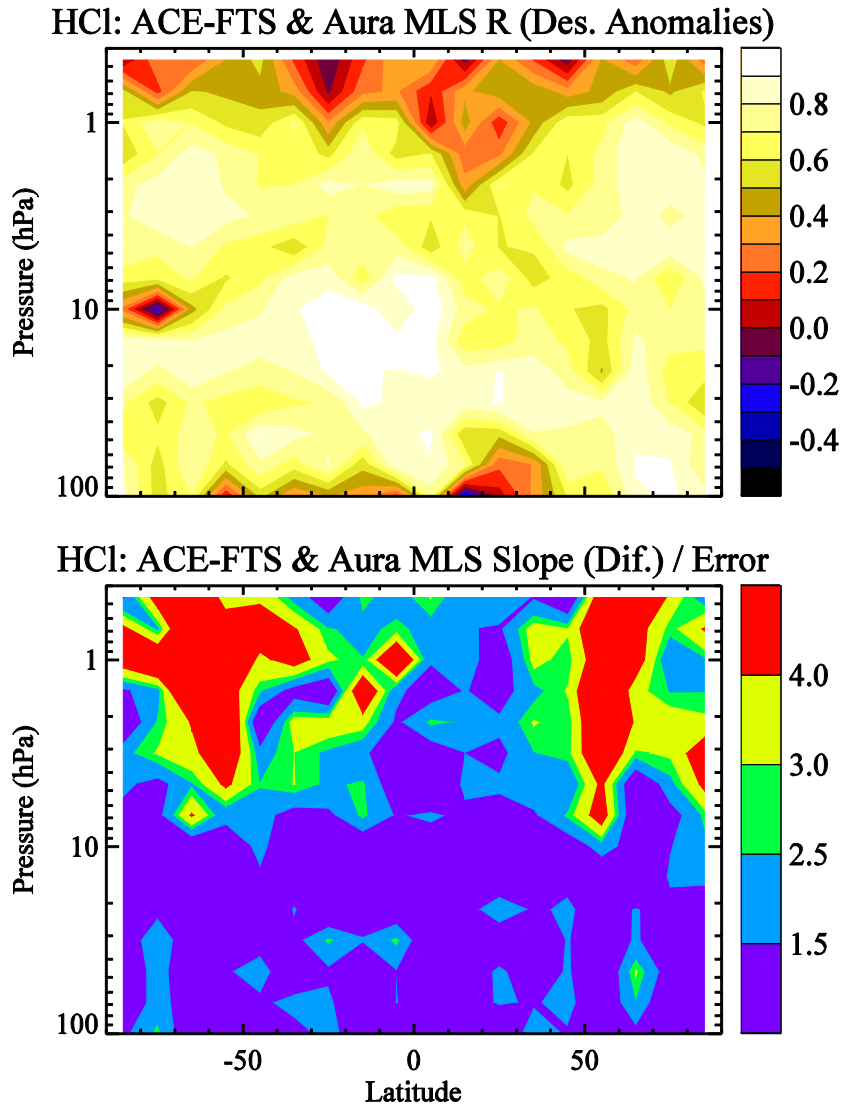
31

32

33

34

**Fig. 3.** Example of HCl time series analyses for 50°N-60°N and 32 hPa. (a) HCl monthly mean source data from ACE-FTS and Aura MLS; the MLS dots are filled when there is time overlap with ACE-FTS, and open if no such overlap exists. Simple linear fits are shown as colored lines for ACE-FTS and for Aura MLS (orange line for all red dots and red line for filled red dots only). Correlation coefficient values (R values) for the two time series are provided in the title. (b) Deseasonalized anomalies for both ACE-FTS and Aura MLS, with corresponding linear fits (and R values). (c) Difference of deseasonalized anomalies (ACE-FTS minus Aura MLS), with linear fit.

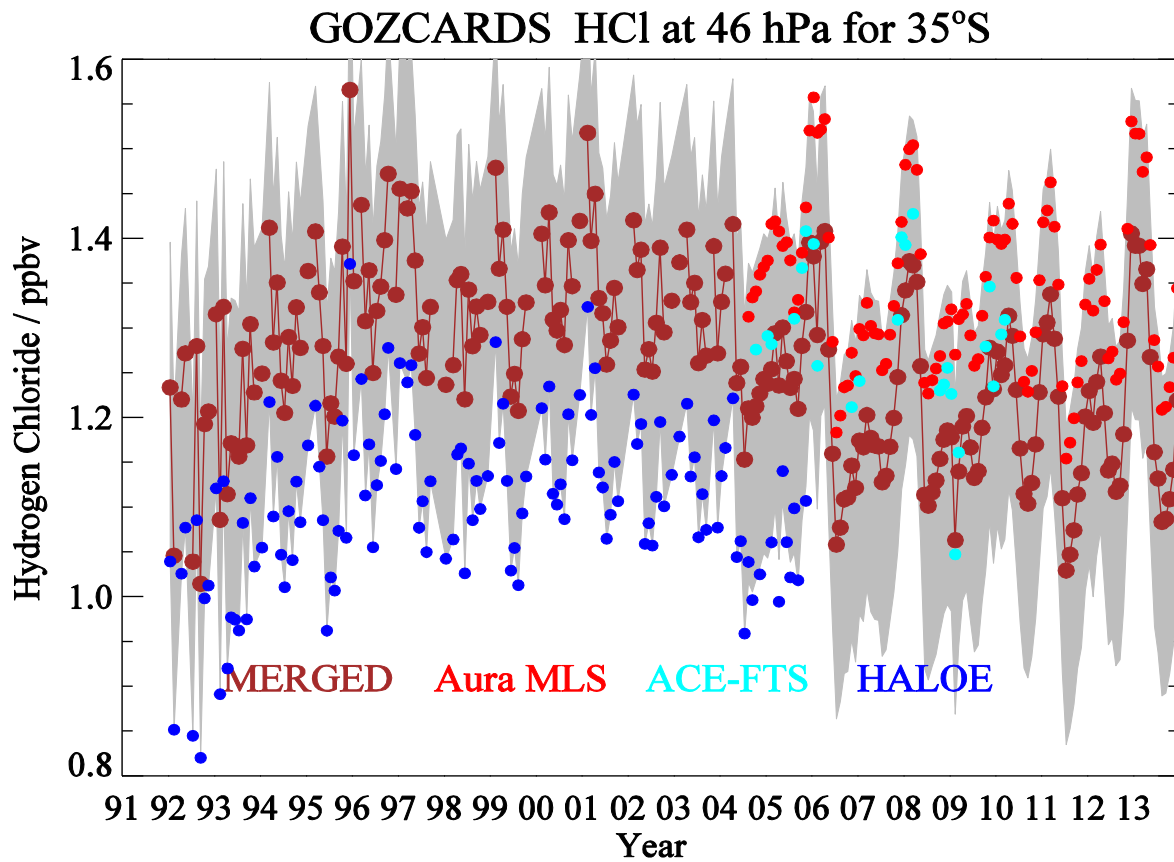


35  
 36 **Fig. 4.** Latitude/pressure contours of time series diagnostics obtained from analyses illustrated in  
 37 Fig. 3 for HCl from Aura MLS and ACE-FTS. Top panel: Correlation coefficient for the deseasonalized  
 38 time series. Bottom panel: Ratio of the slope of the difference between deseasonalized series over the  
 39 error in this slope.

40

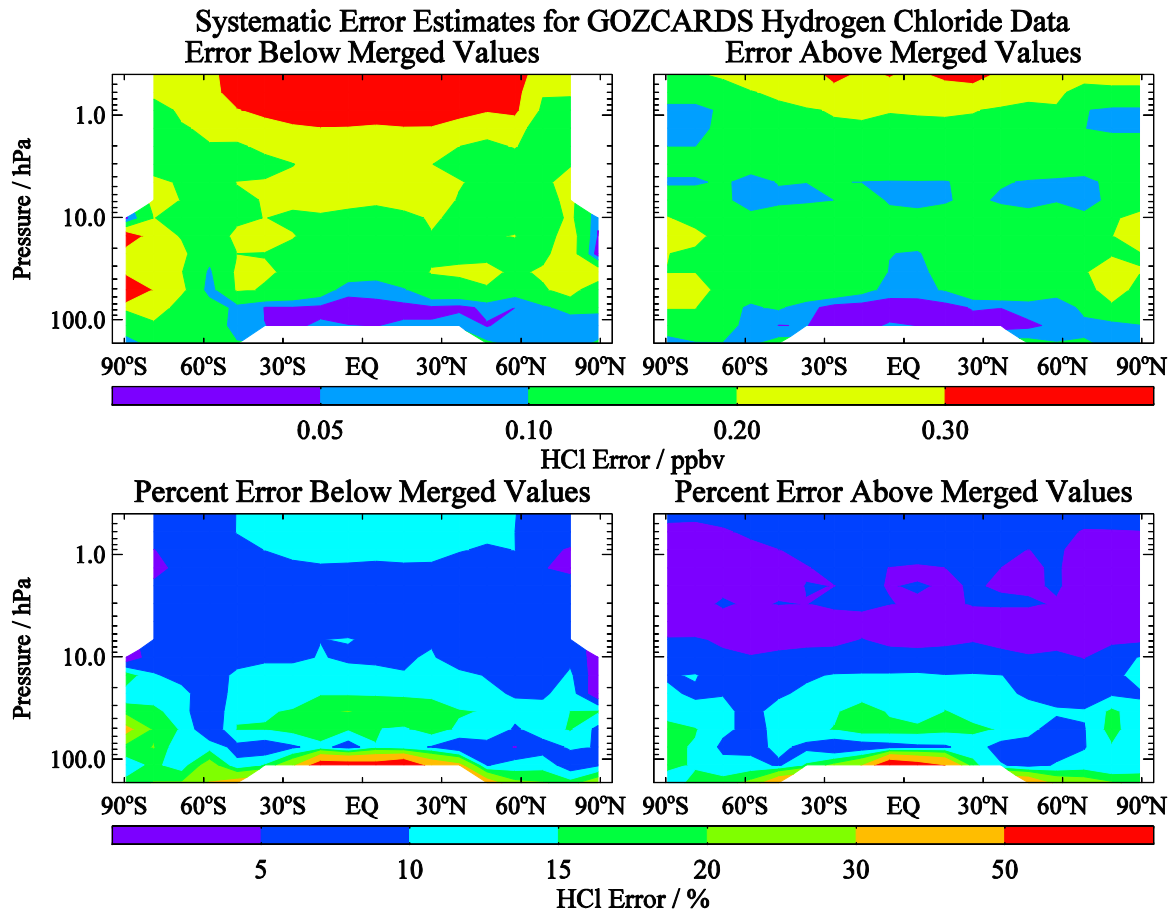
41





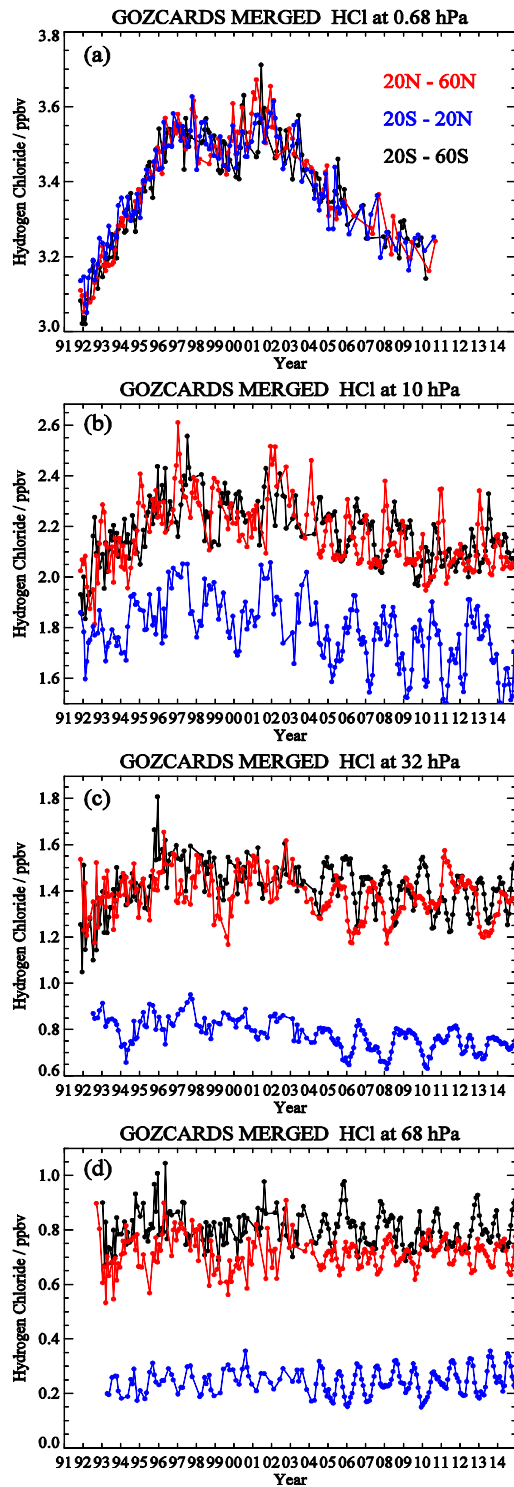
42  
 43  
 44  
 45  
 46  
 47  
 48  
 49  
 50  
 51  
 52  
 53  
 54  
 55  
 56  
 57

**Fig. 5.** Illustration of GOZCARDS HCl monthly averages with systematic error estimates (shown as grey shading) at 46 hPa for 30°S-40°S; see text for the meaning of this shaded region. The source data from HALOE, Aura MLS, and ACE-FTS are shown in different colors (see legend), along with the merged values.



58  
59  
60  
61  
62  
63  
64  
65  
66  
67  
68  
69

**Fig. 6.** Systematic error estimates for GOZCARDS HCl. One error (left panels) is relevant for values lower than (below) the merged values, and one (right panels) for values larger than the merged values; the top panels give the error estimates in ppbv, and the bottom panel errors are expressed as percent of the average merged values over the relevant time periods (see text). These error bars provide a range within which 95% of the source data values lie.

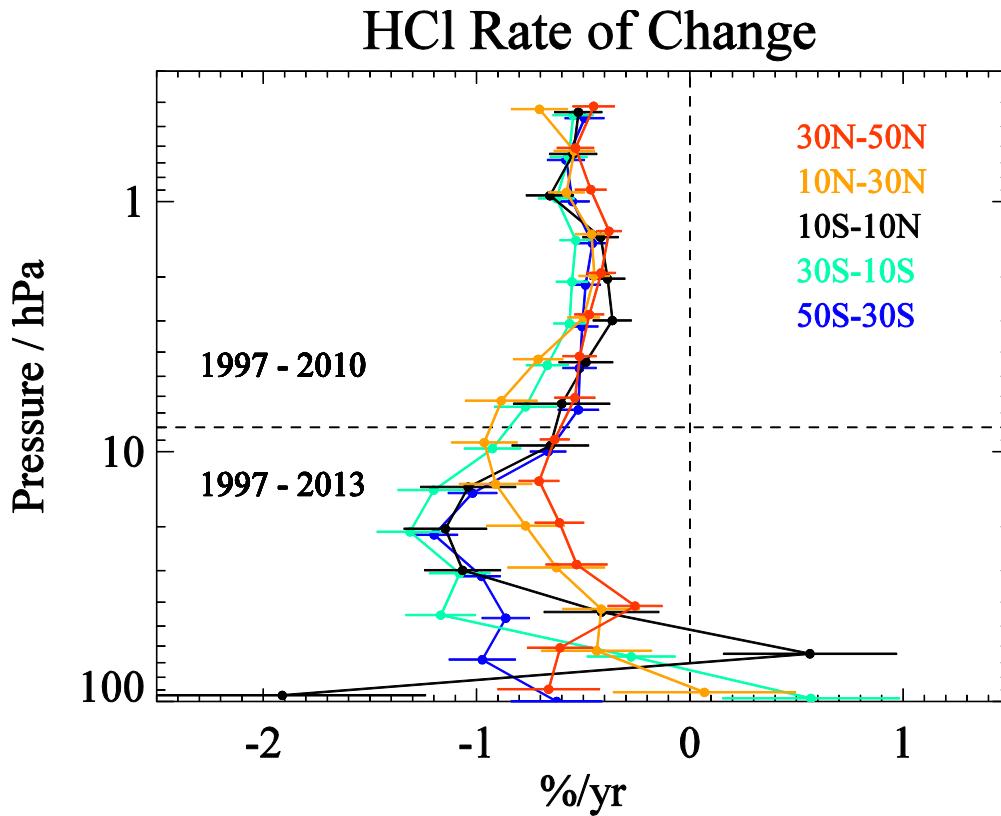


71

72

73 **Fig. 7.** Time series of the GOZCARDS monthly-averaged merged HCl abundance for 3 different latitude

74 bin averages (see color legend in panel (a)) for (a) 0.7 hPa, (b) 10 hPa, (c) 32 hPa, and (d) 68 hPa.



76

77

78 **Fig. 8.** The average rate of change (percent per year) for HCl as a function of pressure for different  
 79 latitude bin averages (see legend) for time periods corresponding to the appropriate GOZCARDS HCl  
 80 values (see text) in the upper stratosphere (Jan. 1997 - Sep. 2010) and lower stratosphere (Jan. 1997 -  
 81 Dec. 2012). Deseasonalized monthly data were used to obtain a long-term trend for these time periods;  
 82 two-sigma error bars are shown.

83

84

85

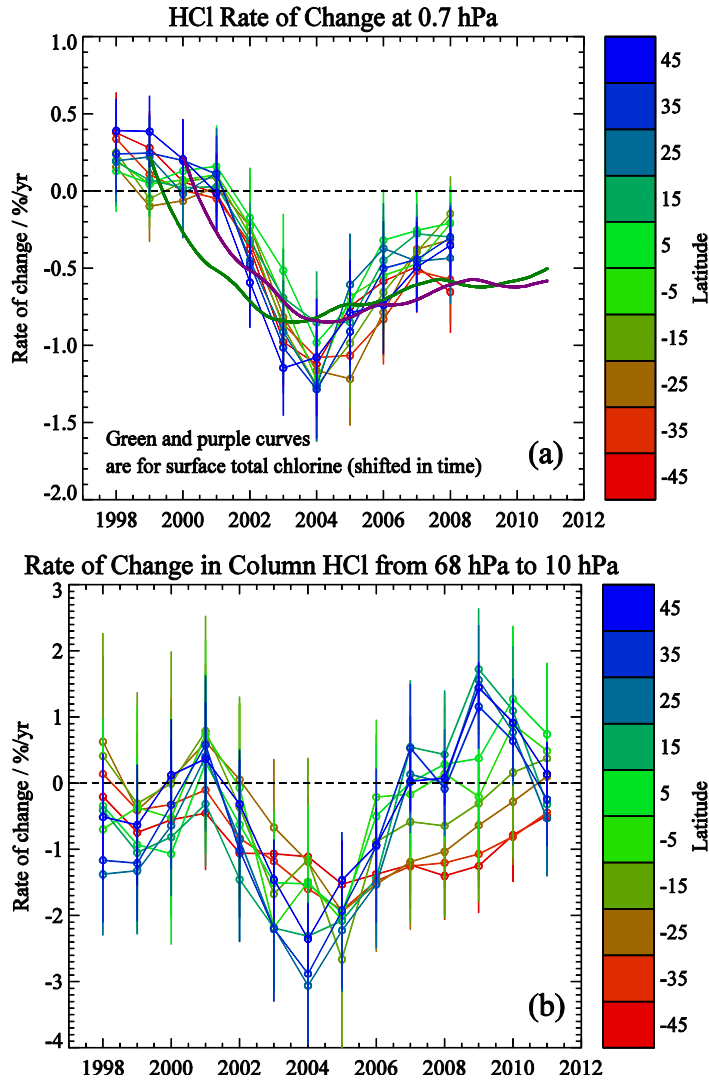
86

87

88

89

90



92

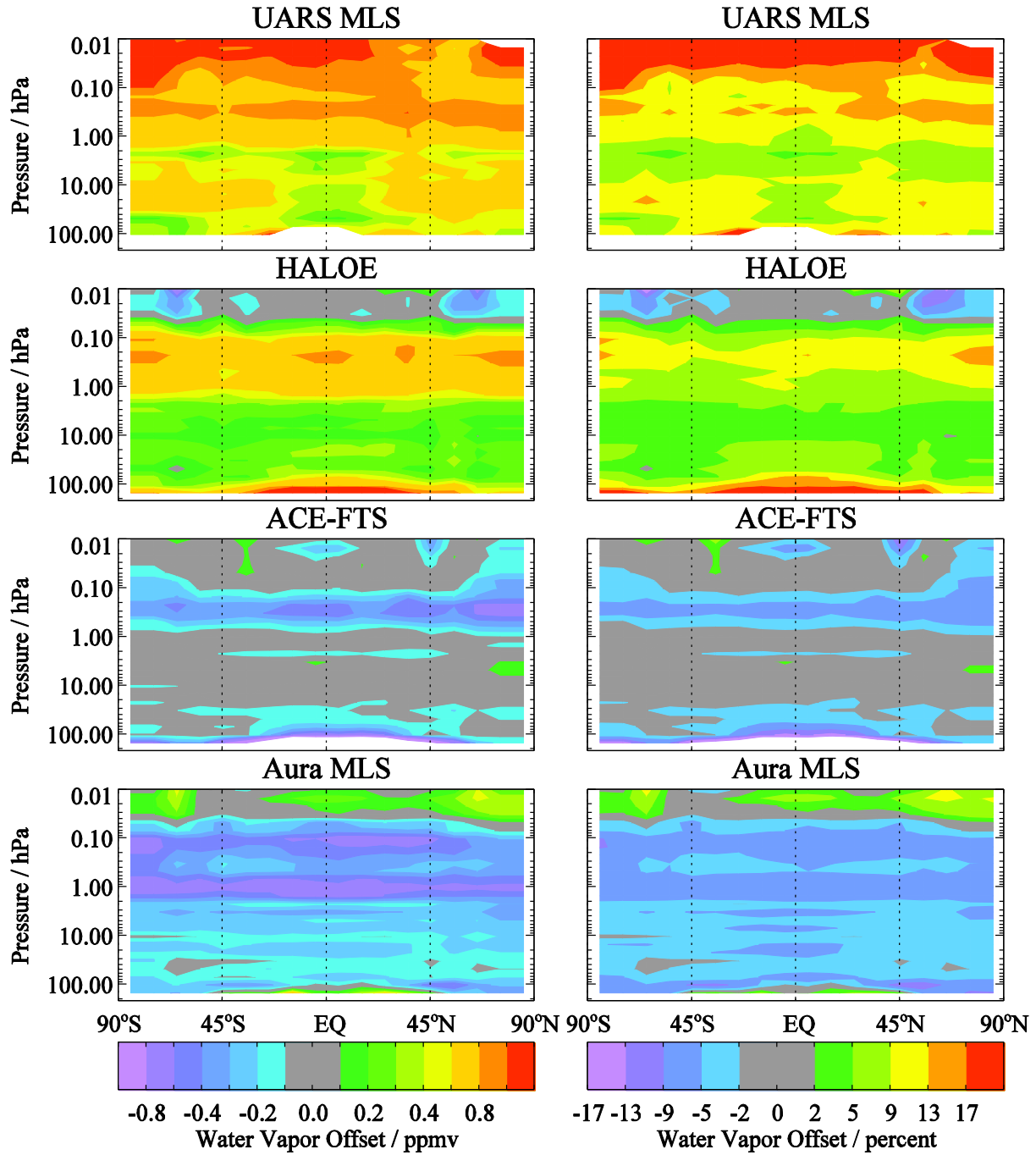
93

94 **Fig. 9.** Rates of change for GOZCARDS HCl (connected open circles) are given as a function of latitude  
 95 in 10° latitude bins for sliding 6-year periods centered on Jan. 1 of each year (e.g., the 1998 point is an  
 96 average for data from 1995 through 2000, and the 2011 point is for data from 2008 through 2013). (a) is  
 97 for changes in upper stratospheric HCl at 0.7 hPa and (b) is for the change in the integrated HCl column  
 98 between 68 hPa and 10 hPa. The two additional curves in (a) represent the rates of change in the  
 99 estimated surface total chlorine from NOAA data (green is for a 6-year time shift, and purple for a  
 100 7-year time shift, to account for transport time to the upper stratosphere); see text for more details. Error  
 101 bars indicate twice the standard errors in the means.

102

103

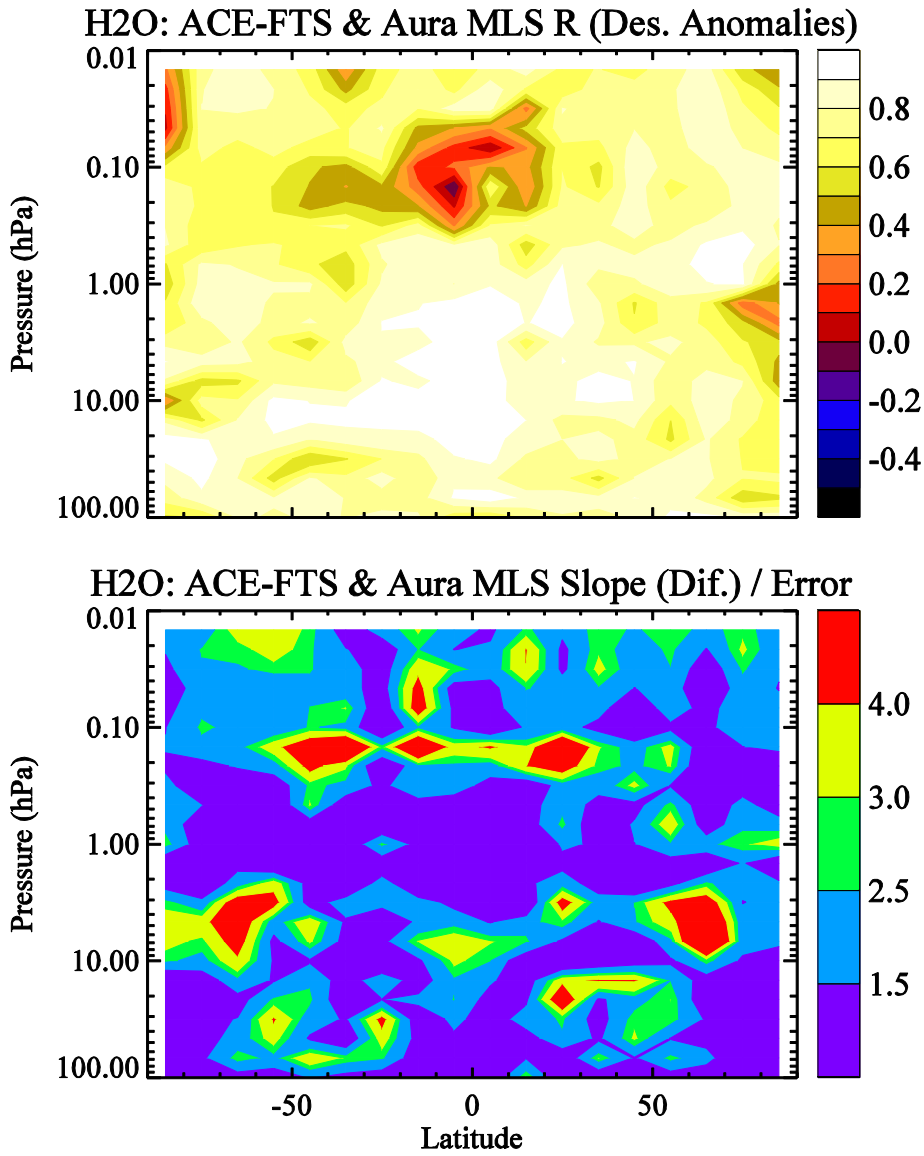
104



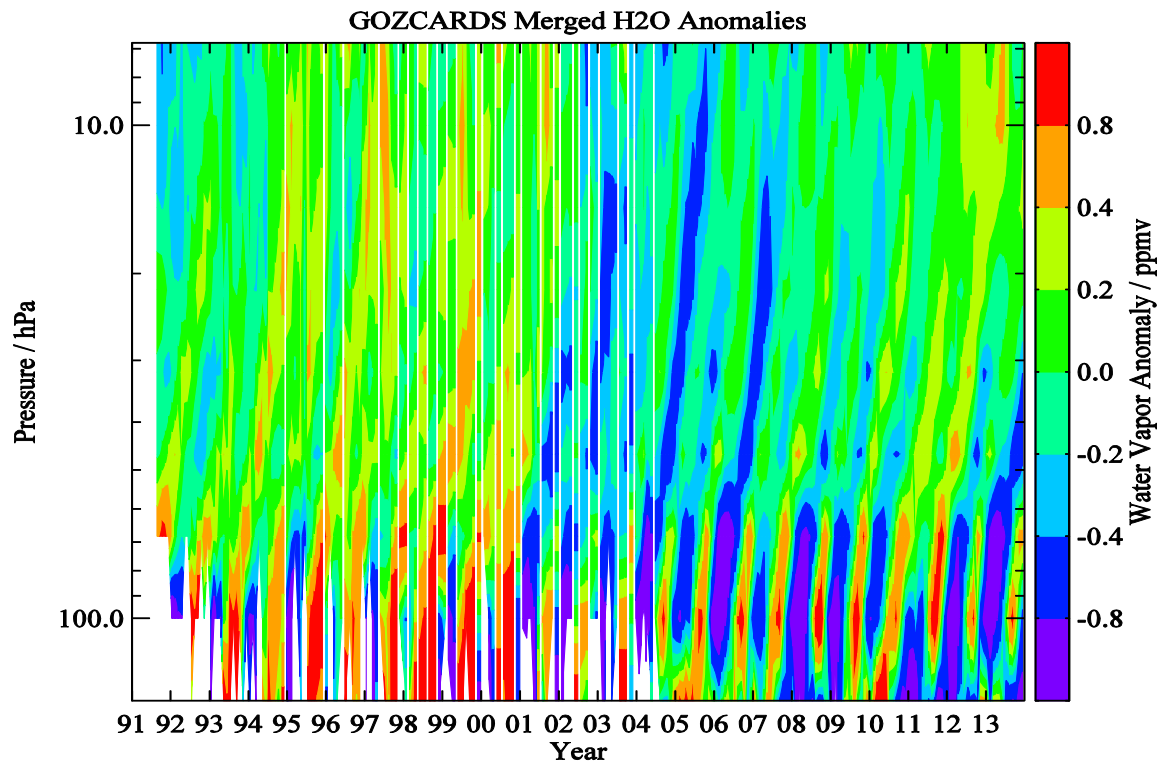
105  
 106  
 107  
 108  
 109  
 110

**Fig. 10.** Offsets applied to the H<sub>2</sub>O source datasets as a function of latitude and pressure, similar to Fig. 2 for HCl.

111  
112  
113



114  
115 **Fig. 11.** Latitude/pressure contours of time series diagnostics for H<sub>2</sub>O from Aura MLS and ACE-FTS;  
116 this is similar to Fig. 4 for HCl.



117

118

119 **Fig. 12.** A depiction of the “tape recorder” evolution for tropical water vapor abundances from 147 to  
120 10 hPa for October 1991 through December 2013. This plot was produced from GOZCARDS merged  
121 H<sub>2</sub>O time series anomalies (differences from the long-term means) for the average of the 4 tropical bins  
122 covering 20°S to 20°N.

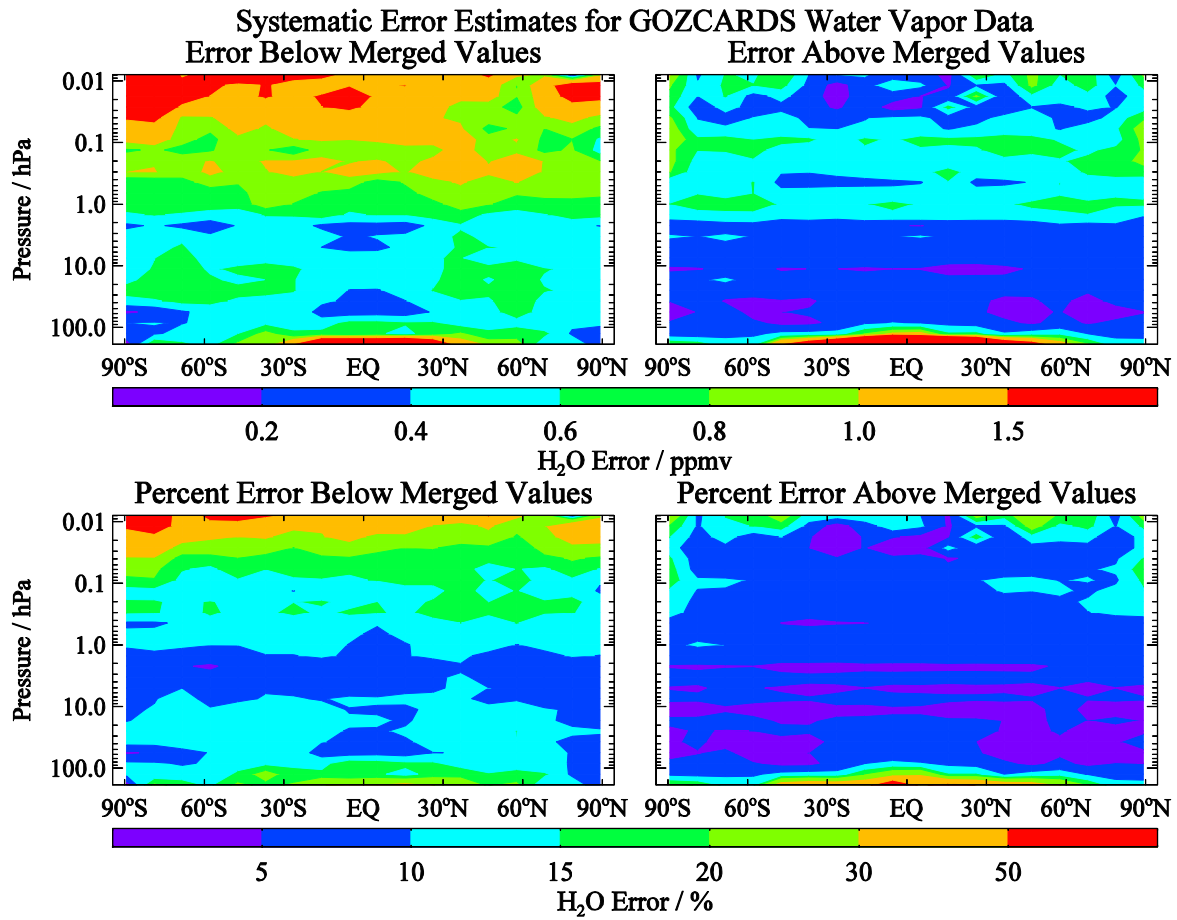
123

124

125

126





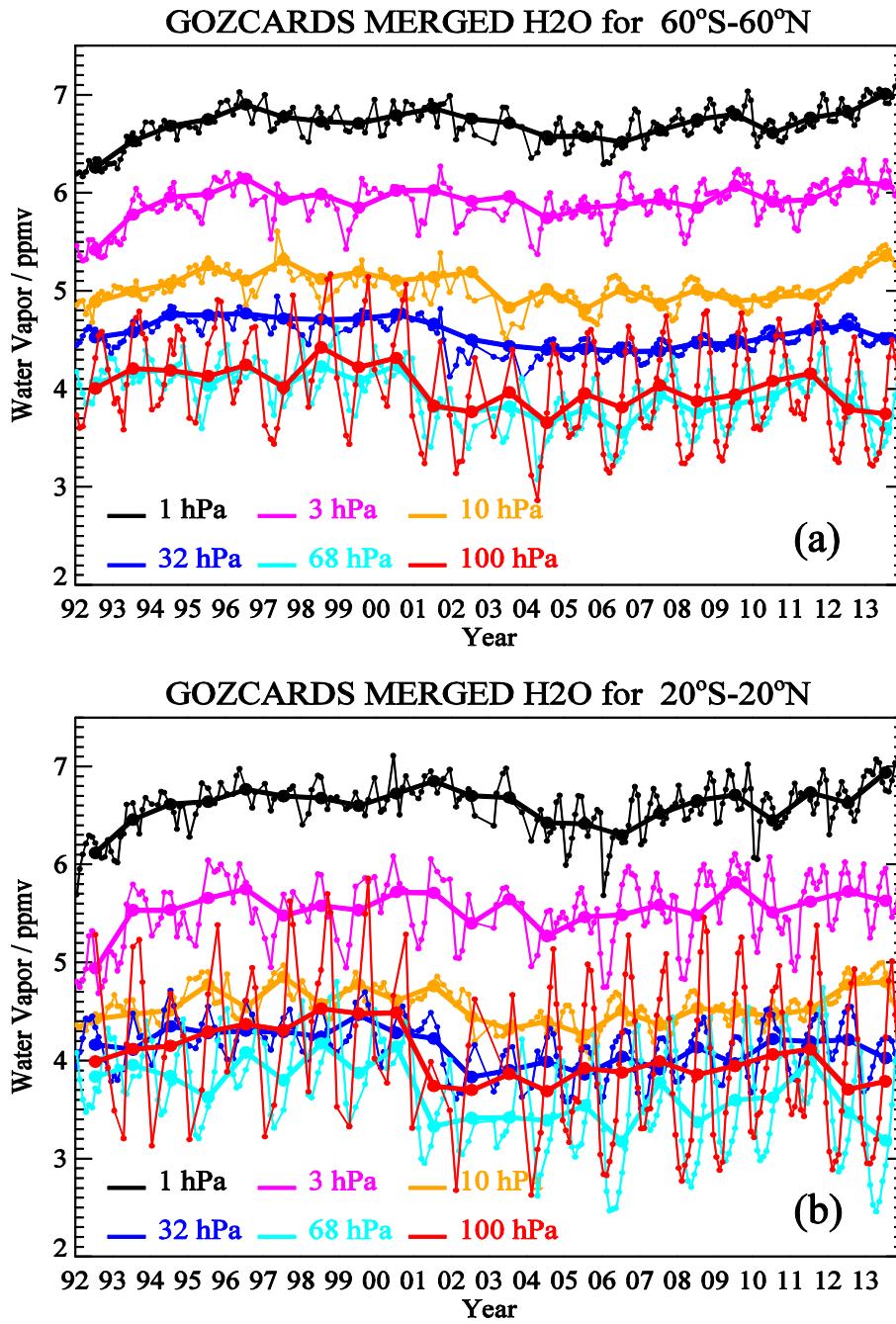
127

128

129 **Fig. 13.** Systematic error estimates for GOZCARDS H<sub>2</sub>O (similar to Fig. 6 for HCl).

130

131



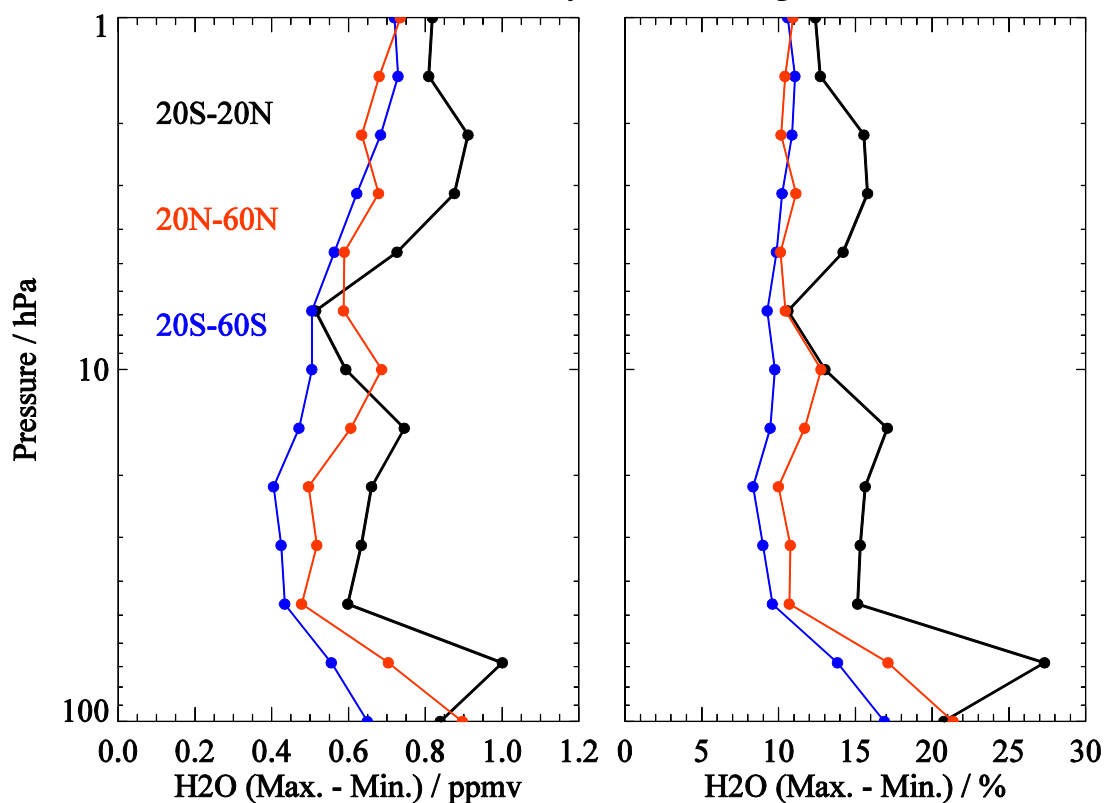
133

134 **Fig. 14.** Variations in stratospheric water vapor from the GOZCARDS H<sub>2</sub>O merged data records (1992  
 135 through 2013) averaged from (a) 60°S to 60°N and (b) 20°S to 20°N. Monthly average values and annual  
 136 averages are shown by thin and thick lines (connecting similarly-colored dots), respectively, for the  
 137 pressure levels indicated in the plot legend.

138

139

### H2O Variability: 1992 through 2013



140

141

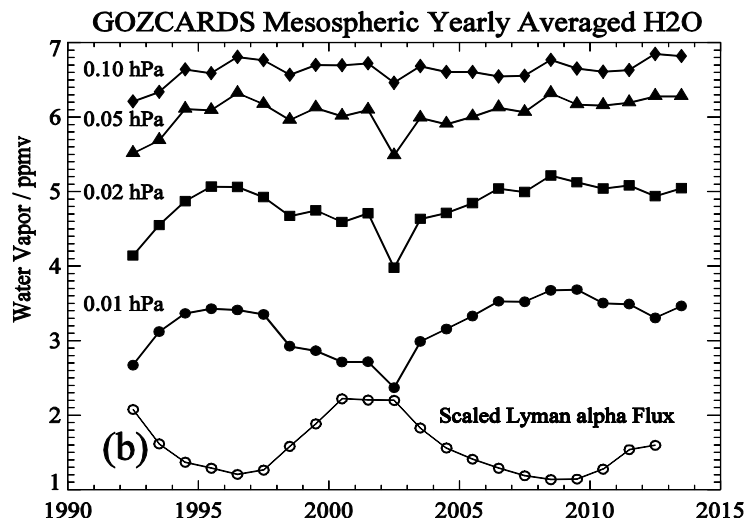
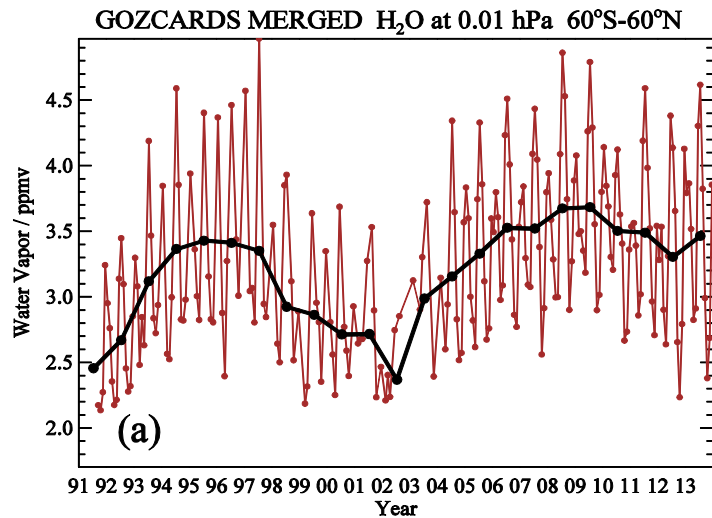
142 **Fig. 15.** Stratospheric water vapor variability on decadal timescales for 1992 through 2013 for tropical  
143 (20°S-20°N in black) and mid-latitude (20°N-60°N in red and 20°S-60°S in blue) zonal means, based on  
144 the GOZCARDS merged H<sub>2</sub>O data record. The variability is expressed here as the difference between  
145 maximum and minimum annual average abundances, from 100 to 1 hPa, in ppmv (left panel) and percent  
146 (right panel).

147

148

149

150



151

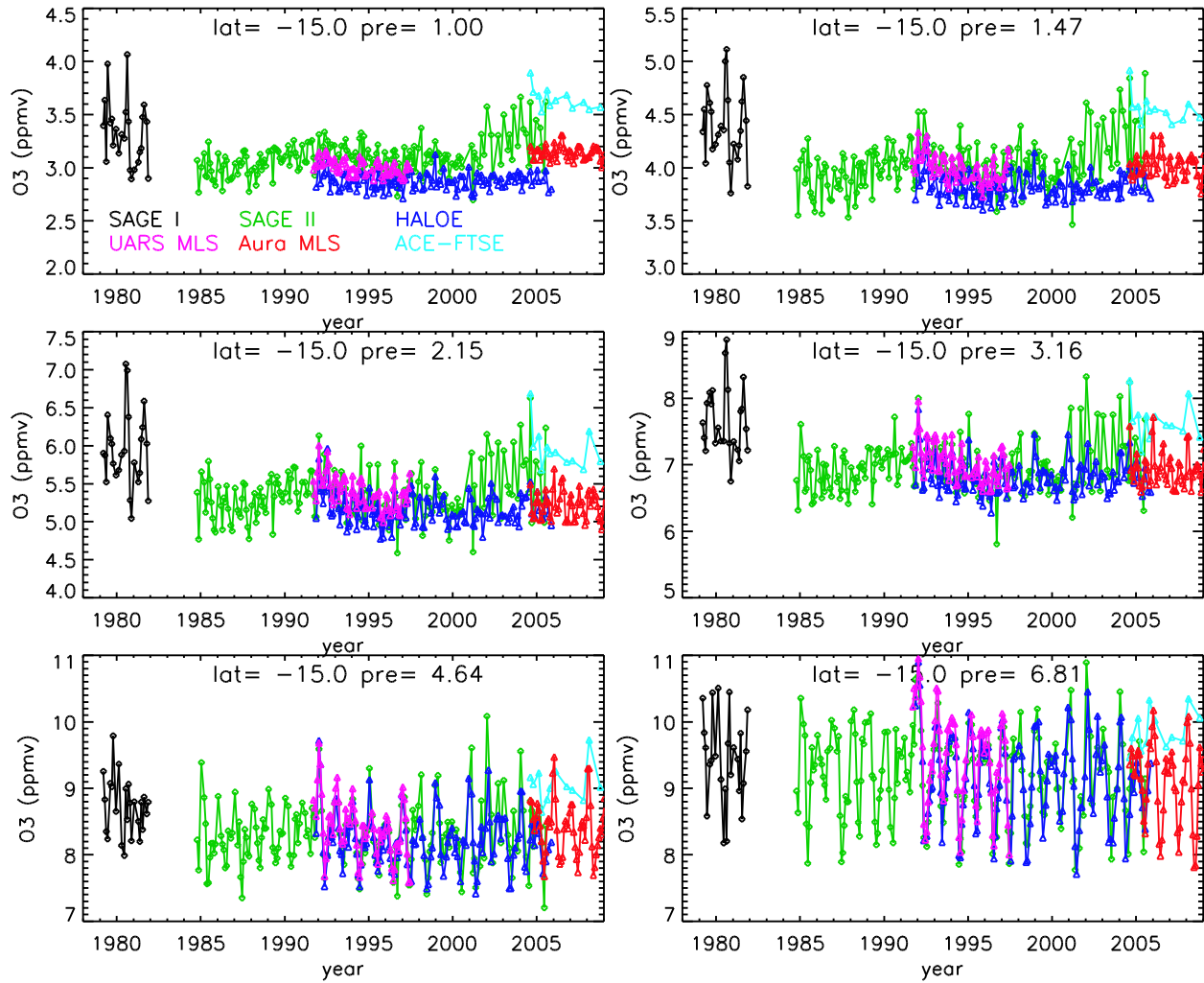
152

153 **Fig. 16.** (a) Variations in upper mesospheric (0.01 hPa) water vapor mixing ratios averaged from 60°S to  
 154 60°N for Oct. 1991 through Dec. 2013, based on the GOZCARDS merged H<sub>2</sub>O data records. Monthly  
 155 average values and annual averages are shown by connected brown dots and connected black dots,  
 156 respectively. (b) GOZCARDS merged H<sub>2</sub>O annual averages (connected filled symbols) from 60°S to  
 157 60°N for 1992 through 2013 at pressure levels between 0.1 and 0.01 hPa. A time series of annually-  
 158 averaged Lyman  $\alpha$  solar flux values (open circles), scaled to arbitrary units, is also displayed (see text).

159

160

161



162

163

164 **Fig. 17.** Time series of monthly zonal mean O<sub>3</sub> for 10°S - 20°S between 1 hPa and 6.8 hPa (with pressure  
 165 values given by "pre") from SAGE I, SAGE II, HALOE, UARS MLS, Aura MLS, and ACE-FTS, all  
 166 color-coded following the legend in top left panel.

167

168

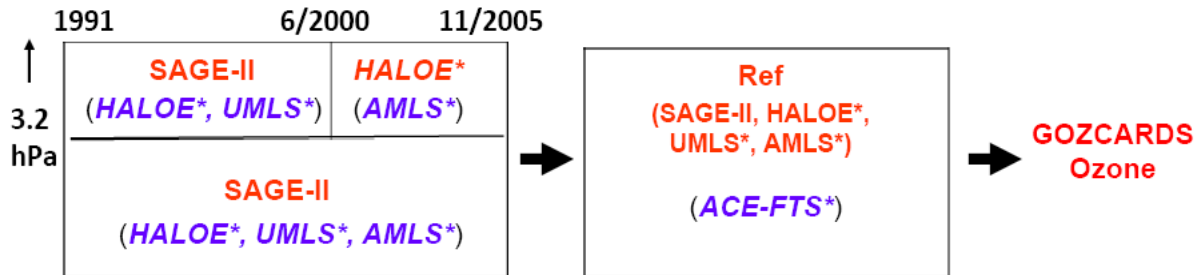
169

170

171

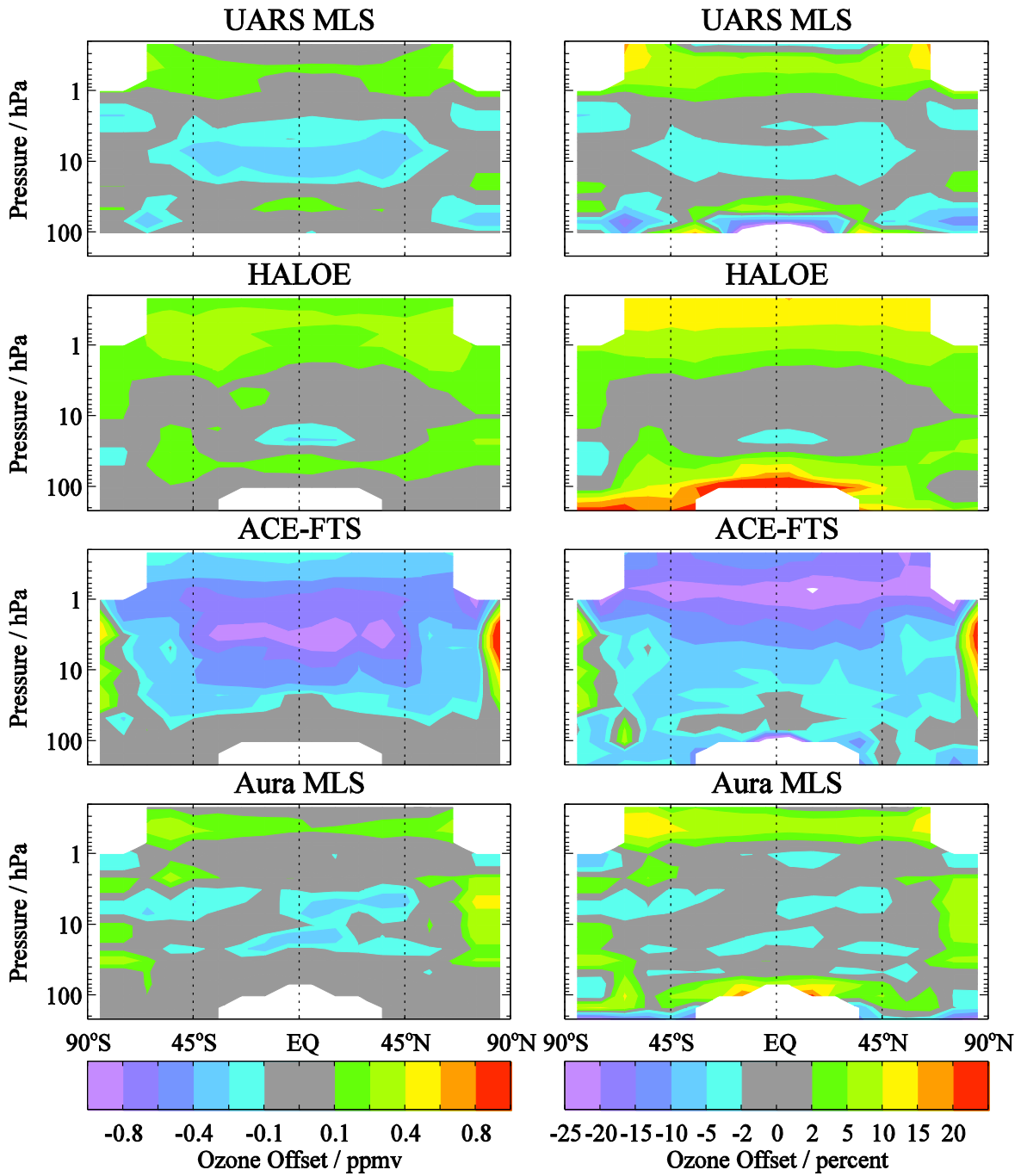
172

173 .  
174  
175



176  
177  
178  
179  
180  
181  
182  
183  
184  
185

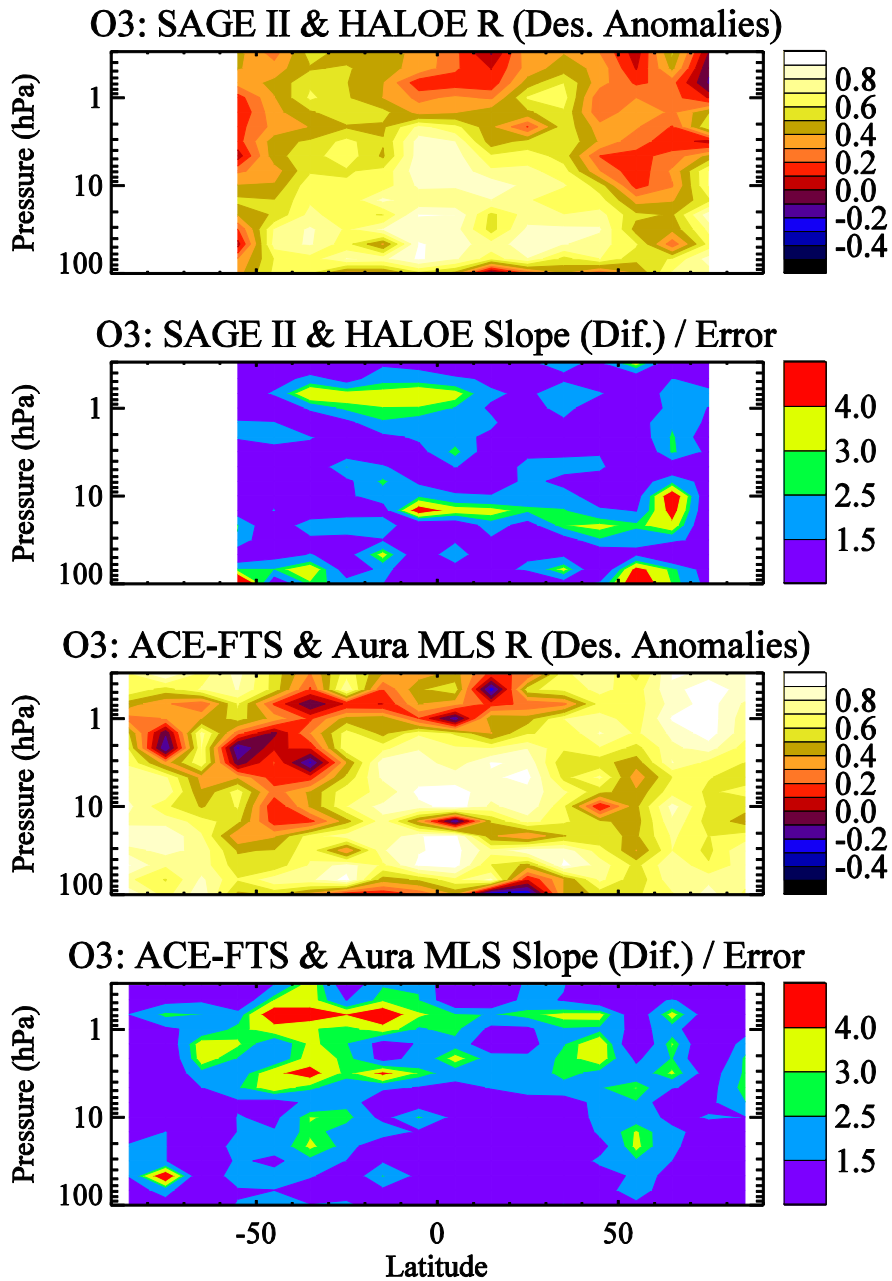
**Fig. 18.** Schematic diagram describing the creation of the merged GOZCARDS monthly zonal mean ozone data record from various satellite datasets. Instruments represented in red inside the boxes are used as a reference. Instruments whose measurements have already been adjusted to a reference are indicated with a “\*” superscript. AMLS refers to Aura MLS and UMLS to UARS MLS. See text for more details.



186

187 **Fig. 19.** Offsets applied to the O<sub>3</sub> source datasets, similar to Fig. 2 for HCl.

188



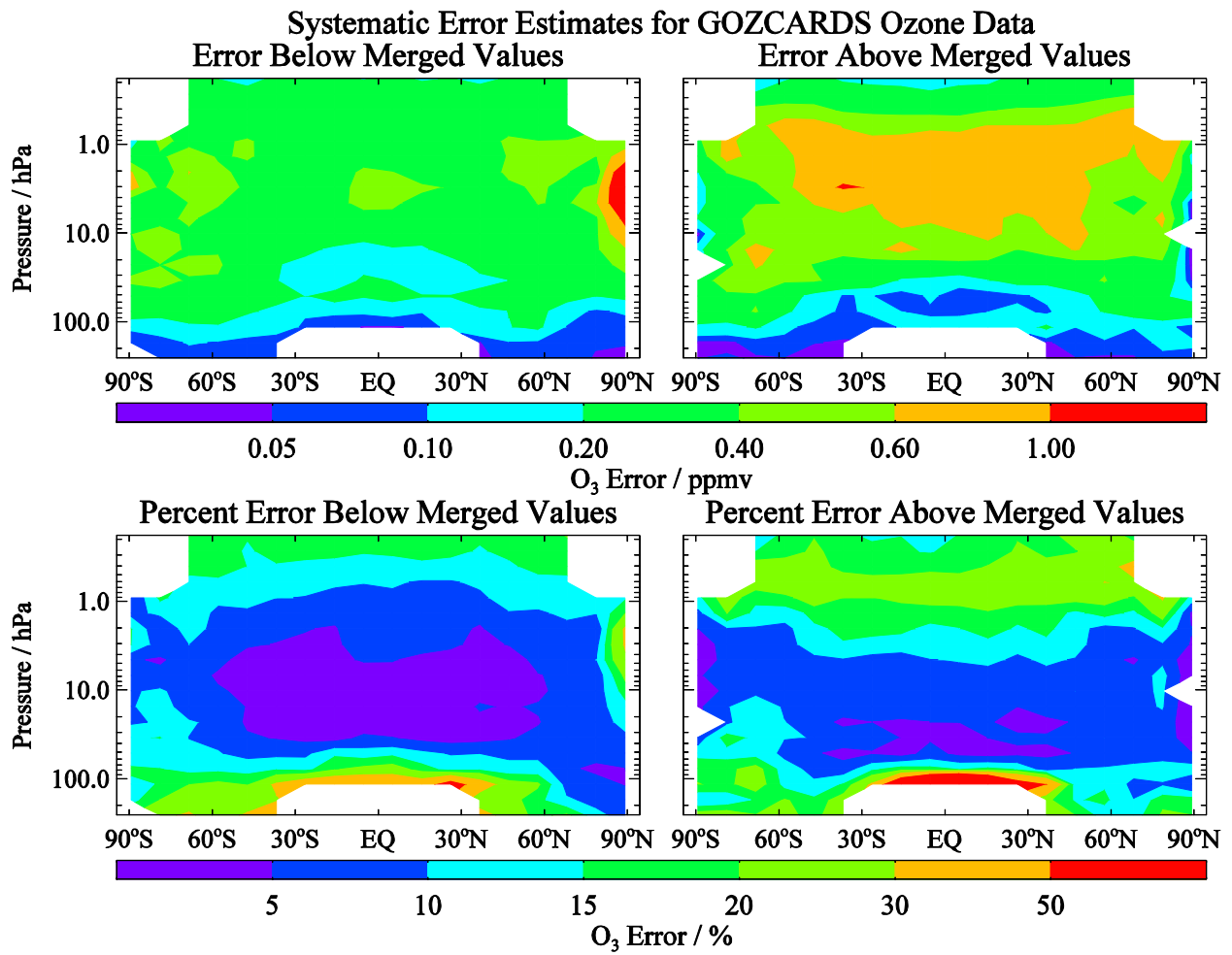
190

191 **Fig. 20.** Latitude/pressure contours of time series diagnostics for O<sub>3</sub> from Aura MLS and ACE-FTS; this  
 192 is similar to Fig. 4 for HCl. The correlation coefficients (R values) and slope trend diagnostics are  
 193 provided for HALOE versus SAGE II in the top two panels (for 1993-1999 as the trend issue for  
 194 converted SAGE II data occurs after mid-2000 and to avoid Pinatubo-related data gaps before 1993) and  
 195 for ACE-FTS versus Aura MLS in the bottom two panels (for 2005-2009).

196

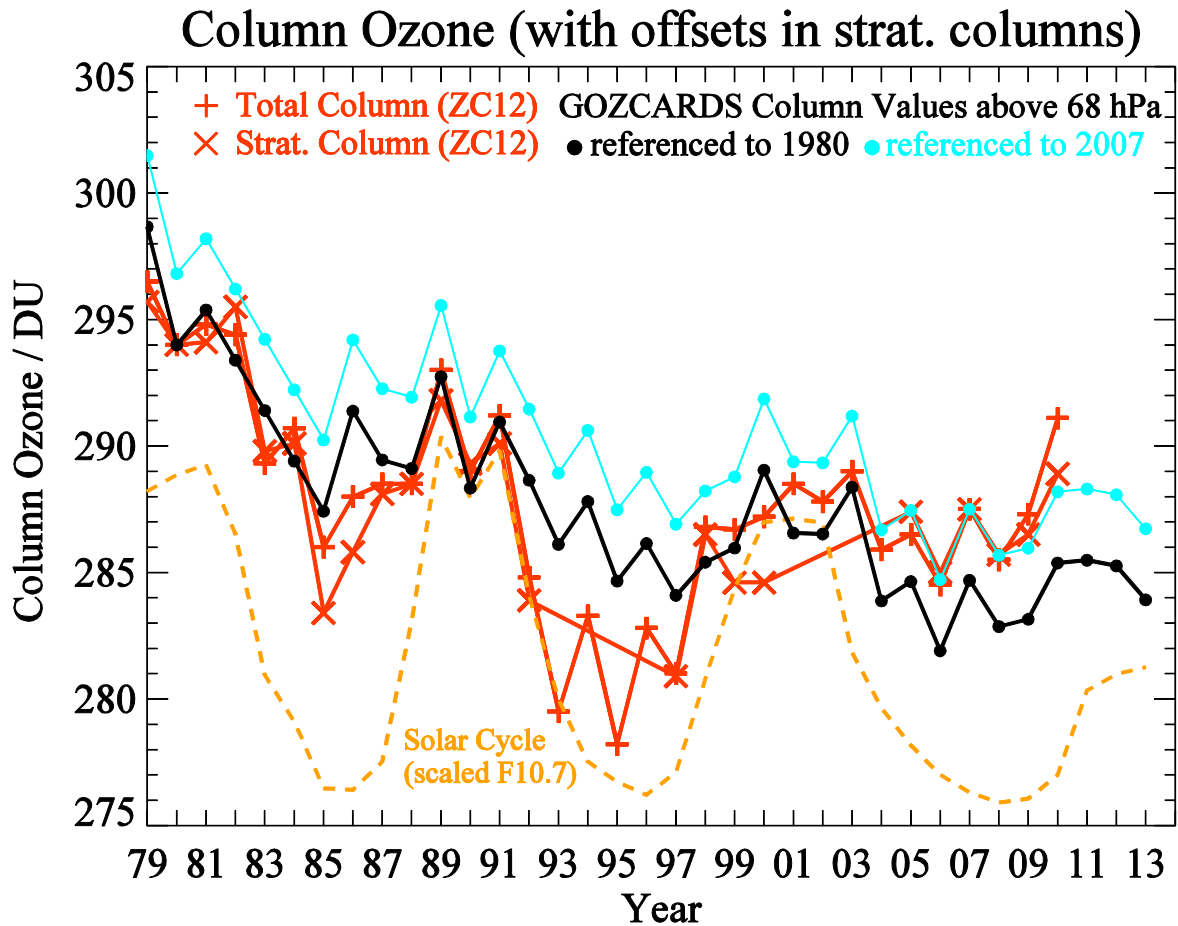


197  
198  
199



200  
201  
202  
203  
204

**Fig. 21.** Systematic error estimates for GOZCARDS O<sub>3</sub> (similar to Fig. 6 for HCl).



206

207

208 **Fig. 22.** Near-global (60°S to 60°N) results for average column ozone (total and stratospheric, from  
 209 *Ziemke and Chandra, 2012*) compared to GOZCARDS O<sub>3</sub> columns above 68 hPa. Stratospheric columns  
 210 are offset to better match the total column values, in order to more easily compare relative variations  
 211 versus time; the black dots and red crosses are referenced to the 1980 total column values, while the cyan  
 212 curves are referenced to 2007 to better illustrate the fits in the later years.

213

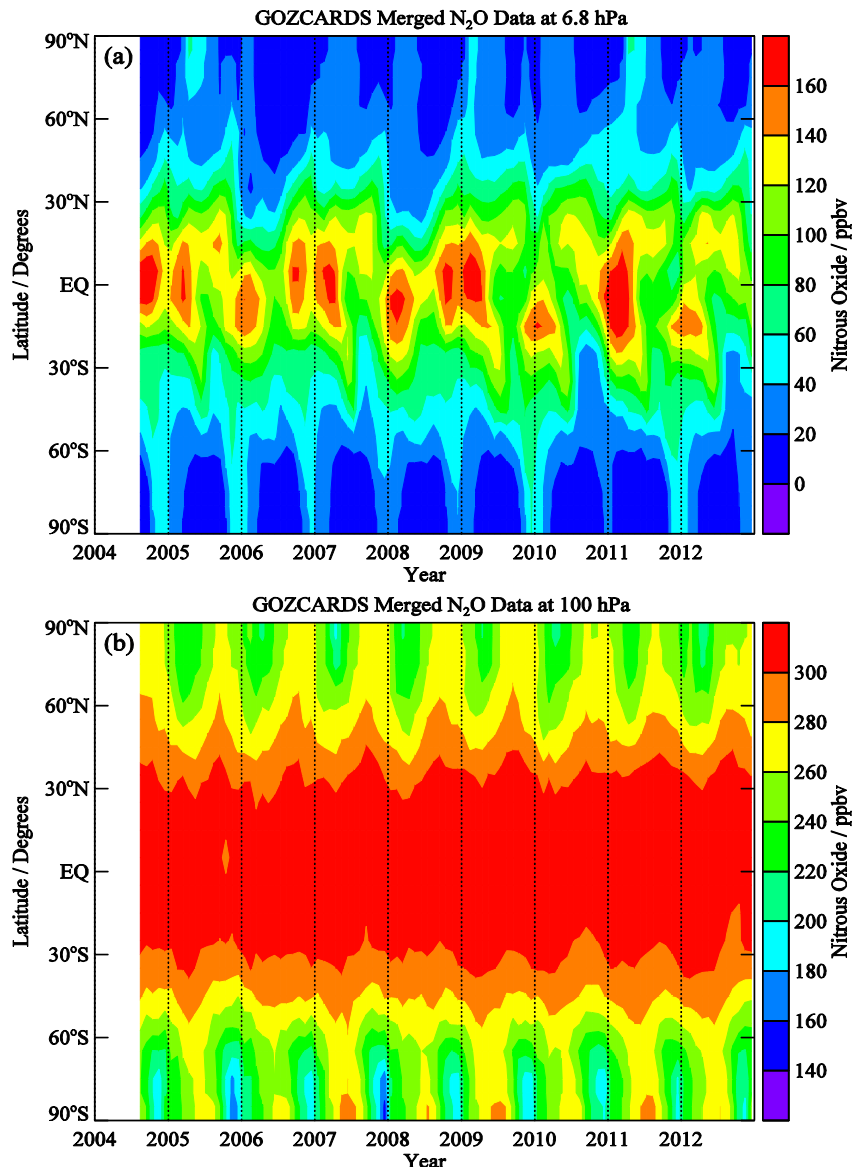
214

215

216

217

218



219

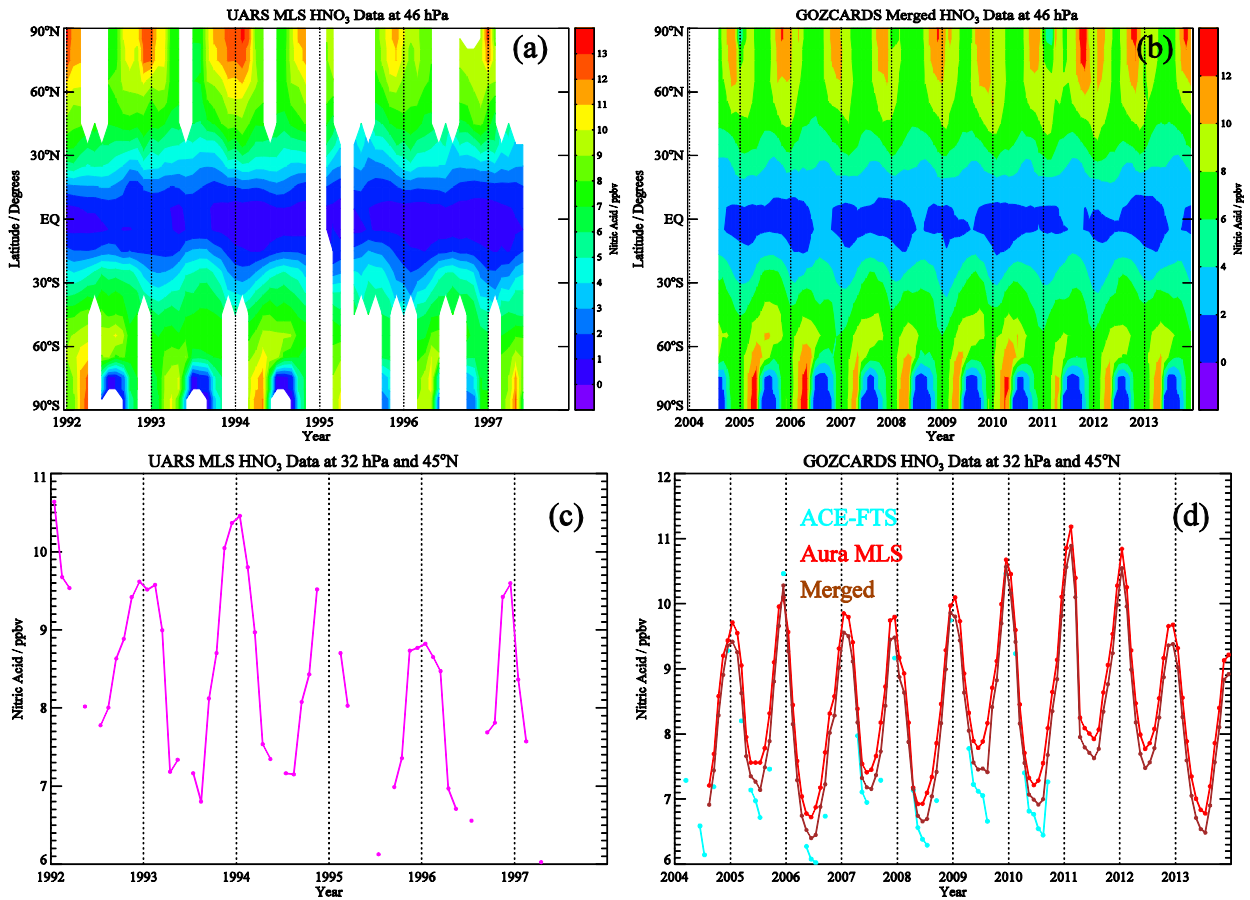
220 **Fig. 23.** Time evolution (Aug. 2004 through 2012) versus latitude of GOZCARDS merged N<sub>2</sub>O (ppbv) at  
 221 (a) 6.8 hPa and (b) 100 hPa.

222

223

224

225



226

227

228 **Fig. 24.** Sample results display the time evolution of satellite-retrieved HNO<sub>3</sub> (ppbv) for two different  
229 periods, 1992-1997 in (a) and (c) versus 2004-2013 in (b) and (d). Panels (a) and (b) are contour plots at  
230 46 hPa from UARS MLS global data and the merged GOZCARDS global data after 2004, respectively;  
231 (c) and (d) show time series at 32 hPa and for the 40°N-50°N latitude bin, with (a) from UARS MLS data,  
232 and (d) from ACE-FTS, Aura MLS, and the merged combination (between the two source data sets).

233

234

1 **Global Ozone Chemistry And Related Datasets for the**  
2 **Stratosphere (GOZCARDS): methodology and sample results**  
3 **with a focus on HCl, H<sub>2</sub>O, and O<sub>3</sub>**

4 **L. Froidevaux<sup>1</sup>, J. Anderson<sup>2</sup>, H.-J. Wang<sup>3</sup>, R. A. Fuller<sup>1</sup>, M. J. Schwartz<sup>1</sup>,**  
5 **M. L. Santee<sup>1</sup>, N. J. Livesey<sup>1</sup>, H. C. Pumphrey<sup>4</sup>, P. F. Bernath<sup>5</sup>,**  
6 **J. M. Russell III<sup>2</sup>, and M. P. McCormick<sup>2</sup>**

7 <sup>1</sup>Jet Propulsion Laboratory, California Institute of Technology, Pasadena, CA, USA

8 <sup>2</sup>Hampton University, Hampton, VA, USA

9 <sup>3</sup>Georgia Institute of Technology, Atlanta, GA, USA

10 <sup>4</sup>The University of Edinburgh, Edinburgh, UK

11 <sup>5</sup>Old Dominion University, Norfolk, VA, USA

12 *Correspondence to:* L. Froidevaux (lucienf@jpl.nasa.gov)

13

14

15

16

17

18

19

20

21

22

23

## 24 **Abstract**

25 We describe the publicly available dataset from the Global OZone Chemistry And Related  
26 Datasets for the Stratosphere (GOZCARDS) project, and provide some results, with a focus on  
27 hydrogen chloride (HCl), water vapor (H<sub>2</sub>O), and ozone (O<sub>3</sub>). This dataset is a global long-term  
28 stratospheric Earth System Data Record (ESDR), consisting of monthly zonal mean time series  
29 starting as early as 1979. The data records are based on high quality measurements from several  
30 NASA satellite instruments and ACE-FTS on SCISAT. We examine consistency aspects  
31 between the various datasets. To merge ozone records, the time series are debiased by calculating  
32 average offsets with respect to SAGE II during periods of measurement overlap, whereas for  
33 other species, the merging derives from an averaging procedure based on overlap periods. The  
34 GOZCARDS files contain mixing ratios on a common pressure/latitude grid, as well as standard  
35 errors and other diagnostics; we also present estimates of systematic uncertainties in the merged  
36 products. Monthly mean temperatures for GOZCARDS were also produced, based directly on  
37 data from the Modern-Era Retrospective analysis for Research and Applications (MERRA).

38 The GOZCARDS HCl merged product comes from HALOE, ACE-FTS and (for the lower  
39 stratosphere) Aura MLS data. After a rapid rise in upper stratospheric HCl in the early 1990s, the  
40 rate of decrease in this region for 1997-2010 was between 0.4 and 0.7%/yr. On shorter timescales  
41 (6 to 8 years), the rate of decrease peaked in 2004-2005 at about 1%/yr, and has since levelled  
42 off, at ~0.5%/yr. With a delay of 6-7 years, these changes roughly follow total surface chlorine,  
43 whose behavior versus time arises from inhomogeneous changes in the source gases. Since the  
44 late 1990s, HCl decreases in the lower stratosphere have occurred with pronounced latitudinal  
45 variability at rates sometimes exceeding 1-2%/yr. *There has been a significant reversal in the  
46 changes of lower stratospheric HCl abundances and columns for 2005-2010, in particular at  
47 northern midlatitudes and in the deep tropics, where short-term increases are observed. However,  
48 lower stratospheric HCl tendencies appear to be reversing after about 2011, with (short-term)  
49 decreases at northern midlatitudes and some increasing tendencies at southern midlatitudes.*

50 For GOZCARDS H<sub>2</sub>O, covering the stratosphere and mesosphere, the same instruments as for  
51 HCl are used, along with UARS MLS stratospheric H<sub>2</sub>O data (1991-1993). We display seasonal  
52 to decadal-type variability in H<sub>2</sub>O from 22 years of data. In the upper mesosphere, the anti-

53 correlation between H<sub>2</sub>O and solar flux is now clearly visible over two full solar cycles. Lower  
54 stratospheric tropical H<sub>2</sub>O has exhibited two periods of increasing values, followed by fairly  
55 sharp drops, the well-documented 2000-2001 decrease, and another recent decrease in 2011-  
56 2013. Tropical decadal variability peaks just above the tropopause. Between 1991 and 2013, both  
57 in the tropics and on a near-global basis, H<sub>2</sub>O has decreased by ~5-10% in the lower  
58 stratosphere, but about a 10% increase is observed in the upper stratosphere and lower  
59 mesosphere. However, recent tendencies may not hold for the long-term, and the addition of a  
60 few years of data can significantly modify trend results.

61 For ozone, we used SAGE I, SAGE II, HALOE, UARS and Aura MLS, and ACE-FTS data to  
62 produce a merged record from late 1979 onward, using SAGE II as the primary reference for  
63 aligning (debiasing) the other datasets. ~~Other adjustments were needed in the upper stratosphere  
64 to circumvent temporal drifts in SAGE II O<sub>3</sub> after June 2000, as a result of the (temperature-  
65 dependent) data conversion from a density/altitude to a mixing ratio/pressure grid.~~ Unlike the 2  
66 to 3% increase in near-global column ozone after the late 1990s reported by some, GOZCARDS  
67 stratospheric column O<sub>3</sub> values do not show a recent upturn of more than 0.5 to 1%; continuing  
68 studies of changes in global ozone profiles, as well as ozone columns, are warranted.

69 A brief mention is also made of other currently available, commonly-formatted GOZCARDS  
70 satellite data records for stratospheric composition, namely those for N<sub>2</sub>O and HNO<sub>3</sub>.

## 71 **1 Introduction**

72 The negative impact of anthropogenic chlorofluorocarbon emissions on the ozone layer,  
73 following the early predictions of Molina and Rowland (1974), stimulated interest in the trends  
74 and variability of stratospheric ozone, a key absorber of harmful ultraviolet radiation. The  
75 discovery of the ozone hole in ground-based data records (Farman et al., 1985) and the  
76 associated dramatic ozone changes during southern hemisphere winter and spring raised the level  
77 of research and understanding regarding the existence of new photochemical processes (see  
78 Solomon, 1999). This research was corroborated by analyses of aircraft and satellite datasets  
79 (e.g., Anderson et al., 1989; Waters et al., 1993), and by independent ground-based data. Global  
80 total column ozone averages in 2006-2009 were measured to be smaller than during 1964-1980  
81 by ~3%, and larger more localized decreases over the same periods reached ~6% in the southern

82 hemisphere midlatitudes (WMO, 2011). Halogen source gas emissions have continued to  
83 decrease as a result of the Montreal Protocol and its amendments. Surface loading of total  
84 chlorine peaked in the early 1990s (WMO, 2011), and subsequent decreases in global  
85 stratospheric HCl and ClO have been measured from satellite-based sensors (Anderson et al.,  
86 2000; Froidevaux et al., 2006; Jones et al., 2011) as well as from the ground (e.g., Solomon et  
87 al., 2006, Kohlhepp et al., 2012). A slow recovery of the ozone layer is expected between the  
88 late 1990s and several decades from now, towards pre-1985 levels (WMO, 2011); **the robust  
89 determination of a long-term global trend requires a sufficiently long and accurate data record. It  
90 is desirable to use high quality datasets for ozone and related stratospheric species for a robust  
91 documentation of past variations and as constraints for global atmospheric models.**

92 The history of global stratospheric observations includes a large suite of satellite-based  
93 instruments, generally well-suited for the elucidation of long-term global change. A review of  
94 differences between past and ongoing satellite measurements of atmospheric composition has  
95 been the focus of the Stratosphere-troposphere Processes And their Role in Climate (SPARC)  
96 Data Initiative (DI); results for stratospheric water vapor and ozone intercomparisons have been  
97 published by Hegglin et al. (2013) and Tegtmeier et al. (2013), respectively, to be followed by a  
98 larger report on intercomparisons of multiple species. Systematic biases reported in these recent  
99 papers tend to mirror past validation work. However, these investigations have not pursued data  
100 merging aspects or the creation of long-term records.

101 Under the Global OZone Chemistry And Related Datasets for the Stratosphere (GOZCARDS)  
102 project, we have created monthly zonally averaged datasets of stratospheric composition on a  
103 common latitude/pressure grid, using satellite-based limb viewing instruments launched as early  
104 as 1979 (for ozone data in particular) and now continuing with instruments launched about a  
105 decade ago. The creation of this Earth System Data Record stays close to the data values  
106 themselves. Therefore, spatial or temporal gaps are typically not filled in; various methods can  
107 be used to try to produce continuous fits to time series, but we viewed this as being outside the  
108 scope of this data record creation. The GOZCARDS products arise from several high quality  
109 satellite datasets, namely from Stratospheric Aerosol and Gas Experiment instruments (SAGE I  
110 and SAGE II), the Halogen Occultation Experiment (HALOE) which flew aboard the Upper  
111 Atmosphere Research Satellite (UARS), the UARS Microwave Limb Sounder (MLS), the



112 Atmospheric Chemistry Experiment Fourier Transform Spectrometer (ACE-FTS) on SCISAT,  
113 and the Aura MLS experiment. Table 1 provides characteristics of the original datasets;  
114 validation papers from the instrument teams and other related studies give a certain degree of  
115 confidence in these datasets. However, the existence of validation references does not imply that  
116 there are no caveats or issues with a particular measurement suite. In this project, we have strived  
117 to optimize data screening and mitigate some undesirable features, such as the impact of outlier  
118 values or the effects of clouds or aerosols. All source datasets still have shortcomings or  
119 imperfections, but we have refrained from arbitrarily removing specific monthly means.

120 Based on original profiles from the various instruments, GOZCARDS “source” monthly  
121 zonal mean values were derived. After data screening, monthly average profiles were created by  
122 vertical interpolation onto the GOZCARDS pressure levels, followed by binning and averaging  
123 into monthly sets. In order to accommodate the lower vertical resolution of some limb viewers,  
124 such as UARS MLS, the GOZCARDS pressure grid was chosen as

$$125 \quad p(i) = 1000 \cdot 10^{-\frac{i}{6}} (\text{hPa}) \quad (1)$$

126 with  $i$  varying from 0 to a product-dependent top; this grid width corresponds to  $\sim 2.7$  km. The  
127 high resolution SAGE O<sub>3</sub> profiles were smoothed vertically onto this grid (see Sect. 5). Given  
128 the sampling of solar occultation instruments, which typically provide 15 sunrise (SR) and 15  
129 sunset (SS) profiles every day (versus the emission-based sampling from MLS), we used latitude  
130 bins of width 10° (18 bins from 80°S-90°S to 80°N-90°N) to construct the monthly zonal means.

131 After the production of GOZCARDS source data files on the above grid, merged (combined)  
132 products were created. This involves the calculation of average biases between monthly zonal  
133 means from different source data during periods of overlap, followed by an adjustment (using  
134 calculated average offsets) of the time series. Non-zero biases always exist between datasets  
135 from different instruments for various reasons, such as systematic errors arising from Level 1  
136 (radiances) or Level 2 (retrievals), different vertical resolutions, or sampling effects. A useful  
137 reference regarding the sampling effects, which can arise spatially (within a latitude bin) or  
138 temporally (within a month), is the recent work by Toohey et al. (2013). They studied sampling  
139 biases from a large suite of satellite-based stratospheric profiling instruments, based on  
140 simulations using fully-sampled model abundance averages versus averaged sampled results  
141 from sub-orbital track locations. The magnitude of such sampling errors is typically inversely

142 related to the number of available profiles routinely sampled, so that larger sampling errors arise  
143 from occultation than from emission measurements, which often sample thousands of profiles  
144 per day. Toohey et al. (2013) found that sampling-related biases can reach 10-15% in some  
145 regions/periods, notably at high latitudes when larger atmospheric variability exists. Sofieva et  
146 al. (2014) have also discussed sampling uncertainty issues for satellite ozone datasets.

147 We have observed very good correlations between GOZCARDS ozone and other long-term  
148 ozone datasets, such as the Stratospheric Water vapor and OzOne Satellite Homogenized  
149 (SWOOSH) dataset (Davis et al., in preparation) and homogenized Solar Backscatter Ultraviolet  
150 (SBUV) data; these analyses (along with related work on H<sub>2</sub>O) will be discussed elsewhere.  
151 Results from GOZCARDS and other data relating to midlatitude ozone trends have appeared  
152 (e.g., Nair et al., 2013). Dissemination of trend results arising from analyses of GOZCARDS  
153 and other ozone profile data is planned as part of the SI<sup>2</sup>N initiative, which stands for  
154 Stratospheric Processes And their Role in Climate (SPARC), International Ozone Commission  
155 (IOC), Integrated Global Atmospheric Chemistry Observations (IGACO-O<sub>3</sub>), and the Network  
156 for the Detection of Atmospheric Composition Change (NDACC). Recent results on such ozone  
157 profile trend comparisons can be found in Tummon et al. (2014) and Harris et al. (2014).

158 This paper starts with a discussion of general data screening issues (Sect. 2), and then  
159 describes the GOZCARDS data production approach and methodology, followed by some  
160 atmospheric results for HCl (Sect. 3), H<sub>2</sub>O (Sect. 4), and O<sub>3</sub> (Sect. 5). We provide specific  
161 diagnostics that indicate generally good correlations and small relative drifts between the main  
162 datasets being used to create the longer-term GOZCARDS merged time series. Section 6 briefly  
163 mentions the availability of a few other GOZCARDS products, namely N<sub>2</sub>O, HNO<sub>3</sub>, and  
164 temperatures derived from MERRA fields. The version of GOZCARDS described here is  
165 referred to as ESDR version 1.01 or ev1.01. ~~Each product's public GOZCARDS data record has  
166 an associated digital object identifier (DOI) along with a relevant dataset reference.~~

167

## 168 **2 GOZCARDS source data and data screening**

169 Data provenance information regarding the various measurements used as inputs for  
170 GOZCARDS is provided in Appendix A (Sect. A.1).

## 171 2.1 GOZCARDS data screening and binning

172 The screening of profiles for GOZCARDS has largely followed guidelines recommended by  
173 the various instrument teams and/or relevant publications; such screening procedures are rarely  
174 all described in one convenient location, so we review this briefly here for the various data sets.  
175 Data screening can reduce the total number of good profiles below our chosen threshold for  
176 flagging zonal monthly means; unless otherwise noted, we only provide monthly means  
177 constructed from 15 or more values in a given latitude/pressure bin.

178 ~~For HALOE, cloud contamination may add retrieval artifacts and HALOE profiles were~~  
179 ~~screened for clouds, following procedures described in Hervig and McHugh (1999); values at~~  
180 ~~and below the cloud level (found in the netCDF files) were excluded. Also, HALOE profiles that~~  
181 ~~may occasionally contain artifacts associated with either a faulty trip angle or constant lockdown~~  
182 ~~angle registration were screened out, per recommendations from the HALOE data processing~~  
183 ~~team (see [http://haloc.gats-inc.com/user\\_docs/index.php](http://haloc.gats-inc.com/user_docs/index.php) for details).~~

184 ~~—For UARS MLS, we used screening recommendations documented by Livesey et al. (2003).~~  
185 ~~In particular, MLS data points whose retrieved precisions are flagged with a negative sign were~~  
186 ~~discarded, ensuring only a negligible contribution to the retrieval from a priori. Also, our data~~  
187 ~~filtering followed the recommendations regarding the “MMAF\_STAT” flag for operational~~  
188 ~~status (we only used values of ‘G’, ‘t’, or ‘T’ for this flag) and the product-specific~~  
189 ~~“QUALITY” flag (for which we only used values equal to 4, thus eliminating bad radiance fits).~~

190 ~~—For Aura MLS data screening, the procedures are generally as follows: we only use profiles~~  
191 ~~with even values of the Status field, Quality values larger than documented thresholds (indicating~~  
192 ~~good radiance fits), Convergence values smaller than documented thresholds (indicating good~~  
193 ~~convergence), and positive (unflagged) values of the estimated precisions. Species-specific~~  
194 ~~validation papers give data screening recommendations, with appropriate flag values for Quality~~  
195 ~~and Convergence; see Livesey et al. (2013) for such references and v3.3 data screening updates.~~

196 ~~—For ACE FTS, a list of profiles with data issues is provided by the ACE FTS team (see~~  
197 ~~[https://database.seisat.ca/validation/data\\_issues\\_table.php](https://database.seisat.ca/validation/data_issues_table.php)) and these have been removed from~~  
198 ~~our database. However, we also found it necessary to remove occasional large outlier values that~~  
199 ~~could significantly impact monthly zonal means by adding a bias (or “noise”) to the time series if~~

200 such screening were not performed; such outliers are not otherwise routinely removed from the  
201 original ACE-FTS profiles. Our outlier screening procedure removed values outside 2.5 times  
202 the standard deviation, as measured from the median values in each latitude/pressure bin, for  
203 each year of data. This was deemed close to optimum by comparing the results to Aura MLS  
204 time series (which usually are not impacted by such outliers), as well as to independent zonal  
205 means (using 5° latitude bins) provided by the ACE-FTS instrument team. Up to 5% of the  
206 profile values in each bin in any given month were typically discarded as a result of this  
207 procedure, but the maximum percentage of discarded values can be close to 10% for a few  
208 months of ACE-FTS version 2.2 data, depending on year and species. Moreover, because of poor  
209 ACE-FTS sampling in the tropics, the threshold value for minimum number of (good) ACE-FTS  
210 profiles determining a monthly zonal average was allowed to be as low as 10 for mid- to high  
211 latitudes, and as low as 6 for low latitudes (bins centered from 25°S to 25°N). Our zonal mean  
212 datasets for ACE-FTS would become too sparse in some years if such lower threshold values  
213 were not used; ~~such data sparseness can introduce limitations (larger error bars) in the~~  
214 ~~determination of trends, for example, although we also performed comparisons versus Aura MLS~~  
215 ~~monthly means to provide some level of confidence in the results. In addition, ACE-FTS single~~  
216 ~~profile values were discarded if the associated error was larger than the mixing ratio or smaller~~  
217 ~~than  $10^{-4}$  times the mixing ratio, following recommendations from the ACE-FTS team.~~

218 The binning of profiles occurs after the screened values are averaged (in each  
219 latitude/pressure bin). Negative monthly means have been flagged (set to -999.0) in the  
220 GOZCARDS files; while a negative mixing ratio that is smaller (in absolute value) than its  
221 associated standard error (or a few times this standard error) can in theory be meaningful, we  
222 deem that occasional small negative monthly means are unlikely to be very useful, scientifically.

223 The organization of profiles on a common pressure grid is straightforward when pressure  
224 values are present in the original files, as is the case for most data used here. Also, the vertical  
225 resolutions are similar for most of the instruments used for GOZCARDS (see more details in  
226 each species-specific section). The UARS MLS, HALOE, and Aura MLS native pressure grids  
227 are either the same as or a superset of the GOZCARDS pressure grid, so these datasets were  
228 readily sampled for the construction of the GOZCARDS monthly means. For ACE-FTS profiles,  
229 pressures are provided along with the fixed altitude grid, and we used linear interpolation versus

230 log(pressure) to convert profiles to the GOZCARDS grid. More details are provided in the O<sub>3</sub>  
231 section for SAGE I and SAGE II, for which density versus altitude is the native representation.

232

### 233 **3 GOZCARDS HCl**

#### 234 **3.1 GOZCARDS HCl source data records**

235 We used HCl datasets from HALOE, ACE-FTS and Aura MLS to generate the monthly zonal  
236 mean source products for GOZCARDS HCl.

237 For the screening of HALOE HCl profiles, in addition to the procedures mentioned in  
238 Sect. 2, a first-order aerosol screening was applied: all HCl values at and below a level where the  
239 5.26 μm aerosol extinction exceeds 10<sup>-3</sup> km<sup>-1</sup> were excluded.

240 For Aura MLS, the ongoing standard HCl product is retrieved using band 14 rather than band  
241 13, which was used to measure HCl for the first 1.5 years after launch, but started deteriorating  
242 rapidly after Feb. 2006. Validation and error characterization for the Aura MLS HCl product  
243 (version 2.2) were provided by Froidevaux et al. (2008). The MLS version 3.3/3.4 HCl data used  
244 here (see Livesey et al., 2013) compare quite well with v2.2, with average biases within 5% in  
245 general. A high bias exists in MLS HCl versus aircraft data at 147 hPa at low latitudes  
246 (Froidevaux et al., 2008). Such regions with large uncertainties and biases are avoided (flagged)  
247 for the production of the GOZCARDS merged HCl dataset.

248 The use of the GOZCARDS source files for Aura MLS HCl, like the use of original Level 2  
249 MLS HCl files, is not recommended for obtaining realistic trends in the upper stratosphere (at  
250 pressures < 10 hPa), even if monthly mean MLS HCl in this region displays reasonable values in  
251 comparison to other satellite-based measurements. Aura MLS switched to a backup band (band  
252 14) to retrieve the daily HCl measurements after band 13 (originally targeted specifically for  
253 HCl) showed signs of rapid degradation in early 2006; as the remaining lifetime for band 13 is  
254 expected to be very short (days as opposed to weeks), this band has only been turned on for a  
255 few days since February 2006. However, for pressures ≥ 10 hPa, the long-term (band 14) HCl  
256 data now being routinely produced is deemed to be robust (because of the broader emission line

257 in this region, in comparison to the measurement bandwidth). These considerations have  
258 implications for how we treat MLS HCl upper stratospheric data in terms of the merging process.

259 Past validation studies have compared MLS HCl (v2.2), ACE-FTS (v2.2) and HALOE (v19)  
260 datasets using coincident pairs of profiles; such work was described by Froidevaux et al. (2008)  
261 for MLS HCl validation and by Mahieu et al. (2008) for ACE-FTS HCl validation. HALOE HCl  
262 values were found to be biased low by ~10-15% relative to both MLS and ACE-FTS, especially  
263 in the upper stratosphere; this low bias versus other (balloon- and space-based) measurements  
264 had been noted in past HALOE validation studies (Russell et al., 1996). Also, HALOE (v19) and  
265 ACE-FTS (v2.2) HCl data tend to lose sensitivity and reliability for pressures less than ~0.4 hPa.

### 266 **3.2 GOZCARDS HCl merged data records**

267 HCl is a good candidate for merging the main satellite data that have provided this measurement  
268 since 1991. Indeed, one can benefit from the strengths of all datasets in the lower stratosphere,  
269 but rely on HALOE and ACE-FTS for upper stratospheric trends, because of the Aura MLS HCl  
270 trend detection issue mentioned above. Aura MLS HCl time series were not included in the  
271 merging at pressures less than 10 hPa, so after November 2005, the GOZCARDS HCl upper  
272 stratospheric trends are dictated only by changes in ACE-FTS abundances. However, in order to  
273 derive the systematic offsets needed to adjust the time series from these three instruments in a  
274 continuous way (in the pressure dimension), we used the absolute Aura MLS HCl measurements  
275 at all pressure levels in 2004 and 2005, during the overlap period between the three instruments.

276 Figure 1 illustrates the merging process for HCl at 32 hPa for the 45°S latitude bin (which  
277 covers 40°S to 50°S). Given that there exists very little overlap between the three sets of  
278 measurements in the same months in 2004 and 2005, especially in the tropics, a simple 3-way  
279 averaging of the datasets is not practical and would lead to significant data gaps. Our  
280 methodology is equivalent to averaging all three datasets during this period (if one had full  
281 coverage from all datasets), but we use Aura MLS as a transfer dataset. This was done by first  
282 averaging ACE-FTS and Aura MLS data, where the datasets overlap, and then including the  
283 third dataset (HALOE) into the merging process with the intermediate (temporary) merged data.  
284 Although HALOE HCl is believed to be biased too low, modifying the HALOE values to  
285 somehow match ACE-FTS or Aura MLS values or a combination of these two datasets was

286 deemed to be too subjective. The combined weight of the other two datasets leads to a merged  
287 HCl dataset that is generally further away from HALOE than it is from either ACE-FTS or Aura  
288 MLS. The top left panel in Fig. 1 shows monthly zonal average GOZCARDS source data for  
289 HALOE, ACE-FTS, and Aura MLS during the overlap period, from Aug. 2004 (when Aura  
290 MLS data started) through Nov. 2005 (when HALOE data ended). The top right panel illustrates  
291 the result of step 1 in the merging procedure, with the temporary merged data values (orange)  
292 resulting from the adjustment of ACE-FTS and Aura MLS values to the mean reference  
293 indicated by the black dashed line; this reference is simply the average (over the overlap period)  
294 of these two datasets, formed from the average of the points which overlap during the same  
295 months, meaning whenever ACE-FTS obtained monthly data (since Aura MLS HCl means exist  
296 every month). The middle left panel shows the result of step 2, namely the merged values  
297 (brown) that arise from merging HALOE values with the temporary merged values (orange)  
298 from step 1. In this second averaging step, we weigh the intermediate merged values by  $2/3$  and  
299 HALOE values by  $1/3$  (leading to a mean reference illustrated by the dashed black line), in order  
300 for this process to be equivalent to averaging all three datasets, each with a weight of  $1/3$ . The  
301 middle right panel shows the source data along with the final merged values during the overlap  
302 period. A simple mathematical description of the above procedure is provided in Appendix A.  
303 The bottom panel shows the same datasets but for 1991 through 2012, after the calculated  
304 additive offsets are applied to the whole source series, thus debiasing the datasets; these adjusted  
305 time series are then merged (averaged) together wherever overlap exists. We tested this  
306 procedure by using one or the other of the two occultation datasets as the initial one in step 1,  
307 and results were not found to differ appreciably. This methodology is used as well for the same  
308 three datasets for the  $H_2O$  merging; we have also checked our procedures and results by using  
309 two independent calculations from different institutions. We also found that the use of  
310 multiplicative adjustments generally produces very similar results as additive offsets. Some  
311 issues were found on occasion with multiplicative offsets, when combining very low mixing  
312 ratios, but additive offsets can also have drawbacks if the merged values end up being slightly  
313 negative, notably as a result of changes that modify the already low HCl values during Antarctic  
314 polar winter. This occurs on occasion as additive offsets tend to be weighted more heavily by the  
315 larger mixing ratios found during non-winter seasons; as a result, we decided not to offset the

316 lower stratospheric HCl source datasets in the polar winter seasons at high latitudes for any of  
317 the years (for interannual consistency). Procedural details regarding the merging of HCl data are  
318 summarized in the Supplementary material.

319 In Fig. 2, we display the offsets that were applied to the three HCl source datasets as a result  
320 of the merging process in each latitude/pressure bin; a positive value means that a dataset is  
321 biased low and needs to be increased (on average) by the offset value. These offsets show that in  
322 general, ACE-FTS and Aura MLS HCl values were adjusted down by 0.1-0.2 ppbv (a decrease  
323 of about 2-10%), while HALOE HCl was adjusted upward by 0.2-0.4 ppbv. Offset values tend  
324 to be fairly constant with latitude and the sum of the offsets equals zero. The generally  
325 homogeneous behaviour versus latitude is a good sign, as large discontinuities would signal  
326 potential issues in the merging (e.g., arising from large variability or lack of sufficient statistics).  
327 Figure S1 provides more detailed examples of some of these (upper and lower stratospheric)  
328 offsets versus latitude, including standard errors based on the variability in the offsets from  
329 month to month during the overlap period. Error bars in the offsets provide an indication of the  
330 results' robustness. Another indication of first-order compatibility between datasets is provided  
331 by a comparison of annual cycles. Figure S2 provides average annual cycle amplitudes obtained  
332 from simple regression model fits to HALOE, ACE-FTS, and Aura MLS series over their  
333 respective periods. While there are a few regions where noise or spikes exist (mainly for ACE-  
334 FTS), large annual amplitudes in the polar regions occur in all the time series; this arises from  
335 HCl decreases in polar winter, followed by springtime increases.

336 A more detailed analysis of interannual variability and trend consistency is provided from  
337 results in Fig. 3, which shows an example of ACE-FTS and Aura MLS time series. ~~We note that  
338 no v2.2 ACE-FTS data (for any species) are used after September 2010, because of a data  
339 processing problem; a fully updated version of ACE-FTS data was not available when the  
340 GOZCARDS data records were constructed.~~ We have used coincident points from these time  
341 series to compare the deseasonalized anomalies (middle panel in Fig. 3) from both instrument  
342 series; correlation coefficient values (R values) are also computed. In the Fig. 3 example, very  
343 good correlations are obtained and no significant trend difference between the anomalies (bottom  
344 panel) is found for ACE-FTS and Aura MLS HCl. A global view for all latitude/pressure bins of  
345 these correlations and drifts is provided in Fig. 4, where the top panel gives R values for



346 deseasonalized anomalies, and the bottom panel gives the ratio of the difference trends over the  
347 error in these trends. The results in Fig. 4 confirm that there are significant trend differences  
348 between the upper stratospheric HCl time series from ACE-FTS and that of Aura MLS (as a  
349 reminder, we did not use Aura MLS HCl for pressures less than 10 hPa). Fig. 4 also shows very  
350 low correlation coefficients from the deseasonalized HCl series in the uppermost stratosphere,  
351 because Aura MLS HCl exhibits unrealistically flat temporal behavior, whereas ACE-FTS HCl  
352 varies more. In the lower stratosphere, there is generally good agreement between the ACE-FTS  
353 and Aura MLS HCl time series, with R values typically larger than 0.7 and difference trend to  
354 error ratios smaller than 1.5. The few low R values for 100 hPa at low latitudes likely reflect  
355 more infrequent ACE-FTS sampling and some (possibly related) outlier data screening issues.

356 Figure S3 illustrates GOZCARDS merged 46 hPa HCl variations versus time; there is clearly  
357 a much more complete global view (with no monthly gaps) after the launch of Aura MLS. Gaps  
358 at low latitudes in 1991 and 1992 are caused by post-Pinatubo aerosol-related issues in the  
359 HALOE record, and gaps in later years arise from the decrease in coverage from UARS. In the  
360 upper stratosphere, there are more gaps compared to 10 hPa and below, as a result of the much  
361 poorer tropical coverage from ACE-FTS and the elimination of MLS data in this region.

362 An indication of systematic errors in the merged values can be obtained by providing  
363 estimates of the range of available monthly mean source data. We have made such a calculation,  
364 although these error values are not part of the public GOZCARDS data files. For each bin, we  
365 computed the ranges of monthly means above and below the merged values that include 95% of  
366 the available source data monthly means. These error bars are not usually symmetric about the  
367 merged values, especially if one dataset is biased significantly in relation to merged values. We  
368 did not have enough datasets here to consider a more statistical approach (such as actual standard  
369 deviations among source datasets). Figure 5 shows the result of such a systematic error  
370 calculation at 46 hPa for the 35°S latitude bin. The lower shaded region range gives the lower  
371 bound, determined by HALOE data, and the upper limit of the grey shading originates from  
372 ACE-FTS data. Figure 6 shows contour plots of these estimated systematic errors in HCl for all  
373 latitudes and pressures. These are fairly conservative error bars; however, even the source data  
374 averages at the 95% boundaries have their own systematic errors (rarely smaller than 5%), so our  
375 estimates do not really encompass all error sources. Error bars representing a range within which

376 95% of the source data values reside (see Figs. 5 and 6) can be a useful guide for data users or  
377 model comparisons; users can readily calculate such ranges (or we can provide these values).

378 ~~Other quantities are provided in the netCDF GOZCARDS files, which are composed of one~~  
379 ~~set of individual yearly files for all source datasets, and one set of yearly files for the merged~~  
380 ~~products. The main data quantities are monthly averages, plus standard deviations and standard~~  
381 ~~errors for these means. The GOZCARDS source files also provide the number of days sampled~~  
382 ~~each month as well as minimum and maximum values for the source datasets. Other information~~  
383 ~~includes average solar zenith angles and local solar times for individual sources. Note that for the~~  
384 ~~species discussed here, sunset and sunrise occultation values in the same latitude bin during a~~  
385 ~~given month are averaged together. Finally, formulae for monthly standard deviations of the~~  
386 ~~merged data are given in Appendix A, where sample time series of the standard deviations and~~  
387 ~~standard errors (not systematic errors) for both source and merged HCl data are also shown.~~

### 388 **3.3 GOZCARDS HCl sample results and discussion**

389 Stratospheric HCl is important because it is the main reservoir of gaseous chlorine and it can be  
390 used to follow the chlorine budget evolution over the past decades. This includes a significant  
391 increase before the mid-1990s as a result of anthropogenic chlorofluorocarbon (CFC) production,  
392 followed by a slower decrease as a result of the Montreal Protocol and subsequent international  
393 agreements to limit surface emissions that were correctly predicted to be harmful to the ozone  
394 layer (Molina and Rowland, 1974; Farman et al., 1985).

395 In Fig. 7, we provide an overview of the HCl evolution since 1991, based on GOZCARDS  
396 average merged HCl for 3 different latitude regions at 4 pressure levels, from the upper  
397 stratosphere to the lower stratosphere. In the upper stratosphere (at 0.7 hPa shown here), the  
398 rapid early rise in HCl was followed by a period of stabilization (1997-2000) and subsequent  
399 decreases. ~~The GOZCARDS HCl time series for pressures less than 10 hPa stop in September~~  
400 ~~2010 because after this, v2.2 ACE FTS data were halted, due to technical retrieval issues with~~  
401 ~~that data version.~~ Rates of decrease for stratospheric HCl and total chlorine have been  
402 documented based on such satellite-based upper stratospheric abundances, which tend to follow  
403 tropospheric source gas trends with a time delay of order 6 years, with some uncertainties in the  
404 modeling of this time delay and related age of air issues (Waugh et al., 2001; Engel et al., 2002;

405 Froidevaux et al., 2006). As summarized in WMO (2011), the average rate of decrease in  
406 stratospheric HCl has typically been measured at  $-0.6\%/yr$  to  $-0.9\%/yr$ , in reasonable agreement  
407 with estimated rates of change in surface total chlorine; see also the HCl upper stratospheric  
408 results provided by Anderson et al. (2000) for HALOE, Froidevaux et al. (2006) for the one and  
409 a half year Aura MLS data record (from the initially used primary band), and Jones et al. (2009)  
410 and Brown et al. (2011) for a combination of HALOE and ACE-FTS datasets. The WMO (2011)  
411 summary of trends also includes results from column HCl data at various NDACC Fourier  
412 transform infrared (FTIR) measurement sites; see Kohlhepp et al. (2012) for a comprehensive  
413 discussion of ground-based results, showing some scatter as a function of latitude. Figure 7  
414 demonstrates that a global-scale decline in mid- to lower stratospheric HCl is visible since about  
415 1997. We also notice that at 68 hPa in the tropics, the long-term rate of change appears to be  
416 near-zero or slightly positive. In addition, there are shorter-term periods in recent years when an  
417 average increasing “trend” would be inferred rather than a decrease, in particular, see the  
418 northern hemisphere data from 2005 through 2012 at 32 hPa.

419 To quantify the rates of change further, we created deseasonalized GOZCARDS merged  
420 monthly zonal mean HCl data for the different latitudes, and we show in Fig. 8 the linear rate of  
421 change that results from simple fits through such series (averaged into  $20^\circ$ -wide latitude bins).  
422 The long-term trends (1997 through 2013 for the lower stratosphere, and 1997 through 2010 for  
423 the upper stratosphere) are generally negative and between about  $-0.5\%/yr$  in the upper  
424 stratosphere and  $-1\%/yr$  in the lower stratosphere, depending on latitude. Some separation  
425 between northern and southern hemisphere results is observed in the lower stratosphere, with  
426 smaller trends in the northern hemisphere. Also, the scatter increases for 68 to 100 hPa and some  
427 positive (or essentially zero) trends occur at low latitudes in this region; however, we have less  
428 confidence in the results at 100 hPa, given the larger scatter and error bars in that region (and the  
429 smaller abundances). ~~Results at more polar latitudes (not shown here) tend to follow the adjacent~~  
430 ~~midlatitude bin results, but with more scatter (and larger error bars), especially for shorter time~~  
431 ~~periods. To explore these rates of change in the lower stratosphere in more detail, Fig. 9 shows~~  
432 ~~the same type of analysis as Fig. 8 for three other time periods and for pressures of 10 hPa or~~  
433 ~~more: (a) for a decade of data from 2003 through 2012, (b) for a shorter 6-yr period from 2006~~  
434 ~~through 2011, and (c) for the most recent 6-yr period from 2008 through 2013. For the results in~~

435 ~~(a), a decadal decrease is still observed for the southern hemisphere bins and some of the tropics~~  
436 ~~in the upper region, but increases can be detected in the northern hemisphere and at the higher~~  
437 ~~pressures in the tropics. In (b), we see an accentuation of this hemispheric asymmetry in the~~  
438 ~~short-term rates of change, with large positive changes in the northern hemisphere, and values on~~  
439 ~~both negative and positive sides between 1 and 3 %/yr in many cases; during this past decade,~~  
440 ~~this 6-yr period (2006–2011) is near the temporal peak of this asymmetric lower stratospheric~~  
441 ~~behavior. In the most recent 6-yr period, however (see (c)), the rates of change have decreased~~  
442 ~~for all the latitude bins shown, with all results from 10 to 68 hPa under 0.5 to 1%/yr (absolute~~  
443 ~~value).~~ Without assigning an exact linear “trend” from these simple analyses, we illustrate here  
444 that there is considerable variability in lower stratospheric HCl short-term behavior, especially  
445 after 2005. Such lower stratospheric changes in HCl have been captured in column HCl FTIR  
446 data, as demonstrated by Mahieu et al. (2013, 2014). In the latter reference, it is shown that total  
447 column (FTIR) results and GOZCARDS lower stratospheric HCl trends agree quite well; also,  
448 these authors’ analyses imply that a relative slowdown in the northern hemispheric circulation is  
449 responsible for these observed recent changes in the lower stratosphere. However, we note from  
450 Fig. 7, that such changes in lower stratospheric HCl appear to be fairly short-term in nature, with  
451 an apparent reversal in behavior occurring at both northern and southern midlatitudes since 2011  
452 (e.g., at 32 hPa). The lower stratospheric changes are distinct from the upper stratospheric long-  
453 term decrease, which we expect to continue, as long as the Montreal Protocol agreements are  
454 fulfilled worldwide and total surface chlorine emissions keep decreasing.

455 The rate of change analyses above were repeated and shown in Fig. 10 for sliding time  
456 periods centered on different years (e.g., a 6-yr average for 2004 means an average from 2001  
457 through 2006) in the upper and lower stratosphere for various latitude bins (covering 50°S to  
458 50°N in 10° steps). As observed in Fig. 10(a), the sliding 6-yr results indicate that there has been  
459 an acceleration in the rate of decrease of upper stratospheric HCl between 2000 and 2004,  
460 followed by a flatter period until 2010 (this being the last year of GOZCARDS data available for  
461 the upper stratosphere, with a 6-yr period centered at the start of 2008). The rate of upper  
462 stratospheric HCl change reached a maximum close to -1%/yr, and has retreated to values near -  
463 0.5%/yr in more recent years. This is roughly in agreement with time-shifted curves showing the  
464 rates of change for surface total chlorine based on National Oceanic and Atmospheric

465 Administration (NOAA) surface data (Montzka et al., 1999), as shown in Fig. 10 (upper panels,  
466 green and purple curves) with the Earth System Research Laboratory Global Monitoring  
467 Division (website) data, time shifted by 6 or 7 years to approximately account for transport  
468 delays into the upper stratosphere. The tropospheric source gases for chlorine have also shown a  
469 reduction in the rate of decrease during the 2<sup>nd</sup> half of the past decade, as discussed by Montzka  
470 et al. (1999) and summarized more recently in WMO (2011). As discussed in the latter report,  
471 this arises from a combination of factors, including the initial rapid decrease in methyl  
472 chloroform (which now plays a much smaller role), slower rates of decrease from the sum of  
473 CFCs in more recent years, and increases in hydrochlorofluorocarbons (HCFCs), along with  
474 small contributions from very short-lived species, all of which requires continued monitoring. In  
475 Fig. 10, the lower stratospheric response is summarized (panel (b)) by considering the rates of  
476 change in partial column density between 68 hPa and 10 hPa. The lower stratospheric rates of  
477 change show more variability with latitude than in the upper stratosphere for short (6-yr) time  
478 periods, and a hemispheric asymmetry exists, peaking in 2009, when positive tendencies are seen  
479 in the northern hemisphere, as opposed to decreases in the south. ~~Figure 10 (panels (e) and (d))~~  
480 ~~also displays the sensitivity to the time period chosen, as we average the different latitudinal~~  
481 ~~results (from the left panels) and add 8-yr sliding periods to this analysis of HCl changes.~~ The  
482 near-global results are not too dependent on whether 6-yr or 8-yr periods are used, but longer  
483 periods tend to smooth out the rates of change; interannual changes, including those arising from  
484 the quasi-biennial oscillation (QBO), will affect short-term results, especially in the lower  
485 stratosphere. It is worth noting (Fig. 10) that the patterns in the upper and lower stratosphere are  
486 qualitatively similar, and that rates of change in surface emissions will impact both regions, but  
487 carefully disentangling this from changes in the dynamics and in other constituents (e.g., CH<sub>4</sub>)  
488 that can affect the partitioning of chlorine species will require more analyses and modeling.

489

## 490 **4 GOZCARDS H<sub>2</sub>O**

### 491 **4.1 GOZCARDS H<sub>2</sub>O source data records**

492 We used water vapor datasets from HALOE, UARS MLS, ACE-FTS, and Aura MLS to generate  
493 the monthly zonal mean source products for GOZCARDS H<sub>2</sub>O.

494 In addition to the data screening procedures mentioned in Sect. 2, screening of HALOE H<sub>2</sub>O  
495 data for high aerosol extinction values was performed, in a way very similar to the method used  
496 for the creation of merged H<sub>2</sub>O for the Stratospheric Water vapor and OzOne Satellite  
497 Homogenized (SWOOSH) dataset (Sean Davis, personal communication, 2013). This method  
498 (see Fig. S4) screens out anomalous HALOE H<sub>2</sub>O values that occurred mainly in 1991-1992,  
499 when the aerosol extinction near 22 hPa exceeded  $5 \times 10^{-4} \text{ km}^{-1}$ ; for pressure levels at and below  
500 22 hPa, we have excluded the corresponding H<sub>2</sub>O values. Also, for upper mesospheric HALOE  
501 data used here, care should be taken during high latitude summer months, as no screening was  
502 applied for the effect of polar mesospheric clouds (PMCs). High biases (by tens of percent) in  
503 H<sub>2</sub>O above ~70 km have been shown to occur as a result of PMCs in the HALOE field of view  
504 (McHugh et al., 2003). Indeed, monthly mean values larger than 8-10 ppmv are observed in  
505 GOZCARDS H<sub>2</sub>O merged data and in HALOE source data for pressures less than ~0.03 hPa. A  
506 more recent HALOE data version (version 20), or the version labeled VPMC based on the above  
507 reference, could be used to largely correct such PMC-related effects, although this was not  
508 implemented for GOZCARDS H<sub>2</sub>O. The Aura MLS and ACE-FTS measurements, obtained at  
509 longer wavelengths than those from HALOE, do not yield such large H<sub>2</sub>O values; a rough  
510 threshold value of 8.5 ppmv could also be used (by GOZCARDS data users) to flag the pre-2005  
511 merged dataset.

512 UARS MLS stratospheric H<sub>2</sub>O for GOZCARDS was obtained from V6 (or V600) H<sub>2</sub>O data.  
513 This data version is identical to the original prototype (named V0104) from Pumphrey (1999),  
514 who noted that UARS MLS H<sub>2</sub>O often exhibits drier values (by 5-10%) than HALOE H<sub>2</sub>O (see  
515 also Pumphrey et al., 2000). The resulting GOZCARDS H<sub>2</sub>O monthly zonal means span the  
516 period from Sep. 1991 through April, 1993. We note that a significant fraction of UARS MLS  
517 tropical data values at 100 hPa are flagged bad (as a result of diminishing sensitivity).

518 Summarizing briefly past validation results, SPARC WAVAS (2000) analyses pointed out the  
519 existence of a small low bias in HALOE stratospheric data versus most other measurements  
520 (from satellites or other means), except for UARS MLS. Lambert et al. (2007) showed  
521 agreement within 5-10% between Aura MLS version 2.2 stratospheric H<sub>2</sub>O and other satellite  
522 data, including ACE-FTS H<sub>2</sub>O (see also Carleer et al., 2008), as well as for comparisons between  
523 Aura MLS and balloon data; Aura MLS H<sub>2</sub>O values are slightly larger than HALOE H<sub>2</sub>O in the

524 stratosphere, with differences increasing to 10-15% in the mesosphere. Changes from MLS v2.2  
525 to v3.3 led to an increase of 0.2-0.3 ppmv in stratospheric values (Livesey et al., 2013). Past  
526 disagreements between aircraft water vapor measurements have made those datasets somewhat  
527 difficult to use as absolute validation of satellite-derived H<sub>2</sub>O in the upper troposphere and lower  
528 stratosphere (UTLS) (Read et al., 2007, Weinstock et al., 2009). An intercomparison of  
529 measurements under controlled chamber conditions has helped to better constrain this issue  
530 (Fahey et al., 2014). Very good agreement exists between Aura MLS UTLS H<sub>2</sub>O and  
531 measurements from Cryogenic Frost point Hygrometers (CFH), as discussed by Read et al.  
532 (2007) and Voemel et al. (2007) for MLS v2.2 data. At the lowest level (147 hPa) used here for  
533 merged H<sub>2</sub>O, the latter study showed a dry bias (by ~10%) in the MLS v2.2 data versus CFH.  
534 Recent comparisons by Hurst et al. (2014) of MLS v3.3 H<sub>2</sub>O data versus Boulder CFH time  
535 series show excellent overall agreement, and no significant trend differences between coincident  
536 profile sets. There is therefore support for systematic uncertainties as low as 5% for lower  
537 stratospheric MLS data. Aura MLS stratospheric H<sub>2</sub>O v3.3 values are slightly larger (by up to  
538 ~5%) than the multi-instrument average from a number of satellite datasets, as discussed in  
539 SPARC Data Initiative comparisons by Hegglin et al. (2013). No large disagreements in  
540 interannual variations were noted by these authors for the GOZCARDS datasets (p < 150 hPa).  
541 From the mid-stratosphere to the upper mesosphere, excellent agreement between ground-based  
542 data from the Water Vapor Millimeter-wave Spectrometer (WVMS) and H<sub>2</sub>O profiles from Aura  
543 MLS and ACE-FTS has been demonstrated by Nedoluha et al. (2007, 2009, 2011).

#### 544 **4.2 GOZCARDS H<sub>2</sub>O merged data records**

545 The merging process for H<sub>2</sub>O is nearly identical to the method used for HCl. The main difference  
546 is an additional step that merges UARS MLS data with the already combined datasets from  
547 HALOE, ACE-FTS, and Aura MLS, by simply adjusting UARS MLS values to the average of  
548 the previously merged series during the early (1991-1993) overlap period; see Fig. S5 for an  
549 illustration at 22 hPa for the 5°N latitude bin. Typically, this requires an upward adjustment of  
550 the UARS MLS H<sub>2</sub>O data, as these values are biased low versus most other datasets;  
551 nevertheless, the fairly short but global record from UARS MLS helps to fill the time series.  
552 After considering the channel drift issues for SAGE II H<sub>2</sub>O (and following past advice from the

553 SAGE II team itself), we decided to use caution and did not include that dataset for GOZCARDS  
554 merging, as some trend results could be affected to an unknown extent. Also, there is probably  
555 some remaining retrieval contamination from volcanic aerosol effects for some time after the  
556 volcanic eruptions of El Chichon (1982) and Mt. Pinatubo (1991), as well as after several smaller  
557 eruptions; see Bauman et al. (2003) for a review of stratospheric aerosol climatology (1984-  
558 1999) and Thomason et al. (2008) for the SAGE II stratospheric aerosol dataset.

559 Minor procedural merging details or issues for H<sub>2</sub>O are included in the Supplement. Also,  
560 data users should be aware of effects from unequal latitudinal sampling when no MLS data exist,  
561 for regions where large latitudinal variations occur, as for H<sub>2</sub>O at 147 hPa (the largest pressure  
562 value). Indeed, global or latitudinal averages can be significantly biased in certain months and  
563 month-to-month variability for such averages increases. This is because of poor sampling of the  
564 full latitudinal variability, prior to Aug. 2004; after this, regular sampling exists from MLS every  
565 month. Such variations in sampling can become an issue for temporal analyses of latitudinal or  
566 global averages, unless additional fits or interpolations to mitigate such effects are undertaken.

567 In Fig. 11, we display the average offsets that were applied to the four H<sub>2</sub>O source datasets;  
568 these offsets follow previously known relative data biases (mentioned earlier). For example, low  
569 biases in UARS MLS H<sub>2</sub>O, especially in the mesosphere, were discussed by Pumphrey (1999)  
570 and the UARS MLS offsets (see Fig. 11) correct that dataset upward. The application of offsets  
571 derived for HALOE and UARS MLS raises the H<sub>2</sub>O time series from these instruments, whereas  
572 negative offsets lower the H<sub>2</sub>O source data from ACE-FTS and Aura MLS. As we found for  
573 HCl, the offset values generally display small variations versus latitude and are therefore fairly  
574 stable systematic adjustments to the time series. Figure S6 displays the amplitudes of the fitted  
575 annual cycles for HALOE, ACE-FTS, and Aura MLS. As for HCl, similar patterns emerge for  
576 these datasets. Wintertime descent into the polar vortex regions is responsible for large annual  
577 cycles at high latitudes, especially in the mesosphere; also, the seasonal impact of dehydration in  
578 the lower stratospheric Antarctic region causes a large annual cycle in Aura MLS high southern  
579 latitude data. Figure 12 provides some statistical information, as done for HCl in Sect. 3.2,  
580 regarding the correlations and trend differences between ACE-FTS and Aura MLS. There are a  
581 few regions with noisier relationships. While slow increases in H<sub>2</sub>O are generally observed by  
582 both instruments in the stratosphere and mesosphere, the tropical region near 0.1 hPa shows a



583 slight decreasing trend for the ACE-FTS points, thus leading to larger discrepancies; it is not  
584 clear what the source of these discrepancies is. While the tropical ACE-FTS data are generally  
585 sampled with a significantly lower temporal frequency, the same applies for all pressure levels;  
586 however, a few outlier points can have a much larger impact when sampling is poorer. There are  
587 also a few other spots, such as near 65°S and 65°N and near 5 hPa with a poor trend value for the  
588 difference series, in comparison to the errors; this may be caused by a combination of poorer  
589 sampling by ACE-FTS and higher atmospheric variability, which can lead to more scatter. At the  
590 highest latitudes in the lower stratosphere, the observed slope differences are more within error  
591 bars, but the larger variability means that a longer record is needed to determine if two time  
592 series really trend differently. The main point here is to show the dataset characteristics and to  
593 point out where the agreement is better or worse than typical. The merged dataset tends to be  
594 much closer to Aura MLS in terms of trends because there are usually many more months of  
595 Aura MLS data than ACE-FTS data, including the fact that the ACE-FTS time series (data  
596 version 2.2) used here was halted for data after late 2010 due to technical retrieval issues.  
597 Therefore, the overall impact of ACE-FTS data on the merged H<sub>2</sub>O series is fairly small.

598 Figure S7 provides a visual representation of the merged GOZCARDS H<sub>2</sub>O fields at  
599 3 hPa and 68 hPa, respectively. Well-known features are displayed in these plots, given the good  
600 global coverage in the post-2004 period in particular. In the upper stratosphere, descent at high  
601 latitudes during the winter months leads to larger H<sub>2</sub>O values, and low latitude QBO features are  
602 also observed. In the lower stratosphere, one observes dehydration evidence at high southern  
603 latitudes in the winter months, as well as a low latitude seasonal “tape recorder” signal; this  
604 phenomenon is driven by tropopause temperatures and has been measured in satellite data since  
605 the early 1990s (Mote et al., 1996; Pumphrey, 1999). A vertical cross-section of this lower  
606 stratospheric tropical (20°S to 20°N) tape recorder in GOZCARDS merged H<sub>2</sub>O for 1991-2013  
607 is shown in Fig. 13; periods of positive anomalies alternate with negative anomalies, including  
608 the post-2000 lows, as well as the most recent decreases in 2012-2013 (see also next section).

609 As we discussed for HCl, we have estimated systematic errors for the merged H<sub>2</sub>O product.  
610 This is illustrated by the contour plots in Fig. 14; these ranges encompass at least 95% of the  
611 monthly mean source data values from HALOE, UARS MLS, ACE-FTS, and Aura MLS above  
612 or below the merged series. These errors typically span 5 to 15% of the mean between 100 and

613 0.1 hPa; errors larger than 30% exist in the tropical upper troposphere (147 hPa), and similarly,  
614 large values in the upper mesosphere arise from the low bias in UARS MLS H<sub>2</sub>O.

### 615 **4.3 GOZCARDS H<sub>2</sub>O sample results and discussion**

616 Stratospheric H<sub>2</sub>O variations have garnered attention in the past two decades, because of the  
617 radiative impacts of water vapor in the UTLS and the connection to climate change, as well as  
618 the stratospheric chemical significance of H<sub>2</sub>O oxidation products. H<sub>2</sub>O can influence changes in  
619 stratospheric and mesospheric ozone via the HO<sub>x</sub> catalytic cycles. H<sub>2</sub>O in the UTLS has a  
620 significant radiative impact (e.g., Forster and Shine, 2002) and has the potential to influence  
621 surface temperature changes in ways that could mitigate surface warming (Solomon et al., 2010)  
622 if H<sub>2</sub>O exhibits a significant drop, as was observed right after 2000. A decrease of about 1 ppmv  
623 was also observed in *in situ* data (Fujiwara et al., 2010; Hurst et al., 2011; Kunz et al., 2013).  
624 Randel et al. (2004, 2006) correlated this post-2000 decrease with a decline in tropical cold point  
625 temperatures. An increasing trend in stratospheric H<sub>2</sub>O since the 1950s (see Rosenlof et al.,  
626 2001) will have a surface warming tendency. We expect to see continued studies of the influence  
627 of cold point temperatures on stratospheric H<sub>2</sub>O and the possible connections to changes in sea  
628 surface temperatures (see Rosenlof and Reid, 2008; Garfinkel et al., 2013). Efforts to better  
629 understand past changes in H<sub>2</sub>O, and their causes and expected impacts, include the references  
630 above, and (among others) Dvortsov and Solomon (2001), Shindell (2001), Nedoluha et al.  
631 (2003), Urban et al. (2007), Dhomse et al. (2008), Scherer et al. (2008), Read et al. (2008), Tian  
632 et al. (2009), Schoeberl et al. (2012), Fueglistaler (2012), Fueglistaler et al. (2013), and the  
633 recent review of the tropical tropopause layer by Randel and Jensen (2013). The reconciliation of  
634 long-term trends in tropopause temperatures with changes in lower stratospheric water vapor is a  
635 task worthy of continued study, using additional datasets as well as model studies.

636 Individual water vapor datasets have been used here to produce a merged record now  
637 spanning more than two decades. Linear trend estimates can be quite sensitive to the starting and  
638 ending points of the time series, even for 22 years of data, and simple linear trends do not best  
639 describe the variations in stratospheric H<sub>2</sub>O over the past two decades. We do not attempt here to  
640 characterize trends or to imply that recent tendencies will carry into the next decade or two.  
641 Rather, as variability is also of interest to climate modelers, we provide information below

642 regarding observed decadal-type (longer-term) variability in stratospheric water vapor. Figure 15  
643 illustrates monthly, annual, and longer-term changes in stratospheric water vapor, based on the  
644 global GOZCARDS merged H<sub>2</sub>O series; this shows the well-known H<sub>2</sub>O minimum in the lower  
645 tropical stratosphere as well as an increasing vertical gradient in the upper stratosphere (as a  
646 result of methane oxidation). As we know from past studies (e.g., Randel et al., 2004), medium-  
647 to long-term changes in H<sub>2</sub>O are large-scale in nature. However, lower stratospheric H<sub>2</sub>O  
648 variations are more accentuated at low latitudes, in comparison to near-global (60°S-60°N)  
649 results. It has long been known (e.g., from the *in situ* balloon-borne measurements of Kley et al.,  
650 1979) that the hygropause is typically located a few km higher than the thermal tropopause; this  
651 is consistent with the tape recorder and Brewer-Dobson circulation concepts. We observe low  
652 water vapor mixing ratios at 68 hPa in the tropics, in comparison to 100 hPa values (near the  
653 tropopause). According to the 22-year GOZCARDS data record, annually-averaged H<sub>2</sub>O values  
654 in the tropics (20°S-20°N) have varied between about 3.2 and 4.2 ppmv at 68 hPa. The rapid  
655 drop between 2000 and 2001 is observed at 100 and 68 hPa, with some dilution of this effect at  
656 higher altitudes. There is a clear difference in long-term behavior between the upper  
657 stratosphere, where changes in methane should have the clearest influence, and the lower  
658 stratosphere, especially in a narrow vertical region above the tropopause, where cold point  
659 temperatures and dynamical changes have a significant impact. To first-order, the last few years  
660 show ~10% larger values in the upper stratosphere than in the early 1990s, while the opposite  
661 holds in the lowest stratospheric region, where a decrease of order 10% is observed over the  
662 same period. The long-term upper stratospheric increase carries into the mesosphere (see below).  
663 Figure 15 also shows that month-to-month and seasonal variations (thin lines) are usually  
664 somewhat larger than the long-term changes in the lower stratosphere, most notably at 100 hPa.

665 In order to provide longer-term variability diagnostics for water vapor, we show in Fig. 16 the  
666 minimum to maximum spread in annual averages (tropics and mid-latitudes) from Fig. 15. These  
667 variability diagnostics are provided for the 22-yr period (1992 to 2013) and also separated into  
668 the two 11-yr periods (thin and dashed lines); as expected, the 22-yr variability is always larger  
669 than the variability in either of the two decadal period subsets. We also note that the tropical  
670 variability is largest just above the tropopause (here this means at the 68 hPa GOZCARDS

671 level), where it reaches 20-28% (or 0.8 to 1 ppmv) depending on the time period. Such  
672 variability diagnostics should be useful for comparisons to various chemistry climate models.

673 The longer-term variability in water vapor increases above the stratopause and reaches close  
674 to 30% in the uppermost mesosphere, as seen in Fig. 17(a); this plot shows the monthly and  
675 annual near-global (60°S-60°N) H<sub>2</sub>O variations at 0.01 hPa. Large seasonal changes in this  
676 region are driven by vertical advection associated with the mesospheric circulation, with each  
677 hemisphere's summertime peaks contributing to the maxima (two per year) in these near-global  
678 averages; such seasonal variations were compared to model results by Chandra et al. (1997),  
679 based on the first few years of HALOE H<sub>2</sub>O data. The strong upper mesospheric variability in  
680 annual-mean H<sub>2</sub>O is known from previous studies of ground-based and satellite H<sub>2</sub>O data  
681 (Chandra et al., 1997; Nedoluha et al., 2009; Remsberg, 2010), and this region is where the solar  
682 (Lyman  $\alpha$ ) influence on H<sub>2</sub>O is strongest. Figure 17(b) displays the near-global variations in  
683 annual upper mesospheric H<sub>2</sub>O from 0.1 to 0.01 hPa. We clearly see increased variability in the  
684 uppermost mesosphere, and decreases in the mixing ratios as a result of H<sub>2</sub>O photodissociation.

## 685 **5 GOZCARDS ozone**

686 A number of discussions relating to signs of ozone recovery have been presented before  
687 (Newchurch et al., 2003; Wohltmann et al., 2007; Yang et al., 2008; Jones et al., 2009; Hassler  
688 et al., 2011; Salby et al., 2011, 2012; Ziemke and Chandra, 2012; Gebhardt et al., 2013;  
689 Kuttipurath et al., 2013; Kirgis et al., 2013; Nair et al., 2013, 2014; Shepherd et al., 2014, Frith et  
690 al., 2014). While there are some indications of small increases in O<sub>3</sub> in the past 10-15 years,  
691 further confirmation of an increase in global O<sub>3</sub> and its correlation with column increases, is  
692 needed, in order to more clearly distinguish between long-term forcings, notably from the 11-yr  
693 solar cycle, slow changes in halogen source gases, temperature changes, and shorter-term  
694 variability. Continuing, good long-term ozone datasets are clearly needed for such studies.

### 695 **5.1 GOZCARDS ozone source data records**

696 We used ozone datasets from SAGE I, SAGE II, HALOE, UARS MLS, ACE-FTS, and Aura  
697 MLS to generate the monthly zonal mean source products for GOZCARDS. Due to time  
698 constraints, we did not use the newer SAGE II version 7 ozone (see Damadeo et al., 2013) as  
699 part of the GOZCARDS merged dataset. Our studies indicate that there are systematic

700 differences of a few percent between SAGE II V6.2 and V7 O<sub>3</sub> on their native coordinates  
701 (number density versus altitude). However, these 2 versions will exhibit different trends, mainly  
702 in the upper stratosphere, after the data are converted to mixing ratios on pressure surfaces (as  
703 shown later). These differences result mainly from different temperature trends between  
704 MERRA and analyses from the National Centers for Environmental Prediction (NCEP), which  
705 are used by the SAGE II V7 and V6.2 retrievals, respectively; the main differences between  
706 MERRA and NCEP temperatures occur in the upper stratosphere for time periods before 1989  
707 and after mid-2000. ~~After June 2000, SAGE II V6.2 O<sub>3</sub> at upper stratospheric pressures ( $\leq 3$ hPa)  
708 is not included in our merged data (see discussions in Sect. 5.2). In addition to the general data  
709 screening methods (Sect. 2), HALOE O<sub>3</sub> was screened for aerosols based on recommendations  
710 from Bhatt et al. (1999). Specifically, the O<sub>3</sub> profiles were screened for instances when either the  
711 5.26  $\mu\text{m}$  aerosol extinction exceeded  $10^{-3} \text{ km}^{-1}$  or a local aerosol extinction minimum was  
712 present near the tropopause; all O<sub>3</sub> values at or below the identified levels were flagged bad.~~

### 713 **5.1.1 Treatment of SAGE ozone profiles**

714 Both SAGE I and SAGE II used solar occultations during satellite sunrise and sunset to measure  
715 vertical profiles of ozone, along with other composition data and aerosol extinction (McCormick  
716 et al., 1989; Cunnold et al., 1989). It takes about 1 month for SAGE I and II to provide near  
717 global coverage (about 80°N to 80°S), with some dependence on season. The SAGE I  
718 measurements started in February 1979 and stopped in November 1981, while SAGE II provided  
719 data between October 1984 and August 2005. In the middle of July 2000, SAGE II had a  
720 problem in its azimuth gimbal system. Although this was corrected by November 2000, the  
721 instrument operation was switched to a 50% duty cycle, with either sunrise or sunset occultations  
722 occurring in monthly alternating periods, until the end of the mission.

723 It has been known that there were altitude registration errors in SAGE I (V5.9) data  
724 (Veiga et al., 1995; Wang et al., 1996). To correct this problem, an empirical altitude correction  
725 method based on Wang et al. (1996) had been applied to SAGE I (V5.9) data; these corrected  
726 SAGE I V5.9 profiles, which had been evaluated in previous trend studies (e.g. SPARC Report,  
727 1998; WMO, 2003), were used to create the GOZCARDS SAGE I product (denoted as version  
728 V5.9\_rev). We did not use reprocessed version 6.1 SAGE I data (L. W. Thomason, personal

729 communication) because the altitude registration problems had not been completely fixed and  
730 new altitude correction criteria should be derived and validated.

731 Ozone data screening details for the original SAGE I and SAGE II datasets are provided in  
732 the Supplementary material. The number density profiles were converted to mixing ratios on  
733 pressure levels by using NCEP temperature and pressure data provided with each profile.  
734 Derived ozone profiles were then interpolated to fixed pressure levels on the following grid:

$$735 \quad p(i) = 1000 \times 10^{-\frac{i}{30}} \text{ (hPa)} \quad i = 0, 1, 2, \dots \quad (2)$$

736 Ozone values at each of the 5 levels centered on every GOZCARDS pressure level were then  
737 averaged (weighted by pressure) to derive mixing ratios at each GOZCARDS pressure level. By  
738 doing this, the SAGE profiles were smoothed to a vertical resolution comparable to that of the  
739 other satellite instruments used in this GOZCARDS work. Monthly zonal means were then  
740 computed for the SAGE ozone datasets on the GOZCARDS-compatible grid.

### 741 **5.1.2 Comparisons of ozone zonal means**

742 O<sub>3</sub> differences between SAGE II and other satellites are shown in Fig. S8. Zonal mean  
743 differences between SAGE II and HALOE are generally within 5% for 1.5 to 68 hPa at mid-  
744 latitudes, and for 1.5 to 46 hPa in the tropics. The relative biases are larger outside those ranges  
745 and increase to ~10% near the tropopause and also near 1 hPa. SAGE II data show better  
746 agreement with UARS and Aura MLS in the upper stratosphere and lower mesosphere, within  
747 5% up to 0.68 hPa and for latitudes outside the polar regions. Aura MLS O<sub>3</sub> compares better with  
748 SAGE II data than does UARS MLS in the tropics for pressures larger than 68 hPa; the high bias  
749 in UARS MLS O<sub>3</sub> at 100 hPa has been discussed previously (Livesey et al., 2003). There are no  
750 months that include both SAGE II and ACE-FTS data in the northern hemisphere tropics (see the  
751 gap in Fig. S8, bottom right panel), largely due to the poorer coverage from ACE-FTS in the  
752 tropics. ACE-FTS O<sub>3</sub> shows the largest positive bias (greater than 10%) with respect to SAGE II,  
753 for pressures less than 1.5 hPa. The high bias in upper stratospheric ACE-FTS ozone has been  
754 mentioned in past validation work using ACE-FTS data (e.g., Froidevaux et al., 2008; Dupuy et  
755 al., 2008). The biases shown here are also consistent with recent O<sub>3</sub> intercomparison studies from  
756 a comprehensive array of satellite instruments by Tegtmeier et al. (2013). It has been known for  
757 some time that the HALOE and SAGE II ozone datasets, which govern the main variations of the

758 GOZCARDS merged ozone values before 2005, agree quite well (within 5%) in absolute value,  
759 and also in terms of temporal trends (Nazaryan et al., 2005), and versus ozonesondes (mostly  
760 above ~20 km or ~50 hPa). Larger percentage differences occur in the lowest region of the  
761 stratosphere at low latitudes, and especially in the upper troposphere, where HALOE values  
762 become significantly smaller than SAGE II data, which are already biased low (by ~50%) versus  
763 sondes (Wang et al., 2002); see also Morris et al. (2002), as well as results of SAGE II and  
764 HALOE comparisons versus solar occultation UV-Visible spectrometer measurements from long  
765 duration balloons (Borchi et al., 2005). We should note here that in this GOZCARDS merging  
766 work, we have largely avoided the upper tropospheric region.

767 Zonal mean differences between SAGE II and Aura MLS show some latitudinal structure  
768 between 1 and 3 hPa, with larger (5-10%) biases in the southern hemisphere, especially for 0 to  
769 30°S (see Fig. S8). There are no such features between SAGE II and HALOE or UARS MLS.  
770 We found that this results from anomalous NCEP temperatures after 2000, which affect SAGE II  
771 data converted from number density/altitude to GOZCARDS VMR/pressure coordinates.  
772 Figure 18 shows an example of the ozone series from SAGE II and other satellite data for 10°S to  
773 20°S from 1 to 6.8 hPa. At 1 hPa, SAGE II ozone drifts and is elevated after mid-2000, when  
774 compared to HALOE. Similar features are found down to pressures near 3 hPa. These anomalous  
775 values can be attributed to abnormal NCEP temperature trends compared to MERRA and  
776 HALOE during the same time period (for detailed views, see Figs. S9 and S10). Issues relating  
777 to anomalous upper stratospheric NCEP temperature trends were noted by McLinden et al.  
778 (2009). Because such NCEP-related artifacts are confirmed by both MERRA and HALOE, we  
779 decided not to include in the merging process any SAGE II O<sub>3</sub> values after June 30, 2000 for  
780 pressures equal to or less than 3.2 hPa. SAGE II ozone is not significantly affected by the  
781 conversion to mixing ratio/pressure coordinates at 4.6 and 6.8 hPa (Fig. 18).

## 782 **5.2 GOZCARDS ozone merged data records**

### 783 **5.2.1 Methodology for GOZCARDS merged ozone**

784 Ozone measurements from SAGE I, SAGE II, HALOE, UARS MLS, Aura MLS and ACE-FTS,  
785 as described in Sect. 5.1, were used to establish a near-continuous monthly zonal mean record

786 from late 1979 through 2012 for the GOZCARDS merged O<sub>3</sub> product (ESDR version 1.01). ~~The~~  
787 ~~monthly means from each instrument were produced after applying the screening described in~~  
788 ~~Sect. 5.1.~~ The SAGE II dataset was used as a reference standard, since it has the longest period  
789 of measurements and has been extensively validated. A GOZCARDS ozone merged data record  
790 is constructed by combining these measurements after removing systematic biases with respect  
791 to SAGE II. This is done by applying additive offsets to all other instrument series, as  
792 determined from average differences between monthly zonal means and SAGE II during overlap  
793 time periods. The merged data are then derived by averaging all available adjusted datasets.  
794 Because there are gaps in overlap between SAGE II and ACE-FTS monthly mean data in some  
795 latitudes (Fig. S7), and as SAGE II ozone VMRs obtained from the vertical grid transformation  
796 were affected by anomalous NCEP temperatures after mid-2000 for pressures smaller than or  
797 equal to 3.2 hPa, a two-step approach is used to generate the merged product. First, SAGE II data  
798 are used as reference for pressures larger than 3.2 hPa to adjust HALOE, UARS MLS and Aura  
799 MLS based on overlapping months between 1991 and Nov. 2005; see the method overview  
800 schematic in Fig. 19. For  $p \leq 3.2$  hPa, SAGE II O<sub>3</sub> is still used as a reference through June 2000,  
801 and HALOE and UARS MLS data are adjusted accordingly. This eliminates the effect of  
802 anomalous NCEP temperatures on SAGE II ozone and leads to more accurate offsets based on  
803 HALOE values, after they have been adjusted to SAGE II. The adjusted HALOE data (denoted  
804 as HALOE\* in Fig. 19) are then used as a reference to derive estimated offsets for Aura MLS O<sub>3</sub>,  
805 using the overlap period with HALOE from Aug. 2004 to Nov. 2005. In step 2, a new reference  
806 value is derived by averaging all available data from SAGE II, HALOE\*, UARS MLS\* and  
807 Aura MLS\*. This new reference value is then used to adjust the ACE-FTS ozone values based  
808 on all overlapping months between March 2004 and Nov. 2005. By including Aura MLS in the  
809 dataset created in step 1, we obtain more complete spatial and temporal coverage than possible  
810 with SAGE II and HALOE, and ensure that there are overlapping months between this combined  
811 dataset and ACE-FTS source data. At the end of step 2, the final merged ozone is derived by  
812 averaging the temporary merged dataset from step 1 with the adjusted ACE-FTS data values.

## 813 **5.2.2 Further considerations regarding GOZCARDS merged ozone data**

814 ~~Diurnal changes in ozone can affect measurement comparisons and could impact data merging.~~  
815 ~~Measurements and models of the ozone diurnal variation from the lower stratosphere to the~~



816 mesosphere have been discussed previously (Ricaud et al., 1996; Haefele et al., 2008; Huang et  
817 al., 2010). Sakazaki et al. (2013) presented diurnal changes measured by the Superconducting  
818 Submillimeter Wave Limb Emission Sounder (SMILES), and Parrish et al. (2014) have analyzed  
819 ground-based microwave ozone profile variations versus local time in conjunction with satellite  
820 datasets. These studies indicate that ozone diurnal variations range from a few percent in the  
821 lower stratosphere to more than 10% in the upper stratosphere and lower mesosphere. SAGE II  
822 and other occultation instruments observe ozone at local sunrise or sunset, and the retrieved  
823 values are generally closer to nighttime values in the upper stratosphere and mesosphere. To  
824 characterize systematic differences between satellite data, coincident profiles with small  
825 differences in space and time are most often used; an example of mean differences and standard  
826 deviations between SAGE II and Aura MLS using both coincident profile and zonal mean  
827 methods is provided in Fig. S11. SAGE II and coincident Aura MLS nighttime  $O_3$  values agree  
828 within  $\sim 5\%$  between 0.46 and 100 hPa, except in the tropical lower stratosphere where  
829 comparisons are noisier due to weak  $O_3$  signals and strong dynamical variability. Differences  
830 between zonal mean SAGE II and Aura MLS data are very close to the differences from  
831 averaged coincident values, except for pressures less than 2 hPa, where differences between the  
832 methods increase from a few % to  $\sim 10\%$  at 0.3 hPa, consistent with what one expects from the  
833 diurnal cycle. Biases between SAGE II and Aura MLS based on coincident profiles versus zonal  
834 means could be different by more than 5% in the upper stratosphere and above. Zonal mean  
835 differences are likely to be less representative of “true” differences between the two instruments.  
836 By combining SAGE II with Aura MLS data adjusted by zonal mean biases, we provide a series  
837 adjusted to the average of sunrise and sunset, as measured by SAGE II. However, if Aura MLS  
838 data were adjusted by biases obtained using the coincident method, an upper stratospheric offset  
839 of several percent and artificial trends due to such a diurnal cycle effect could be introduced.

840 —Even in the absence of diurnal variations, measurements from occultation sensors can yield  
841 larger sampling errors than those from more densely sampled emission measurements (Toohey  
842 et al., 2013). The use of long term data with consistent sampling should be an advantage for  
843 trend detection. Avoiding SAGE II data after mid-2000 also mitigates potential artifacts arising  
844 from different SAGE II sunrise/sunset sampling patterns versus time. The HALOE sampling  
845 remained fairly balanced between SR and SS events over its mission duration, although there

846 ~~were also more data gaps in the later years. Similarly, the Aura MLS ozone data generated here~~  
847 ~~are averaged from local times roughly in the middle of the day and the middle of the night, with~~  
848 ~~repeatable and stable patterns over the years; ACE-FTS sampling patterns are also quite stable.~~

849 Figure 20 displays the average ozone offsets obtained from the calculated biases versus  
850 SAGE II data. The effect of a high bias in upper stratospheric and lower mesospheric ozone from  
851 ACE-FTS relative to other datasets is made evident by the need to apply a negative offset as  
852 large as 25% to the ACE-FTS series. Most of the stratospheric offsets applied to the other  
853 instrument datasets are in the 5-10% range; a lowering of O<sub>3</sub> from UARS MLS, HALOE, and  
854 Aura MLS in the lower mesosphere is generally required to match the SAGE II values. Sampling  
855 differences and data sparseness may be responsible for larger offsets at the highest latitudes. In  
856 these regions, more caution is required with the merged data, which is also less amenable to  
857 long-term analyses because of data gaps and larger variability (especially prior to 2004).

858 As shown in the Supplement (Fig. S12), we observe strong similarities in the ozone annual  
859 cycle amplitude patterns from SAGE II, HALOE, ACE-FTS, and Aura MLS over their  
860 respective measurement periods (e.g., peaks at midlatitudes near 10 hPa and 1.5 hPa). The  
861 middle stratospheric peaks are a result of the annual cycle in oxygen photolysis, whereas  
862 temperature variations drive the annual cycle in the upper stratosphere (Perliski et al., 1989).  
863 This sort of comparison provides some (first-order) reassurance regarding the consistency of the  
864 various datasets. For further details, Fig. 21 provides diagnostics similar to those presented for  
865 HCl and H<sub>2</sub>O, namely the correlation coefficients and significance ratios for the slopes of the  
866 deseasonalized anomaly time series from SAGE II versus HALOE as well as from ACE-FTS  
867 versus Aura MLS (for 1992 through 1999, and 2005 through 2009, respectively). These  
868 diagnostic results for ACE-FTS and Aura MLS are of a quality that is comparable to the  
869 HALOE/SAGE II results; poorer fits occur mostly at high latitudes and in the upper stratosphere.  
870 Poorer correlations at upper altitude appear largely tied to a decrease in the amount of valid data  
871 in this region (especially at high latitudes), coupled with a relatively small variability. For  
872 regions with poorer agreement between ACE-FTS and Aura MLS, we often see small variability  
873 in the series from Aura MLS but larger changes (scatter) in the ACE-FTS series. Larger  
874 differences in trends between SAGE II and HALOE were noted by Nazaryan et al. (2005) at low  
875 latitudes near 50 km; this is also indicated by our simple linear fits (not shown here) to the

876 GOZCARDS source datasets from these two instruments and the existence of poorer agreements  
877 in Fig. 21 (2<sup>nd</sup> panel from top) for the slope of the differenced (anomaly) series in that region.  
878 The existence of good correlations in interannual ozone variations between a large number of  
879 satellite measurements was discussed by Tegtmeier et al. (2013). Regarding temporal drifts, Nair  
880 et al. (2012) have shown that small drifts (mostly within about  $\pm 0.5\%/yr$  for the 20-35 km  
881 region) exist between most of the datasets from six ozone lidar sites and coincident HALOE,  
882 SAGE II, and Aura MLS measurements; similar results were obtained at two of these sites by  
883 Kirgis et al. (2013). Other recent or ongoing studies (in particular, the comprehensive study by  
884 Hubert et al., 2015) corroborate the very good stability of the longer-term ozone datasets used for  
885 GOZCARDS, which relies most heavily on data from SAGE II and Aura MLS. Jones et al.  
886 (2009) also studied the consistency of various satellite datasets (including SAGE II and HALOE)  
887 for 1979-2008; they concluded that small relative drifts existed between their averaged series and  
888 individual instrument series, although they did find that larger inter-instrument drifts exist in the  
889 extra-tropical upper stratosphere. While we feel justified in the use of the longer-term time series  
890 and generally robust datasets chosen for GOZCARDS O<sub>3</sub>, data users should still note the  
891 existence of a few regions with poorer correlations or trend agreement (and, therefore, larger  
892 uncertainties) between different satellite ozone datasets, as indicated in Fig. 21. Long-term  
893 merged datasets from GOZCARDS and other sources should undergo continued scrutiny from  
894 the community, as done recently for trends by Tummon et al. (2014) and Harris et al. (2014).  
895 Sample cross-sectional views of two slices through the GOZCARDS merged O<sub>3</sub> field are  
896 provided in the Supplement (Fig. S13). Figure 22 shows estimated systematic errors from our  
897 calculation of the 95% ranges for the monthly mean source data used here, both above and below  
898 the merged values. In this case, as SAGE II is used as a reference dataset, the applied offsets  
899 (Fig. 20) correlate quite well with this plot depicting the ranges about SAGE II values. Minimum  
900 error bars can be slightly lower than 5% for the middle stratosphere at low latitudes, where ozone  
901 values are largest. This view of systematic error bars is generally consistent with results by  
902 Tegtmeier et al. (2013), who used a standard deviation measure, based on the larger set of  
903 satellite datasets analyzed for the SPARC Data Initiative. They also found that the regions with  
904 lowest errors (scatter) are in the middle stratosphere at low to mid-latitudes, where most monthly  
905 mean satellite data fit within  $\pm 5\%$  of the multi-instrument mean.

### 906 **5.3 GOZCARDS ozone sample results and discussion**

907 Nair et al. (2013) used regression analyses to compare profile trend results from GOZCARDS  
908 merged O<sub>3</sub> at northern midlatitudes versus a combined O<sub>3</sub> dataset from lidar and coincident  
909 satellite data at the Observatoire de Haute Provence (OHP), France. They showed that good  
910 consistency exists for the decreasing ozone time period, from the early 1980s to 1997, and for the  
911 upper stratospheric increase since 1997, but some differences exist in the lower stratosphere  
912 during this second time period, when the GOZCARDS results show a near-zero trend in  
913 comparison to small positive trends from the combined (and more localized) dataset. The above  
914 results for the declining time period agree broadly with earlier work (for the 1979-1997 period)  
915 by Jones et al. (2009), who averaged various satellite ozone datasets and produced trend  
916 estimates; however, these authors obtained only a small positive, but statistically insignificant,  
917 linear trend for the post-1997 phase, most likely because of too short a time series at that time.  
918 Gebhardt et al. (2013) analyzed ozone profile trends from SCIAMACHY on ENVISAT, and  
919 compared this to trends from Aura MLS, Optical Spectrograph and InfraRed Imager System  
920 (OSIRIS) on the Odin satellite, and sondes; their results include the detection of localized ozone  
921 increases in the mid-stratosphere at low latitudes; see also Bourassa et al. (2014), who analyzed  
922 merged SAGE II and (OSIRIS) observations for 1984-2013, as well as results from Kyrölä et al.  
923 (2013) on combined SAGE II and Global Ozone Monitoring by Occultation of Stars (GOMOS)  
924 records for 1984-2012, and Eckert et al. (2014), who investigated ENVISAT MIPAS trends for  
925 2002-2012. The shortness of data records since 1997, coupled with relative variability and  
926 potential drifts between various measurements may explain some differences in recent trend  
927 results, notably for the post-1997 period. More comprehensive analyses from the SI<sup>2</sup>N initiative  
928 have focused on an intercomparison of profile changes from a variety of datasets, including  
929 GOZCARDS and other merged records (Tummon et al., 2014; Harris et al., 2014).

930 Here, we investigate ozone column results based on the global GOZCARDS dataset, given  
931 the work by Ziemke and Chandra (2012), hereafter generally referenced to as ZC12; these  
932 authors analyzed total column and stratospheric column data from satellite measurements, and  
933 their analyses yielded a rather strong near-global (60°S-60°N) average ozone increase since  
934 1998. Their stratospheric column measurements depend on the convective-cloud differential  
935 (CCD) method, which uses Total Ozone Mapping Spectrometer (TOMS) and Ozone Monitoring

936 Instrument (OMI) column ozone data over convective clouds near the tropopause; below the  
937 clouds, little sensitivity exists, so the method can lead to stratospheric column estimates,  
938 especially in the tropics, where good cloud-related data of this kind exist. For midlatitudes, their  
939 methodology has focused on ozone data over the Pacific, along with a few assumptions relating  
940 to cloud heights and longitudinal invariance, in order to try to represent zonal mean stratospheric  
941 columns (see also Ziemke et al., 2005). In Fig. 23, we show the near-global total and  
942 stratospheric column values from ZC12 (J. Ziemke, private communication, 2013), along with  
943 (unscaled) GOZCARDS column densities down to three pressure levels (68, 100, and 215 hPa)  
944 for mid-latitudes (30°S-60°S and 30°N-60°N), low latitudes (30°S-30°N), and a near-global  
945 range (60°S-60°N). In an absolute sense, the GOZCARDS near-global columns above 215 hPa  
946 are larger than the ZC12 stratospheric columns, but quite close to the total column amounts from  
947 ZC12. Not too surprisingly, the GOZCARDS column values above 100 hPa are slightly lower  
948 than the stratospheric columns from ZC12, as the latter columns (estimated down to cloud tops)  
949 will capture more of the lower stratosphere in the extra-tropics. Most of the near-global decrease  
950 comes from the midlatitudes, as more of the lower stratospheric column resides in these regions,  
951 in an absolute sense. Randel and Thompson (2011) obtained small decreases (-2 to -4% per  
952 decade) in tropical lower stratospheric ozone for 1985-2009, from a combination of SAGE II  
953 ozone and sonde data from the Southern Hemisphere Additional Ozonesondes (SHADOZ)  
954 network. A fairly strong increase is observed from 2008 to 2010 at northern midlatitudes (orange  
955 curves); Steinbrecht et al. (2011) attributed large ozone enhancements in that region in 2010 to a  
956 coupling between the quasi-biennial and Arctic oscillations (and the North Atlantic oscillation).  
957 Long-term halogen source gas reductions that have occurred since the mid-1990s should only  
958 lead to an ozone increase of a few DU since 1997 (Steinbrecht et al., 2011).

959 In Fig. 24, we compare the changes in 60°S-60°N ZC12 column ozone data to the  
960 GOZCARDS column amounts above 68 hPa for that region; note that GOZCARDS values do  
961 not provide for a continuous long-term time series down to pressures of 100 hPa (or more) in the  
962 SAGE I years (1979-1981). To eliminate biases between stratospheric columns as calculated  
963 using the CCD methodology and the GOZCARDS fixed bottom pressure approach, we reference  
964 all stratospheric columns to the 1980 total column value. These column series include the SAGE  
965 I data record and are linearly interpolated between 1981 and 1984, when no GOZCARDS source

966 datasets exist. We observe that the relative changes in GOZCARDS columns follow the ZC12  
967 curves within a few DU in the downward phase until about 1992, but the 1992-1997 decrease in  
968 total columns does not compare very well. Some of this discrepancy may be because total  
969 columns capture a stronger decrease from levels below 68 hPa, not fully represented in  
970 GOZCARDS columns; there are also gaps in ZC12 stratospheric columns in 1993-1996 and  
971 other years. Focusing on the late period for GOZCARDS data from Aura MLS and ACE-FTS,  
972 we also show the GOZCARDS columns above 68 hPa, referenced to 2007 instead of 1980.  
973 There is a good match in the variations between GOZCARDS and ZC12 columns during 2005-  
974 2010, in agreement with the fact that very good correlations were obtained by ZC12 between  
975 Aura MLS column variations and stratospheric column data from the CCD technique. The ZC12  
976 values for stratospheric and total columns are in good agreement, although the stratospheric  
977 values have gaps when not enough data were present for near-global estimates. Also, the large  
978 increase in ZC12 data from 1997 to 1998 is not matched very well by GOZCARDS column data.

979 We removed the solar cycle from the deseasonalized anomalies, as was done in the ZC12  
980 study, namely via a regression fit and subtraction of that component from the time series. In the  
981 resulting plots (see Fig. 25), a 3-year smoothing is also applied (as done by ZC12). We focus in  
982 these plots on the total time period from 1979 onward, and therefore, on the GOZCARDS  
983 columns above 68 hPa. While agreement exists at the few DU level between the ZC12 relative  
984 changes and the GOZCARDS columns, the apparent ‘recovery’ in the ZC12 datasets is quite  
985 large (~3%) and is not matched by the changes in GOZCARDS columns. The latter columns  
986 show an increase of less than 0.8% between 2001 and 2011, with some decrease (by ~ 0.5%)  
987 from 2011 to 2013. We note that the recent analyses by Sheperd et al. (2014), who used a  
988 chemistry-climate model constrained by observed meteorology to investigate potential causes of  
989 long-term total column ozone variations, show a partial return, in 2010, towards the 1980 ozone  
990 levels (for 60°S-60°N), but not nearly as much as implied by ZC12, neither in the model, nor in  
991 the observations. It is possible that the discrepancies lie in the various datasets and their merging;  
992 for example, it would be worthwhile to check if homogenized SBUV column O<sub>3</sub> data show  
993 results that are substantially different from those of ZC12. Alternatively, the discrepancies could  
994 mainly reflect differences between the coverage or meaning of the different ozone columns used  
995 here (because of different methodologies, grids and/or sampling to properly determine a near-

996 global result). Although most column discrepancies are not that large as a percent of the total  
997 column values, a better consensus regarding the recovery of near-global ozone columns (and  
998 profile values discussed in other recent references) will be desirable in the future.

## 999 **6 Other GOZCARDS data records**

1000 We now briefly mention the three other datasets that were part of the delivery of GOZCARDS  
1001 records for public dissemination in 2013, namely N<sub>2</sub>O, HNO<sub>3</sub>, and temperature. For N<sub>2</sub>O and  
1002 HNO<sub>3</sub>, the somewhat simpler merging procedure consisted of averaging the source datasets from  
1003 ACE-FTS and Aura MLS over the overlap time period (Aug. 2004 through Sep. 2010) to obtain  
1004 the additive offsets for each of the two individual records. We then simply used the  
1005 correspondingly-adjusted and averaged series to create the merged results; this procedure is the  
1006 same as we described for the first step in the HCl (or H<sub>2</sub>O) merging process.

### 1007 **6.1 N<sub>2</sub>O**

1008 This data set starts in August 2004, when the Aura MLS data record began; the only dataset after  
1009 Sep. 2010 is the Aura MLS N<sub>2</sub>O (version 3.3) data record, because we no longer had ACE-FTS  
1010 version 2.2 data after that time due to ACE-FTS data processing issues mentioned earlier.  
1011 Because of degradation in the main target MLS N<sub>2</sub>O band (near 640 GHz) after the first few  
1012 months of 2013, the N<sub>2</sub>O standard MLS product will be reprocessed for the whole Aura MLS  
1013 period using an alternate measurement band and an updated software version. As discontinuities  
1014 in the version 3.3 MLS data are introduced after mid-2013, when the standard N<sub>2</sub>O product was  
1015 replaced with results from the 190 GHz band, there are currently no GOZCARDS N<sub>2</sub>O zonal  
1016 mean data after 2012 based on the original (640 GHz) MLS N<sub>2</sub>O measurement band.

1017 Validation results for the first few years of Aura MLS and ACE-FTS N<sub>2</sub>O data were provided  
1018 by Lambert et al. (2007) and Strong et al. (2008), respectively. Livesey et al. (2013) provided a  
1019 minor update regarding the v3.3 Aura MLS N<sub>2</sub>O data used here, which show typically small  
1020 differences (within ±5%) in comparison to v2.2 data. The references mentioned above showed  
1021 that excellent agreement (mostly within 5%) exists between the stratospheric ACE-FTS and Aura  
1022 MLS N<sub>2</sub>O profiles. Plots showing the average offsets applied to both MLS and ACE-FTS N<sub>2</sub>O  
1023 series as a function of latitude and pressure are provided in Fig. S14. These plots are in



1024 agreement (in magnitude and in sign) with the above-referenced studies; the two datasets yield  
1025 typical offsets (one half of the average differences) of less than 5%. Also, very good temporal  
1026 agreement between these two time series (for 2004-2010) is illustrated by the quality of the N<sub>2</sub>O  
1027 diagnostic information displayed in Fig. S15 (computed as for other MLS and ACE-FTS  
1028 comparisons discussed in this work). This generally shows very highly correlated fields, with  
1029 insignificant drifts between the two separate time series of deseasonalized N<sub>2</sub>O data; the poorest  
1030 correlations are obtained near 100 hPa in the tropics.

1031 Figure 26 shows sample contour plots for the N<sub>2</sub>O merged field (2004-2012); as seen from the  
1032 bottom panel (100 hPa), wintertime descent brings low N<sub>2</sub>O values down at high latitudes (inside  
1033 the polar vortices). N<sub>2</sub>O is a conserved tracer in the lower stratosphere and its variations near the  
1034 tropopause have implications regarding age of air. Variations in upper stratospheric N<sub>2</sub>O are  
1035 clearly affected by seasonal and dynamical effects; this is evident from the striking semi-annual,  
1036 annual and QBO-related patterns displayed in Fig. 26 for the 6.8 hPa level (top panel).

## 1037 **6.2 HNO<sub>3</sub>**

1038 As for N<sub>2</sub>O, we merged the HNO<sub>3</sub> data from ACE-FTS (version 2.2) and Aura MLS (version  
1039 3.3) from Aug. 2004 onward, and included only the adjusted MLS dataset after Sep. 2010. The  
1040 average offsets applied to MLS and ACE-FTS time series as a function of latitude and pressure  
1041 for HNO<sub>3</sub> are provided in Fig. S16. The typical offsets (one half of the average differences) for  
1042 HNO<sub>3</sub> are less than ~10% (and less than 0.5 ppbv). Despite somewhat larger percent absolute  
1043 differences than for N<sub>2</sub>O between Aura MLS and ACE-FTS HNO<sub>3</sub>, there is very good agreement  
1044 as a function of time between these two datasets in the stratosphere. This is illustrated by the  
1045 quality of the HNO<sub>3</sub> diagnostic information provided in Fig. S17; the poorest correlations are  
1046 obtained at or below the tropical tropopause.

1047 Comparisons of v3.3 Aura MLS and v2.2 ACE-FTS nitric acid profiles have shown good  
1048 agreement (see also Livesey et al., 2013), as the MLS HNO<sub>3</sub> v3.3 values are now generally larger  
1049 than in v2.2, for which validation results were provided by Santee et al. (2007). Wolff et al.  
1050 (2008) also compared MLS (v2.2) and ACE-FTS (v2.2) coincident profiles, and obtained similar  
1051 results; in addition, they demonstrated that very good agreement exists between the HNO<sub>3</sub>  
1052 profiles from ACE-FTS and coincident profiles from MIPAS on Envisat. Also, comparisons



1053 between Aura MLS HNO<sub>3</sub> (v3.3) profiles and wintertime HNO<sub>3</sub> profiles retrieved by a Ground-  
1054 based Millimeter-wave Spectrometer (GBMS) in Thule, Greenland, during the first 3 months of  
1055 2010, 2011, and 2012 have shown good agreement, mostly within 10-15% (Fiorucci et al., 2013).

1056 Figure 27 (top two panels) displays the HNO<sub>3</sub> fields at 46 hPa from the UARS MLS period  
1057 (1991-1997) as well as from the 2004-2013 period, for which a merged GOZCARDS product  
1058 was produced, based on Aura MLS and ACE-FTS source datasets. Also shown (bottom two  
1059 panels) are time series for 45°N and 32 hPa from both these periods; the bottom right panel  
1060 includes the source and merged time series. We have performed additional investigations (not  
1061 shown here) which lead us to believe that small upward adjustments to the UARS MLS HNO<sub>3</sub>  
1062 values (by about 10%) are needed to better cross-correlate these datasets across the two distinct  
1063 time periods; such relative biases are within the expected systematic errors. This is based on a  
1064 consideration of ground-based Fourier Transform infrared column HNO<sub>3</sub> data covering the full  
1065 time period, as well as past GBMS HNO<sub>3</sub> profile retrievals. Also, Aura MLS and ACE-FTS  
1066 HNO<sub>3</sub> data match ground-based and other correlative data quite well, and typically better than  
1067 the (intrinsically poorer quality) UARS MLS HNO<sub>3</sub> data. However, obtaining an optimum global  
1068 set of adjustments for the UARS MLS nitric acid field will be limited by the number of sites with  
1069 such ground-based data (as well as by the different vertical resolutions for these datasets versus  
1070 MLS). More collaborative work regarding such analyses is needed in order to find the optimum  
1071 adjustments to help tie together these two time periods for this species. Although we did not  
1072 deliver the UARS MLS HNO<sub>3</sub> source data files for GOZCARDS, we could provide these  
1073 monthly zonal mean series upon request, keeping the above caveats in mind.

### 1074 **6.3 Temperature**

1075 Finally, in terms of the initial set of delivered GOZCARDS products, and for the convenience of  
1076 stratospheric composition data users, we have used temperatures (T) from the Modern-Era  
1077 Retrospective Analysis for Research and Applications (MERRA) to produce a monthly mean  
1078 GOZCARDS temperature data set from 1979 onward. MERRA is a NASA Goddard reanalysis  
1079 (Rienecker et al., 2011) for the satellite era using Goddard Earth Observing System Data  
1080 Assimilation System version 5 (GEOS-5); T is from the DAS 3d analyzed state MAI6NVANA,  
1081 version 5.2 files (such as MERRA300.prod.assim.inst6\_3d\_ana\_Nv.20110227.hdf). Data from

1082 four daily MERRA files (for 00, 06, 12, and 18 hr UT) were averaged to provide daily mean  
1083 temperature fields (appropriate for a mean time of 09 hr). Vertical interpolation was performed  
1084 onto the GOZCARDS pressure grid, which, for temperature, covers 30 pressures levels from  
1085 1000 hPa to 0.0147 hPa. Averaged values were stored for the 10° GOZCARDS latitude bins, and  
1086 daily results were binned to create the GOZCARDS monthly temperature data set (version 1.0).

## 1087 **7 Summary and conclusions**

1088 We have reviewed the MEaSUREs GOZCARDS project's production of merged data records of  
1089 stratospheric composition using carefully screened satellite data, starting in 1979 with SAGE I  
1090 O<sub>3</sub> and continuing with Aura MLS and ACE-FTS data. The source datasets have a high degree of  
1091 maturity, and we have reinforced our confidence in their usefulness through investigations of  
1092 various diagnostics (offsets, annual cycle amplitudes, temporal correlations and trend differences  
1093 of deseasonalized series). We have focused here on the relatively long-term data records for HCl,  
1094 H<sub>2</sub>O, and O<sub>3</sub>. These records are publicly available as GOZCARDS ESDR version 1.01 and can  
1095 be referenced using DOI numbers (Froidevaux et al., 2013b, Anderson et al., 2013, and Wang et  
1096 al., 2013, for the above species, respectively). The other GOZCARDS data records mentioned  
1097 here also have dataset references, namely Schwartz et al. (2013) for the MERRA-based  
1098 temperature records, and Froidevaux et al. (2013c, 2013d) for N<sub>2</sub>O and HNO<sub>3</sub>, respectively.  
1099 Table 2 provides a summary of the monthly mean datasets produced for GOZCARDS. Yearly  
1100 netCDF files were delivered to the GES DISC for public access (see  
1101 <http://mirador.gsfc.nasa.gov>, where a README document is also available, see Froidevaux et  
1102 al., 2013a). Temperature records based on MERRA are also included on the GOZCARDS grid  
1103 (see Sect. 1). The merging methodology follows from the determination of mean biases (for each  
1104 pressure level and 10° latitude bin) between satellite instrument datasets, based on the overlap  
1105 periods between the various series. Each species is treated separately: for ozone, SAGE II data  
1106 are the chosen reference, whereas for other species, the approach is equivalent to an average of  
1107 the datasets during the periods of overlap. The merged data files contain the average offset  
1108 values that were applied to each source data time series, along with standard deviations and  
1109 standard errors. The GOZCARDS README document provides more details about the  
1110 GOZCARDS data file quantities, including local time and solar zenith angle information, and a  
1111 list of days with available data for each month. We have also presented here a compilation of

1112 systematic error estimates about the merged values. While it is difficult to identify error sources  
1113 specifically, we find that typical estimated systematic errors (ranging from ~5% to 15% for  
1114 composition data) are consistent with the magnitude of observed relative biases.

1115 The GOZCARDS HCl merged record in the upper stratosphere enables us to track long-term  
1116 changes in this reservoir for stratospheric chlorine, and by implication, total stratospheric  
1117 chlorine. The long-term increase in HCl prior to the late 1990s, and the subsequent gentler  
1118 decrease in the 21st century, are delayed manifestations of changes in the sum of the surface  
1119 source gas abundances as a result of regulations from the Montreal Protocol (and its  
1120 amendments). From 1997 to 2010, the average rate of change in upper stratospheric HCl (50°S to  
1121 50°N) was about -0.4 to -0.7%/yr. There are smaller rates of decrease and a flattening or slight  
1122 turn-around after 2003. In the lower stratosphere, where Aura MLS data weigh in heavily, recent  
1123 short-term variations have shown a flattening out and, in particular for northern midlatitudes and  
1124 at 50-70 hPa for the deep tropics, a significant reversal and increasing trend, compared to the  
1125 decrease from the late 1990s to about 2004. Mahieu et al. (2014) have discussed the reversal in  
1126 total column HCl trends for 2007-2012 (for northern, not southern midlatitudes), based on  
1127 ground-based FTIR series at various sites; they also showed that column trends agree with those  
1128 from lower stratospheric GOZCARDS abundances for the appropriate latitude bands. However,  
1129 lower stratospheric HCl tendencies appear to be reversing in recent years (2011-2014), with  
1130 decreases at northern midlatitudes (see Fig. 7 for 32 hPa) and some increasing tendencies at  
1131 southern midlatitudes (Fig. 7). Continued data will be needed to track such short-term changes in  
1132 HCl, but we expect to see long-term global HCl decreases in both upper and lower stratosphere,  
1133 as long as the Montreal Protocol and its amendments are adhered to; also, surface chlorine shows  
1134 smaller rates of decrease in recent years, for reasons that are largely understood (Sect. 3).

1135 For water vapor, we have merged monthly mean datasets for 1991-2013 from the same  
1136 satellite instruments as for HCl using the same basic methodology, except for the addition of  
1137 1991-1993 UARS MLS data, and the inclusion of Aura MLS H<sub>2</sub>O data for all pressures. Mostly  
1138 at the uppermost (mesospheric) altitudes, large variations that are anti-correlated with solar flux  
1139 are clearly observed over the past two 11-yr solar cycles, as discussed previously by others,  
1140 using shorter data records. Net long-term trends in lower stratospheric water vapor are quite  
1141 small if one considers the past 22 years, but there has been considerable interannual change, as

1142 mentioned also in past work using satellite data and Boulder sonde records. Notably, the steep  
1143 drop (by 0.5-0.8 ppmv depending on latitude and pressure from 46 to 100 hPa) from 2000 to  
1144 2001 is clearly visible in the GOZCARDS record. While the trends have been generally positive  
1145 in the decade following 2001 (see Sect. 3), the 68 and 100 hPa levels show equally steep  
1146 decreases again from 2011 to 2013 (from  $\sim 0.5$  ppmv for 60°S to 60°N averages to  $\sim 0.8$  ppmv in  
1147 the 20°S-20°N bin at 68 hPa); see also Urban et al. (2014). Long-term stratospheric trends may  
1148 be observable most readily in the upper stratosphere. In the past 22 years, long-term global H<sub>2</sub>O  
1149 increases of order 10% are observed in the upper stratosphere and lower mesosphere, whereas a  
1150 decrease of nearly 10% has occurred in the lower stratosphere (near 70-100 hPa). However, there  
1151 is no regular monotonic change on decadal timescales, especially in the tropical lower  
1152 stratosphere, where fairly sharp decreases followed by steadier increases may be a recurrent  
1153 pattern. This remains to be better understood, with ongoing global datasets; Fueglistaler (2012)  
1154 recently discussed the possibility of stepwise changes in water vapor. We have displayed the  
1155 seasonal and decadal variability in stratospheric and mesospheric H<sub>2</sub>O based on the GOZCARDS  
1156 records for the past 22 years. As one might expect from the well-documented temperature  
1157 influence on the tropical lower stratosphere, the H<sub>2</sub>O variability based on maximum minus  
1158 minimum yearly averages, is largest in the tropics and just above the tropopause. The elucidation  
1159 of lower stratospheric water vapor changes over multiple decades is complicated by the  
1160 significant low frequency variability in this region, and the occurrence of sudden changes; the  
1161 addition of a few years of data can significantly modify trend results. More accurate studies of  
1162 seasonal to decadal water vapor variability will be enabled by continuing merged H<sub>2</sub>O data from  
1163 the lower stratosphere to the upper mesosphere. A reduction in model spread for stratospheric  
1164 H<sub>2</sub>O is likely easier to achieve than tighter model results for water vapor (and ice water content)  
1165 in the upper troposphere (for this region, see the data/model comparisons by Jiang et al., 2012).  
1166 We should continue to improve model comparison results for H<sub>2</sub>O (see, for example, Gettelman  
1167 et al., 2010), although some studies should still focus on non-zonal aspects such as the Asian  
1168 monsoon or Western Pacific regions, rather than zonal means like GOZCARDS.

1169 For ozone, we have used measurements from SAGE I, SAGE II, HALOE, UARS MLS, Aura  
1170 MLS and ACE-FTS to produce a merged data record from late 1979 onward, after adjusting the  
1171 monthly zonal mean series to SAGE II averages. Some complications arose because of the

1172 conversion of the original SAGE II profiles from a density/altitude grid to the GOZCARDS  
1173 mixing ratio/pressure grid. In particular, we observed temperature-related temporal drifts in the  
1174 converted SAGE II series, as a result of the NCEP temperature data used in this conversion,  
1175 mostly in the upper stratosphere after June 2000 (see also McLinden et al., 2009). To circumvent  
1176 this issue, we used HALOE upper stratospheric O<sub>3</sub> (p < 4 hPa) as a reference for July 2000 to  
1177 November 2005, after applying offsets to the HALOE series. Aura MLS and ACE-FTS provide  
1178 the continuing data past 2004. The resulting GOZCARDS merged ozone profiles for northern  
1179 midlatitudes have recently been used in regression analyses (Nair et al., 2013) to reveal  
1180 significant decreases in the whole stratosphere during 1984-1996. Nair et al. (2014) extended this  
1181 work to a broader range of latitudes; they found significant increasing trends in upper  
1182 stratospheric GOZCARDS ozone since 1997, but no significant positive trends in the lower  
1183 stratosphere. Studies of GOZCARDS (and other) O<sub>3</sub> profile trends have been recently discussed  
1184 as part of the SI<sup>2</sup>N analyses (Tummon et al., 2014; Harris et al., 2014), among other efforts.

1185 Here, we looked into the consistency of column ozone data between stratospheric  
1186 GOZCARDS results and the study by Ziemke and Chandra (2012), who noted, using a simple  
1187 regression model, that a fairly rapid change (“recovery”) in near-global ozone columns from  
1188 TOMS and OMI data could be inferred since the mid-1990s. We show here that, unlike the 2 to  
1189 3% net increase in near-global column ozone reported by ZC12 after the late 1990s, the similarly  
1190 analyzed GOZCARDS record does not show such a strong reversal (or an upturn of more than  
1191 0.5-1% since that period). Reasons for these differences could include data coverage or  
1192 merging-related issues in either dataset, as well as differences in column sensitivities, as column  
1193 ozone data down to certain pressures (as used in GOZCARDS analyses) cannot be exactly  
1194 equivalent to stratospheric or total column estimates from ZC12; for example, changes that occur  
1195 at the lowest altitudes may not be that well captured (for all latitudes) by GOZCARDS-derived  
1196 columns. Further studies regarding the consistency of various column ozone results and a  
1197 recovery tendency are warranted; a recent global total ozone study (Sheperd et al., 2014) also  
1198 points to less of a return towards the 1980 levels than implied by ZC12.

1199 We also briefly described the creation of N<sub>2</sub>O and HNO<sub>3</sub> GOZCARDS data records, based on  
1200 Aura MLS and ACE-FTS monthly mean time series. The agreement between these two  
1201 instruments’ datasets for these species was shown to be generally very good. For HNO<sub>3</sub>, UARS

1202 MLS HNO<sub>3</sub> source datasets in the GOZCARDS format are available from the authors. However,  
1203 a small upward adjustment (of order 10%) to the UARS MLS values is most likely needed based  
1204 on our preliminary work comparing these time series to HNO<sub>3</sub> column results from FTIR  
1205 measurements. More detailed work should help determine if adjustments can indeed be made in  
1206 a more generalized way to the global UARS MLS HNO<sub>3</sub> dataset; lacking this, one should ensure  
1207 that the error bars reflect the likely biases that can affect the continuity between satellite HNO<sub>3</sub>  
1208 datasets before and after 2000, given the multi-year gap in satellite coverage for this species.

1209 **There is a Supplement related to this article.**

1210 *Acknowledgements.* We dedicate this work to the memory of Professor Derek Cunnold (Georgia  
1211 Institute of Technology) who was a member of the original GOZCARDS proposal. The  
1212 GOZCARDS data generation could not have been possible without the past work from  
1213 instrument teams for SAGE I, SAGE II, HALOE, UARS MLS, Aura MLS, and ACE-FTS, and  
1214 related data usage documentation. At JPL, we thank Joe Waters for his leadership role in making  
1215 MLS instruments and datasets possible and Bill Read for his key role; thanks to Vince Perun for  
1216 MERRA-related work, and to Brian Knosp and Robert Thurstans for database and computer  
1217 management assistance. Work at JPL was performed under contract with the National  
1218 Aeronautics and Space Administration. We also thank Kaley Walker and Ashley Jones for  
1219 comments regarding ACE-FTS data, Gloria Manney and William Daffer for help in making the  
1220 original ACE-FTS data profiles available, and Joe Zawodny and Larry Thomason for their  
1221 contributions and comments regarding SAGE data. We acknowledge the work of the GMAO  
1222 team responsible for MERRA data used to generate the GOZCARDS temperatures, specifically,  
1223 Steven Pawson and Jianjun Jin for discussions and cross-checks regarding temperature data. We  
1224 acknowledge Jerry Ziemke for the ozone column data (from Ziemke and Chandra, 2012), and  
1225 Sean Davis for discussions on data usage and screening, and the creation of long-term series. For  
1226 early HNO<sub>3</sub>-related work connecting ground-based data to MLS datasets, we thank Giovanni  
1227 Muscari and Irene Fiorucci. We are thankful for the NOAA Earth System Research Laboratory  
1228 (ESRL) Global Monitoring Division (GMD) website information and data on total surface  
1229 chlorine. We obtained solar flux data for the Ottawa/Penticton sites from the NOAA National  
1230 Geophysical Data Center (NGDC) website ([www.ngdc.noaa.gov](http://www.ngdc.noaa.gov)), for which we also  
1231 acknowledge the National Research Council of Canada.

1232 **References**

1233

1234 Anderson, J. G., Brune, W. H., and Proffitt, M. H.: Ozone destruction by chlorine radicals within the  
1235 Antarctic vortex: The spatial and temporal evolution of ClO–O<sub>3</sub> anticorrelation based on in situ ER-2  
1236 data, *J. Geophys. Res.*, 94, 11,465-11,479, 1989.

1237 Anderson, J., Russell, J. M., Solomon, S., and Deaver, L. E.: HALOE confirmation of stratospheric  
1238 chlorine decreases in accordance with the Montreal Protocol, *J. Geophys. Res.*, 105, 4483-4490, 2000.

1239 Anderson, J., Froidevaux, L., Fuller, R. A., Bernath, P. F., Livesey, N. J., Pumphrey, H. C., Read, W. G.,  
1240 and Walker, K. A.: GOZCARDS Merged Data for Water Vapor Monthly Zonal Means on a Geodetic  
1241 Latitude and Pressure Grid, version 1.01, Greenbelt, MD, USA: NASA Goddard Earth Science Data and  
1242 Information Services Center, accessible from doi:10.5067/MEASURES/GOZCARDS/DATA3003, 2013.

1243 Barath, F., Chavez, M. C., Cofield, R. E., Flower, D. A., Frerking, M. A., Gram, M. B.,  
1244 Harris, W. M., Holden, J. R., Jarnot, R. F., Kloezeman, W. G., Klose, G. J., Lau, G. K.,  
1245 Loo, M. S., Maddison, B. J., Mattauch, R. J., McKinney, R. P., Peckham, G. E., Pickett, H. M., Siebes,  
1246 G., Soltis, F. S., Suttie, R. A., Tarsala, J. A., Waters, J. W., and Wilson, W. J.: The Upper Atmosphere  
1247 Research Satellite Microwave Limb Sounder Experiment, *J. Geophys. Res.*, 98, 10751-10762, 1993.

1248 Bauman, J. J., Russell, P. B., Geller, M. A., and Hamill, P.: A stratospheric aerosol climatology from  
1249 SAGE II and CLAES measurements: 2. Results and comparisons, 1984–1999, *J. Geophys. Res.*, 108  
1250 (D13), 4383, doi:10.1029/2002JD002993, 2003.

1251 Bernath, P. F., McElroy, C. T., Abrams, M. C., Boone, D., Butler, M., Camy-Peyret, C.,  
1252 Carleer, M., Clerbaux, C., Coheur, P.-F., Colin, R., DeCola, P., DeMaziere, M., Drummond, J. R.,  
1253 Dufour, D., Evans, W. F. J., Fast, H., Fussen, D., Gilbert, K., Jennings, D. E., Llewellyn, E. J., Lowe, R.  
1254 P., Mahieu, E., McConnell, J. C., McHugh, M., McLeod, S. D., Michaud, R., Midwinter, C., Nassar, R.,  
1255 Nichitiu, F., Nowlan, C., Rinsland, C. P., Rochon, Y. J., Rowlands, N., Semeniuk, K., Simon, P., Skelton,  
1256 R., Sloan, J. J., Soucy, M.-A., Strong, K., Tremblay, P., Turnbull, D., Walker, K. A., Walkty, I., Wardle,  
1257 D. A., Wehrle, V., Zander, R., and Zou, J.: Atmospheric Chemistry Experiment (ACE): Mission  
1258 overview, *Geophys. Res. Lett.*, 32, L15S01, doi:10.1029/2005GL022386, 2005.

1259 Bhatt, P. P., Remsberg, E. E., Gordley, L. L., McInerney, J. M., Brackett, V. G., and  
1260 Russell, III, J. M.: An evaluation of the quality of Halogen Occultation Experiment ozone profiles in the  
1261 lower stratosphere, *J. Geophys. Res.*, 104 (D8), 9261-9275, 1999.

- 1262 Borchi, F., Pommereau, J.-P., Garnier, A., and Pinharanda, M.: Evaluation of SHADOZ sondes, HALOE  
1263 and SAGE II ozone profiles at the tropics from SAOZ UV-Vis remote measurements onboard long  
1264 duration balloons, *Atmos. Chem. Phys.*, 5, 1381-1397, 2005.
- 1265 Bourassa, A. E., Degenstein, D. A., Randel, W. J., Zawodny, J. M., Kyrölä, E., McLinden, C. A., Sioris,  
1266 C. E., and Roth, C. Z., Trends in stratospheric ozone derived from merged SAGE II and Odin-OSIRIS  
1267 satellite observations, *Atmos. Chem. Phys.*, 14, 6983-6994, doi:10.5194/acp-14-6983-2014, 2014.
- 1268 Brown, A. T., Chipperfield, M. P., Boone, C., Wilson, C., Walker, K. A., and Bernath, P.: Trends in  
1269 atmospheric halogen containing gases since 2004, *J. Quant. Spec. Rad. Trans.*, 112, 2552-2566, 2011.
- 1270 Carleer, M. R., Boone, C. D., Walker, K. A., Bernath, P. F., Strong, K., Sica, R. J., Randall, C., Vomel, E.  
1271 H., Kar, J., Hopfner, M., Milz, M., von Clarmann, T., Kivi, R., Valverde-Canossa, J., Sioris, C. E., Izawa,  
1272 M. R. M., Dupuy, E., McElroy, C. T., Drummond, J. R., Nowlan, C. R., Zou, J., Nichitiu, F., Lossow, S.,  
1273 Urban, J., Murtagh, D., and Dufour, D. G.: Validation of water vapour profiles from the Atmospheric  
1274 Chemistry Experiment (ACE), *Atmos. Chem. Phys. Discuss.*, 8, 4499-4559, 2008.
- 1275 Chandra, S., Jackman, C. H., Fleming, E. L., and Russell, J. M.: The seasonal and long term changes in  
1276 mesospheric water vapor, *Geophys. Res. Lett.*, 24, No. 6, 639-642, 1997.
- 1277 Chu, W. P., and McCormick, M. P.: Inversion of Stratospheric Aerosol and Gaseous Constituents From  
1278 Spacecraft Solar Extinction Data in the 0.38-1.0  $\mu\text{m}$  Wavelength Region, *Appl. Opt.*, 18, No. 9, 1404-  
1279 1413, 1979.
- 1280 Cunnold, D. M., Chu, W. P., Barnes, R. A., McCormick, M. P., and Veiga, R. E.: Validation of SAGE II  
1281 ozone measurements, *J. Geophys. Res.*, 94, 8447-8460, 1989.
- 1282 Damadeo, R. P., Zawodny, J. M., Thomason, L. W., and Iyer, N.: SAGE version 7.0 algorithm:  
1283 application to SAGE II, *Atmos. Meas. Tech.*, 6, 3539-3561, doi:10.5194/amt-6-3539-2013, 2013.
- 1284 Davis, S., et al., in preparation, 2014.
- 1285 Dhomse, S., Weber, M., and Burrows, J.: The relationship between tropospheric wave forcing and  
1286 tropical lower stratospheric water vapor, *Atmos. Chem. Phys.*, 8, 471-480, doi:10.5194/acp-8-471-2008,  
1287 2008.



1288 Dupuy, E., Walker, K. A., Kar, J., Boone, C. D., McElroy, C. T., Bernath, P. F.,  
 1289 Drummond, J. R., Skelton, R., McLeod, S. D., Hughes, R. C., Nowlan, C. R., Dufour, D. G., Zou, J.,  
 1290 Nichitiu, F., Strong, K., Baron, P., Bevilacqua, R. M., Blumenstock, T., Bodeker, G. E., Borsdorff, T.,  
 1291 Bourassa, A. E., Bovensmann, H., Boyd, I. S., Bracher, A., Brogniez, C., Burrows, J. P., Catoire, V.,  
 1292 Ceccherini, S., Chabrillat, S., Christensen, T., Coffey, M. T., Cortesi, U., Davies, J., De Clercq, C.,  
 1293 Degenstein, D. A., De Maziere, M., Demoulin, P., Dodion, J., Firanski, B., Fischer, H., Forbes, G.,  
 1294 Froidevaux, L., Fussen, D., Gerard, P., Godin-Beekmann, S., Goutail, F., Granville, J., Griffith, D.,  
 1295 Haley, C. S., Hannigan, J. W., Hopfner, M., Jin, J. J., Jones, A., Jones, N. B., Jucks, K., Kagawa, A.,  
 1296 Kasai, Y., Kerzenmacher, T. E., Kleinbohl, A., Klekociuk, A. R., Kramer, I., Kullmann, H.,  
 1297 Kuttippurath, J., Kyrölä, E., Lambert, J.-C., Livesey, N. J., Llewellyn, E. J., Lloyd, N. D., Mahieu, E.,  
 1298 Manney, G. L., Marshall, B. T., McConnell, J. C., McCormick, M. P., McDermid, I. S., McHugh, M.,  
 1299 McLinden, C. A., Mellqvist, J., Mizutani, K., Murayama, Y., Murtagh, D. P., Oelhaf, H., Parrish, A.,  
 1300 Petelina, S. V., Piccolo, C., Pommereau, J.-P., Randall, C. E., Robert, C., Roth, C., Schneider, M., Senten,  
 1301 C., Steck, T., Strandberg, A., Strawbridge, K. B., Sussmann, R., Swart, D. P. J., Tarasick, D. W., Taylor,  
 1302 J. R., Tetard, C., Thomason, L. W., Thompson, A. M., Tully, M. B., Urban, J., Vanhellefont, F.,  
 1303 Vigouroux, C., von Clarmann, T., von der Gathen, P., von Savigny, C., Waters, J. W., Witte, J. C., Wolff,  
 1304 M., and Zawodny, J. M.: Validation of ozone measurements from the Atmospheric Chemistry Experiment  
 1305 (ACE), *Atmos. Chem. Phys.*, 9, 287–343, doi:10.5194/acp-9-287-2009, 2009.

1306 Dvortsov, V. L. and Solomon, S.: Response of the stratospheric temperatures and ozone to past and future  
 1307 increases in stratospheric humidity. *J. Geophys. Res.*, 106, 7505-7514, 2001.

1308 Eckert, E., von Clarmann, T., Kiefer, M., Stiller, G. P., Lossow, S., Glatthor, N., Degenstein, D. A.,  
 1309 Froidevaux, L., Godin-Beekmann, S., Leblanc, T., McDermid, S., Pastel, M., Steinbrecht, W., Swart, D.  
 1310 P. J., Walker, K. A., and Bernath, P. F.: Drif-corrected trends and periodic variations in MIPAS IMK/IAA  
 1311 ozone measurements, *Atmos. Chem. Phys.*, 14, 2571-2589, doi:10.5194/acp-14-2571-2014, 2014.

1312 Engel, A., Strunk, M., Muller, M., Haase, H.-P., Poss, C., Levin, I., and Schmidt, U.: The temporal  
 1313 development of total chlorine in the high latitude stratosphere based on reference distributions of mean  
 1314 age derived from CO<sub>2</sub> and SF<sub>6</sub>, *J. Geophys. Res.*, 107, 4136, doi:10.1029/2001JD000584, 2002.

1315 Fahey, D. W., Gao, R.-S., Möhler, O., Saathoff, H., Schiller, C., Ebert, V., Krämer, M., Peter, T.,  
 1316 Amarouche, N., Avallone, L. M., Bauer, R., Bozoki, Z., Christensen, L. E., Davis, S. M., Durrey, G.,  
 1317 Dyroff, C., Herman, R. L., Hunsmann, S., Khaykin, S. M., Mackrodt, P., Meyer, J., Smith, J. B., Spelten,  
 1318 N., Troy, R. F., Vömel, H., Wagner, S., and Wienhold, F. G.: The AquaVIT-1 intercomparison of

1319 atmospheric water vapor measurement techniques, *Atm. Meas. Tech. Discuss.*, 7, 3159-3251,  
1320 doi:10.5194/amtd-7-3159-2014, 2014.

1321 Farman, J. C., Gardiner, B. G., and Shanklin, J. D.: Large losses of total ozone in Antarctica reveal  
1322 seasonal ClOx/NOx interaction, *Nature*, 315, 207-210, 1985.

1323 Fiorucci, I., Muscari, G., Froidevaux, L., and Santee, M. L.: Ground-based stratospheric O<sub>3</sub> and HNO<sub>3</sub>  
1324 measurements at Thule, Greenland: an intercomparison with Aura MLS observations, *Atmos. Meas.*  
1325 *Tech.*, 6, 2441–2453, doi:10.5194/amt-6-2441-2013, 2013.

1326 Forster, P. M. de F., and Shine, K. P.: Assessing the climate impact of trends in stratospheric water vapor,  
1327 *Geophys. Res. Lett.*, 29 (6), 1086, doi:10.1029/2001GL013909, 2002.

1328 Frith, S. M., Kramarova, N. A., Stolarski, R. S., McPeters, R. D., Bhartia, P. K., and Labow, G. J.: Recent  
1329 changes in total column ozone based on the SBUV Version 8.6 Merged Ozone Data Set, *J. Geophys.*  
1330 *Res.*, 119, 9735-9751, doi:10.1029/2014JD021889, 2014.

1331 Froidevaux, L., Livesey, N. J., Read, W. G., Salawitch, R. J., Waters, J. W., Drouin, B., MacKenzie, I. A.,  
1332 Pumphrey, H. C., Bernath, P., Boone, C., Nassar, R., Montzka, S., Elkins, J., Cunnold, D., and  
1333 Waugh, D.: Temporal decrease in upper atmospheric chlorine, *Geophys. Res. Lett.*, 33, L23813,  
1334 doi:10.1029/2006GL027600, 2006.

1335 Froidevaux, L., Jiang, Y. B., Lambert, A., Livesey, N. J., Read, W. G., Waters, J. W.,  
1336 Browell, E. V., Hair, J. W., Avery, M. A., McGee, T. J., Tiwgg, L. W., Sumnicht, G. K., Jucks, K. W.,  
1337 Margitan, J. J., Sen, B., Stachnik, R. A., Toon, G. C., Bernath, P. F., Boone, C. D., Walker, K. A.,  
1338 Filipiak, M. J., Harwood, R. S., Fuller, R. A., Manney, G. L., Schwartz, M. J., Daffer, W. H., Drouin, B. J.,  
1339 Cofield, R. E., Cuddy, D. T., Jarnot, R. F., Knosp, B. W., Perun, V. S., Snyder, W. V., Stek, P. C.,  
1340 Thurstans, R. P., and Wagner, P. A.: Validation of Aura Microwave Limb Sounder stratospheric and  
1341 mesospheric ozone measurements, *J. Geophys. Res.*, 113, doi:10.1029/2007JD008771, D15S20, 2008.

1342 Froidevaux, L., Fuller, R., Schwartz, M., Anderson, J., and Wang, R.: README Document for the  
1343 Global OZoneChemistry And Related trace gas Data records for the Stratosphere (GOZCARDS) project,  
1344 Goddard Earth Sciences Data and Information Services Center (GES DISC), <http://disc.gsfc.nasa.gov>,  
1345 NASA Goddard Space Flight Center, Code 610.2, Greenbelt, MD 20771 USA, 2013a.

1346 Froidevaux, L., Anderson, J., Fuller, R. A., Bernath, P. F., Livesey, N. J., Russell III, J. M., and  
1347 Walker, K.A.: GOZCARDS Merged Data for Hydrogen Chloride Monthly Zonal Means on a Geodetic

1348 Latitude and Pressure Grid, version 1.01, Greenbelt, MD, USA: NASA Goddard Earth Science Data and  
1349 Information Services Center, accessible from doi:10.5067/MEASURES/GOZCARDS/DATA3002,  
1350 2013b.

1351 Froidevaux, L., Fuller, R. A., Lambert, A., Livesey, N. J., Bernath, P. F., Livesey, N. J., and Walker,  
1352 K.A.: GOZCARDS Merged Data for Nitrous Oxide Monthly Zonal Means on a Geodetic Latitude and  
1353 Pressure Grid, version 1.01, Greenbelt, MD, USA: NASA Goddard Earth Science Data and Information  
1354 Services Center, accessible from doi:10.5067/MEASURES/GOZCARDS/DATA3013, 2013c.

1355 Froidevaux, L., Fuller, R. A., Santee, M. L., Manney, G. L., Livesey, N. J., Bernath, P. F., and Walker,  
1356 K.A.: GOZCARDS Merged Data for Nitric Acid Monthly Zonal Means on a Geodetic Latitude and  
1357 Pressure Grid, version 1.01, Greenbelt, MD, USA: NASA Goddard  
1358 Earth Science Data and Information Services Center, accessible from  
1359 doi:10.5067/MEASURES/GOZCARDS/DATA3008, 2013d.

1360 Fueglistaler, S.: Step-wise changes in stratospheric water vapor? *J. Geophys. Res.*, 117, D13302,  
1361 doi:10.1029/2012JD017582, 2012.

1362 Fueglistaler, S., Liu, Y. S., Flannaghan, T. J., Haynes, P. H., Dee, D. P., Read, W. J., Remsberg, E. E.,  
1363 Thomason, L. W., Hurst, D. F., Lanzante, J. R., and Bernath, P. F.: The relation between atmospheric  
1364 humidity and temperature trends for stratospheric water, *J. Geophys. Res.*, 118, 1052–1074,  
1365 doi:10.1002/jgrd.50157, 2013.

1366

1367 Fujiwara, M., Vomel, H., Hasebe, F., Shiotani, M., Ogino, S.- Y., Iwasaki, S., Nishi, N.,  
1368 Shibata, T., Shimizu, K., Nishimoto, E., Valverde Canossa, J. M., Selkirk, H. B., and  
1369 Oltmans, S. J.: Seasonal to decadal variations of water vapour in the tropical lower stratosphere observed  
1370 with balloon-borne cryogenic frost point hygrometers, *J. Geophys. Res.*, 115, D18304,  
1371 doi:10.1029/2010JD014179, 2010.

1372

1373 Garfinkel, C. I., Waugh, D. W., Oman, L. D., Wang, L., and Hurwitz, M. M.: Temperature trends in the  
1374 tropical upper troposphere and lower stratosphere: Connections with sea surface temperatures and  
1375 implications for water vapor and ozone, *J. Geophys. Res. Atmos.*, 118, 9658–9672,  
1376 doi:10.1002/jgrd.50772, 2013.

1377

1378 Gebhardt, C., Rozanov, A., Hommel, R., Weber, M., Bovensmann, H., Burrows, J. P., Degenstein, D.,

1379 Froidevaux, L., and Thompson, A. M.: Stratospheric ozone trends and variability as seen by  
1380 SCIAMACHY from 2002 to 2012, *Atmos. Chem. Phys.*, 14, 831–846, doi:10.5194/acp-14-831-2014,  
1381 2014.

1382

1383 Gettelman, A., Hegglin, M. I., Son, S.-W., Kim, J., Fujiwara, M., Birner, T., Kremser, S.,  
1384 Rex, M., Añel, J. A., Akiyoshi, H., Austin, J., Bekki, S., Braesike, P., Brühl, C., Butchart, N.,  
1385 Chipperfield, M., Dameris, M., Dhomse, S., Garny, H., Hardiman, S. C., Jöckel, P.,  
1386 Kinnison, D. E., Lamarque, J. F., Mancini, E., Marchand, M., Michou, M., Morgenstern, O., Pawson, S.,  
1387 Pitari, G., Plummer, D., Pyle, J. A., Rozanov, E., Scinocca, J., Shepherd, T. G., Shibata, K., Smale, D.,  
1388 Teyssèdre, H., and Tian, W.: Multimodel assessment of the upper troposphere and lower stratosphere:  
1389 Tropics and global trends, *J. Geophys. Res.*, 115, D00M08, doi:10.1029/2009JD013638, 2010.

1390 Gordley, L. L., Russell III, J. M., Mickley, L. J., Frederick, J. E., Park, J. H., Stone, K. A., Beaver, G. M.,  
1391 McNerney, J. M., Deaver, L. E., Toon, G. C., Murcray, F. J., Blatherwick, R. D., Gunson, M. R., Abbatt,  
1392 J. P. D., Mauldin III, R. L., Mount, G. H., Sen, B., and Blavier, J.-F.: Validation of nitric oxide and  
1393 nitrogen dioxide measurements made by the Halogen Occultation Experiment for UARS platform, *J.*  
1394 *Geophys. Res.*, 101, 10241-10266, 1996.

1395 Haefele, A., Hocke, K., Kampfer, N., Keckhut, P., Marchand, M., Bekki, S., Morel, B.,  
1396 Egorova, T., and Rozanov, E.: Diurnal changes in middle atmospheric H<sub>2</sub>O and O<sub>3</sub>: Observations in the  
1397 Alpine region and climate models, *J. Geophys. Res.*, 113, D17303, doi:10.1029/2008JD009892, 2008.

1398 Harris, N. R. P., et al., Past changes in the Vertical Distribution of Ozone, Part III: Analysis and  
1399 interpretation of trends, in preparation, 2014.

1400 Hassler, B., Bodeker, G. E., Solomon, S., and Young, P. J.: Changes in the polar vortex: Effects on  
1401 Antarctic total ozone observations at various stations, *Geophys. Res. Lett.*, 38, L01805,  
1402 doi:10.1029/2010GL045542, 2011.

1403 Hegglin, M. I., Tegtmeier, S., Anderson, J., Froidevaux, L., Fuller, R., Funke, B., Jones, A., Lingenfelter,  
1404 G., Lumpe, J., Pendlebury, D., Remsberg, E., Rozanov, A., Toohey, M., Urban, J., von Clarmann, T.,  
1405 Walker, K. A., Wang, R., and Weigel, K.: SPARC Data Initiative: Comparison of water vapor  
1406 climatologies from international satellite limb sounders, *J. Geophys. Res. Atmos.*, 118, 11,824–11,846,  
1407 doi: 10.1002/jgrd.50752, 2013.

1408 Hervig, M., and McHugh, M.: Cirrus detection using HALOE measurements, *Geophys. Res. Lett.*, 26,  
1409 No. 6, 719-722, 1999.

1410 Huang, F. T., Mayr, H. G., Russell III, J. M., and Mlynczak, M. G.: Ozone diurnal variations in the  
1411 stratosphere and lower mesosphere, based on measurements from SABER on TIMED,  
1412 *J. Geophys. Res.*, 115, D24308, doi:10.1029/2010JD014484, 2010.

1413 Hubert, D., et al., Ground-based assesment of the bias and long-term stability of fourteen limb and  
1414 occultation ozone profile data records, in preparation, 2014.

1415 Hurst, D. F., Oltmans, S. J., Vomel, H., Rosenlof, K. H., Davis, S. M., Ray, E. A., Hall, E. G., and  
1416 Jordan, A. F.: Stratospheric water vapor trends over Boulder, Colorado: Analysis of the 30 year Boulder  
1417 record, *J. Geophys. Res.*, 116, D02306, doi:10.1029/2010JD015065, 2011.

1418 Hurst, D. F., Lambert, A., Read, W. G., Davis, S. M., Rosenlof, K. H., Hall, E. G., Jordan, A. F., and  
1419 Oltmans, S. J.: Validation of Aura Microwave Limb Sounder stratospheric water vapor measurements by  
1420 the NOAA frost point hygrometer, *J. Geophys. Res. Atmos.*, 119, 1612-1625,  
1421 doi:10.1002/2013JD020757, 2014.

1422 Jiang, J. H., Su, H., Zhai, C., Perun, V. S., Del Genio, A., Nazarenko, L. S., Donner, L. J., Horowitz, L.,  
1423 Seman, C., Cole, J., Gettelman, A., Ringer, M. A., Rotstayn, L., Jeffrey, S., Wu, T., Brient, F., Dufresne,  
1424 J.-L., Kawai, H., Koshiro, T., Watanabe, M., L'Écuyer, T. S., Volodin, E. M., Iversen, T., Drange, H.,  
1425 Mesquita, M. D. S., Read, W. G., Waters, J. W., Tian, B., Teixeira, J., and Stephens, G. L.: Evaluation of  
1426 cloud and water vapor simulations in CMIP5 climate models using NASA "A-Train" satellite  
1427 observations, *J. Geophys. Res.*, 117, D14105, doi:10.1029/2011JD017237, 2012.

1428 Jiang, Y. B., Froidevaux, L., Lambert, A., Livesey, N. J., Read, W. G., Waters, J. W.,  
1429 Bojkov, B., Leblanc, T., McDermid, I. S., Godin-Beekmann, S., Filipiak, M. J., Harwood, R. S.,  
1430 Fuller, R. A., Daffer, W. H., Drouin, B. J., Cofield, R. E., Cuddy, D. T., Jarnot, R. F., Knosp, B. W.,  
1431 Perun, V. S., Schwartz, M. J., Snyder, W. V., Stek, P. C., Thurstans, R. P., Wagner, P. A., Allaart, M.,  
1432 Andersen, S. B., Bodeker, G., Calpini, B., Claude, H., Coetzee, G., Davies, J., De Backer, H., Dier, H.,  
1433 Fujiwara, M., Johnson, B., Kelder, H., Leme, N. P., Koenig-Langlo, G., Kyrölä, E., Laneve, G.,  
1434 Fook, L.S., Merrill, J., Morris, G., Newchurch, M., Oltmans, S., Parrondos, M.C., Posny, F., Schmidlin, F.,  
1435 Skrivankova, P., Stubi, R., Tarasick, D., Thompson, A., Thouret, V., Viatte, P., Vomel, H., von Der  
1436 Gathen, P., Yela, M., and Zablocki, G.: Validation of the Aura Microwave Limb Sounder Ozone by

1437 Ozonesonde and Lidar Measurements, *J. Geophys. Res.*, 112, D24S34, , doi:10.1029/2007JD008776,  
1438 2007.

1439 Jones, A., Urban, J., Murtagh, D. P., Eriksson, P., Brohede, S., Haley, C., Degenstein, D., Bourassa, A.,  
1440 von. Savigny, C., Sonkaew, T., Rozanov, A., Bovensmann, H., and Burrows, J.: Evolution of  
1441 stratospheric ozone and water vapour time series studied with satellite measurements, *Atmos. Chem.*  
1442 *Phys.*, 9, 6055-6075, doi:10.5194/acp-9-6055-2009, 2009.

1443 Jones, A., Urban, J., Murtagh, D. P., Sanchez, C., Walker, K. A., Livesey, N. J., Froidevaux, L., and  
1444 Santee, M. L.: Analysis of HCl and ClO time series in the upper stratosphere using satellite data sets,  
1445 *Atmos. Chem. Phys.*, 11, 5321-5333, doi:10.5194/acp-11-5321-2011, 2011.

1446 Kirgis, G., Leblanc, T., McDermid, I. S., and Walsh, T. D.: Stratospheric ozone interannual variability  
1447 (1995–2011) as observed by Lidar and Satellite at Mauna Loa Observatory, HI and Table Mountain  
1448 Facility, CA, *Atmos. Chem. Phys.*, 13, 5033–5047, doi:10.5194/acp-13-5033-2013, 2013.

1449

1450 Kley, D., Stone, E. J., Henderson, W. R., Drummond, J. W., Harrop, W. J., Schmeltekopf, A. L.,  
1451 Thompson, T. L., and Winkler, R. H.: In Situ Measurements of the Mixing Ratio of Water Vapor in the  
1452 Stratosphere, *J. Atmos. Sci.*, 36, 2513-2524, 1979.

1453

1454 Kohlhepp, R., Ruhnke, R., Chipperfield, M. P., De Maziere M., Notholt, J., Barthlott, S., Batchelor, R. L.,  
1455 Blatherwick, R. D., Blumenstock, T., Coffey, M. T., Demoulin, P., Fast, H., Feng, W., Goldman, A.,  
1456 Griffith, D. W. T., Hamann, K., Hannigan, J. W., Hase, F., Jones, N. B., Kagawa, A., Kaiser, I., Kasai, Y.,  
1457 Kirner, O., Kouker, W., Lindenmaier, R., Mahieu, E., Mittermeier, R. L., Monge-Sanz, B., Morino, I.,  
1458 Murata, I., Nakajima, H., Palm, M., Paton-Walsh, C., Raffalski, U., Reddman, T., Rettinger, M.,  
1459 Rinsland, C. P., Rozanov, E., Schneider, M., Senten, C., Servais, C., Sinnhuber, B.-M., Smale, D., Strong,  
1460 K., Sussmann, R., Taylor, J. R., Vanhaelewyn, G., Warneke, T., Whaley, C., Wiehle, M., and Wood, S.  
1461 W.: Observed and simulated time evolution of HCl, ClONO<sub>2</sub>, and HF total column abundances, *Atmos.*  
1462 *Chem. Phys.*, 12, 3527–3557, doi:10.5194/acp-12-3527-2012, 2012.

1463

1464 Kunz, A., Müller, R., Homonnai, V., Jánosi, I. M., Hurst, D., Rap, A., Forster, P. M., Rohrer, F., Spelten,  
1465 N., and Riese, M.: Extending water vapor trend observations over Boulder into the tropopause region:  
1466 Trend uncertainties and resulting radiative forcing, *J. Geophys. Res. Atmos.*, 118,  
1467 doi:10.1002/jgrd.50831, 2013.

1468 Kuttippurath, J., Lefevre, F., Pommereau, J.-P., Roscoe, H. K., Goutail, F., Pazmino, A., and Shanklin, J.  
1469 D.: Antarctic ozone loss in 1979–2010: first sign of ozone recovery, *Atmos. Chem. Phys.*, 13, 1625–1635,  
1470 doi:10.5194/acp-13-1625-2013, 2013.

1471 Kyrölä, E., Laine, M., Sofieva, V., Tamminen, J., Päivärinta, S.-M., Tukiainen, S., Zawodny, J., and  
1472 Thomason, L.: Combined SAGE II-GOMOS ozone profile data set for 1984-2011 and trend analysis of  
1473 the vertical distribution of ozone, *Atmos. Chem. Phys.*, 13, 10,645-10,658, doi:10.5194/acp-13-10645-  
1474 2013, 2013.

1475 Lambert, A., Read, W. G., Livesey, N. J., Santee, M. L., Manney, G. L., Froidevaux, L.,  
1476 Wu, D. L., Schwartz, M. J., Pumphrey, H. C., Jimenez, C., Nedoluha, G. E., Cofield, R. E., Cuddy, D. T.,  
1477 Daffer, W. H., Drouin, B. J., Fuller, R. A., Jarnot, R. F., Knosp, B. W., Pickett, H. M., Perun, V. S.,  
1478 Snyder, W. V., Stek, P. C., Thurstans, R. P., Wagner, P. A., Waters, J. W., Jucks, K. W., Toon, G. C.,  
1479 Stachnik, R. A., Bernath, P. F., Boone, C. D., Walker, K. A., Urban, J., Murtagh, D., Elkins, J. W., and  
1480 Atlas, E.: Validation of the Aura Microwave Limb Sounder stratospheric water vapour and nitrous oxide  
1481 measurements, *J. Geophys. Res.*, 112, D24S36, doi:10.1029/2007JD008724, 2007.

1482 Livesey, N. J., Read, W. J., Froidevaux, L., Waters, J. W., Santee, M. L., Pumphrey, H. C., Wu, D. L.,  
1483 Shippony, Z., and Jarnot, R. F.: The UARS Microwave Limb Sounder version 5 dataset: Theory,  
1484 characterization and validation, *J. Geophys. Res.*, 108 (D13), 4378, doi:10.1029/2002JD002273, 2003.

1485 Livesey, N. J., Read, W. G., Froidevaux, L., Lambert, A., Manney, G. L., Pumphrey, H. C., Santee, M.  
1486 L., Schwartz, M. J., Wang, S., Cofield, R. E., Cuddy, D. T., Fuller, R. A., Jarnot, R. F., Jiang, J. H.,  
1487 Knosp, B. W., Stek, P. C., Wagner, P. A., and Wu, D. L.: EOS MLS Version 3.3/3.4 Level 2 data quality  
1488 and description document, Tech. rep., Jet Propulsion Laboratory, available from <http://mls.jpl.nasa.gov/>,  
1489 2013.

1490 Mahieu, E., Duchatelet, P., Demoulin, P., Walker, K. A., Dupuy, E., Froidevaux, L., Randall, C., Catoire,  
1491 V., Strong, K., Boone, C. D., Bernath, P. F., Blavier, J.-F., Blumenstock, T., Coffey, M., DeMaziere, M.,  
1492 Griffith, D., Hannigan, J., Hase, F., Jones, N., Jucks, K. W., Kagawa, A., Kasai, Y., Mebarki, Y.,  
1493 Mikuteit, S., Nassar, R., Notholt, J., Rinsland, C. P., Robert, C., Schrems, O., Senten, C., Smale, D.,  
1494 Taylor, J., Tetard, C., Toon, G. C., Warneke, T., Wood, S. W., Zander, R., and Servais, C.: Validation of  
1495 ACE-FTS v2.2 measurements of HCl, HF, CCl<sub>3</sub>F and CCl<sub>2</sub>F<sub>2</sub> using space-, balloon- and ground-based  
1496 instrument observations, *Atmos. Chem. Phys.*, 8, 6199-6221, doi:10.5194/acp-8-6199-2008.

1497 Mahieu, E., Zander, R., Bernath, P. F., Boone, C. D., and Walker, K. A.: Recent trend anomaly of  
1498 hydrogen chloride (HCl) at northern mid-latitudes derived from Jungfraujoch, HALOE, and ACE-FTS  
1499 infrared solar observations, in: *The Atmospheric Chemistry Experiment ACE at 10: a solar occultation*  
1500 *anthology*, Bernath, P. (Ed.), Deepak Publishing, Hampton, VA, 239-249, 2013.

1501 Mahieu, E., Chipperfield, M. P., Notholt, J., Anderson, J., Bernath, P. F., Blumenstock, T., Coffey, M. T.,  
1502 Dhomse, S., Feng, W., Franco, B., Froidevaux, L., Griffith, D. W. T., Hannigan, J., Hase, F., Hossaini, R.,  
1503 Jones, N. B., Morino, I., Murata, I., Nakajima, H., Palm, M., Paton-Walsh, C., Reddman, T.,  
1504 Russell III, J. M., Schneider, M., Servais, C., Smale, D., and Walker, K. A.: Increase in northern  
1505 stratospheric hydrogen chloride over recent years, submitted, 2014.

1506 McCormick, M. P., Zawodny, J. M., Veiga, R. E., Larsen, J. C., and Wang, P. H.: An overview of SAGE-  
1507 I and II ozone measurements, *Planetary and Space Science*, 37, No. 12, 1567-1586, 1989.

1508 McHugh, M., Hervig, M., Magill, B., Thompson, R. E., Remsberg, E., Wrotny, J., and  
1509 Russell, J. M.: Improved mesospheric temperature, water vapor, and polar mesospheric cloud extinctions  
1510 from HALOE, *Geophys. Res. Lett.*, 30, 8, doi: 10.1029/2002GL016859, 2003.

1511 McLinden, C. A., Tegtmeier, S., and Fioletov, V.: Technical Note: A SAGE-corrected SBUV zonal-mean  
1512 ozone data set, *Atmos. Chem. Phys.*, 9, 7963–7972, doi:10.5194/acp-9-7963-2009, 2009.

1513 McPeters, R. D., Bhartia, P. K., Haffner, D., Labow, G. J. and Flynn, L.: The v8.6 SBUV Ozone Data  
1514 Record: An Overview, *J. Geophys. Res.*, 118, 8032-8039, doi:10.1002/jgrd.50597, 2013.

1515 Molina, M. J., and Rowland, F. S.: Stratospheric sink for chlorofluoromethane: chlorine atom-catalyzed  
1516 destruction of ozone, *Nature*, 249, 810-812, 1974.

1517 Montzka, S. A., Butler, J. H., Elkins, J. W., Thompson, T. M., Clarke, A. D., and Lock, L. T.: Present  
1518 and future trends in the atmospheric burden of ozone-depleting halogens, *Nature*, 398, 690-694, 1999.

1519 Morris, G. A., Gleason, J. F., Russell III, J. M., Schoeberl, M. R., and McCormick, M. P.: A comparison  
1520 of HALOE V19 with SAGE II V6.00 ozone observations using trajectory mapping, *J. Geophys. Res.*,  
1521 107, D13, 4177, doi:10.1029/2001JD000847, 2002.

1522 Mote, P. W., Rosenlof, K. H., McIntyre, M. E., Carr, E. S., Gille, J. C., Holton, J. R., Kinnersley, J. S.,  
1523 Pumphrey, H. C., Russell III, J. M., and Waters, J. W.: An atmospheric tape recorder: The imprint of  
1524 tropical tropopause temperatures on stratospheric water vapor,  
1525 *J. Geophys. Res.*, 101, 3989–4006, 1996.



1526 Nair, P. J., Godin-Beekmann, S., Froidevaux, L., Flynn, L. E., Zawodny, J. M., Russell III, J. M.,  
1527 Pazmino, A., Ancellet, G., Steinbrecht, W., Claude, H., Leblanc, T., McDermid, S., van Gijssel, J. A. E.,  
1528 Johnson, B., Thomas, A., Hubert, D., Lambert, J.-C., Nakane, H., and Swart, D. P. J.: Relative drifts and  
1529 stability of satellite and ground-based stratospheric ozone profiles at NDACC lidar stations, *Atmos.*  
1530 *Meas. Tech.*, 5, 1301–1318, doi: 10.5194/amt-5-1301-2012, 2012.

1531 Nair, P. J., Godin-Beekmann, S., Kuttippurath, J., Ancellet, G., Goutail, F., Pazmiño, A., Froidevaux, L.,  
1532 Zawodny, J. M., Evans, R. D., Wang, H.-J., Anderson, A., and Pastel, M.: Ozone trends derived from the  
1533 total column and vertical profiles at a northern mid-latitude station, *Atmos. Chem. Phys.*, 13, 10373–  
1534 10384, doi:10.5194/acp-13-10373-2013, 2013.

1535

1536 Nair, P. J., Froidevaux, L., Kuttippurath, J., Zawodny, J. M., Russell III, J. M., Steinbrecht, W., Claude,  
1537 H., Leblanc, T., van Gijssel, J. A. E., Johnson, B., Swart, D. P. J., Thomas, A., Querel, R., Wang, R., and  
1538 Anderson, J.: Subtropical and mid-latitude ozone trends: implications for recovery, submitted, 2014.

1539 Nazaryan, H., McCormick, M. P., and Russell III, J. M.: New studies of SAGE II and HALOE ozone  
1540 profile and long-term change comparisons, *J. Geophys. Res.*, 110, D09305, doi:10.1029/2004JD005425,  
1541 2005.

1542 Nedoluha, G. E., Bevilacqua, R. M., Gomez, R. M., Hicks, B. C., Russell III, J. M., and  
1543 Connor, B. J.: An evaluation of trends in middle atmospheric water vapor as measured by HALOE,  
1544 WVMS, and POAM, *J. Geophys. Res.*, 108 (D13), 4391, doi:10.1029/2002JD003332, 2003.

1545 Nedoluha, G. E., Gomez, R. M., Hicks, B. C., Bevilacqua, R. M., Russell III, J. M.,  
1546 Connor, B. J., and Lambert, A.: A comparison of middle atmospheric water vapor as measured by  
1547 WVMS, EOS-MLS, and HALOE, *J. Geophys. Res.*, 112, D24S39, doi:10.1029/2007JD008757, 2007.

1548

1549 Nedoluha, G. E., Gomez, R. M., Hicks, B. C., Wrotny, J. E., Boone, C., and Lambert, A.: Water vapor  
1550 measurements in the mesosphere from Mauna Loa over solar cycle 23, *J. Geophys. Res.*, 114, D23303,  
1551 doi:10.1029/2009JD012504, 2009.

1552

1553 Nedoluha, G., Gomez, R. M., Hicks, B. C., Helmboldt, J., Bevilacqua, R. M., and Lambert, A.: Ground-  
1554 based microwave measurements of water vapor from the midstratosphere to the mesosphere, *J. Geophys.*  
1555 *Res.*, 116, D02309, doi:10.1029/2010JD014728., 2011.

1556

1557 Newchurch, M. J., Yang, E. S., Cunnold, D. M., Reinsel, G. C., Zawodny, J. M., and  
1558 Russell III, J. M.: Evidence for slowdown in stratospheric ozone loss: First stage of ozone recovery, *J.*  
1559 *Geophys. Res.*, 108, D16, doi:10.1029/2003JD003471, 2003.

1560 Parrish, A., Boyd, I. S., Nedoluha, G. E., Bhartia, P. K., Frith, S. M., Kramarova, N. A.,  
1561 Connor, B. J., Bodeker, G. E., Froidevaux, L., Shiotani, M., and Sakazaki, T.: Diurnal variations of  
1562 stratospheric ozone measured by ground-based microwave remote sensing at the Mauna Loa NDACC  
1563 site: measurement validation and GEOSCCM model comparison, *Atmos. Chem. Phys.*, 7255-7272,  
1564 doi:10.5194/acp-14-7255-2014, 2014.

1565 Perliski, L. M., Solomon, S., and London, J.: On the interpretation of seasonal variations of stratospheric  
1566 ozone, *Planet. Space Sci.*, 37, 12, 1527-1538, 1989.

1567 Pumphrey, H. C.: Validation of a new prototype water vapor retrieval for UARS MLS,  
1568 *J. Geophys. Res.*, 104 (D8), 9399–9412, 1999.

1569 Pumphrey, H. C., Clark, H. L., and Harwood, R. S.: Lower stratospheric water vapor as measured by  
1570 UARS MLS, *Geophys. Res. Lett.*, 27, 1691–1694, 2000.

1571 Randel, W. J., Wu, F., Oltmans, S. J., Rosenlof, K., and Nedoluha, G. E.: Interannual changes of  
1572 stratospheric water vapor and correlations with tropical tropopause temperatures, *J. Atmos. Sci.*, 61,  
1573 2133–2148, 2004.

1574  
1575 Randel, W. J., Wu, F., Voemel, H., Nedoluha, G. E., and Forster, P.: Decreases in stratospheric water  
1576 vapor after 2001: links to changes in the tropical tropopause and the Brewer-Dobson circulation, *J.*  
1577 *Geophys. Res.*, 111, D12312, doi:10.1029/2005JD006744, 2006.

1578  
1579 Randel, W.J., and Jensen, E. J.: Physical processes in the tropical tropopause layer and their role in a  
1580 changing climate, *Nature Geosci.*, 6, 169-176, doi:10.1038/ngeo1733, 2013.

1581  
1582 Randel, W. J., and Thompson, A. M.: Interannual variability and trends in tropical ozone derived from  
1583 SAGE II satellite data and SHADOZ ozonesondes, *J. Geophys. Res.*, 116, D07303,  
1584 doi:10.1029/2010JD015195, 2011.

1585  
1586 Read, W. G., Lambert, A., Bacmeister, J., Cofield, R. E., Christensen, L. E., Cuddy, D. T., Daffer, W.  
1587 H., Drouin, B. J., Fetzer, E., Froidevaux, L., Fuller, R., Herman, R., Jarnot, R. F., Jiang, J. H., Jiang, Y.

1588 B., Kelly, K., Knosp, B. W., Kovalenko, L. J., Livesey, N. J., Liu, H.-C., Manney, G. L., Pickett, H. M.,  
1589 Pumphrey, H. C., Rosenlof, K. H., Sabouchi, X., Santee, M. L., Schwartz, M. J., Snyder, W. V., Stek, P.  
1590 C., Su, H., Takacs, L. L., Thurstans, R. P., Voemel, H., Wagner, P. A., Waters, J. W., Webster, C. R.,  
1591 Weinstock, E. M., and Wu, D. L.: Aura Microwave Limb Sounder upper tropospheric and lower  
1592 stratospheric H<sub>2</sub>O and relative humidity with respect to ice validation, *J. Geophys. Res.*, 112, D24S35,  
1593 doi:10.1029/2007JD008752, 2007.

1594

1595 Read, W. G., Schwartz, M. J., Lambert, A., Su, H., Livesey, N. J., Daffer, W. H., and  
1596 Booe, C. D.: The roles of convection, extratropical mixing, and in-situ freeze-drying in the Tropical  
1597 Tropopause Layer, *Atmos. Chem. Phys.*, 8, 6051–6067, doi:10.5194/acp-8-6051-2008, 2008.

1598

1599 Remsberg, E.: Observed seasonal to decadal scale responses in mesospheric water vapor,  
1600 *J. Geophys. Res.*, 115, D06306, doi:10.1029/2009JD012904, 2010.

1601

1602 Ricaud, P., de La Noë, J., Connor, B. J., Froidevaux, L., Waters, J. W., Harwood, R. S., MacKenzie, I. A.,  
1603 and Peckham, G. E.: Diurnal variability of mesospheric ozone as measured by the UARS microwave limb  
1604 sounder instrument: Theoretical and ground-based validations, *J. Geophys. Res.*, 101 (D6), 10,077–  
1605 10,089, doi:10.1029/95JD02841, 1996.

1606

1607 Rienecker, M., Suarez, M. J., Gelaro, R., Todling, R., Bacmeister, J., Liu, E., Bosilovich, M. G.,  
1608 Schubert, S. D., Takacs, L., Kim, G.-K., Bloom, S., Chen, J., Collins, D., Conaty, A.,  
1609 da Silva, A., Gu, W., Joiner, J., Koster, R. D., Lucchesi, R., Molod, A., Owens, T., Pawson, S., Pegion,  
1610 P., Redder, C. R., Reichle, R., Robertson, J., F. R., Ruddick, A. G., Sienkiewicz, M., and Woollen, J.:  
1611 MERRA: NASA's Modern-Era Retrospective Analysis for Research and Applications, *J. Climate*, 24,  
1612 3624–3648, doi:10.1175/JCLI-D-11-00015.1, 2011.

1613

1614 Rosenlof, K. H., and Reid, G. C.: Trends in the temperature and water vapor content of the tropical lower  
1615 stratosphere: Sea surface connection, *J. Geophys. Res.*, 113, D06107, doi:10.1029/2007JD009109, 2008.

1616

1617 Rosenlof, K. H., Chiou, E.-W., Chu, W. P., Johnson, D. G., Kelly, K. K., Michelsen, H. A., Nedoluha, G.  
1618 E., Remsberg, E. E., Toon, G. C., and McCormick, M. P.: Stratospheric water vapor increases over the  
1619 past half-century, *Geophys. Res. Lett.*, 28, 1195–1198, doi:10.1029/2000GL012502, 2001.

1620 Russell III, J. M., Gordley, L. L., Park, J. H., Drayson, S. R., Hesketh, D. H., Cicerone, R. J., Tuck, A. F.,  
1621 Frederick, J. E., Harries, J. E., and Crutzen, P.: The Halogen Occultation Experiment, *J. Geophys. Res.*,  
1622 98, 10777-10797, 1993.

1623 Russell III, J. M., Deaver, L. E., Luo, M., Park, J. H., Gordley, L. L., Tuck, A. F., Toon, G. C., Gunson ,  
1624 M. R., Traub, W. A., Johnson, D. G., Jucks, K. W., Murcray, D. G., Zander, R.,  
1625 Nolt, I. G., and Webster, C. R.: Validation of hydrogen chloride measurements made by the Halogen  
1626 Occultation Experiment from the UARS platform, *J. Geophys. Res.*, 101 (D6), 10,151– 10,162, 1996.

1627 Sakazaki, T., Fujiwara, M., Mitsuda, C., Imai, K., Manago, N., Naito, Y., Nakamura, T., Akiyoshi, H.,  
1628 Kinnison, D., Sano, T., Suzuki, M., and Shiotani, M.: Diurnal ozone variations in the stratosphere  
1629 revealed in observations from the Superconducting Submillimeter-Wave Lime-Emission Sounder  
1630 (SMILES) on board the International Space Station (ISS), *J. Geophys. Res. Atmos.*, 118, 2991-3006,  
1631 doi:10.1002/jgrd.50220, 2013.

1632 Santee, M. L., Lambert, A., Read, W. G., Livesey, N. J., Cofield, R. E., Cuddy, D. T.,  
1633 Daffer, W. H., Drouin, B. J., Froidevaux, L., Fuller, R. A., Jarnot, R. F., Knosp, B. W.,  
1634 Manney, G. L., Perun, V. S., Snyder, W. V., Stek, P. C., Thurstans, R. P., Wagner, P. A.,  
1635 Waters, J. W., Muscari, G., de Zafra, R. L., Dibb, J. E., Fahey, D. W., Popp, P. J., Marcy, T. P., Jucks, K.  
1636 W., Toon, G. C., Stachnik, R. A., Bernath, P. F., Boone, C. D., Walker, K. A.,  
1637 Urban, J., and Murtagh, D.: Validation of the Aura Microwave Limb Sounder HNO<sub>3</sub> measurements, *J.*  
1638 *Geophys. Res.*, 112, D24S40, doi:10.1029/2007JD008, 2007.

1639 Salby, M., Titova, E., and Deschamps, L.: Rebound of Antarctic ozone, *Geophys. Res. Lett.*, 38, L09702,  
1640 doi:10.1029/2011GL047266, 2011.

1641 Salby, M. L., Titova, E. A., and Deschamps, L.: Changes of the Antarctic ozone hole: Controlling  
1642 mechanisms, seasonal predictability, and evolution, *J. Geophys. Res.*, 117, D10111,  
1643 doi:10.1029/2011JD016285, 2012.

1644 Schoeberl, M. R., Dessler, A. E., and Wang, T.: Simulation of stratospheric water vapor and trends using  
1645 three reanalyses, *Atmos. Chem. Phys.*, 12, 6475–6487, doi:10.5194/acp-12-6475-2012, 2012.

1646 Schwartz, M. J., Froidevaux, L., Fuller, R. A., and Pawson, S.: GOZCARDS Merged Data for  
1647 Temperature Monthly Zonal Means on a Geodetic Latitude and Pressure Grid, version 1.01, Greenbelt,

1648 MD, USA: NASA Goddard Earth Science Data and Information Services Center, accessible from  
1649 doi:10.5067/MEASURES/GOZCARDS/DATA3023, 2013.

1650 Scherer, M., Vömel, H., Fueglistaler, S., Oltmans, S. J., and J. Staehelin, J.: Trends and variability of  
1651 midlatitude stratospheric water vapour deduced from the re-evaluated Boulder balloon series and  
1652 HALOE, *Atmos. Chem. Phys.*, 8, 1391–1402, doi:10.5194/acp-8-1391-2008, 2008.

1653

1654 Sheperd, T. G., Plummer, D. A., Scinocca, J. F., Hegglin, M. I., Fioletov, V. E., Reader, M. C., Remsberg,  
1655 E., von Clarmann, T., and Wang, H. J.: Reconciliation of halogen-induced ozone loss with the total-  
1656 column ozone record, *Nature Geoscience*, 7, 443-449, doi:10.1038/NGEO2155, 2014.

1657

1658 Shindell, D. T.: Climate and ozone response to increased stratospheric water vapor,  
1659 *Geophys. Res. Lett.*, 28, 1551-1554, doi:10.1029/1999GL011197, 2001.

1660 Solomon P. M., Barrett, J., Mooney, T., Connor, B., Parrish, A., and Siskind, D. E.: Rise and decline of  
1661 active chlorine in the stratosphere, *Geophys. Res. Lett.*, 33, L18807, doi:10.1029/2006GL027029, 2006.

1662 Sofieva, V. F., Kalakoski, N., Päivärinta, S.-M., Tamminen, J., Laine, M., and Froidevaux, L.: On  
1663 sampling uncertainty of satellite profile ozone measurements, *Atmos. Meas. Tech.*, 7, 1891–1900,  
1664 doi:10.5194/amt-7-1891-2014, 2014.

1665 Solomon, S.: Stratospheric ozone depletion: A review of concepts and history, *Rev. Geophys.*, 37, 275–  
1666 316, doi:10.1029/1999RG900008, 1999.

1667 Solomon, S., Rosenlof, K., Portmann, R., Daniel, J., Davis, S., Sanford, T., and Plattner, G.-K.:  
1668 Contributions of Stratospheric Water Vapor to Decadal Changes in the Rate of Global Warming, *Science*,  
1669 237, 1219-1223, 2010.

1670 SPARC: Assessment of Trends in the Vertical Distribution of Ozone, edited by N. Harris, R. Hudson and  
1671 C. Phillips, SPARC/IOC/GAW, WMO Ozone Research and Monitoring Project Report No. 43, 1998.

1672 SPARC WAVAS: Assessment of upper tropospheric and stratospheric water vapour, World Climate  
1673 Research Programme, WCRP-113, WMO/TD-No.1043, 261-264, 2000.

1674 Steinbrecht, W., Koehler, U., Claude, H., Weber, M., Burrows, J. P., and van der A, R. J.: Very high  
1675 ozone columns at northern mid latitudes in 2010, *Geophys. Res. Lett.*, 38, L06803,

1676 doi:10.1029/2010GL046634, 2011.

1677 Strong, K., Wolff, M. A., Kerzenmacher, T. E., Walker, K. A., Bernath, P. F., Blumenstock, T., Boone,  
1678 C., Catoire, V., Coffey, M., De Maziere, M., Demoulin, P., Duchatelet, P., Dupuy, E., Hannigan, J.,  
1679 Hopfner, M., Glatthor, N., Griffith, D. W. T., Jin, J. J., Jones, N., Jucks, K., Kuellmann, H., Kuttippurath,  
1680 J., Lambert, A., Mahieu, E., McConnell, J. C., Mellqvist, J., Mikuteit, S., Murtagh, D. P., Notholt, J.,  
1681 Piccolo, C., Raspollini, P., Ridolfi, M., Robert, C., Schneider, M., Schrems, O., Semeniuk, K., Senten, C.,  
1682 Stiller, G. P., Strandberg, A., Taylor, J., Tetard, C., Toohey, M., Urban, J., Warneke, T., and Wood, S.:  
1683 Validation of ACE-FTS N<sub>2</sub>O measurements, *Atmos. Chem. Phys.*, 8, 4759-4786, doi:10.5194/acp-8-  
1684 4759-2008, 2008.

1685 Tegtmeier, S., Hegglin, M. I., Anderson, J., Bourassa, A., Brohede, S., Degenstein, D., Froidevaux, L.,  
1686 Fuller, R., Funke, B., Gille, J., Jones, A., Kasai, Y., Krüger, K., Kyrölä, E., Lingenfelter, G., Lumpe, J.,  
1687 Nardi, B., Neu, J., Pendlebury, D., Remsberg, E., Rozanov, A., Smith, L., Toohey, M., Urban, J., von  
1688 Clarmann, T., Walker, K. A., and Wang, H. J.: The SPARC Data Initiative: A comparison of ozone  
1689 climatologies from international satellite limb sounders, *J. Geophys. Res. Atmos.*, 118, 12,229–12,247,  
1690 doi: 10.1002/2013JD019877, 2013.

1691 Thomason, L. W., Burton, S. P., Iyer, N., Zawodny, J. M., and Anderson, J.: A revised water vapor  
1692 product for the Stratospheric Aerosol and Gas Experiment (SAGE) II version 6.2 data set,  
1693 *J. Geophys. Res.*, 109 (D6), 9, 2004.

1694 Thomason, L. W., Burton, S. P., Luo, B.-P., and Peter, T.: SAGE II measurements of stratospheric  
1695 aerosol properties at non-volcanic levels, *Atmos. Chem. Phys.*, 8, 983–995, doi:10.5194/acp-8-983-2008,  
1696 2008.

1697 Thomason, L. W., Moore, J. R., Pitts, M. C., Zawodny, J. M., and Chiou, E.-W.: An evaluation of the  
1698 SAGE III Version 4 aerosol extinction coefficient and water vapor data products, *Chem. Phys. Discuss.*,  
1699 9, 22,177-22,222, 2009.

1700 Tian, W., Chipperfield, M. P., and Lu, D.: Impact of increasing stratospheric water vapor on ozone  
1701 depletion and temperature change, *Adv. in Atmos. Sci.*, 26, 3, 423–437, 2009.

1702 Toohey, M., Hegglin, M. I., Tegtmeier, S., Anderson, J., Añel, J. A., Bourassa, A., Brohede, S.,  
1703 Degenstein, D., Froidevaux, L., Fuller, R., Funke, B., Gille, J., Jones, A., Kasai, Y., Krüger, K., Kyrölä,  
1704 E., Neu, J. L., Rozanov, A., Smith, L., Urban, J., von Clarmann, T., Walker, K. A., and Wang, R.:

1705 Characterizing sampling bias in the trace gas climatologies of the SPARC Data Initiative, *J. Geophys.*  
1706 *Res. Atmos.*, 118, 11,847–11,862, doi: 10.1002/jgrd.5087, 2013.

1707 Tummon, F., Hassler, B., Harris, N. R. P., Staehelin, J., Steinbrecht, W., Anderson, J.,  
1708 Bodeker, G. E., Bourassa, A., Davis, S. M., Degenstein, D., Frith, S. M., Froidevaux, L.,  
1709 Kyrölä, E., Laine, M., Long, C., Penckwitt, A. A., Sioris, C. E., Rosenlof, K. H., Roth, C.,  
1710 Wang, H. J., and Wild, J.: Intercomparison of vertically resolved merged satellite ozone data sets:  
1711 interannual variability and long-term trends, *Atmos. Chem. Phys. Discuss.*, 14, 25687-25745, doi:  
1712 10.5194/acpd-14-25687-2014, 2014.

1713 Urban, J., Lautié, N., Murtagh, D. P., Eriksson, P., Kasai, Y., Lossow, S., Dupuy, E.,  
1714 de LaNoë, J., Frisk, U., Olberg, M., Flochmoën, E. Le., and Ricaud, P.: Global observations of middle  
1715 atmospheric water vapour by the Odin satellite: An overview, *Planet. Space Sci.*, 55, 9, 1093-1102, 2007.

1716 Urban, J., Lossow, S., Stiller, G., and Read, W.: Another drop in water vapor, *EOS Transactions,*  
1717 *American Geophysical Union*, 95, 27, 245-252, doi:10.1002/2014EO270001, 2014.

1718 Veiga, R.E., Cunnold, D. M., Chu, W. P., and McCormick, M. P.: Stratospheric Aerosol and Gas  
1719 Experiments I and II comparisons with ozonesondes. *J. Geophys. Res.*, 100 (D5), 9073-9090, 1995.

1720 Voemel, H., Barnes, J. E., Forno, R. N., Fujiwara, M., Hasebe, F., Iwasaki, S., Kivi, R., Komala, N.,  
1721 Kyrölä, E., Leblanc, T., Morel, B., Ogino, S.-Y., Read, W. G., Ryan, S. C., Saraspriya, S., Selkirk, H.,  
1722 Shiotani, M., Valverde Canossa, J., and Whiteman, D. N.: Validation of Aura Microwave Limb Sounder  
1723 water vapor by balloon-borne Cryogenic Frost point Hygrometer measurements, *J. Geophys. Res.*, 112,  
1724 D24S37, doi:10.1029/2007JD008698, 2007.

1725 Wang, H. J., Cunnold, D. M., and Bao, X.: A critical analysis of Stratospheric Aerosol and Gas  
1726 Experiment ozone trends *J. Geophys. Res.*, 101 (D7), 12495-12514, 1996.

1727 Wang, H. J., Cunnold, D. M., Thomason, L. W., Zawodny, J. M., and Bodeker, G. E.: Assessment of  
1728 SAGE version 6.1 ozone data quality, *J. Geophys. Res.*, 107 (D23),  
1729 doi: 10.1029/2002JD002418, 2002.

1730 Wang, H. J., Cunnold, D. M., Treppe, C., Thomason, L. W., and Zawodny, J. M.: SAGE III solar ozone  
1731 measurements: Initial results, *Geophys. Res. Lett.*, 33, L03805, doi:10.1029/2005GL025099, 2006.

1732 Wang, R., Froidevaux, L., Anderson, J., Fuller, R. A., Bernath, P. F., McCormick, M. P., Livesey, N. J.,  
1733 Russell III, J. M., Walker, K. A., and Zawodny, J. M.: GOZCARDS Merged Data for Ozone Monthly  
1734 Zonal Means on a Geodetic Latitude and Pressure Grid, version 1.01, Greenbelt, MD, USA: NASA

1735 Goddard Earth Science Data and Information Services Center, accessible from  
1736 doi:10.5067/MEASURES/GOZCARDS/DATA3006, 2013.

1737 Waters, J. W., Microwave limb sounding, in *Atmospheric Remote Sensing by Microwave Radiometry*,  
1738 ed. by M. Janssen, chap. 8, John Wiley, New York, 1993.

1739 Waters, J. W., Froidevaux, L., Read, W. G., Manney, G. L., Esilon, L. S., Flower, D. A., Jarnot, R. F., and  
1740 Harwood, R. S.: Stratospheric ClO and ozone from the Microwave Limb Sounder on the Upper  
1741 Atmosphere Reseach Satellite, *Nature*, 362, 597-602, 1993.

1742 Waters, J. W., Froidevaux, L., Harwood, R. S., Jarnot, R. F., Pickett, H. M., Read, W. G., Siegel, P. H.,  
1743 Cofield, R. E., Filipiak, M. J., Flower, D. A., Holden, J. R., Lau, G. K., Livesey, N. J., Manney, G. L.,  
1744 Pumphrey, H. C., Santee, M. L., Wu, D. L., Cuddy, D. T., Lay, R. R., Loo, M. S., Perun, V. S., Schwartz,  
1745 M. J., Stek, P. C., Thurstans, R. P., Boyles, M. A., Chandra, S., Chavez, M. C., Chen, G.-S., Chudasama,  
1746 B. V., Dodge, R., Fuller, R. A., Girard, M. A., Jiang, J. H., Jiang, Y., Knosp, B. W., LaBelle, R. C., Lam,  
1747 J. C., Lee, K. A., Miller, M., Oswald, J. E., Patel, N. C., Pukala, D. M., Quintero, O., Scaff, D. M.,  
1748 Snyder, W. V., Tope, M. C., Wagner, P. A., and Walch, M. J.: The Earth Observing System Microwave  
1749 Limb Sounder (EOS MLS) on the Aura satellite, *IEEE Trans. Geosci. Remote Sens.*, 44 (5), 1075–1092,  
1750 doi:10.1109/TGRS.2006.873771, 2006.

1751 Waugh, D. W., Considine, D. B., and Fleming, E. L.: Is Upper Stratospheric Chlorine Decreasing as  
1752 Expected?, *Geophys. Res. Lett.*, 28(7), 1187–1190, 2001.

1753 Weinstock, E. M., Smith, J. B., Sayres, D. S., Pittman, J. V., Spackman, J. R., Hints, E. J., Hanisco, T.  
1754 F., Moyer, E. J., St. Clair, J. M., Sargent, M. R., and Anderson, J. G.: Validation of the Harvard Lyman- $\alpha$   
1755 in situ water vapor instrument: Implications for the mechanisms that control stratospheric water vapor, *J.*  
1756 *Geophys. Res.*, 114, D23301, doi:10.1029/2009JD012427, 2009.

1757 WMO (World Meteorological Organization): *Scientific Assessment of Ozone Depletion: 2002*, Global  
1758 Ozone Research and Monitoring Project – Report No. 47, Geneva, Switzerland, 2003.

1759 WMO (World Meteorological Organization), *Scientific Assessment of Ozone Depletion: 2010*, Global  
1760 Ozone Research and Monitoring Project – Report No. 52, Geneva, Switzerland, 2011.

1761 Wohltmann, I., Lehmann, R., Rex, M., Brunner, D., and Mader, J.A.: A process-oriented regression  
1762 model for column ozone, *J. Geophys. Res.*, 112, D12304, doi:10.1029/2006JD007573, 2007.

1763 Wolff, M. A., Kerzenmacher, T., Strong, K., Walker, K. A., Toohey, M., Dupuy, E., Bernath, P. F.,  
1764 Boone, C. D., Brohede, S., Catoire, V., von Clarmann, T., Coffey, M., Daffer, W. H., De Maziere, M.,



1765 Duchatelet, P., Glatthor, N., Griffith, D. W. T., Hannigan, J., Hase, F., Hopfner, M., Huret, N., Jones, N.,  
1766 Jucks, K., Kagawa, A., Kasai, Y., Kramer, I., Kullmann, H., Kuttippurath, J., Mahieu, E., Manney, G.,  
1767 McElroy, C. T., McLinden, C., Mebarki, Y., Mikuteit, S., Murtagh, D., Piccolo, C., Raspollini, P.,  
1768 Ridolfi, M., Ruhnke, R., Santee, M., Senten, C., Smale, D., Tetard, C., Urban, J., and Wood, S.:  
1769 Validation of HNO<sub>3</sub>, ClONO<sub>2</sub>, and N<sub>2</sub>O<sub>5</sub> from the Atmospheric Chemistry Experiment Fourier Transform  
1770 Spectrometer (ACE-FTS), *Atmos. Chem. Phys.*, 8, 3529–3562, doi:10.5194/acp-8-3529-2008, 2008.

1771 Yang, E.-S., Cunnold, D. M., Newchurch, M. J., Salawitch, R., McCormick, J. M. P., Russell III, J. M.,  
1772 Zawodny, J. M., and Oltmans, S. J.: First stage of Antarctic ozone recovery, *J. Geophys. Res.*, 113,  
1773 D20308, doi:10.1029/2007JD009675, 2008.

1774 Ziemke, J. R., and Chandra, S.: Development of a climate record of tropospheric and stratospheric  
1775 column ozone from satellite remote sensing: evidence of an early recovery of global stratospheric ozone,  
1776 *Atmos. Chem. Phys.*, 12, 5737-5753, doi:10.5194/acp-12-5737-2012, 2012.

1777 Ziemke, J. R., Chandra, S., and Bhartia, P. K.: A 25-year data record of atmospheric ozone from TOMS  
1778 Cloud Slicing: Implications for trends in stratospheric and tropospheric ozone, *J. Geophys. Res.*, 110,  
1779 D15105, doi:10.1029/2004JD005687, 2005.

1780

## 1781 **Appendix A**

### 1782 **A.1. GOZCARDS data provenance**

1783 The general origin of the datasets is summarized here. Data coverage from limb sounders  
1784 (including the instruments used here) is displayed nicely in the work by Toohey et al. (2013).

#### 1785 ***SAGE I***

1786 SAGE I was launched February 18, 1979, aboard the Applications Explorer Mission-B  
1787 (AEM-B) satellite. SAGE I was a sun photometer using solar occultation (Chu and McCormick,  
1788 1979), and it collected a global database for nearly three years on stratospheric aerosol, O<sub>3</sub>, and  
1789 NO<sub>2</sub>. For more information, the reader is referred to <http://sage.nasa.gov/SAGE1>.

#### 1790 ***SAGE II***

1791 SAGE II was launched aboard the Earth Radiation Budget Satellite (ERBS) in October 1984  
1792 and its data gathering period ended in August 2005. During each sunrise and sunset, SAGE II  
1793 measured stratospheric aerosols, O<sub>3</sub>, NO<sub>2</sub>, and H<sub>2</sub>O via solar occultation. This long dataset has  
1794 proven very valuable in determining past ozone trends. For more information on and data access  
1795 to the (V6.2) dataset used for GOZCARDS, the reader is referred to <http://sage.nasa.gov/SAGE2>.

#### 1796 ***HALOE***

1797 Since its launch on September 12, 1991 from the Space Shuttle Discovery until November  
1798 2005, UARS HALOE collected profiles of atmospheric composition and temperature. HALOE  
1799 (Russell et al., 1993) used solar occultation to measure vertical profiles of O<sub>3</sub>, HCl, HF, CH<sub>4</sub>,  
1800 H<sub>2</sub>O, NO, NO<sub>2</sub>, temperature, aerosol extinction, and aerosol composition and size distribution.  
1801 More information and access to the HALOE data can be obtained from <http://haloe.gats-inc.com>  
1802 and <http://disc.sci.gsfc.nasa.gov/UARS/data-holdings/HALOE>. For GOZCARDS purposes, we  
1803 have used Version 19 HALOE netCDF data files available at <http://haloe.gats-inc.com>.

#### 1804 ***UARS MLS***

1805 This instrument observed the Earth's limb in microwave emission using three radiometers, at  
1806 frequencies near 63, 183 and 205 GHz (Waters, 1993; Barath et al., 1993), providing unique

1807 daily global information on stratospheric ClO, along with other profiles, including O<sub>3</sub>, H<sub>2</sub>O,  
1808 HNO<sub>3</sub>, temperature, and cloud ice water content. The stratospheric H<sub>2</sub>O data ceased on April 15,  
1809 1993, after the failure of the 183 GHz radiometer. After March 15, 1994, measurements became  
1810 increasingly sparse in order to conserve the life of the MLS antenna scan mechanism and UARS  
1811 power. Data exist until July 28, 1999, although for GOZCARDS, only data through mid-June  
1812 1997 are used, as data sparseness and degradation of the 63 GHz radiometer led to less ‘trend-  
1813 quality’ data after this. Sampling patterns follow the alternating yaw cycles imposed on MLS by  
1814 the precessing UARS orbit; MLS measurements were obtained continuously for all latitudes  
1815 between 34°S and 34°N, with higher latitudes covered in either the northern or southern  
1816 hemisphere with a roughly 36-day cycle. Livesey et al. (2003) provide more information on the  
1817 UARS MLS instrument, retrievals, and results. For data access, the reader is directed to the  
1818 relevant Goddard Earth Sciences and Information Services Center (GES DISC) data holdings at  
1819 <http://disc.sci.gsfc.nasa.gov/UARS/data-holdings/MLS>. L3AT data files were used as the basis  
1820 for the production of the GOZCARDS UARS MLS monthly source datasets.

### 1821 *ACE-FTS*

1822 ACE-FTS is the primary instrument onboard the SCISAT satellite, launched on August 12, 2003.  
1823 It is a high spectral resolution (0.02 cm<sup>-1</sup>) Michelson interferometer operating from 2.2 to  
1824 13.3 μm (750-4400 cm<sup>-1</sup>); see Bernath et al. (2005) for an overview of the ACE mission. The  
1825 instrument can simultaneously measure temperature and many trace gases (including all the  
1826 species mentioned here for GOZCARDS), thin clouds, and aerosols, using the solar occultation  
1827 technique. ACE-FTS data version 2.2, along with the version 2.2 update for ozone, were used  
1828 here for GOZCARDS. For access to the public ACE-FTS datasets, with a routine measurement  
1829 start date of March 2004, the reader is directed to <http://www.ace.uwaterloo.ca>.

### 1830 *Aura MLS*

1831 MLS is one of four instruments on NASA's Aura satellite, launched on July 15th 2004. Aura  
1832 MLS is a greatly enhanced version of the UARS MLS experiment, providing better spatial  
1833 coverage, vertical resolution, and vertical range, along with more continuous data over its  
1834 lifetime (and with ongoing measurements at the time of writing). The instrument includes

1835 radiometers at 118, 190, 240, and 640 GHz, and a 2.5 THz module (Waters et al., 2006). Aura  
 1836 MLS provides measurements of many chemical species, cloud ice, temperature and geopotential  
 1837 height. Continuous measurements have been obtained since August 2004, with the exception of  
 1838 OH, for which sparser measurements exist since August 2010, in order to preserve the life of the  
 1839 THz module. For more information and access to the Aura MLS datasets, the reader is referred to  
 1840 <http://disc.sci.gsfc.nasa.gov/Aura/data-holdings/MLS>. For GOZCARDS, we use the currently  
 1841 recommended Aura MLS data versions (version 2.2/2.3 for ozone and 3.3/3.4 for other species).

## 1842 **A.2. Calculation details for the iterative merging procedure**

1843 Given three time series, the merging procedure that we use first combines two out of the three  
 1844 time series,  $y_1(i)$  and  $y_2(i)$  (where index  $i$  represents time for each monthly mean value in a given  
 1845 latitude/pressure bin). We first obtain the temporary merged series  $m_1(i)$  via:  
 1846 
$$m_1(i) = (1/2) (y_1(i) + y_2(i)) \quad (1)$$

1847 with the average offsets for  $y_1(i)$  and  $y_2(i)$  being  $(1/(2 n_{12})) \sum (y_1(i) - y_2(i))$  and -1 times this value,  
 1848 respectively;  $n_{12}$  is the number of overlapping data points between the two time series. Then, we  
 1849 merge together the time series  $m_1(i)$  and  $y_3(i)$ , keeping the weightings equal for all 3 time series  
 1850 (1/3 for each), so that we calculate the new merged time series  $m(i)$  via:

$$1851 \quad m(i) = w_m m_1(i) + w_3 y_3(i) = (1/3) (y_1(i) + y_2(i) + y_3(i)) \quad (2)$$

1852 which will hold if the weights are  $w_m = 2/3$  and  $w_3 = 1/3$  (given equation (1) for  $m_1(i)$ ). The  
 1853 average reference value (to which the adjustments of  $m_1(i)$  and  $y_3(i)$  in the 2<sup>nd</sup> step are made) is  
 1854 given by  $(1/n_m) \sum ( (2/3) m_1(i) + (1/3) y_3(i) )$ , where  $n_m$  represents the number of (overlapping  
 1855 pairs of) data values used in step 2. For the HCl and H<sub>2</sub>O data merging procedure, we always use  
 1856 the Aura MLS time series as one of the first two series involved in the initial merging step, for  
 1857 example as  $y_1(i)$ , in order to maximize the overlap between the first two series and obtain more  
 1858 robust offset values. Then, we use the 3<sup>rd</sup> time series; the order used for HALOE and ACE-FTS  
 1859 (i.e., whether we use HALOE or ACE-FTS for  $y_2$  or  $y_3$ ) makes very little difference.

## 1860 **Calculation of the standard deviation for the merged data values**

1861 The average and standard deviation (square root of variance) for each  $y_k$  value (i.e. for each  
 1862 monthly zonal mean in a particular lat/p bin) are calculated from equations (3) and (4) below:

1863 
$$\bar{y}_k = \frac{1}{n_{yk}} \sum_j y_{kj} \quad (3)$$

1864 and, for the variance,

1865 
$$\sigma_{yk}^2 = \frac{1}{n_{yk} - 1} \sum_j (y_{kj} - \bar{y}_k)^2 \quad (4)$$

1866 where index “ $j$ ” corresponds to individual data values within a month, index  $k$  represents a given  
 1867 instrument (data source), and  $n$  is the total number of data values for a given bin and source  
 1868 (instrument) time series point in time (or month). Each value  $\bar{y}_k$  above is a monthly average  
 1869 (although we also use instead the simpler notation  $y_k$ ), with standard deviation about the mean  
 1870  $\sigma_{yk}$ . Now, given the merged series  $u(i)$  (where index  $i$  runs over a large number of months), the  
 1871 standard deviation of each merged data point (for a given month) can be obtained by considering  
 1872 the original datasets  $y_{kj}$  that were used to construct  $u$ . Specifically, we have the variance for the  
 1873 merged dataset

1874 
$$\sigma_u^2 = \frac{1}{n_u - 1} \sum_j (u_j - u_{ref})^2 \quad (5)$$

1875 where  $u_{ref}$  is the merged value (which is not necessarily chosen to be the average value  $\bar{u}$ ) and  
 1876 the  $u_j$  values represent the union of adjusted data values that make up the merged product, with  
 1877 the index  $j$  for this combined dataset covering all values (up to the total  $n_u$ ) obtained from the  
 1878 original source values  $y_{kj}$ . In practice, we do not keep track of the individual data values that  
 1879 went into making the averages for the series  $y_k$  that are being merged, and we need to obtain  $\sigma_u$   
 1880 based solely on the values  $\bar{y}_k$ ,  $\sigma_{yk}$ , and the original number of points for each dataset  $y_k$ ,  
 1881 namely  $n_{yk}$ . If we consider all the original values, we have a combined dataset with  $n_u$  points,  
 1882 such that  $n_u = \sum_k n_{yk}$ . Now, expanding equation (5), we get

1883 
$$(n_u - 1) \sigma_u^2 = \sum_j (u_j^2 + u_{ref}^2 - 2u_{ref} u_j) \quad (6)$$

1884 or

1885  $(n_u - 1) \sigma_u^2 = \sum_j u_j^2 + n_u u_{ref}^2 - 2u_{ref} \sum_j u_j$  (7)

1886 Expanding (4) for each individual dataset  $y_k$ , we get

1887  $(n_{y_k} - 1) \sigma_{y_k}^2 = \sum_j y_{kj}^2 + \bar{y}_k^2 - 2\bar{y}_k \sum_j y_{kj}$  (8)

1888 which leads to

1889  $\sum_j u_j^2 = \sum_{k,j} y_{kj}^2 = \sum_k (n_{y_k} - 1) \sigma_{y_k}^2 + \sum_k n_{y_k} \bar{y}_k^2$ , (9)

1890 so that extracting the variance from equation (7) now leads to

1891  $S_u^2 = \frac{1}{(n_u - 1)} ( \underset{k}{\overset{\circ}{\mathbf{a}}}(n_{y_k} - 1) S_{y_k}^2 + \underset{k}{\overset{\circ}{\mathbf{a}}} n_{y_k} \bar{y}_k^2 + n_u u_{ref}^2 - 2u_{ref} \underset{k}{\overset{\circ}{\mathbf{a}}} n_{y_k} \bar{y}_k )$  (10)

1892 The adjusted time series are obtained from the original series  $y_k$  as  $Y_k$ , and we can write

1893 Equation (4) in the same manner for the  $Y_k$  data values, namely

1894  $\sigma_{Y_k}^2 = \frac{1}{n_{y_k} - 1} \sum_j (Y_{kj} - \bar{Y}_k)^2$  (11)

1895 with  $\sigma_{Y_k} = \sigma_{y_k}$  as the adjustments (offsets) are performed in an additive manner; if these

1896 adjustments were performed using multiplicative factors, those factors would also have to be

1897 considered in a multiplicative way to get the new  $\sigma_{Y_k}$  values. We can thus write (10) for the

1898 adjusted datasets as:

1899  $S_u^2 = \frac{1}{(n_u - 1)} ( \underset{k}{\overset{\circ}{\mathbf{a}}}(n_{y_k} - 1) S_{y_k}^2 + \underset{k}{\overset{\circ}{\mathbf{a}}} n_{y_k} \bar{Y}_k^2 + n_u U_{ref}^2 - 2U_{ref} \underset{k}{\overset{\circ}{\mathbf{a}}} n_{y_k} \bar{Y}_k )$  (12)

1900 Equation (12) for the standard deviation of the merged dataset simplifies if the original datasets

1901 are adjusted to exactly the same reference value  $ref$  ( $\bar{Y}_k = ref$ ) and the merged value  $U_{ref}$  is

1902 also equal to that value, as the sum of the last 3 terms in Eq. (10) (with  $Y_k$  replacing  $y_k$ ) then

1903 reduces to  $n_u ref^2 + n_u ref^2 - 2n_u ref^2$ , which is zero. In this case, one obtains

1904 
$$s_u^2 = \frac{1}{(n_u - 1)} \left( \sum_k (n_{yk} - 1) s_{yk}^2 \right) \quad (13)$$

1905 However, in general, one should use equation (12) for the standard deviation of the merged  
 1906 dataset, given the adjusted datasets  $\bar{Y}_k$  and the merged (or reference) value  $U_{ref}$ . Also, we often  
 1907 use a merged value equal to the average of the original data (over a given overlap period), so that

1908 
$$U_{ref} = \frac{1}{n_y} \sum_k \bar{y}_k \quad (14)$$

1909 where  $n_y$  is the total number of datasets ( $y_k$ ), as opposed to having the merged value place more  
 1910 weight on the larger datasets (e.g., for emission-type measurements versus occultation-type), in

1911 which case one would consider using  $U_{ref} = \frac{1}{n_u} \sum_k n_{yk} \bar{y}_k$ . For ozone, we use a particular dataset

1912 (SAGE II ozone) as the primary reference, but equation (12) can be used to obtain the standard  
 1913 deviation for the merged dataset (about the SAGE II reference) in that case also. While it is  
 1914 useful to have the formalism above for obtaining the merged dataset standard deviation  $\sigma_u$ , we

1915 often find significant differences between the standard deviations of various datasets, so that this  
 1916 effect will have the greatest influence on the results, as opposed to the impact of the last 3 terms

1917 in the summation (in (12)). Finally, it is easy to test equation (12) (and we have done so) by  
 1918 using synthetic series and calculating the standard deviation of the combined set. In reality, the

1919 standard deviations of the time series monthly mean values are typically larger for MLS than for  
 1920 ACE-FTS, mainly because of the more complete sampling of variability from the daily global

1921 measurements acquired by MLS. Sample plots for standard deviations and standard errors in the  
 1922 case of HCl are shown in Fig. A1. As expected, merged standard deviations follow the standard

1923 deviations from HALOE HCl before Aug. 2004 and those from MLS HCl after this time.  
 1924 However, the merged standard errors for the MLS time period follow the smaller MLS standard

1925 errors, because these values vary inversely with the square root of the number of values sampled,  
 1926 and are therefore made smaller by the significantly larger daily and monthly MLS sampling rate

1927 and coverage.

1928

1929 **A.3. Procedural merging details for GOZCARDS HCl, H<sub>2</sub>O, and O<sub>3</sub>**

1930 **A.3.1. HCl**

- 1931 - The vertical data range for valid HCl merged values is between 0.46 hPa and 147 hPa  
1932 (inclusive), as a result of data sparseness or data quality issues outside these ranges.
- 1933 - At 147 hPa, no merged HCl values exist for latitude bins from 35°S to 35°N inclusive,  
1934 because of unrealistically large Aura MLS HCl values in this region; also, there is not enough  
1935 data at this level to provide a meaningful product from HALOE and ACE-FTS data alone.
- 1936 - Because of occasional small negative merged values during southern hemisphere polar  
1937 winter, we did not apply HCl data offsets in the lower stratosphere for the 65°S through 85°S  
1938 bins from June through September and for pressures larger than or equal to 15 hPa. For  
1939 vertical continuity purposes, we applied this method to all lower stratospheric pressure levels,  
1940 although the small negative merged values only occurred in a small fraction of cases and the  
1941 impact on the merged values is not large. Seasonal variations in other bins are milder and did  
1942 not lead to such an Antarctic winter issue; also, this issue did not affect other species.
- 1943 - As Aura MLS and ACE-FTS data exist in the 85°N and 85°S bins, but there are no HALOE  
1944 measurements, we could not use our standard merging procedure there. We simply extended  
1945 the offsets from the adjacent bins (at 75°N and 75°S) to these two bins to obtain a merged  
1946 record after 2004 that exhibits continuity versus latitude.
- 1947 - At 100 hPa, we used HCl offsets from the 5°S bin for the 5°N bin, as there was insufficient  
1948 data from the three combined datasets in the latter bin to calculate meaningful offsets and  
1949 merge the datasets. This procedure seems reasonable, given that the time series in these two  
1950 adjacent tropical latitude bins (during years outside the 2004/2005 overlap period) look  
1951 continuous and stable enough to justify identical adjustments in both bins and to avoid a data  
1952 gap in the merged series at 5°N, although this does imply somewhat larger error bars at 5°N.

1953

1954 **A.3.2. H<sub>2</sub>O**

- 1955 - The vertical data range for valid H<sub>2</sub>O merged values is between 0.01 hPa and 147 hPa  
1956 (inclusive). Some H<sub>2</sub>O data exist at 147 hPa for low latitudes, but more careful work would  
1957 be needed to extend the merged data globally in such a region.



- 1958 - Users should keep in mind the PMC-related caveats mentioned in Sect. 4 for summer at high  
1959 latitudes in the upper mesosphere, prior to the end of the HALOE dataset (Nov. 2005).
- 1960 - As for HCl, we could not use our standard merging procedure at the two most poleward  
1961 latitude bins; we simply extended the offsets from the adjacent bins (at 75°N and 75°S) to  
1962 these polar bins to obtain a merged record after 2004 that exhibits continuity versus latitude.
- 1963 - Also as for HCl, at 100 hPa, we used H<sub>2</sub>O offsets from the 5°S bin for the 5°N bin, as there  
1964 was insufficient data from the combined datasets in the latter bin to calculate meaningful  
1965 offsets and merge the datasets. This procedure avoids a data gap in the merged series at 5°N.

### 1966 **A.3.3. O<sub>3</sub>**

#### 1967 *Screening of SAGE O<sub>3</sub> data*

1968 For SAGE I O<sub>3</sub>, the main uncertainty is aerosol interference, especially below 15 to 20 km. All  
1969 SAGE I values below (in altitude) where the aerosol extinction at 1.0 μm reaches a value larger  
1970 than  $1.0 \times 10^{-3} \text{ km}^{-1}$  are removed from the analysis (L. W. Thomason, personal communication).

1971 For SAGE II ozone, the screening steps are based on Wang et al (2002) as follows:

- 1972 - We removed the entire ozone profile when any reported error bar value exceeded 10%  
1973 between 30 and 50 km, in order to filter out outliers affected by “short events” (Wang et al.,  
1974 2002), which mainly occurred between mid-1993 and mid-1994, when SAGE II had a battery  
1975 problem. In order to preserve power, sunset measurements were started later than normal  
1976 while sunrise measurements were ended earlier. These “short events” had fewer  
1977 extraterrestrial solar irradiance measurements for calibration and normalization.
- 1978 - We used aerosol extinctions and extinction ratios to remove data affected by clouds, and  
1979 aerosols from the June 1991 Mt. Pinatubo eruption. O<sub>3</sub> data were removed when the aerosol  
1980 extinction at 0.525 μm exceeded  $6 \times 10^{-3} \text{ km}^{-1}$ , thus removing data affected by this eruption  
1981 for months and even years, in the lower stratosphere. For cases with extinctions less than  
1982  $6 \times 10^{-3} \text{ km}^{-1}$  but greater than  $1 \times 10^{-3} \text{ km}^{-1}$ , and extinction ratios ( $0.525 \text{ μm} / 1.02 \text{ μm}$ )  $\leq 1.4$ , the  
1983 corresponding data were removed for additional filtering. Although more stringent criteria  
1984 could be used to remove a few more outliers, this would also remove many more “good”  
1985 ozone data that are not affected by aerosol/cloud. Fortunately, any artifacts from these few  
1986 unfiltered data values are greatly reduced after binning the data into monthly zonal means.

- 1987 - We removed anomalously low O<sub>3</sub> values resulting from very small SAGE II transmittances;  
 1988 O<sub>3</sub> error values in these cases were capped at 300% by the algorithm. Such low O<sub>3</sub> values  
 1989 (sometimes low by 2-3 orders of magnitude) generally occur close to the tropopause and in  
 1990 the troposphere, and can be identified by using this 300% error flag (Wang et al., 2002).  
 1991 - It was found that SAGE II ozone data could be affected during high sun-orbit beta angle  
 1992 conditions (Wang et al., 1996). SAGE II profiles immediately following fully sunlit orbits  
 1993 with absolute values of beta greater than 40° are eliminated from monthly zonal means.

1994

1995 *Other merging details for O<sub>3</sub>*

- 1996 - SAGE I monthly mean source data are used for the merged dataset in the tropical bins (25°S  
 1997 to 25°N) from 1 through 68 hPa only and, at higher latitudes, from 1 through 100 hPa only.  
 1998 - The vertical range for valid O<sub>3</sub> merged values is between 0.2 hPa and 215 hPa (inclusive),  
 1999 with the lower altitude bound varying with latitude. The merged product at 147 and 215 hPa  
 2000 has valid data only for the 35° to 85° latitude bins. Indeed, we limited merged data mostly to  
 2001 stratospheric values (larger than ~ 0.1 ppmv); the upper troposphere is more of a challenge  
 2002 for such a merging activity, given smaller abundances, more challenging measurements, and  
 2003 a larger impact from different instrument resolutions. The upper range limit was chosen to  
 2004 enable studies of the upper stratosphere and lower mesosphere, even if this is a region where  
 2005 diurnal ozone change occurs; arguments we have presented (see main text) suggest that the  
 2006 GOZCARDS merged ozone time series variations should not be subject to a large impact  
 2007 from diurnal variations, although high altitude regions should still be treated with caution.  
 2008 - We omitted the use of UARS MLS at 100 hPa for low latitudes (from 25°S to 25°N), as these  
 2009 monthly values are biased quite high and also exhibit too large a seasonal cycle amplitude, in  
 2010 comparison to HALOE and SAGE II data; this appears to relate to a UARS MLS artifact.  
 2011 - Since there is no (monthly) overlap between SAGE II and HALOE versus UARS MLS or  
 2012 Aura MLS in the 85°N and 85°S latitude bins, the same offsets as for 75°N and 75°S  
 2013 (respectively) are applied to the datasets at these two extreme latitude bins, in order to  
 2014 minimize latitudinal discontinuities in the merged data record.

2015 - Because of discontinuities that appeared in merged O<sub>3</sub> at high latitudes above the stratopause,  
2016 particularly in the 75°S bin, we flagged merged values for 75° and 85° (N and S) as bad, for  
2017 pressures less than 1 hPa. This issue could be the result of a few bad data points or not  
2018 enough data overlap. To minimize artifacts, we left the resolution of this issue for future  
2019 investigations; also, the reduced amount of occultation data at these high latitudes makes the  
2020 usefulness of a merged product with poorly sampled seasonal changes somewhat marginal  
2021 (for certain years at least, the number of monthly values drops significantly at high latitudes).  
2022  
2023

**Table 1.** Characteristics of instrument datasets used to create GOZCARDS ESDRs (version ev1.01).

<b>Instrument and Data Versions</b>	<b>Platform</b>	<b>Type of measurement</b>	<b>Time period (GOZCARDS source files)</b>	<b>Vertical Resolution (km)</b>	<b>Retrieved quantity and stratospheric vertical grid spacing</b>
SAGE I V5.9_rev O <sub>3</sub>	AEM-2	Solar occultation VIS/UV and near-IR	Feb. 1979 - Nov. 1981	1	Density on altitude grid 1 km spacing
SAGE II V6.2 O <sub>3</sub>	ERBS	Solar occultation VIS/UV and near-IR	Oct. 1984 - Aug. 2005	0.5 - 1	Density on altitude grid 0.5 km spacing
HALOE V19	UARS	Solar occultation mid-IR	Oct. 1991 - Nov. 2005	2.5	Volume Mixing Ratio on pressure grid with 30 levels per decade (LPD) change in p
MLS V5 O <sub>3</sub> V6 H <sub>2</sub> O	UARS	Limb emission microwave / sub-mm	Oct. 1991 - June 1997 (May 1993 end for strat. H <sub>2</sub> O)	<b>H<sub>2</sub>O</b> 3 - 4 (strat.) 5 - 12 (mes.)  <b>O<sub>3</sub></b> 3.5 - 5 (strat.) 5 - 8 (mes.)	Volume Mixing Ratio on pressure grid with 6 LPD in stratosphere  6 LPD in stratosphere
ACE-FTS V2.2 (V2.2 update for O <sub>3</sub> )	SCISAT	Solar occultation mid-IR	Mar. 2004 through Sep. 2010 (2009 for O <sub>3</sub> )	3 - 4	Volume Mixing Ratio on 1 km grid spacing (height and p provided)
MLS V3.3 V2.2 O <sub>3</sub>	Aura	Limb emission microwave / sub-mm	Aug. 2004 through 2012	<b>HCl</b> 3 - 5  <b>H<sub>2</sub>O</b> 3 - 4 (p > 0.1 hPa) 5 - 9 (0.1-0.01 hPa)  <b>O<sub>3</sub></b> 3	Volume Mixing Ratio on pressure grid with 6 LPD  12 LPD  6 LPD

2027 **Table 2.** Products and instrument source data making up the available GOZCARDS data records.

<b>Merged Products</b> and pressure range	<b>Source Datasets</b> (and years used)
<b>HCl</b> 147 – 0.5 hPa	HALOE (1991-2005), ACE-FTS (2004-2010), Aura MLS (2004 onward)
<b>H<sub>2</sub>O</b> 147 – 0.01 hPa	HALOE (1991-2005), UARS MLS (1991-1993), ACE-FTS (2004-2010), Aura MLS (2004 onward)
<b>O<sub>3</sub></b> 215 – 0.2 hPa	SAGE I (1979-1981), SAGE II (1984-2005), HALOE (1991-2005), UARS MLS (1991-1997), ACE-FTS (2004-2009), Aura MLS (2004 onward)
<b>HNO<sub>3</sub></b> 215 – 1 hPa	ACE-FTS (2004-2010), Aura MLS (2004 onward)
<b>N<sub>2</sub>O</b> 100 – 0.5 hPa	ACE-FTS (2004-2010), Aura MLS (2004 onward)
<b>Temperature</b> 1000 – 0.015 hPa	GMAO MERRA (1979 onward)

2028

2029

2030

2031 **Fig. 1.** Merging procedure illustration for HCl. Top left panel shows the HCl monthly mean source data  
2032 during the overlap period (Aug. 2004 - Nov. 2005) for HALOE, ACE-FTS, and Aura MLS. Top right  
2033 panel illustrates step 1 in the merging procedure, with the temporary merged data values (orange)  
2034 resulting from the adjustment of ACE-FTS and Aura MLS values to the reference indicated by the black  
2035 dashed line. Middle left panel shows the result of step 2, namely the merged values arising from merging  
2036 HALOE data with the temporary merged values from step 1; the black dashed line is the new average  
2037 reference value, obtained from a 2/3 and 1/3 weighting of the dashed orange and dashed blue line values,  
2038 respectively (see text). Middle right panel shows all the source data and the final merged values during  
2039 the overlap period. Bottom panel shows the source and merged time series from 1991 through 2012 after  
2040 the calculated additive offsets are applied to the whole source datasets, which are then merged (averaged)  
2041 together wherever overlap between instruments exists.

2042  
2043 **Fig. 2.** Offsets applied to the HCl source datasets (top panels for HALOE, middle panels for ACE-FTS,  
2044 bottom panels for Aura MLS) as a function of latitude and pressure. The left column gives offsets in ppbv  
2045 and the right column provides offsets as a percent of the zonal average merged mixing ratios during the  
2046 overlap period (Aug. 2004 – Nov. 2005) used here to compute the average offsets.

2047  
2048 **Fig. 3.** Example of HCl time series analyses for 50°N-60°N and 32 hPa. (a) HCl monthly mean source  
2049 data from ACE-FTS and Aura MLS; the MLS dots are filled when there is time overlap with ACE-FTS,  
2050 and open if no such overlap exists. Simple linear fits are shown as colored lines for  
2051 ACE-FTS and for Aura MLS (orange line for all red dots and red line for filled red dots only).  
2052 Correlation coefficient values (R values) for the two time series are provided in the title.  
2053 (b) Deseasonalized anomalies for both ACE-FTS and Aura MLS, with corresponding linear fits (and R  
2054 values). (c) Difference of deseasonalized anomalies (ACE-FTS minus Aura MLS), with linear fit.

2055  
2056 **Fig. 4.** Latitude/pressure contours of time series diagnostics obtained from analyses illustrated in  
2057 Fig. 3 for HCl from Aura MLS and ACE-FTS. Top panel: Correlation coefficient for the deseasonalized  
2058 time series. Bottom panel: Ratio of the slope of the difference between deseasonalized series over the  
2059 error in this slope.

2060

2061

2062 **Fig. 5.** Illustration of GOZCARDS HCl monthly averages with systematic error estimates (shown as grey  
2063 shading) at 46 hPa for 30°S-40°S; see text for the meaning of this shaded region. The source data from  
2064 HALOE, Aura MLS, and ACE-FTS are shown in different colors (see legend), along with the merged  
2065 values.

2066  
2067 **Fig. 6.** Systematic error estimates for GOZCARDS HCl. One error (left panels) is relevant for values  
2068 lower than (below) the merged values, and one (right panels) for values larger than the merged values; the  
2069 top panels give the error estimates in ppbv, and the bottom panel errors are expressed as percent of the  
2070 average merged values over the relevant time periods (see text). These error bars provide a range within  
2071 which 95% of the source data values lie.

2072  
2073 **Fig. 7.** Time series of the GOZCARDS monthly-averaged merged HCl abundance for 3 different latitude  
2074 bin averages (see color legend in panel (a)) for (a) 0.7 hPa, (b) 10 hPa, (c) 32 hPa, and (d) 68 hPa.

2075  
2076 **Fig. 8.** The average rate of change (percent per year) for HCl as a function of pressure for different  
2077 latitude bin averages (see legend) for time periods corresponding to the appropriate GOZCARDS HCl  
2078 values (see text) in the upper stratosphere (Jan. 1997 - Sep. 2010) and lower stratosphere (Jan. 1997 -  
2079 Dec. 2012). Deseasonalized monthly data were used to obtain a long-term trend for these time periods;  
2080 two-sigma error bars are shown.

2081  
2082 **Fig. 9.** Same as Fig. 8, but for the lower stratosphere only and using different time periods to illustrate  
2083 shorter-term changes in this region. Average rates of change in HCl are given for (a) 2003 through 2012,  
2084 a decade exhibiting significant differences between northern and southern hemispheric change, (b) the  
2085 6-year period 2006 through 2011, when the largest changes occurred, and (c) the most recent 6-year  
2086 period 2008 through 2013, when a significant decrease in the variability took place.

2087

2088

2089

2090

2091 **Fig. 10.** Rates of change for GOZCARDS HCl (connected open circles) are given as a function of latitude  
2092 in 10° latitude bins for sliding 6-year periods centered on Jan. 1 of each year (e.g., the 1998 point is an  
2093 average for data from 1995 through 2000, and the 2011 point is for data from 2008 through 2013). (a) is  
2094 for changes in upper stratospheric HCl at 0.7 hPa and (b) is for the change in the integrated HCl column  
2095 between 68 hPa and 10 hPa. The two additional curves in (a) represent the rates of change in the  
2096 estimated surface total chlorine from NOAA data (green is for a 6-year time shift, and purple for a  
2097 7-year time shift, to account for transport time to the upper stratosphere); see text for more details. Panels  
2098 (c) and (d) are similar to (a) and (b), respectively, in terms of the pressure levels used, but the rates of  
2099 change are averaged over all latitude bins covering 50°S to 50°N for two sets of sliding time periods  
2100 (black is for 6-year periods, red is for 8-year periods). As in (a), surface total chlorine variations are also  
2101 displayed in panel (c). Error bars indicate twice the standard errors in the means.

2102  
2103 **Fig. 11.** Offsets applied to the H<sub>2</sub>O source datasets as a function of latitude and pressure, similar to  
2104 Fig. 2 for HCl.

2105  
2106 **Fig. 12.** Latitude/pressure contours of time series diagnostics for H<sub>2</sub>O from Aura MLS and ACE-FTS;  
2107 this is similar to Fig. 4 for HCl.

2108  
2109 **Fig. 13.** A depiction of the “tape recorder” evolution for tropical water vapor abundances from 147 to  
2110 10 hPa for October 1991 through December 2013. This plot was produced from GOZCARDS merged  
2111 H<sub>2</sub>O time series anomalies (differences from the long-term means) for the average of the 4 tropical bins  
2112 covering 20°S to 20°N.

2113  
2114 **Fig. 14.** Systematic error estimates for GOZCARDS H<sub>2</sub>O (similar to Fig. 6 for HCl).

2115  
2116 **Fig. 15.** Variations in stratospheric water vapor from the GOZCARDS H<sub>2</sub>O merged data records (1992  
2117 through 2013) averaged from (a) 60°S to 60°N and (b) 20°S to 20°N. Monthly average values and annual  
2118 averages are shown by thin and thick lines (connecting similarly-colored dots), respectively, for the  
2119 pressure levels indicated in the plot legend.

2120



2121 **Fig. 16.** Stratospheric water vapor variability on decadal timescales for 1992 through 2013 (thick lines)  
2122 for tropical (20°S-20°N in black) and mid-latitude (20°N-60°N in red and 20°S-60°S in blue) zonal  
2123 means, based on the GOZCARDS merged H<sub>2</sub>O data record. The variability is expressed here as the  
2124 difference between maximum and minimum annual average abundances, from 100 to 1 hPa, in ppmv (left  
2125 panel) and percent (right panel). The 22-year period is broken up into two 11-year periods to illustrate  
2126 how the variability changes from the 1<sup>st</sup> period (dashed lines) to the 2<sup>nd</sup> period (thin solid lines).

2127

2128 **Fig. 17.** (a) Variations in upper mesospheric (0.01 hPa) water vapor mixing ratios averaged from 60°S to  
2129 60°N for Oct. 1991 through Dec. 2013, based on the GOZCARDS merged H<sub>2</sub>O data records. Monthly  
2130 average values and annual averages are shown by connected brown dots and connected black dots,  
2131 respectively. (b) GOZCARDS merged H<sub>2</sub>O annual averages (connected filled symbols) from 60°S to  
2132 60°N for 1992 through 2013 at pressure levels between 0.1 and 0.01 hPa. A time series of annually-  
2133 averaged Lyman  $\alpha$  solar flux values (open circles), scaled to arbitrary units, is also displayed (see text).

2134

2135 **Fig. 18.** Time series of monthly zonal mean O<sub>3</sub> for 10°S - 20°S between 1 hPa and 6.8 hPa (with pressure  
2136 values given by "pre") from SAGE I, SAGE II, HALOE, UARS MLS, Aura MLS, and ACE-FTS, all  
2137 color-coded following the legend in top left panel.

2138

2139 **Fig. 19.** Schematic diagram describing the creation of the merged GOZCARDS monthly zonal mean  
2140 ozone data record from various satellite datasets. Instruments represented in red inside the boxes are used  
2141 as a reference. Instruments whose measurements have already been adjusted to a reference are indicated  
2142 with a "\*" superscript. AMLS refers to Aura MLS and UMLS to UARS MLS. See text for more details.

2143

2144 **Fig. 20.** Offsets applied to the O<sub>3</sub> source datasets, similar to Fig. 2 for HCl.

2145

2146

2147

2148 **Fig. 21.** Latitude/pressure contours of time series diagnostics for O<sub>3</sub> from Aura MLS and ACE-FTS; this  
2149 is similar to Fig. 4 for HCl. The correlation coefficients (R values) and slope trend diagnostics are  
2150 provided for HALOE versus SAGE II in the top two panels (for 1993-1999 as the trend issue for  
2151 converted SAGE II data occurs after mid-2000 and to avoid Pinatubo-related data gaps before 1993) and  
2152 for ACE-FTS versus Aura MLS in the bottom two panels (for 2005-2009).

2153

2154 **Fig. 22.** Systematic error estimates for GOZCARDS O<sub>3</sub> (similar to Fig. 6 for HCl).

2155

2156 **Fig. 23.** Column ozone values (DU) from ZC12 (in red) for 60°S-60°N and from GOZCARDS averages  
2157 in different latitude bins (see legend). The connected dots are for GOZCARDS column ozone densities  
2158 above 68 hPa from 1979 through 2013. The lines with no symbols and the connected open dots are also  
2159 for GOZCARDS columns, but for values above 100 hPa and above 215 hPa, respectively, for 1985  
2160 through 2013; there are no blue open dots because of the lack of GOZCARDS merged ozone data in the  
2161 tropics for pressures larger than 100 hPa, during 1985-2013.

2162

2163 **Fig. 24.** Near-global (60°S to 60°N) results for average column ozone (total and stratospheric, from  
2164 *Ziemke and Chandra, 2012*) compared to GOZCARDS O<sub>3</sub> columns above 68 hPa. Stratospheric columns  
2165 are offset in order to more easily compare relative variations versus time; the black dots and red crosses  
2166 are referenced to the 1980 total column values, while the cyan curves are referenced to 2007 to better  
2167 illustrate the fits in the later years.

2168

2169 **Fig. 25.** Change in column ozone after removal of solar cycle signal and with 3-year smoothing applied;  
2170 (a) gives relative changes in DU, and (b) shows percent changes relative to the average GOZCARDS  
2171 stratospheric columns in 1979. Black symbols are from the GOZCARDS column values above 68 hPa,  
2172 averaged over 60°S-60°N. Red symbols, for comparison, are from the ZC12 data over the same latitude  
2173 range (after removal of the fitted solar cycle signal).

2174

2175 **Fig. 26.** Time evolution (Aug. 2004 through 2012) versus latitude of GOZCARDS merged N<sub>2</sub>O (ppbv) at  
2176 (a) 6.8 hPa and (b) 100 hPa.

2177

2178 **Fig. 27.** Sample results display the time evolution of satellite-retrieved HNO<sub>3</sub> (ppbv) for two different  
2179 periods, 1992-1997 in (a) and (c) versus 2004-2013 in (b) and (d). Panels (a) and (b) are contour plots at  
2180 46 hPa from UARS MLS global data and the merged GOZCARDS global data after 2004, respectively;  
2181 (c) and (d) show time series at 32 hPa and for the 40°N-50°N latitude bin, with (a) from UARS MLS data,  
2182 and (d) from ACE-FTS, Aura MLS, and the merged combination (between the two source data sets).

2183

2184

2185

2186

2187 **Fig. A1.** Illustration of the standard deviations (in (a)) and standard errors (in (b)) for monthly  
2188 mean GOZCARDS HCl (source and merged records) at 46 hPa for 30°S-40°S. Source data from  
2189 HALOE, Aura MLS, and ACE-FTS are given by the filled colored dots (see legend); each  
2190 standard deviation is simply obtained from the range of values measured during the month. The  
2191 large open brown circles give standard deviations for the merged HCl product; this Appendix  
2192 provides the formulae to calculate these quantities.

2193

2194

2195

2196 **Fig. S1:** Illustration of the latitudinal dependence of the HCl offsets for HALOE, ACE-FTS, and Aura  
2197 MLS at two pressure levels (top panel for 0.46 hPa, bottom panel for 46 hPa). Error bars represent twice  
2198 the standard error in the derived offsets (based on variability during the overlapping period). Larger  
2199 standard error values indicate that there were either fewer points of overlap or larger offset variability  
2200 (standard deviations); we found that both of these factors contribute.

2201

2202 **Fig. S2:** Latitude/pressure contours of the fitted mean annual amplitudes (ppbv) from HCl time series for  
2203 HALOE, ACE-FTS, and Aura MLS, based on their respective measurement periods (see text).

2204

2205 **Fig. S3:** Time evolution (Oct. 1991 through 2013) versus latitude of GOZCARDS merged HCl (ppbv) at  
2206 46 hPa.

2207

2208 **Fig. S4:** HALOE sunrise measurements of H<sub>2</sub>O versus the 3.46 μm extinction coefficient for 1992, 1993,  
2209 and 1999 at 22 hPa. The green vertical line represents the aerosol extinction value ( $5 \times 10^{-4} \text{ km}^{-1}$ ) used to  
2210 screen anomalous HALOE H<sub>2</sub>O values. It is apparent that anomalously low H<sub>2</sub>O values occurred in 1992  
2211 when the 3.46 μm aerosol extinction exceeded about  $5 \times 10^{-4} \text{ km}^{-1}$ . These artifacts were confined to 1991  
2212 and 1992; for these years, and for pressure levels at and below 22 hPa, the corresponding H<sub>2</sub>O data values  
2213 were excluded. This screening method eliminates about 10% of the global (lower stratospheric)  
2214 measurements in 1992.

2215

2216 **Fig. S5:** Merging procedure illustration for H<sub>2</sub>O at 5°N and 22hPa. This is similar to Fig. 2 (for HCl), but  
2217 an additional step is illustrated for the end of this procedure, whereby stratospheric H<sub>2</sub>O data from UARS  
2218 MLS are adjusted to the early portion of the merged time series that was obtained after the 2<sup>nd</sup> step; this  
2219 adds more coverage (more brown dots in the bottom panel for 1991-1993).

2220

2221 **Fig. S6:** Latitude/pressure contours of the fitted mean annual amplitudes (ppmv) from H<sub>2</sub>O time series for  
2222 HALOE, ACE-FTS, and Aura MLS, based on their respective measurement periods.

2223

2224 **Fig. S7:** Time evolution (Oct. 1991 through 2013) versus latitude of GOZCARDS merged H<sub>2</sub>O (ppmv) at  
2225 3.2 hPa (top panel) and 68 hPa (bottom panel).

2226

2227 **Fig. S8:** Monthly zonal mean ozone differences (%) between SAGE II and (a) HALOE,  
2228 (b) UARS MLS (UMLS for short), (c) Aura MLS (AMLS for short), and (d) ACE-FTS during their  
2229 respective overlap periods. Differences are expressed (in percent) as  $100 \times [(SAGE II - Other) / (Other)]$ .  
2230 Shaded areas indicate negative values.

2231

2232 **Fig. S9:** Monthly zonal mean temperature differences between NCEP (used by SAGE II) and HALOE  
2233 temperatures relative to MERRA for 10°S - 20°S between 1 and 6.8 hPa, per color-coding indicated in  
2234 bottom left panel; “pre” represents the pressure value. From 1 to 2.1 hPa, differences between NCEP and  
2235 MERRA are generally within  $\pm 4$ K before mid-2000. After that time, NCEP temperatures show a sharp  
2236 increase and are systematically higher than MERRA values by 5 to 10K. However, this divergence and  
2237 trend are not seen in HALOE temperatures. NCEP temperatures between 3.2 and 6.8 hPa are smaller than  
2238 MERRA after mid-2000; negative trends (versus MERRA) also occur in the HALOE data at these levels.

2239

2240 **Fig. S10:** Relative trends (K/decade) in zonal mean temperature differences for NCEP – MERRA and  
2241 HALOE – MERRA (color-coded as in Fig. S9) in the upper stratosphere. NCEP temperatures show  
2242 positive trends versus MERRA of  $\sim 2$ -5 K/decade between 2.1 and 1 hPa for all latitudes. However,  
2243 HALOE temperatures show no significant trends versus MERRA, except at 1.5 hPa in the southern  
2244 hemisphere. For pressures between 3.2 and 6.8 hPa, the temperature analyses are not conclusive; although  
2245 NCEP values show negative trends of  $\sim 2$ -3 K/decade versus MERRA, they agree with HALOE.

2246

2247 **Fig. S11:** Mean differences and standard deviations (horizontal bars) between SAGE II and Aura MLS  
2248 ozone in three different latitude bins: 20°S to 60°S (left panel), 20°S to 20°N (middle panel), and 20°N to  
2249 60°N (right panel). Results based on monthly zonal mean and coincident profiles (see text for coincidence  
2250 criteria) during overlap periods are shown in red and blue, respectively. To choose collocated profiles,  
2251 coincidence criteria of  $\pm 1^\circ$  in latitude and  $\pm 8^\circ$  in longitude were used; the time difference criterion was  
2252 chosen as 12 hours, but only nighttime measurements from Aura MLS were used.

2253

2254 **Fig. S12:** Latitude/pressure contours of the fitted mean annual amplitudes (ppmv) from O<sub>3</sub> time series for  
2255 SAGE II, HALOE, ACE-FTS, and Aura MLS, based on their respective measurement periods.

2256

2257 **Fig. S13:** Illustration of the time evolution of the GOZCARDS merged O<sub>3</sub> data field versus latitude at  
2258 68 hPa (top panel) and versus pressure for the 40°N-50°N latitude bin (bottom panel).

2259

2260 **Fig. S14:** Offsets applied to the N<sub>2</sub>O source datasets (top panels for ACE-FTS, bottom panels for Aura  
2261 MLS) as a function of latitude and pressure. The left column gives offsets in ppbv and the right column  
2262 provides offsets as a percent of the zonal average merged mixing ratios during the overlap period (Aug.  
2263 2004 – Sep. 2010) used here to compute the average offsets.

2264

2265 **Fig. S15:** Latitude/pressure contours of time series diagnostics derived from Aura MLS and ACE-FTS  
2266 N<sub>2</sub>O data comparisons (and obtained from analyses similar to those illustrated in Fig. 6 for HCl). Top  
2267 panel: Correlation coefficient for the deseasonalized time series. Bottom panel: Ratio of the slope of the  
2268 difference between deseasonalized series over the error in this slope.

2269

2270 **Fig. S16:** Offsets applied to the HNO<sub>3</sub> source datasets (top panels for ACE-FTS, bottom panels for Aura  
2271 MLS) as a function of latitude and pressure. The left column gives offsets in ppbv and the right column  
2272 provides offsets as a percent of the zonal average merged mixing ratios during the overlap period (Aug.  
2273 2004 – Sep. 2010) used here to compute the average offsets.

2274

2275 **Fig. S17:** Latitude/pressure contours of time series diagnostics derived from Aura MLS and ACE-FTS  
2276 HNO<sub>3</sub> data comparisons (and obtained from analyses similar to those illustrated in Fig. 6 for HCl). Top  
2277 panel: Correlation coefficient for the deseasonalized time series. Bottom panel: Ratio of the slope of the  
2278 difference between deseasonalized series over the error in this slope.

2279

2280